EDITED BY
IGOR KRASNIKOV

PROCESSES AND CONTROL SYSTEMS: SYNTHESIS, MODELING, OPTIMIZATION

Collective monograph

Technology Center

2025

UDC 681.5
K81

Published in 2025
by TECHNOLOGY CENTER PC®
Kharkiv, Ukraine

K81 **Authors:**
Edited by Igor Krasnikov
Anatolii Babichenko, Igor Krasnikov, Juliya Babichenko, Oleksandr Dzevochko, Yana Kravchenko, Ihor Lysachenko, Valerii Samsonkin, Valerii Druz, Oksana Yurchenko, Vitalii Budashko, Oksana Glazeva, Albert Sandler, Sergii Khniunin, Valentyn Bogach, Yurii Zhuravlov, Petro Lezhniuk, Viacheslav Komar, Vladyslav Lysyi, Yuliia Malohulko, Volodymyr Netrebskyi, Olena Sikorska, Oleksandr Povazhnyi, Volodymyr Kukhar, Oleksiy Koyfman, Khrystyna Malii, Volodymyr Pashynskyi
Processes and control systems: synthesis, modeling, optimization: monograph / I. Krasnikov and others. Kharkiv: TECHNOLOGY CENTER PC, 2025. — 187 p.

The collective monograph is devoted to the study of modern approaches to modeling, optimization and increasing the efficiency of control systems in complex technical complexes. The presented material covers issues of heat and power processes, operational data analytics, optimal regulation of mobile power plants, intelligent local power grids and digital monitoring of industrial equipment. The focus is on methods of identifying uncertainties, implementing adaptive algorithms, using mathematical models and three-dimensional control technologies. The monograph demonstrates the interaction of theoretical principles and applied solutions, reflecting the transition of engineering systems from static structures to dynamic objects with built-in mechanisms of self-diagnosis and optimization. The work summarizes tools that contribute to the formation of a new technical paradigm based on the integration of modeling, control and predictive analysis.
Figures 81, Tables 19, References 192 items.

DOI: 10.15587/978-617-8360-19-1
ISBN 978-617-8360-19-1 (on-line)

Cite as: Krasnikov, I. (Ed.) (2025). Processes and control systems: synthesis, modeling, optimization: monograph. Kharkiv: TECHNOLOGY CENTER PC, 187. doi: http://doi.org/10.15587/978-617-8360-19-1

AUTHORS

CHAPTER 1

ANATOLII BABICHENKO
PhD, Associate Professor
Department of Technology System Automation and Ecology Monitoring
National Technical University "Kharkiv Polytechnic Institute"
ORCID: https://orcid.org/0000-0002-8649-9417

IGOR KRASNIKOV
PhD, Associate Professor
Department of Technology System Automation and Ecology Monitoring
National Technical University "Kharkiv Polytechnic Institute"
ORCID: https://orcid.org/0000-0002-7663-1816

JULIYA BABICHENKO
PhD, Associate Professor
Department of Heat Engineering, Heat Engines and Energy Management
Ukrainian State University of Railway Transport
ORCID: https://orcid.org/0000-0002-5345-7595

OLEKSANDR DZEVOCHKO
PhD, Associate Professor
Department of Technology System Automation and Ecology Monitoring
National Technical University "Kharkiv Polytechnic Institute"
ORCID: https://orcid.org/0000-0002-1297-1045

YANA KRAVCHENKO
PhD
Department of Technology System Automation and Ecology Monitoring
National Technical University "Kharkiv Polytechnic Institute"
ORCID: https://orcid.org/0000-0002-6311-8060

IHOR LYSACHENKO
PhD, Associate Professor
Department of Technology System Automation and Ecology Monitoring
National Technical University "Kharkiv Polytechnic Institute"
ORCID: https://orcid.org/0000-0002-3723-8587

CHAPTER 2

VALERII SAMSONKIN
Doctor of Technical Sciences, Professor
Department of Transport Technology and Process Control Traffic
National Transport University
ORCID: https://orcid.org/0000-0002-1521-2263

VALERII DRUZ
Doctor of Biological Sciences, Professor
Department of Radioelectronic and Biomedical Computerised Means and Technologies
National Aerospace University "Kharkiv Aviation Institute"
ORCID: https://orcid.org/0009-0004-5808-2456

OKSANA YURCHENKO
PhD, Associate Professor
Department of Management of Commercial Activity of Railways
National Transport University
ORCID: https://orcid.org/0000-0001-6834-692X

CHAPTER 3

VITALII BUDASHKO
Doctor of Technical Sciences, Professor, Director
Educational and Scientific Institute of Automation and Electrical Engineering
National University "Odessa Maritime Academy"
ORCID: https://orcid.org/0000-0003-4873-5236

OKSANA GLAZEVA
PhD, Associate Professor
Department of Electrical Engineering and Electronics
National University "Odessa Maritime Academy"
ORCID: https://orcid.org/0000-0002-4992-7697

ALBERT SANDLER
PhD, Associate Professor
Department of the Theory of Automatic Control and Computer Technology
National University "Odessa Maritime Academy"
ORCID: https://orcid.org/0000-0002-0709-0542

SERGII KHNIUNIN
PhD, Associate Professor
Department of Information Technology
International Humanitarian University
ORCID: https://orcid.org/0000-0001-5941-5372

VALENTYN BOGACH
PhD, Associate Professor
Department of Engineering Mechanics and Ship Repair
National University "Odessa Maritime Academy"
ORCID: https://orcid.org/0000-0002-0822-0003

YURII ZHURAVLOV
PhD, Associate Professor
Department of Engineering Mechanics and Ship Repair
National University "Odessa Maritime Academy"
ORCID: https://orcid.org/0000-0001-7342-1031

CHAPTER 4

PETRO LEZHNIUK
Doctor of Technical Sciences, Professor
Department of Electric Power Stations and Systems
Vinnytsia National Technical University
ORCID: https://orcid.org/0000-0003-0338-2131

VIACHESLAV KOMAR
Doctor of Technical Sciences, Professor, Head of Department
Department of Electric Power Stations and Systems
Vinnytsia National Technical University
ORCID: https://orcid.org/0000-0003-4969-8553

VLADYSLAV LYSYI
PhD Student
Department No. 3 Wind Power
Institute of Renewable Energy of the National Academy of Sciences of Ukraine
ORCID: https://orcid.org/0009-0007-0211-9100

YULIIA MALOHULKO
PhD, Associate Professor
Department of Electric Power Stations and Systems
Vinnytsia National Technical University
ORCID: https://orcid.org/0000-0002-6637-7391

VOLODYMYR NETREBSKYI
PhD, Associate Professor
Department of Electric Power Stations and Systems
Vinnytsia National Technical University
ORCID: https://orcid.org/0000-0003-2855-1253

OLENA SIKORSKA
PhD, Associate Professor
Department of Electric Power Stations and Systems
Vinnytsia National Technical University
ORCID: https://orcid.org/0000-0001-7341-9724

CHAPTER 5

OLEKSANDR POVAZHNYI
Doctor of Economic Sciences, Professor, Rector
Technical University "Metinvest Polytechnic" LLC
ORCID: https://orcid.org/0000-0002-9835-6464

VOLODYMYR KUKHAR
Doctor of Technical Sciences, Professor, Vice-Rector for Research
Department of Metallurgy and Production Organization
Technical University "Metinvest Polytechnic" LLC
ORCID: https://orcid.org/0000-0002-4863-7233

OLEKSIY KOYFMAN
PhD, Associate Professor, Head of Department
Department of Automation, Electrical and Robotic Systems
Technical University "Metinvest Polytechnic" LLC
ORCID: https://orcid.org/0000-0003-2075-7417

KHRYSTYNA MALII
PhD, Associate Professor, Head of Research Department
Department of Metallurgy and Production Organization
Technical University "Metinvest Polytechnic" LLC
ORCID: https://orcid.org/0000-0002-9046-4268

VOLODYMYR PASHYNSKYI
Doctor of Technical Sciences, Associate Professor, Head of Department
Department of Materials Science and Applied Mechanics
Technical University "Metinvest Polytechnic" LLC
ORCID: https://orcid.org/0000-0003-0118-4748

ABSTRACT

The collective monograph focuses on the study of modeling methods, analytical assessment and optimization of complex technical systems in industry and energy. The presented materials cover the tasks of heat transfer, operational reliability, mobile control, distributed energy and predictive monitoring, forming a holistic scientific and applied basis for the implementation of engineering solutions in real production conditions. The monograph is aimed at systematizing methods that ensure increased efficiency of technological facilities through mathematical analysis, digital measurements and adaptive control.

The first section examines in detail the processes of secondary condensation in large-capacity ammonia synthesis units of the AM-1360 type. Special attention is paid to methods for experimental identification of thermophysical parameters that determine the operation of heat exchangers in unsteady modes. Refined mathematical models of heat transfer have been constructed and the influence of structural deviations on energy consumption parameters has been assessed. It is shown that the use of adaptive software control allows to adjust temperature profiles, reduce the load on refrigeration units and increase the resource of heat engineering equipment. The presented results can be taken into account during the modernization of technological lines of the chemical industry.

The second section is devoted to the analysis of the operational reliability of transport systems based on large sets of statistical data. A methodology for detecting latent deviations and "repeated anomalies" that are not recorded by standard control means is proposed. An assessment of negative statistics and time trends is carried out, which allow to establish potential areas of infrastructure degradation. The feasibility of the transition from reactive maintenance to preventive management is substantiated, when decisions are based not on the fact of failure, but on early signs of its occurrence. This approach creates the basis for the implementation of predictive diagnostics systems in transport.

The third section considers the issue of optimal regulation of azimuthal power plants of marine vessels. Based on parametric modeling, the influence of external disturbances and variable loads on the behavior of the ship complex was investigated. Adaptive controller structures were developed that ensure course stability, reduce energy consumption, and increase the accuracy of maneuvering operations. Criteria for selecting control laws for operating conditions where traditional PID methods lose their effectiveness were outlined. The results confirm the possibility of integrating new-type controllers into ship motion systems.

The fourth section is devoted to the architecture of autonomous microgrid-class electric power systems. The principles of coordination between generation, storage, and consumption of electricity using multi-agent subsystems are considered. Mechanisms for maintaining stability in the event of loss of connection to the centralized network are substantiated, and the issue of load balancing in abnormal modes is also considered. The presented models demonstrate the possibility of forming a flexible energy infrastructure capable of providing guaranteed power supply to technological equipment without involving dispatch control.

The fifth section presents approaches to predictive maintenance of metallurgical equipment using the example of the lining of induction crucible furnaces. The technology of 3D laser profiling is proposed for spatial reconstruction of the inner surface of the lining and determination of zones of marginal wear. Criteria for permissible deviation of geometry are established and a methodology for calculating the residual resource of the lining layer is developed. Practical results confirm that the transition to condition-based monitoring allows to reduce emergency downtime and economic losses associated with the destruction of working units.

The summarized results of the monograph can be used during the design, adjustment and operation of automation systems, energy facilities and industrial units. The presented methods create the basis for the development of integrated control systems in which mathematical modeling is combined with digital monitoring and preventive intervention. The materials of the publication constitute a scientific contribution to the development of engineering practice, focused on increasing technological reliability and optimizing the life cycle of technical systems.

CONTENTS

List of Tables x
List of Figures xi
Circle of readers and scope of application xii

Introduction 1

Chapter 1. Technological aspects of computer control of the secondary condensation complex in ammonia production under uncertainty 4
1.1 Features of operating conditions and formation of an array of experimental data for a secondary condensation technological complex 7
1.2 Identification of heat exchange and condensation-separation processes in the secondary condensation process complex 17
1.3 Synthesis of the hardware and technological design of the secondary condensation complex and determination of the general structure of its control system 20
1.4 Investigation of the patterns of influence of phlegm drainage intensity on the efficiency of the circulating gas cooling process in low-temperature evaporators 26
1.5 Technical structure of the computer-integrated system for optimal software Control 34
Conclusions 35
References 36

Chapter 2. Management of transport systems and processes based on a unified theory of self-organizing systems 39
2.1 Terminology and interpretation in the field of transport technologies, processes and systems ... 40
2.2 A method for detecting hidden statistical patterns in traffic management 43
2.3 The concept and key principles of the MDHSP 44
2.4 The essence of the idea and use of the MDHSP 51
2.4.1 Identification of the current state of the system based on the norm of its functioning .. 51
2.4.2 Substantiation/support of the management decision ≡Block D 56
2.5 System behavior norm 59
2.6 Integrated system control model based on norms and bottlenecks 66
Conclusions 73
References 74

Chapter 3. Improvement of the method of linear-quadratic control of azimuthal drivers of the combined propulsion complex 76

3.1 Determination of the motion model of a marine vehicle under conditions of incomplete information 79
3.2 Iterative adaptation of ship motion models in accordance with the algorithmization of the motion controller functioning 84
3.3 Iterative matching of the selected position point with the motion controller linearization function 88
3.4 Adaptation of defined state spaces according to the algorithmization of the controller operation 89
3.5 Structuring a linear quadratic regulator (LQR) as a linearization object 92
3.6 Physical modeling of a marine-based vehicle 95
3.7 Simulation studies of the change in the yaw speed based on the defined state space 97
Conclusions 113
References 113

Chapter 4. Intelligentization of control systems for local electric power systems 118
4.1 Conditions for balancing power and electricity in the LES 119
4.2 Reducing imbalances between predicted and actual RES generation through a combination of methods 126
4.3 Formation of an intellectual control system for the LES mode as part of the electric power system 132
4.3.1 LES as an object of an intelligent control system 132
4.3.2 Intelligent control system of the LES mode 135
4.4 Local electric power system formed from microgrid 137
4.5 Increasing the efficiency of electrical networks through their intellectualization 140
Conclusions 143
References 144

Chapter 5. Improving condition monitoring and maintenance framework for refractory linings in induction melting furnaces through continuous improvement methods 147
5.1 Technical background and methods for improving lining durability 150
5.2 Methods for improving the durability of refractory linings 153
5.3 Methods for monitoring the condition of refractory linings 154
5.4 Heuristic methods application 155
5.4.1 Method of control questions (MCQ) 156
5.4.2 Focal objects method (FOM) 158
5.4.3 Algorithm for solving inventive problems (ASIP) 159
5.5 Functional value analysis 164
Conclusions 167
References 168

LIST OF TABLES

1.1 Experimental data on the operating modes of the condensation column 15
1.2 Experimental data on the operating modes of the primary condensation unit and the ARU evaporator 16
1.3 Generalised indicators of the quality of the information obtained 17
1.4 Results of calculations of the actual heat transfer coefficient of the condensation column based on experimental data 18
1.5 Results of calculations of the efficiency indicators of the heat exchange process of the condensation column according to the design and actual thermal resistance 18
1.6 Efficiency indicators of the heat exchange process of the ARU evaporator according to experimental data 19
1.7 Main target indicators of the condensation column operating modes based on the results of mathematical modelling 20
1.8 Calculated indicators of the evaporator operating modes ARU 29
2.1 Structure of the control parameter systematization database (DB) 57
2.2 Filling in the refined database 58
3.1 Parameters of the SBV model and thrusters 112
5.1 Specifications of EGES induction furnaces (Turkey) with crucible capacities of 1 tonne and 3 tonnes 152
5.2 Systematization of methods for improving the durability of refractory linings in induction steelmaking furnaces 153
5.3 Methods for monitoring the condition of refractory linings in induction steelmaking furnaces 155
5.4 Application of ASIP to the use of a laser system for determining the lining thickness of an induction steelmaking furnace 161
5.5 Numbers and names of inventive principles and proposed solutions 162
5.6 Main stages of FVA in evaluating the effectiveness of materials for repairing the lining of an induction crucible furnace 164
5.7 Distribution of repair material functions for furnace lining (as per item 1 in Table 5.6) according to the ABC principle for the target objective of extending the inter-repair period 165
5.8 Calculation of cost coefficients for constituent materials used to repair an induction crucible furnace 166

LIST OF FIGURES

1.1 Process diagram of the secondary condensation complex with the main parameter control points using the TDC-3000 information and control complex: CC1 — circulation compressor; CC2 — condensation column; VP1, VP2 — evaporator; ARU1, ARU2 — absorption refrigeration unit; TRU — turbo compressor refrigeration unit; EM — electric motor 9

1.2 Dependence of individual indicators of heat exchange efficiency in the condensation column and cooling capacity of refrigeration systems on the cooling temperature of the circulating gas in the evaporators for the initial data of mode No. 5 in Table 1.1 21

1.3 Effect of circulation gas temperature at the inlet of the condensation column 22

1.4 Influence of the heat exchange surface of the additional heat exchanger *FD* on the distribution of temperatures at the outlets of the circulating gas at its maximum thermal load at the inlet temperature Θ_{MTP}^{IN} = 45°C 22

1.5 Equipment and technological design of a secondary condensation complex with increased energy efficiency: CC — condensation column; CG — circulation gas; ABC — nitrogen-hydrogen mixture; ARU — absorption refrigeration unit; SEU — steam ejector refrigeration unit; HTE and LTE — high-temperature and low-temperature evaporators, respectively; AH — additional heat exchanger 23

1.6 Generalised structure of an adaptive system for optimising the operating mode of a control object 25

1.7 Generalised block diagram of the evaporator research algorithm 28

1.8 Dependence of the efficiency indicators of the ARU evaporator on the change in pressure P_{MTP} (---- — P_{MTP} = 0.29 MPa; - - - - — P_{MTP} = 0.3 MPa) and the control action of the phlegm flow rate M_F: *a* — phlegm concentration ξ_{Φ}, refrigerant boiling temperature in the intertube space Φ_{MTP}, refrigerant vapour flow rate at the evaporator outlet cooling temperature CG Φ_{2C}; *b* — cooling capacity Φ_0, heat transfer coefficient *K*, effective heat exchange surface F_X, mean logarithmic temperature difference $\Delta\Phi^{CP}$ 30

1.9 Dependence of the cooling temperature Φ_{2C} and the cooling capacity Φ_0 of the ARU on the control action of the phlegm flow M_Φ at different values of the refrigerant concentration ξ_X^{IN} at the evaporator inlet 31

1.10 Dependence of the cooling temperature of the central heating system Φ_{2C} and the cooling capacity of the ARU Φ_0 on the control action of the phlegm flow rate M_Φ at different refrigerant flow rate M_X^{IN} at the evaporator inlet 32

1.11 Dependence of the cooling temperature of the central heating system Φ_{2C} and the cooling capacity of the automatic control system Φ_0 on the control action of the phlegm flow rate M_Φ at different values of ammonia concentration in the central heating system Θ_{2C} at the evaporator inlet 32

1.12 Generalised technical structure of the automated system for optimal software control of the ARU evaporator 34

2.1 The set of scientific directions that form the theoretical basis of the MDHSP 44
2.2 The first sign of a bottleneck – "outlier" 46
2.3 The second sign of a bottleneck – "negative trend" – is marked with a red line for four observation time periods 47
2.4 Uniform manifestation of components of the control parameter classifier 47
2.5 Systematization of failure statistics cases 48
2.6 Interaction of cause-and-effect classifiers for transport events 50
2.7 System control based on the norm as a functional optimum 52
2.8 Methodology for substantiating a management decision based on the bottleneck principle 56
2.9 Determination of the probability of the system's activity states and the residence time 62
2.10 Change in the parameters of the normal distribution of the control parameter depending on the state of the system: *a* – regularity of change in the probability density of the current statistics of the control parameter (PR); *b* – dependence of the PR variation on the state 63
2.11 Change of the distribution center according to the increase in tension in the system activity 65
2.12 Shift of the location and width of the functional optimum zone 65
2.13 Integrated system control model based on the system behavior norm and the bottleneck principle 66
2.14 Formation of current statistics of the system status control parameter over time 67
2.15 Functional diagram of block 4 "Determination of significant prerequisites" 72
3.1 Appearance of the AT physical model located in the stern of the physical model of the multifunctional propulsion complex with a variable structure 78
3.2 Standard notation for describing the ship's motion according to (3.1) and (3.2) 80
3.3 Position and angle of rotation of motor *i* 82
3.4 Representation of feedback and reference gain of the system 93
3.5 Gearbox connecting the ECM to the AT screw 95
3.6 Physical model of the thruster with two degrees of freedom: 1 — ECM power cable and the cable of the drive of changing the angle of inclination; 2 — driving gear of the baller rotation drive; 3 — baller; 4 — bearing shield; 5 — feedback spring of the drive of changing the angle of inclination; 6 — power cable; 7 — support bearing; 8 — gland entries; 9 — cable of the drive of changing the angle of inclination; 10 — stabilizing wings; 11 — GFK; 12 — luminescent tag for remote measurement of the frequency of GFK rotation; 13 — connection point of the baller with the AT body; 14 — AT body with the AT ECM located in the middle 96
3.7 Block diagram of the AT ECM closed-loop torque control system: Ψ_p and Ψ_{calc} — the values of the set and calculated fluxes, I_{sa}, I_{sb} — the measured values of the stator currents 97
3.8 Block diagram of the ECM speed controller 97
3.9 Transient characteristic of zero angle linearization 98
3.10 Input signals of zero angle linearization: *a* — rotation speed; *b* — angle α 99

3.11 Linearization at zero angle: *a* — speed; *b* — drift speed 100
3.12 Transient response with non-zero angle α 101
3.13 Input signals with non-zero angle α: *a* — propeller rotation frequency; *b* — angle α 102
3.14 Dependences of speeds with non-zero angle α: *a* — speed of movement; *b* — drift speed 103
3.15 Differential input signals at a given zero angle α 104
3.16 Differential transient response for zero angle α 105
3.17 Differential speeds at zero angle α: *a* — longitudinal motion; *b* — drift 105
3.18 Differential speeds of rotation of the APU at zero angle α 106
3.19 Differential transient response with non-zero angle α 107
3.20 Differential speeds at a non-zero angle α: *a* — longitudinal motion; *b* — drift 108
3.21 Differential rotational speeds with a non-zero angle 108
3.22 Differential input signals at a given non-zero angle α 109
3.23 Position and angle of rotation of motor *i* 109
3.24 Setting step characteristic limits 110
3.25 Limit settings: *a* — longitudinal acceleration; *b* — drift acceleration 111
3.26 Rotation speed limit settings 111
3.27 Angle α limit settings 112
4.1 Electricity balancing in a balancing group (local electrical system) 121
4.2 Structural diagram of the automation of the forecasting process for wind power plants as part of a balancing group 123
4.3 Structure of the AREGFS full-scale simulation test system 125
4.4 Combination of different methods to reduce imbalance 127
4.5 Correction of the forecast graph for: *a* — PVPP; *b* — WPP generation 128
4.6 Example of adjusting PVPP generation based on error control results δ 129
4.7 Daily electricity consumption graphs in LES 130
4.8 Local electric power system as part of the EES 134
4.9 Examples of coverage of the daily electricity consumption schedule of a LES 135
4.10 Hierarchical structure of the intelligent LES system 136
4.11 LES of the MHP complex: *a* – 110/35/10 kV substations; *b* – biogas production complex 138
4.12 10 kV LES with microgrid based on photovoltaic modules and energy storage system 139
4.13 Local electrical system formed from microgrid 139
4.14 Fragment of the scheme of Vinkivtsi DEN 140
4.15 Structural diagram of Vinkivtsi LES 141
4.16 Structure of losses in electrical networks of the Vinkivtsi substation 142
4.17 Loss structure at the Vinkivtsi substation in transformers and 10 kV power transmission lines 142
4.18 Structure of losses in the electrical networks of the Vinkivtsi substation in the mode with a PVPP 142
4.19 Loss structure at the Vinkivtsi substation in the mode with a PVPP 143
5.1 View of a typical coreless induction crucible furnace (modified by the author based on an open-source illustration from KEMA educational resource): *a* — schematic; *b* — general 149

5.2 Melting in a 3-tonne induction furnace produced by EGES (Turkey): *a* – overall appearance of the unit; *b* – the crucible is enclosed to minimize heat loss and limit the escape of metal vapors into the work area; *c* – the interior of the furnace visible after tapping 151
5.3 Steel casting using a 3-tonne induction melting furnace from EGES (Turkey): *a* – pouring molten metal from the furnace into a ladle; *b* – skimming slag from the surface of the melt; *c* – filling molds during the casting stage 151
5.4 Relining of a 3-tonne capacity induction furnace (produced by EGES, Turkey): *a* – inductor workspace prepared for lining; *b* – meconite being readied for application to the furnace lining; *c* – lining the furnace bottom; *d* – placing the furnace lining machine inside the unit using a crane; *e* – charging the furnace for the sintering stage 152
5.5 Improvement of the system for monitoring the residual refractory lining thickness using the focal objects method: analysis of the properties of randomly selected objects 158
5.6 Procedure for solving an inventive problem using G. S. Altshuller's matrix (ASIP) 160
5.7 Formulation of the technical contradiction using the "If – Then – But" formula when applying a laser system for measuring the thickness (3D scanning of the condition) of the refractory lining 160
5.8 Functional-value diagram for the repair of an induction crucible furnace 166

CIRCLE OF READERS AND SCOPE OF APPLICATION

The monograph is intended for scientists, teachers, postgraduate students and researchers working in the field of modeling, optimization and digital control of technical systems. It can also be useful for practicing engineers involved in the design, operation and modernization of industrial equipment, in particular in the chemical production, energy, transport and metallurgy industries. The publication considers engineering activities not as a static discipline, but as a process of continuous development, in which technological innovations are combined with analytical thinking and responsibility for the quality of technical solutions.

INTRODUCTION

Modern industrial engineering is in a state of deep renewal. Processes are understood as heat exchange, energy, transport and production cycles, for which models of states and flows are built, operating ranges are determined and requirements for stability and productivity are formulated. Production systems are transformed under the influence of digital technologies, increased requirements for energy efficiency and the need to maintain continuous reliability of equipment in changing conditions. If earlier the creation of an automated system was perceived as a completed stage after its launch, now each technical object requires constant adaptation, re-verification and refinement of models. In such conditions, the combination of classical physical and mathematical approaches with methods of digital monitoring, data analysis and adaptive control becomes the basis of engineering thinking focused on practical results. This monograph forms a systemic vision of current scientific and applied tasks in the field of complex process control, covering heat and energy chains of chemical production, operational analytics of transport infrastructure, motion control tasks in marine engineering, architecture of local electrical networks and digital monitoring of high-temperature equipment.

The subject of the research is methods of modeling, identification and optimal control under conditions of operational uncertainty. Special attention is paid to the synthesis of structures and control laws taking into account technological constraints, the synthesis of measuring and diagnostic circuits to ensure state observability, as well as the synthesis of quality criteria in multi-criteria parameter tuning. The practical goal is to create approaches that allow moving from declarative concepts to engineering solutions compatible with the existing infrastructure of enterprises and technical safety regulations. To do this, models are developed that can reproduce the real dynamics of units based on field data, parameters are refined based on the results of experimental identification, numerical optimization methods are used to select modes, adaptive control algorithms are formed that correct the effects in the event of changes in external and internal conditions. This combination ensures a reduction in operating costs, increased energy efficiency and a reduction in the risk of emergency shutdowns, while maintaining technological discipline and compliance with standards.

Particular attention is paid to modeling heat and mass exchange processes and their identification under real modes. The passport characteristics of heat exchangers often differ from the actual values of heat transfer coefficients, therefore, checking assumptions, calibrating models and re-verification are mandatory stages of constructing correct calculations. Refined descriptions make it possible to identify critical sections of the circuit, assess the impact of local deviations on the energy balance, and propose control schemes that combine the use of available resources with a reduction in the load on refrigeration units. The effect of such solutions is manifested in the reduction of temperature differences, stabilization of operating points, and extension of the equipment life without major reconstruction.

Operational data analytics is considered as a mechanism for increasing reliability and safety. Arrays of registration data generated at the unit and infrastructure levels contain latent patterns that are not detected by traditional control approaches.

The combination of statistical analysis, time trend detection, and work with negative statistics allows to create early warning indicators and move from reactive to preventive maintenance. This makes it possible to identify risk concentration points in advance, coordinate intervention schedules with the real technical condition, avoid irrational downtime, and increase the overall availability of systems. Motion control tasks in a changing environment require a combination of rigorous theoretical principles with testing on model and full-scale installations. Parametric modeling, stability assessment, and the use of optimal regulation ensure the formation of control laws that maintain accuracy and reliability under disturbances. For ship power plants, this means increased maneuverability, reduced energy consumption, and reduced load on nodes in conditions of variable hydro- and aerodynamics. Practical integration of such algorithms requires clear quality criteria, verification of sensitivity to parametric uncertainty and a regulated tuning procedure.

The development of local electrical networks and distributed energy makes the issue of the architecture of coordination of generation, storage and consumption relevant. Hierarchical control models and multi-agent approaches provide tools for load balancing, maintaining electricity quality and ensuring autonomous modes in case of disruption of communication with the centralized network. Integration of renewable sources and local storage requires synchronization mechanisms, forecasting of consumption and production profiles, as well as algorithms for prioritizing critical consumers. Such solutions increase the stability of technological processes and make it possible to plan work taking into account fluctuations in external power supply.

Digital monitoring of high-temperature equipment transfers maintenance from calendar intervals to state-oriented logic. Three-dimensional profiling of working surfaces, reconstruction of wear geometry and quantitative assessment of deformations allow building criteria for residual resource, coordinating intervention schedules with the real state of the nodes, minimizing emergency stops and reducing costs. The advantage is the possibility of implementing such monitoring in stages, with adaptation to existing technological procedures and quality control tools.

The methodological basis of the monograph is based on the synthesis of modeling, numerical optimization, statistical analytics and practical validation. The developed approaches form a closed loop from measurements to decision-making. Within a single loop from measurements to decisions, modeling of states and disturbances, synthesis of structures and control laws, as well as optimization of modes taking into account efficiency criteria and safety restrictions are sequentially carried out. First, data collection and cleaning are carried out, then parameter identification and model construction, then optimization of modes and formation of control algorithms, after which testing and correction of solutions taking into account feedback. This logic allows to adapt the results to the constraints of the production environment and maintain the reproducibility of effects when external conditions change.

Along with the advantages, implementation barriers are also recognized. These include limited funding, heterogeneity of the equipment fleet, uneven digital readiness of personnel, the need to harmonize with current safety and health standards, issues of cyber security and maintaining data integrity. Practical steps to overcome these barriers include phased pilot implementations at selected sites, training of engineering and technical personnel, integration of new methods into existing production management

systems, as well as the creation of procedures for quality control of modeling and verification of results. Such a pragmatic approach increases confidence in the proposed solutions and reduces the time to obtain a measurable effect.

The practical significance of the presented developments lies in the possibility of their phased integration into production processes without radical reconstruction. The proposed tools allow to form technical tasks for modernization, configure modes taking into account the real dynamics of processes, implement condition monitoring systems and build a maintenance policy that is consistent with the actual resource of elements. The materials of the monograph can be used as a methodological basis for engineers and operation specialists who are responsible for the reliability and economic efficiency of production.

The content of the subsequent sections specifies the above principles at the level of models, algorithms and applied results. Identification and tuning methods, examples of validation on real data, justification of the choice of parameters and quality criteria, as well as recommendations for phased implementation in industrial conditions are presented. The proposed approach harmonizes processes and control systems through a combination of synthesis, modeling and optimization, which corresponds to the stated problems of the monograph.

DOI: 10.15587/978-617-8360-19-1.CH1

Anatolii Babichenko, Igor Krasnikov, Juliya Babichenko,
Oleksandr Dzevochko, Yana Kravchenko, Ihor Lysachenko

CHAPTER 1

TECHNOLOGICAL ASPECTS OF COMPUTER CONTROL OF THE SECONDARY CONDENSATION COMPLEX IN AMMONIA PRODUCTION UNDER UNCERTAINTY

ABSTRACT

The object of the study is the technological complex of secondary condensation of large-tonnage ammonia synthesis units of the AM-1360 series, which provides final cooling and separation of condensed production ammonia from circulating gas. The possibility of increasing the energy efficiency of production by modernising the equipment and technological design of the TCC has been established. This is achieved by removing the energy-intensive turbocompressor refrigeration unit (TRU) with electric drive from the circuit and creating an adaptive system of optimal software control.

The feasibility of applying a systematic approach to solving such a complex problem, based on mathematical modelling and process identification, has been demonstrated. The operating conditions of the TCSC and the primary condensation unit have been analysed. The results of the research have established uncertainties in the functioning of such components as the condensation column (CC) and low-temperature evaporators (LTE), which are connected to the operating circuit of two absorption refrigeration units (ARU) and TRU.

Algorithms have been developed for forming an information array of experimental data and numerical assessment of uncertainties, in particular heat transfer coefficients in the CC and LTE, as well as ammonia concentration at the outlet of the primary condensation unit and CC. The algorithms provide for the separation of transient modes in the operation of the TCSC, verification of stationarity, reproducibility of the process and the hypothesis of normality of empirical distribution, which determines the possibility of using a stochastic approximation method for numerical estimation of uncertainties.

Based on the results of processing the experimental data, a discrepancy between the actual and design heat transfer coefficients was established, which is due to an underestimation of the condensation thermal resistance. The heat exchange processes in the CC and LTE as part of the ARU were identified, and equations were obtained for determining the heat transfer coefficients, heat transfer, condensation thermal resistance, and ammonia concentration in the CG at the CC inlet and outlet.

Mathematical modelling was used to determine the conditions for the necessary temperature distribution in the TCSC to exclude the TRU from the circuit and reduce the cooling temperature of the CG in the LTE by 5°C compared to the initial version at maximum heat load from the CG at the inlet of the complex. The developed TCSC scheme is characterised by greater energy efficiency due to the use of only heat-utilising

refrigeration systems of the ARU and steam ejector units (SEU), which utilise the heat of material flows with both low temperature potential (up to 150°C) and ultra-low (up to 90°C).

Using mathematical modelling of LTE, a pattern of extreme dependence of cooling capacity and cooling temperature of the central heating system on the phlegm flow rate has been established. Achieving maximum cooling capacity, and therefore minimum cooling temperature of the central heating system at a certain temperature head, is determined by the critical regime of bubble boiling of the refrigerant. The dependencies of the cooling temperature of the central heating system on the control action of the phlegm flow rate have been determined, which characterise the shift of the extreme under conditions of changing values of the disturbance vector coordinates, and, consequently, the change in the energy efficiency indicators of ammonia production (annual natural gas consumption).

Algorithmic support has been developed to solve the problems of identification, obtaining a mathematical model of the LTE evaporator and numerical estimation of the optimal state vector (cooling temperature of the central heating system). The use of the algorithm implemented in the MATLAB package provides a solution to the optimisation problem in real time using a step-type non-gradient method with the application of one-dimensional extremum search methods. The technical structure of a computer-integrated system for optimal software control of the temperature regime of a low-temperature evaporator, adapted to the existing information system of an industrial synthesis unit, has been determined.

KEYWORDS

Ammonia production, secondary condensation, mathematical modelling of heat transfer processes, computer-integrated technology, optimal software control.

Synthetic ammonia is the most important product of the chemical industry. The continuous increase in the production of this product is due to the need to increase crop yields by applying nitrogen-containing mineral fertilisers to the soil. This need, in turn, is linked to the expected growth of the world population to almost 9.6 billion by 2050 [1]. Considering the latter and the availability of large amounts of arable land, ammonia and fertilisers will always be strategic commodities for Ukraine, determining the economic security of the state. At the same time, the main raw material in ammonia production technology is and will remain natural gas in the coming decades, which, compared to heavy oil and coal as raw materials, reduces energy costs by 1.3 and 1.7 times, respectively [2].

Modern ammonia synthesis units are complex energy-technological complexes with a large number of interconnected departments. Despite the diversity of equipment and technology, catalysts and equipment used to implement the processes, they are built in almost all countries according to the unified ideology of Kellogg Braun & Root (USA). The synthesis unit is based on the traditional Haber-Bosch closed circulation scheme with a two-stage system for condensing production ammonia from circulation gas [3].

The nitrogen industry in Ukraine is based on medium-pressure synthesis units with a capacity of 1,360 tons per day (AM-1360 series), which are significantly inferior in terms of energy consumption to

technologies from such world-renowned manufacturers as Haldor Topsoe (Denmark), Imperial Chemical Industries (UK), and Kellogg Braun & Root (USA), by almost 25% [4], and more than twice as much in terms of electricity consumption. At the same time, the efficiency of the units of leading manufacturers is largely achieved by the use of secondary condensation (TCSC) in the technological complex to drive turbo compressor cooling systems with medium pressure water vapor extraction (4 MPa), which is obtained by utilizing high-potential heat at the reforming stages and conducting ammonia synthesis at a lower pressure of up to 15 MPa [5]. The use of such technology directly in units operating in Ukraine is impossible due to the higher synthesis pressure (over 20 MPa). In such circumstances, there is not enough steam to drive the compressor systems. The insufficient amount of steam is obtained in an additional steam boiler, which significantly reduces the efficiency of domestic units. Therefore, in AM-1360 series synthesis units, a turbo compressor refrigeration unit (TRU) is used in addition to two low-temperature evaporators (LTE), along with two heat-using absorption refrigeration units (ARU), a turbo compressor refrigeration unit (TRU) with an electric drive is also used, the share of electricity of which is up to 40% of the total consumption of the entire production.

The simplest option for improving production efficiency would be to use a third ARU instead of a TRU. However, this is impossible due to the lack of units from both domestic and leading manufacturers that utilize waste heat streams with temperatures above 1000°C, which are necessary for the operation of the ARU by supplying heat to its generator-rectifier. In such circumstances, an alternative to ARU and TRU could be steam ejector refrigeration units (SEU), which, when using a refrigerant (ammonia) with a low boiling point, allow the utilization of heat from material flows with temperatures even below 900°C. However, today, in all synthesis units without exception, this heat is not utilized and is discharged into the environment through air cooling devices [6].

SEUs, compared to ARUs and TRUs, are characterized by lower thermodynamic efficiency. It can be increased by increasing the pressure and boiling point of the refrigerant in the evaporator [7]. However, recommendations on the possibility of using SEUs in chemical production, in particular ammonia, are practically absent in the literature. Therefore, this work focuses on research into the possibility of using SEUs for cooling the central gas in the general scheme of the AM-1360 series TCSC unit, the results of which can be applied to improve the technological design of cooling systems for synthesis units of various leading manufacturers in order to increase their energy efficiency by replacing complex and powerful steam-driven turbo compressor refrigeration systems. At the same time, the 4 MPa pressure water vapor from these units can be used to generate electricity, which will further increase their energy efficiency.

A characteristic feature of the TCSC is the presence of a condensation column. In this case, the direct flow of the heat transfer fluid at the inlet of the condensation column (CC) goes through the intertube space to two evaporators of the high-pressure system. The return flow of the heat transfer fluid from these high-pressure systems is directed to the separation part of the CC, and then to its tube space. This flow direction ensures the regeneration of "cold" and the separation of condensed ammonia from the refrigerant, to which a fresh nitrogen-hydrogen mixture (NHM) is supplied through the condensate layer. The operation of the TCSC due to the use of air cooling in the complex of primary condensation and refrigerant condensation in the ARU leads to constant seasonal and daily changes in the heat load on the evaporators, and therefore

is characterized by instability. All this causes fluctuations in the cooling temperature of the central heating system (secondary condensation) within a fairly wide range from –80°C to 50°C and causes not only parametric uncertainty in the operation of the facility, but also, due to the large tonnage of production, leads to significant economic losses. According to research, an increase in this temperature by even 10°C leads to a decrease in the energy efficiency of production due to an increase in annual natural gas consumption by 307.3 thousand nm^3 [8]. Therefore, minimizing the secondary condensation temperature by removing the TRU from the TCSC operation scheme through the creation of a high-quality control system under external disturbances is a pressing issue in the overall process of improving the energy efficiency of ammonia production.

The most effective way to solve such a complex task is to apply a systematic approach, one of the main components of which is systemic-structural and systemic-control [9]. The first is aimed at identifying the optimal structure of the technological system, and the second is aimed at studying its functioning and creating an adaptive system of optimal software control under the influence of external and internal disturbances. The scientific basis for this approach to final decision-making on this complex task is mathematical modeling and process identification [10]. Therefore, based on a systematic approach and using the example of TCSC, this paper presents some of the results of the authors' research, focusing on: the specifics of operating conditions, the formation of information arrays of experimental data and parametric identification of non-stationary static objects; mathematical modeling of multidimensional objects with uncertainties; synthesis of an energy-efficient structure of a technological complex using heat-using refrigeration units and an adaptive system of optimal software control based on the estimation of state coordinates.

1.1 FEATURES OF OPERATING CONDITIONS AND FORMATION OF AN ARRAY OF EXPERIMENTAL DATA FOR A SECONDARY CONDENSATION TECHNOLOGICAL COMPLEX

The operation of the TCSC technological equipment takes place under conditions of seasonal and daily changes in thermal load, which is caused by the use of air-cooling devices and a separator in the previous primary condensation unit. Under such circumstances, the temperature and pressure of primary condensation are subject to random changes, which, as is known, determine the concentration at the outlet of this unit. At the same time, the temperature of the central heating system and the concentration of ammonia in the central heating system at the inlet of the complex vary in the ranges of 35–45°C and 9–12% vol., respectively, and, consequently, at the inlet of the evaporators. An increase in this concentration not only increases the heat load, but also reduces the heat transfer coefficient due to the formation of additional condensation thermal resistance [11]. In addition, to determine the heat flows in the condensation column, it is necessary to know the concentration of ammonia in the CG at the outlet of its pipe space [12]. The value of this concentration is determined by the efficiency of the separation process, the calculation of which cannot be performed using analytical methods and depends on many uncontrollable factors. This also causes uncertainty in this concentration. A numerical assessment of these uncertainties for such linear technological objects is most often performed using the stochastic approximation method [13, 14], which has been sufficiently tested in industrial conditions.

The simplest way to eliminate these uncertainties would be to use an automatic analyser. However, the conditions of measurement, namely the presence of ammonia in the form of a vapour-liquid mixture and excessively high pressure in the central heating system, prevent the use of this method. In this regard, it is no coincidence that on existing synthesis units, the measurement of ammonia concentration in the central heating system is carried out using laboratory analyses, which are performed periodically, only once a day. Under such conditions and existing daily fluctuations in atmospheric air temperature, this method leads to complete uncertainty in the concentration of ammonia in the CG at certain periods. This complicates the real-time identification of heat exchange processes in the mathematical model of both the LTE and the CC. Thus, the task of identifying the processes of the mathematical model is complicated by the presence of interrelated uncertainties in the concentration of ammonia and the heat transfer coefficient, the solution of which is of particular importance in the process of obtaining mathematical models of LTE and CC. However, information on the numerical assessment of interrelated uncertainties is not sufficiently covered in the literature [15] and requires the development of a separate research algorithm for its application in the creation of an adequate mathematical model.

The significant metal intensity of the technological equipment and the complexity of the technological design of the TCSC contribute to the excessive inertia of heat exchange processes. This is especially true for the CC, whose total mass is almost 300 tonnes and is characterised by feedback on the CG flow. Therefore, under certain conditions, a situation may arise that makes it impossible to adapt the parameter to its actual value. In such circumstances, the identification of non-stationary static technological objects for the purpose of numerical estimation of the heat transfer coefficient requires the creation of an algorithmic basis for separating transient modes.

Thus, the established relationship between the uncertainties of the heat transfer coefficient, the concentration of ammonia in the heat carrier at the inlet and outlet of the column, and the numerical evaluation of uncertainties under existing conditions are of particular importance in the overall process of creating an automated system for the operational generation of a mathematical model of the evaporator and condensation column.

The formation of an array of experimental data on the elimination of transient modes of operation of the TCSC industrial synthesis unit of the AM-1360 series was carried out using the TDC-3000 microprocessor information and control complex from Honeywell and, in part, laboratory analyses of ammonia concentrations in the central gas. The method for determining the concentration is based on the absorption of ammonia by water, followed by titration of the ammonia water with sulphuric acid. The concentration of ammonia was determined by the amount of acid used to titrate the ammonia water. A generalised diagram of the TCSC with the main parameter control points according to the technological regulations is shown in **Fig. 1.1**.

Samples for laboratory analysis to determine the composition of the CG (ammonia, argon, methane, nitrogen, hydrogen) at the inlet and outlet of the CC were taken once per shift (8 hours). Therefore, the frequency of collection of all other data on the parameters of the TCSC operation was also once per shift. The analyses were performed using a NeoCHROM (Ukraine) industrial chromatograph, and the ammonia content in the CG was determined analytically using a standard method in the workshop laboratory.

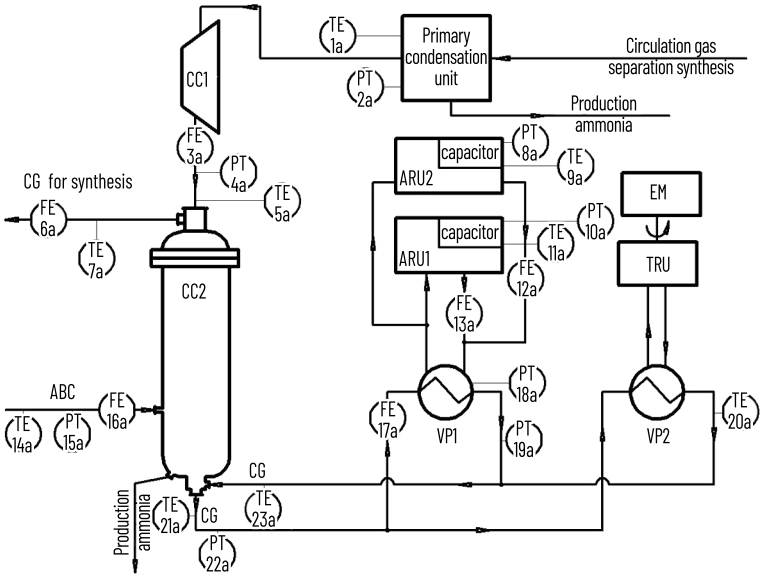

Fig. 1.1 Process diagram of the secondary condensation complex with the main parameter control points using the TDC-3000 information and control complex: CC1 — circulation compressor; CC2 — condensation column; VP1, VP2 — evaporator; ARU1, ARU2 — absorption refrigeration unit; TRU — turbo compressor refrigeration unit; EM — electric motor

In the process of developing the algorithm for forming the information array, equations of the mathematical description of the condensation column [16] were used, which, unlike the well-known ones, take into account both the condensation of ammonia in the intertube space and its evaporation in the tube space. The algorithm contains two convergence cycles. The first forms modes that ensure the convergence of heat flows due to heat exchange in the separation part due to heat exchange between the CG, the liquid ammonia layer and the NHM in order to determine the temperature of the CG at the inlet of the pipe space of the condensation column. The second cycle ensures the final formation of data on the input and output variables of the object under conditions of convergence of heat flows from the pipe and inter-pipe space of the heat exchange part of the condensation column. The algorithm includes the following main functional blocks [17]:

Block 1. Calling the task for solution after a specified period of time or at the operator's command.

Block 2. Opening the FORM file that serves this task.

Block 3. Subroutine for reading the necessary information from the DANI file, which stores information about the input and output variables and design characteristics of the object, obtained from the TDC-3000 information and control complex.

Blocks 4 and 5. Setting the initial temperature approximation $\Theta_{TP}^{C} = \Theta_{TP}^{B}$ with an approximation step of 0.001°C to determine the heat flows V_{ABC} (W) and V'_{ABC} (W) from NHM to the liquid ammonia layer and the heat source according to the equations:

$$\Phi_{ABC} = M_{ABC} C_{ABC} (\Theta_{ABC}^{C} - \Theta_{TP}^{C}); \tag{1.1}$$

$$\Phi'_{ABC} = \Phi_{MTP}^{C} + \Phi_{B}^{C}; \tag{1.2}$$

$$\Phi_{MTP}^{C} = M_{MTP}^{C} C_{MTP}^{C} (\Theta_{TP}^{C} - \Theta_{TP}^{B}) + M_{B}^{C} r^{C} + M_{G}^{Caver} C_{G}^{C} (\Theta_{TP}^{C} - \Theta_{TP}^{B}); \tag{1.3}$$

$$\Phi_{B}^{C} = G_{B}^{C} r^{C}; \tag{1.4}$$

$$G_{B}^{C} = V_{ABC} \frac{a_{NH_3}^{C} 0.771}{100 - a_{NH_3}^{C}}, \tag{1.5}$$

where Φ_{ABC}, Φ_{B}^{C}, Φ_{MTP}^{C} – amount of heat transferred to NHM, evaporation due to heat exchange in the liquid ammonia layer and heating of the central heating system; C_{ABC}, C_{MTP}^{C}, C_{G}^{C} – average heat capacities of NHM, the gas phase of the central heating system and liquid ammonia in the central heating system flow from the evaporator, kJ/(kg °C); M_{ABC}, M_{MTP}^{C}, M_{B}^{C}, M_{G}^{Caver}, G_{B}^{C} – mass flow rates of NHM, evaporated ammonia in the CG stream, liquid ammonia in the CG stream and evaporated ammonia due to heat exchange in the liquid ammonia layer, kg/s; V_{ABC} – volumetric flow rate of NHM, nm^3/s; Θ_{ABC}^{C}, Θ_{TP}^{C}, Θ_{TP}^{B} – temperatures of NHM at the column inlet, CG at the inlet of the column heat exchanger tube space, and CG at the evaporator outlet, °C; $a_{NH_3}^{C}$ – ammonia concentration in the CG stream at the column outlet, % vol.; r^{C} – ammonia vaporisation heat, kJ/kg.

Block 6. Evaluation of the convergence condition error $\delta = \left(\Phi_{ABC}^{1} - \Phi_{ABC}\right) < 3\%$ and transition to the second cycle if it is fulfilled.

Blocks 7 and 8. Determination of heat flows from the pipe side Φ_{TP}^{K} (W) and inter-pipe side Φ_{MTP}^{K} (W) of the heat exchanger space of the condensation column using the formulas:

$$\Phi_{TP}^{K} = M_{TP}^{G} C_{TP}^{C} (\Theta_{TP}^{K} - \Theta_{TP}^{C}) + M_{G}^{C} (i_{P}^{K} - i_{G}^{C}), \tag{1.6}$$

$$\Phi_{MTP}^{K} = M_{MTP}^{G} C_{MTP}^{C} (\Theta_{MTP}^{K} - \Theta_{MTP}^{B}) + M_{CK}^{K} r_{MTP} + (K_{G}^{K} - 0.5 M_{CK}^{K}) C_{G}^{C} (\Theta_{MTP}^{K} - \Theta_{MTP}^{B}), \tag{1.7}$$

where M_{TP}^{G}, M_{MTP}^{G} – gas phase flow rate of the central heating system, kg/s; M_{CK}^{K}, M_{G}^{K}, M_{G}^{C} – flow rates of condensed ammonia and liquid ammonia at the inlet between the intertube and tube space of the heat exchanger, kg/s; i_{P}^{K}, i_{G}^{C} – enthalpy of vapour and liquid ammonia at the inlet and outlet of the tube space of the heat exchanger, kJ/kg; C_{G}^{C}, C_{MTP}^{C}, C_{TP}^{G} – average heat capacities of liquid ammonia in the intertube space, gas phases of the intertube and tube space of the heat exchanger, kJ/(kg °C); r_{MTP} – heat of condensation of ammonia, kJ/kg; Θ_{TP}^{K}, Θ_{MTP}^{K}, Θ_{MTP}^{B} – temperatures of the heat transfer medium at the outlet of the pipe space, at the inlet and outlet of the intertube space of the heat exchanger, °C.

Block 9. Evaluation of the convergence condition error $\delta_2 = \left(\Phi^K_{MTP} - \Phi^K_{TP}\right) < 5\%$, in which case the transition to the calculation of heat transfer coefficients is carried out.

Block 10. Calculation of heat flow Φ^K heat transfer coefficients using the formulas adopted in the design K^K_P and the actual coefficient K^K_E for the condensation column:

$$K^K_P = \frac{1}{\frac{1}{a_{MTP}} + R^P_T + \frac{1}{a_{TP}}}; \tag{1.8}$$

$$K^K_E = \frac{\Phi^K}{F\Delta\Theta_{CP}}; \tag{1.9}$$

$$a_{MTP} = 1.3A\varepsilon_f (W_{MTP})^{0.56} (d_{OUT})^{-0.44}; \tag{1.10}$$

$$a_{TP} = A(W_{TP})^{0.8} (d_{IN})^{-0.2}; \tag{1.11}$$

$$\Phi^K = 0.5\left(\Phi^K_{TP} + \Phi^K_{MTP}\right), \tag{1.12}$$

where a_{TP} – heat transfer coefficients from the pipe and inter-pipe space, W/(m^2/°C); R^P_T = 0.000354 – design thermal resistance coefficient, m^2·K/W; $\Delta\Theta_{CP}$ – average temperature difference, °C; F – heat transfer surface, m^2; W_{TP}, W_{MTP} – weight velocity of the coolant in the pipe and inter-pipe space per unit of surface, kg/(m^2·s); ε_f – correction coefficient for the angle of attack; d_{IN}, d_{OUT} – internal and external diameter of heat exchange pipes, m; A – coefficient that takes into account the thermophysical properties of the heat transfer medium.

Block 11. Calculation of heat flow Φ_0, heat transfer coefficients according to the formulas adopted in the design K^B_P and the actual coefficient K^B_E for the evaporator:

$$K^B_E = \frac{\Phi_0}{F \cdot \Delta\Theta_{CP}}; \tag{1.13}$$

$$\Phi_0 = M_G C^{CP}_G \left(\Theta_{1C} - \Theta_{2C}\right) + M_{KC} C^{CP}_K \left(\Theta_{1C} - \Theta_{2C}\right) + M_K r^{CP} + M^{OUT}_P C^{aver}_P \left(\Theta_{1C} - \Theta_{2C}\right); \tag{1.14}$$

$$M_K = 0.771 \cdot V_C \left(a^{PIN}_{NH_3} - a^{POUT}_{NH_3}\right); \tag{1.15}$$

$$K^B_P = \frac{1}{\frac{1}{a_{MTP}} + R^P_T + \frac{1}{a_{TP}}}; \tag{1.16}$$

$$a_{TP} = A \cdot W^{0.8}_{TP} \cdot d^{-0.2}_{IN}; \tag{1.17}$$

$$a_{MTP} = 2.2 \cdot q^{0.7}_F \cdot P^{0.21}_{MTP}; \tag{1.18}$$

$$A = 16.28 \cdot \left(\frac{\lambda_C}{\mu_C^{0.8}} \right) \cdot \left(\frac{Pr}{0.73} \right)^{0.4}, \quad (1.19)$$

where W_{TP} is the weight velocity of the coolant per unit surface area in the pipe space, kg/(m^2·s); d_{IN} is the internal diameter of the pipes, m; q_F is the specific heat flux, W/m^2; λ_C is the thermal conductivity of the coolant, W/(m·K); μ_C is the dynamic viscosity of the coolant, Pa·s; Pr is the Prandtl number; $R_T^P = 0.000356$ is thermal resistance coefficient, m^2·K/W; Φ_0 is heat flux (cooling capacity), W; F is evaporator heat transfer surface, m^2; Θ_{CP} is mean logarithmic temperature difference, °C; M_G, M_{KS}, M_K, M_P are mass flow rate of the gas phase of the refrigeration circuit, average ammonia condensate, condensed ammonia and ammonia vapour phase in the refrigeration circuit, kg/s; C_G^{CP}, C_K^{CP}, C_P^{CP} are average specific heat capacities of the gas phase of the central heating system, ammonia condensate and ammonia vapour, kJ/(kg·K); r_{CP} is average heat of condensation of ammonia, kJ/kg; Θ_{1C}, Θ_{2C} are temperature of the refrigerant at the evaporator inlet and outlet, °C; V_C is volumetric flow rate of the refrigerant, nm^3/s; $a_{NH_3}^{PIN}$, $a_{NH_3}^{POUT}$ are concentration of ammonia vapour in the refrigerant at the inlet and outlet, % vol.

Block 12. The discrepancy between the design and actual heat transfer efficiency indicators was assessed by the total thermal resistance R_E^T for the evaporator and condensation column using the formula

$$R_E^T = \frac{1}{K_E} - \left[\frac{1}{a_{MTP}} + \frac{1}{a_{TP}} \right]. \quad (1.20)$$

Block 13. Formation of an array of current STAB data of stable values of object quantities with respect to Φ_{ABC}, Φ^K, Φ_0, R_E^T, M_{KC}, M_{CK}, K_P, K_E and technological parameters, and printing of results.

Block 14. Closing the FORM file and exiting the task.

The developed algorithm structure allows forming a stable information array of current data and separating transient modes. This makes it possible to calculate the actual heat transfer coefficient and, consequently, the condensation thermal resistance.

The possibility of applying a probabilistic-statistical (stochastic) approach for numerical estimation of uncertainties requires, as is known, verification of a number of conditions [6, 18]. In order to implement such verification, algorithmic support has been developed for processing experimental data obtained at the previous stage of forming the information array. The algorithm ensures verification of the stationarity and reproducibility of the process, the hypothesis of the normality of the empirical distribution, and the approximation of ammonia concentrations in the central gas according to the functional dependence established in accordance with existing theoretical provisions. The algorithm includes the following functional blocks [19]:

Block 1. Calling the task to be solved after a specified period of time or at the operator's command.

Block 2. Open the STOCH program file that serves this task.

Block 3. Subroutine for reading the necessary information from the STAB file, which stores information about the input and output variables of the TCSC obtained in the process of forming the information array.

Block 4. For each independent variable, the number of series of experiments $i = 1 \div k$ is determined, into which the experimental data is divided, as well as the number of experimental data $j = 1 \div m$ in each series ($i = 4$, $j = 3$).

Blocks 5 and 6. Calculation of the Cochran criterion G_p to verify the reproducibility of the process, establishment of the tabulated value G_T with the number of degrees of freedom k, m and a significance level of 5% with verification of the reproducibility condition using the formulas:

$$G_p = \frac{max\left\{\sigma_i^2(a)\right\}}{S_a^2}; \tag{1.21}$$

$$S_a^2 = \sum_{i=1}^{k}\sigma_i^2(a); \tag{1.22}$$

$$\sigma_i^2(a) = \frac{1}{m-1}\sum_{j=1}^{m}\left(a^{ij} - \overline{a^i}\right)^2; \tag{1.23}$$

$$\overline{a^i} = \frac{1}{m}\sum_{j=1}^{m}a^{ij}; \tag{1.24}$$

$$G_P < G_T. \tag{1.25}$$

Block 7 and 8. Calculation of Fisher's criterion F_p to verify the stationarity of the process, establish a tabulated value for the number of degrees of freedom and a significance level of 5% with verification of the stationarity condition using the equations:

$$F_p = \sigma_\Sigma^2 / \sigma_0^2; \tag{1.26}$$

$$\sigma_0 = S_a^2 / k; \tag{1.27}$$

$$\sigma_\Sigma^2 = \frac{m}{k-1}\sum_{i=1}^{k}\left(\overline{a^i} - \overline{a^{ij}}\right); \tag{1.28}$$

$$\overline{a^{ij}} = \frac{1}{k}\sum_{i=1}^{k}\overline{a^i}; \tag{1.29}$$

$$F_P < F_T. \tag{1.30}$$

Block 9. Determination of sample asymmetry A and excess E, as well as theoretical dispersion of asymmetry $\sigma(A)$ and excess $\sigma(E)$ using the following formulas:

$$A = \frac{1}{N\cdot\sigma_a^3}\sum_{u=1}^{N}\left(a_u - \overline{a_u}\right)^3; \tag{1.31}$$

$$E = \frac{1}{N\cdot\sigma_a^4}\sum_{u=1}^{N}\left(a_u - \overline{a_u}\right)^4 - 3; \tag{1.32}$$

$$\sigma(A) = \frac{6(N-1)}{(N+1)(N+3)}; \tag{1.33}$$

$$\sigma(E) = \frac{24N(N-2)(N-3)}{(N+1)^2(N+3)(N+5)}, \tag{1.34}$$

where σ_a is the standard deviation of the output parameter relative to the mean.

Block 10. Verification of the hypothesis of normality of the empirical distribution, which is accepted if the following conditions are met:

$$|A| \le 3\sqrt{\sigma(A)}; \tag{1.35}$$

$$|E| \le 5\sqrt{\sigma(E)}. \tag{1.36}$$

Block 11. If the above conditions are met, close the STOCH file and exit the task.

Based on the results of processing the experimental data using the above algorithms, a sample of 100 TCSC operating modes was formed, some of which are presented in **Tables 1.1** and **1.2**.

As an example, **Table 1.3** presents selected results of the quality check of the obtained data set. Analysis of these results shows that the process in the selected time interval is sufficiently reproducible and stationary, and the empirical distribution practically corresponds to the normal law.

The developed algorithm structure allows switching to Statistica or MATLAB (Optimisation Toolbox) packages to perform correlation and regression analysis and determine functional dependencies for numerical estimates of ammonia concentrations in the central gas at the outlet of the primary condensation unit (inlet to the condenser) $a^{IN}_{NH_3}$ and at the outlet of the pipe space of the condensation column $a^{TP}_{NH_3}$, which, according to existing theoretical provisions, should be searched for using the following equations:

$$a^{in}_{NH_3} = f\left(P_{TP}, \Theta_{TP}\right); \tag{1.37}$$

$$a^{TP}_{NH_3} = f\left(V_{ABC}, V^{C}_{MTP}, \Theta^{B}_{TP}, a^{IN}_{NH_3}, P\right), \tag{1.38}$$

where P_{TP}, Θ_{TP} – pressure and temperature of primary condensation, respectively; V_{ABC} – NHM flow rate; V^{C}_{MTP} – CG flow rate in the intertube space of the column; Θ^{B}_{TP} – CG temperature at the evaporator outlet; P – CG pressure.

Table 1.1 Experimental data on the operating modes of the condensation column

Parameter names			Mode numbers						
			1	2	3	4	5	6	7
Circulation gas at the column inlet	V^{C}_{MTP} flow rate $\cdot 10^3$, nm^3/hour		639.23	621.25	627.08	625.53	621.59	613.08	613.08
	Pressure P_C, MPa		24	22.4	23	23.0	22.8	22.2	22.2
	Temperature Θ^{K}_{MTP}, °C		37	42	35	40	39	34	40
	Concentration, % vol.	hydrogen $a^{MTP}_{H_2}$	55.7	55.9	55.7	56.5	54.4	55.2	55.6
		methane $a^{MTP}_{H_4}$	8.4	8.0	8	8.2	8.2	8.2	7.8
		nitrogen $a^{MTP}_{H_2}$	18.9	19.6	20.0	19.0	19.5	18.7	18.9
		argon a^{MTP}_{Ar}	6.9	6.8	7	7.9	7.6	7.6	7
		ammonia $a^{MTP}_{NH_3}$	10.1	8.6	9.3	8.4	10.3	10.3	10.4
Nitrogen-hydrogen mixture at the separator inlet	Flow rate $V_{NHM} \cdot 10^3$, nm^3/hour		174	175	175	176	174	173	169
	Pressure P_{NHM}, MPa		24.2	23.2	24	23.5	23.2	23.2	23.2
	Temperature Θ^{C}_{ABC}, °C		35	36	35	41	43	36	40
Temperature Θ^{B}_{MTP}, °C			16	19	13	17	16	12	17
Central heating temperature at the evaporator outlet, Θ^{B}_{TP}, °C			–0.5	–	–	–5	–6	–7	–4
Circulation gas at the column outlet	V^{C}_{TP} flow rate $\cdot 10^3$, nm^3/hour		774.2	771.35	770.7	776.1	758.08	747.58	745.12
	Temperature Θ^{K}_{TP}, °C		25	24	22	24	24	21	24
	Concentration, % vol	hydrogen $a^{TP}_{H_2}$	62.2	62.3	61.7	62.4	62.3	61.9	62.8
		methane $a^{TP}_{CH_4}$	7.2	6.8	6.9	6.9	7.1	7	6.5
		nitrogen $a^{TP}_{N_2}$	21.3	21.3	21.9	20.6	20.5	21.2	20.8
		argon a^{TP}_{Ar}	6.0	5.9	6.0	6.6	6.6	6.6	6.3
		ammonia $a^{TP}_{NH_3}$	3.3	3.7	3.5	3.5	3.5	3.3	3.6

Note: NHM composition (% vol.) – $a^{ABC}_{H_2} = 76.3$; $a^{ABC}_{CH_4} = 0.4$; $a^{ABC}_{N_2} = 23.2$; $a^{ABC}_{Ar} = 0.1$
Source: [16]

Table 1.2 Experimental data on the operating modes of the primary condensation unit and the ARU evaporator

Parameter names			Mode numbers						
			1	2	3	4	5	6	7
CG at the outlet of the primary condensation unit	Flow rate $V_{0C} \cdot 10^{-3}$, nm³/hour		639.2	638.4	643.4	631	623.4	640.0	634.8
	Pressure P_{PC}, MPa		22.1	22	22	22.0	22.7	22.4	24
	Temperature ΘP_C, °C		28	36	29	30	25	29	22
	Concentration,% vol.	$a^{IN}_{H_2}$	55.7	56	55.6	56.8	57.2	56.2	56.2
		$a^{IN}_{N_2}$	18.9	18.9	19.2	17.6	18.8	19.5	20
		$a^{IN}_{CH_4}$	8.4	8.3	8.7	8.8	8	7.7	8.4
		a^{IN}_{Ar}	6.9	6.9	6.7	6.8	6.9	6.8	7.3
		$a^{IN}_{NH_3}$	10.1	9.9	9.8	10	9.1	9.8	8.1
Central heating temperature	at the evaporator inlet Θ_{1C}, °C		16	23	15	18	13	18	18
	at the evaporator outlet Θ_{2C}, °C		–5	–1	–8	–6	–3	4	–6
Central heating consumption at the evaporator inlet $V_C \cdot 10^{-3}$, nm³/hour			319.6	316.2	321	315.5	311.7	320.0	317.4
Central heating pressure P_C, MPa			23.5	23	23	22.7	23.5	23.8	24.8
Intertube space of the evaporator when connected to a two-ARU circuit	Refrigerant boiling pressure P_{MTR}, MPa		0.19	0.25	0.17	0.2	0.2	0.25	0.20
	Refrigerant boiling point Θ_{MTR}, °C		–13	–8	–15	–13	–8	–2	–12
	Refrigerant concentration at inlet ξ^{IN}_X, kg/kg		0.989	0.991	0.993	0.995	0.997	0.996	0.995
	Phlegm consumption M_F, t/year		0.902	1.158	0.541	0.465	0.102	0.142	0.937
	Refrigerant consumption at the inlet M^{IN}_X, t/year		15.995	19.174	16.885	17.507	10.878	10.410	17.313
	Liquid refrigerant inlet temperature Θ^{IN}_X, °C		26	28	29	27	20	25	27

*Note:*there was one ARU in operation*
Source: [19]

Table 1.3 Generalised indicators of the quality of the information obtained

Indicator name		Designation	Numerical value
Average concentration		$\overline{a_{ij}}$	9.85
Maximum sample variance for a single series		$\sigma_i^2(a)$	0.45
Total sum of variances		S_a^2	1.002
Cochran's criterion	calculated	G_p	0.4491
	tabulated	G_m	0.6841
Reproducibility dispersion		σ_0^2	0.25
Residual dispersion		σ_Σ^2	0.2041
Fisher's criterion	calculated	F_p	0.8164
	tabulated	F_B	8.84
Selective	asymmetry	$\lvert A\rvert$	$1.037 \cdot 10^{-3}$
Excess		$\lvert E\rvert$	2.999
Condition for theoretical dispersions	asymmetry	$3\sqrt{\sigma(A)}$	0.644
	of excess	$5\sqrt{\sigma(E)}$	2.064

Source: [19]

1.2 IDENTIFICATION OF HEAT EXCHANGE AND CONDENSATION–SEPARATION PROCESSES IN THE SECONDARY CONDENSATION PROCESS COMPLEX

In order to solve the problem of identifying heat exchange processes in the CC, calculations were made of the total actual thermal resistance R_T^E, the actual heat transfer coefficient K_E^K and the design coefficient K_P^K using equations (1.6)–(1.11), (1.20) given in Section 1.1 of the algorithm for forming the information array. The calculation results are summarised in **Tables 1.4** and **1.5**, where the mode numbers correspond to the numbers in **Table 1.1**.

As can be seen from **Tables 1.4** and **1.5**, the heat transfer coefficient in real conditions K_E^K is almost two times less than the coefficient K_P^K calculated using the equations adopted in the design. According to existing theoretical provisions [20], this discrepancy is due to the presence of additional condensation thermal resistance.

Table 1.4 Results of calculations of the actual heat transfer coefficient of the condensation column based on experimental data

Parameter names			Mode numbers						
			1	2	3	4	5	6	7
Heat flows, MW	Separation section	Φ^C_{ABC}	2.128	2.302	2.233	2.733	2.861	2.512	2.535
		Φ^C_{MTP}	0.523	0.488	0.523	1.000	1.139	0.895	0.814
		Φ^C_B	1.605	1.826	1.721	1.732	1.721	1.616	1.709
	Heat exchanger	Φ^K_{TP}	9.687	10.595	9.687	10.932	10.978	10.187	10.443
		Φ^K_{MTP}	9.874	11.129	10.048	10.804	10.850	9.955	10.932
Θ^C_{TP}, at the outlet of the separation section, °C			0.89	–0.68	–0.61	–2.23	–2.84	–4.5	–1.75
Heat balance discrepancy, %			1.9	4.9	3.8	1.7	1.1	2.2	4.7
Heat transfer coefficient K^K_E, W/m²·K			340.3	271.9	349.9	292.1	304.2	322.3	290.1
Condensed ammonia consumption M_{SK}, t/year			14.4	18.1	14	16.9	16.6	14.43	17

Source: [16]

Table 1.5 Results of calculations of the efficiency indicators of the heat exchange process of the condensation column according to the design and actual thermal resistance

Name of parameters	Mode numbers						
	1	2	3	4	5	6	7
Heat transfer coefficient α_{TP}, W/m²·K	1790.12	1780.65	1801.8	1797.95	1764.68	1761.93	1727.63
Heat transfer coefficient α_{MTP}, W/m²·K	1454.49	1418.31	1447.51	1443.06	1460.13	1431.65	1423.98
Heat transfer coefficient K^K_P, W/m²·K	645	636.91	645.39	644.32	642.89	636.91	635.52
Total thermal resistance R^E_T, m²·K/W	0.00169	0.00241	0.00161	0.00217	0.00203	0.00183	0.00216

Source: [16]

The calculated values in **Table 1.4** and **1.5** show that there is a non-random relationship between the total thermal resistance coefficient R^E_T and the consumption of condensed ammonia M_{CK}. Based on the

results of processing these indicators using the least squares method, an equation was obtained for the numerical estimation of the uncertainty of this coefficient [21]

$$R_T^E = 2.102 \cdot 10^{-5} \cdot M_{CK}^2 - 0.0004674 \cdot M_{CK} + 0.0040679. \quad (1.39)$$

The error in calculations using equation (1.39) does not exceed 6%.

The identification of the heat exchange process in the evaporator was performed using an experimental data set, some of which are presented in **Table 1.2**. The results of calculations of the heat transfer coefficient K_E and the total thermal resistance R_T^E according to equations (1.13)–(1.19) are summarised in **Table 1.6**, where the mode numbers correspond to the numbers in **Table 1.2**.

Table 1.6 Efficiency indicators of the heat exchange process of the ARU evaporator according to experimental data

Name of indicators	Mode numbers						
	1	2	3	4	5	6	7
Cooling capacity Φ_0, MW	4.59	5.53	5.01	5.24	3.38	3.23	5.22
Average consumption of ammonia condensate M_{KS}, t/year	19.1	16.78	18	18.04	16.1	17.7	13.2
Heat transfer coefficient α_{MTR}, W/(m^2·K)	1310.3	1581.6	1360.5	1453.2	1069.3	1085.3	1448.8
Heat transfer coefficient α_{TP}, W/(m^2·K)	3917.3	3889.6	3932.1	3779.7	3783.9	3915.8	3929.7
Total thermal resistance $R_T^{\text{Å}} \cdot 10^4$, (m^2·K)/W	8.2631	6.2330	6.4841	6.4540	5.1315	6.9836	5.3671
Heat transfer coefficient K_E, W/(m^2·K)	541.6	660.4	610.1	625.7	584.2	533.2	673.8

Source: [19]

As can be seen from **Table 1.6**, the heat transfer coefficient in real conditions K_E is on average almost 1.8 times less than the coefficient K_P = 1130.4 W/(m^2·K), calculated using equations (1.16)–(1.19) accepted in the design, and the total thermal resistance R_T^P at the level of 0.000356 (m^2·K)/W. As in the previous case, this discrepancy is due to the presence of additional condensation thermal resistance. A numerical estimate of this resistance based on the approximation results can be represented by the following equation

$$R_T^E = \left(0.0956 M_{KC}^2 - 2.5111 M_{KC} + 21.081\right) 10^{-4}. \quad (1.40)$$

The error in calculations using equation (1.40) does not exceed 14%.

Based on the results of processing experimental data on ammonia concentration $a_{NH_3}^{IN}$ at the inlet (**Table 2.4**) and outlet $a_{NH_3}^{OUT}$ of the heat exchanger using the MATLAB package, the following equations were obtained for their numerical estimation, which have the following form [19, 21]:

$$a_{NH_3}^{IN} = 22.068 - 0.6272P_{TP} + 0.05245\Theta_{TP}; \quad (1.41)$$

$$a_{NH_3}^{TP} = -7.78 + 0.02441 \cdot V_{ABC} + 0.01176 \cdot V_{MTP}^{C} + \\ +0.0327 \cdot \left(\Theta_{TP}^{B} + 273\right) + 0.085 \cdot a_{NH_3}^{MTP} - 0.0635 \cdot P. \quad (1.42)$$

The error in calculations using equations (1.41) and (1.42) does not exceed 6%.

1.3 SYNTHESIS OF THE HARDWARE AND TECHNOLOGICAL DESIGN OF THE SECONDARY CONDENSATION COMPLEX AND DETERMINATION OF THE GENERAL STRUCTURE OF ITS CONTROL SYSTEM

Equations (1.1)–(1.7), (1.10), (1.11), (1.20), (1.39) and (1.42), obtained as a result of the identification of heat exchange processes, constitute a mathematical model of the condensation column.

Table 1.7 presents some of the results of calculating the target indicators for the CC operating modes obtained in the process of mathematical modelling. The mode numbers in **Table 1.7** correspond to the numbers in **Table 1.1.**

Table 1.7 Main target indicators of the condensation column operating modes based on the results of mathematical modelling

Heat transfer efficiency indicators	Mode numbers						
	1	2	3	4	5	6	7
Heat flow of the separation part Φ^{C}, MW	2.162	2.298	2.248	2.729	2.78	2.534	2.536
Heat flow of the heat exchanger Φ^{K}, MW	10.22	10.772	9.927	10.855	10.929	10.604	10.690
Heat transfer coefficient of the heat exchanger K, W/m^2·K	332.51	275.67	339.29	289.8	296.31	324.48	289.61
Circulation gas consumption at the pipe space outlet $V_{TP}^{C} \cdot 10^3$, nm^3/hour	777.67	770.59	771.89	775.93	758.78	749.59	745.42
Circulation gas temperature at the outlet of the pipe space Θ_{TP}^{K}, °C	22.8	25.5	21.5	23.7	22.9	20	24.5
Circulation gas temperature at the inlet to the pipe space Θ_{TP}^{C}, °C	0.896	–0.575	–0.774	–2.194	–2.948	–4.8	–1.8
Temperature of the circulating gas at the evaporator inlet Θ_{MTP}^{B}, °C	15.17	19	13	16.9	15.8	10.4	17.6
Ammonia concentration in the circulating gas at the outlet of the pipe space, $a_{NH_3}^{TP}$, % vol.	3.7	3.6	3.6	3.4	3.59	3.56	3.6

Source: [16]

A comparison of experimental data (**Table 1.4**) and data obtained during modelling (**Table 1.7**) shows that the calculation error does not exceed the approximation error according to equations (1.39) and (1.42), i.e. 6%. Such convergence allows us to conclude that it is possible to use the mathematical model of CC for the synthesis of the technical structure of increased energy efficiency of TCSC.

Fig. 1.2 shows some of the results of mathematical modelling of the CC. They allow us to quantitatively assess the increase in thermal load on the LTE evaporators under real operating conditions compared to those assumed in the design. The dependencies shown in **Fig. 1.2** were obtained at a maximum CG inlet temperature of 45°C, which is observed in real conditions.

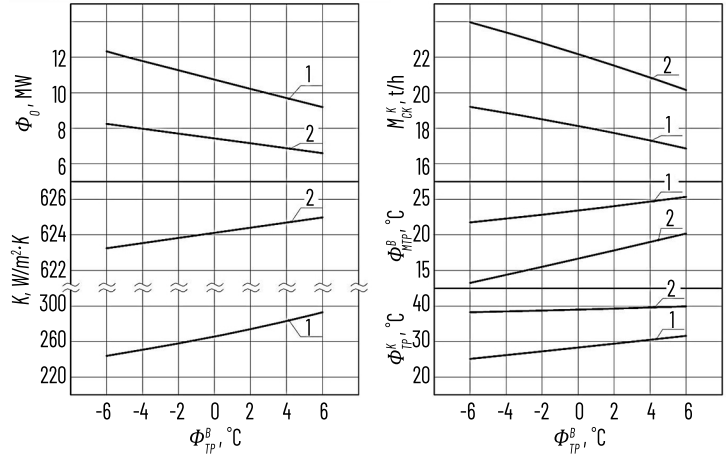

Fig. 1.2 Dependence of individual indicators of heat exchange efficiency in the condensation column and cooling capacity of refrigeration systems on the cooling temperature of the circulating gas in the evaporators for the initial data of mode No. 5 in **Table 1.1**

Source: [16]

According to **Fig. 1.2**, maintaining the specified temperature at 5°C requires an increase in the cooling capacity of refrigeration systems by 4 MW relative to the design value of 8.12 MW. This increase is due to a decrease in the actual heat transfer coefficient K_E to 247.7 W/m^2·K compared to the coefficient K_P = 623.4 W/m^2·K, which is due to the presence of additional condensation thermal resistance due to ammonia condensation M_{SK}. As a result, there is an increase in the temperature Θ^B_{MTP} at the inlet of low-temperature evaporators from 13.8°C to 22°C and a decrease in the temperature Θ^K_{TP}, at the outlet of the CC tube space from 38.4°C to 25.7°C.

The dependencies shown in **Fig. 1.3** and **1.4** allow us to determine the conditions (shown in dotted lines) for not only excluding the TRU from the synthesis unit operation scheme, but also reducing the cooling temperature of the CG in the evaporators (LTE1, LTE2) to a minimum level of 5°C using only two ARUs. However,

this requires a reduction in the heat load on the LTE evaporators in terms of temperature, which can be achieved by installing an additional heat exchanger (AH) for deeper cold recovery.

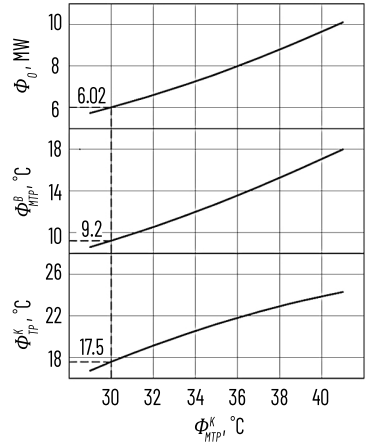

Fig. 1.3 Effect of circulation gas temperature at the inlet of the condensation column
Source: [16]

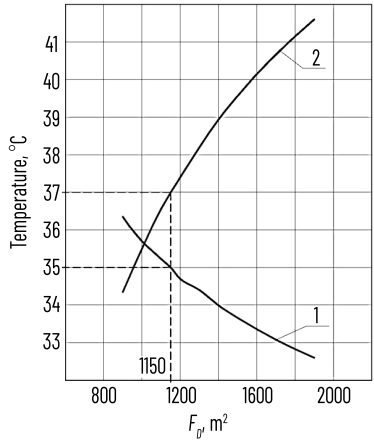

Fig. 1.4 Influence of the heat exchange surface of the additional heat exchanger *FD* on the distribution of temperatures at the outlets of the circulating gas at its maximum thermal load at the inlet temperature Θ^{IN}_{MTP} = 45°C
Source: [16]

Analysis of the dependencies shown in **Fig. 1.3** and **1.4** indicates that at a circulating gas temperature of Θ^{K}_{MTP} = 30°C at the inlet to the cooling unit, the cooling temperature can be stabilised at the minimum (regulatory) level of 5°C with only two automatic control units. At the same time, their cooling capacity must be even lower than the existing 6.28 MW, namely 6.02 MW. It is impossible to fulfil this condition even by installing a AH according to **Fig. 1.4**. Therefore, it is advisable to install a AH in front of the high-temperature evaporator (HTE) heat exchanger with a significantly smaller, i.e. optimal, heat exchange surface F_D = 1150 m^2. The boiling temperature of ammonia in the intertube space is not higher than 24°C, and the pressure of 0.9915 MPa ensures a decrease in the temperature of the direct flow of the cooling agent from 35°C to 30°C. The boiling temperature regime in the HTE can be ensured by connecting it to the cycle of the steam ejector refrigeration unit (SERU), as shown in **Fig. 1.5** [16, 21].

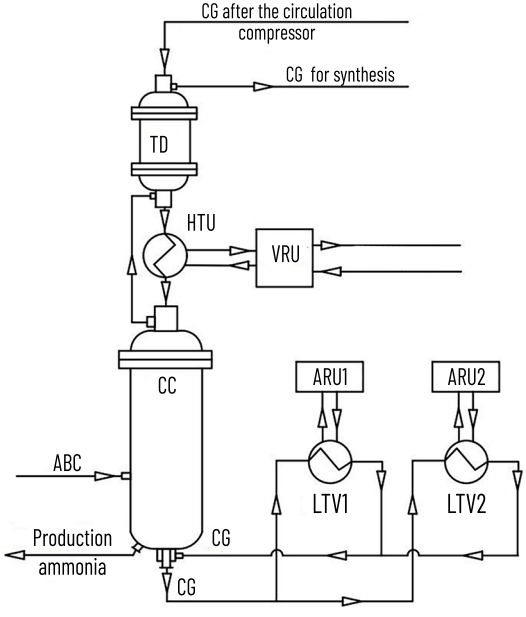

Fig. 1.5 Equipment and technological design of a secondary condensation complex with increased energy efficiency: CC — condensation column; CG — circulation gas; ABC — nitrogen-hydrogen mixture; ARU — absorption refrigeration unit; SEU — steam ejector refrigeration unit; HTE and LTE — high-temperature and low-temperature evaporators, respectively; AH — additional heat exchanger
Source: [21]

The injection coefficient of the SEU jet compressor was determined using a well-proven algorithm [22]. Due to the use of air-cooling devices in the SEU, the injection coefficient was set according to the achievable

compression pressure, the value of which was limited to 1.6 MPa. This allows even in the summer period to ensure a high temperature (40°C) of ammonia vapour condensation after the jet compressor.

According to the calculation results, the injection coefficient is at least 0.4. With this coefficient, 20 t/h of working steam from the SEU steam generator with a pressure of 3 MPa is sufficient to inject 8 t/h of ammonia steam from the HTE evaporator. This will provide a cooling capacity of 2.48 MW. The total amount of refrigerant steam and working steam for air condensers will be 28 t/h, the condensation of which can be provided by three condensers with an electricity consumption of 600 kWh. To obtain 20 t/h of working steam, 515 t/h of monoethanolamine (MEA) solution from the first stream of the MEA purification section through a steam generator is sufficient, i.e. 20·974.4/3.78·(85–75) = 515 t/h. The numerical values in this calculation are as follows: the specific heat of vaporisation of ammonia at a temperature of 65°C and a pressure of 3 MPa is 974.4 kJ/kg; the specific heat capacity of the MEA solution is 3.78 kJ/kg·K; the inlet and outlet temperatures of the MEA solution are 85°C and 75°C, respectively. Due to such heat utilisation, the load on the air coolers of this solution and heat emissions into the atmosphere are reduced.

This technological design allows reducing the total cooling capacity at the secondary condensation stage from 11.16 MW to 8.5 MW. This is due to deeper recovery and utilization of low-potential heat in the SEU with a MEA solution flow temperature of up to 90°C. At the same time, due to the exclusion of the TRU from the unit's operating scheme, electricity consumption will be reduced by 3.4 thousand kWh. Despite this reduction in cooling capacity, it is possible to reduce and stabilise the cooling temperature of the central heating system in the evaporators from 0°C to –5°C at its maximum temperature at the inlet to the condensation column. This maximum load is typical for the operation of the synthesis unit for about 4 months in the spring-summer period. A 5°C decrease in temperature during this period will also reduce natural gas consumption by 190 m^3/hour in an additional steam boiler for producing water vapour at a pressure of 10 MPa. This will result in annual natural gas savings of approximately 550 thousand nm^3. The advantage of the proposed structure is that it ensures the cooling temperature regime of the central heating system only with the help of heat-using refrigeration systems that utilise both low-temperature heat in the ARU and ultra-low-temperature heat in the SEU.

The central place in this TCSC structure is occupied by LTE evaporators, the efficiency of which ultimately determines the secondary condensation temperature. The evaporators are immersed shell-and-tube heat exchangers with U-shaped tubes. The CG is cooled in the tube space by ammonia boiling in the intertube space. The peculiarity of the evaporation process of liquid ammonia (refrigerant) is that it enters the evaporator with water impurities. To remove water, a process of draining phlegm from the evaporator is provided [23]. Insufficient phlegm drainage causes water to accumulate in the evaporator. This leads to a decrease in ammonia concentration, an increase in pressure and cooling temperature, and, consequently, a decrease in cooling capacity. Excessive drainage causes a loss of refrigerant, which reduces cooling capacity and cooling temperature. Thus, the phlegm flow rate $M_{\Phi}(t)$ is one of the main controlling influences of the control vector $Y(t)$, which determines the optimal state vector x^{OPT}. However, there is practically no information in periodicals on determining the quantitative dependence of the influence of the flow rate $M_{\Phi}(t)$ on the efficiency of the heat exchange process and, consequently, on the cooling temperature regime of the central heating system. This absence is due to the widespread use of ARU with low cooling capacity.

In such installations, periodic phlegm drainage is mainly carried out, and the impact of this process on the efficiency of production is not so significant [24]. For refrigeration units with high cooling capacity, over 3 MW, used in ammonia production, this impact can be quite significant. The task of determining the quantitative dependence of the control vector $M_{\phi}(t)$ on the optimal state vector x^{OPT} and creating an algorithm for optimisation can be most effectively solved using a mathematical model of the evaporator.

The purpose and place of the mathematical model is clearly illustrated by the generalised structure of the adaptive system for optimising the operating mode of the control object, shown in **Fig. 1.6** [25].

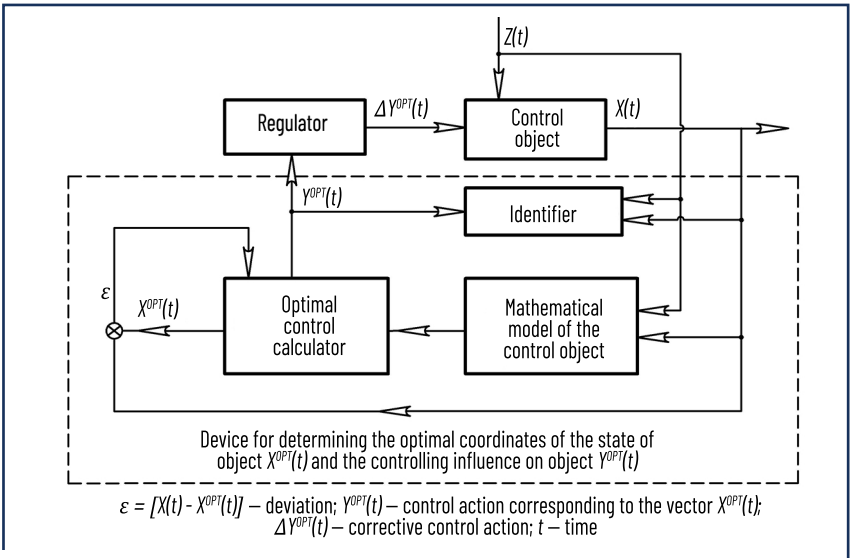

Fig. 1.6 Generalised structure of an adaptive system for optimising the operating mode of a control object
Source: [19]

With regard to the evaporator, the task of synthesising an algorithm for minimising the cooling temperature of the central heating system under certain constraints can be represented in general terms as follows:

$$\varphi\left(x,Y,z\right)\rightarrow min\left(extr\right)\Rightarrow x^{OPT}, \tag{1.43}$$

$$x=F\left(Y,z\right), \tag{1.44}$$

where φ is the objective function; x, z are the coordinate vectors corresponding to the state of the object and disturbances of a certain dimension; Y is the vector of control actions; F is the operator of the mathematical model of the evaporator.

The operation of the LTE evaporator is influenced by a large number of disturbance factors, both external from the primary condensation unit and internal from the ARU. All this will cause a shift in the optimal state coordinates (cooling temperature of the central heating system) and control action (phlegm flow rate). Determining these coordinates and identifying the patterns of the disturbance vector's influence on the shift of the optimal state coordinates can be achieved through mathematical modelling, which requires the construction of a mathematical model of the LTE and the development of algorithmic research tools.

1.4 INVESTIGATION OF THE PATTERNS OF INFLUENCE OF PHLEGM DRAINAGE INTENSITY ON THE EFFICIENCY OF THE CIRCULATING GAS COOLING PROCESS IN LOW-TEMPERATURE EVAPORATORS

In the process of developing a mathematical model of an evaporator, uncertainties in its description are due to a number of assumptions. Among them, the following can be highlighted: saturation of ammonia vapour throughout the entire intertube space, negligible heat of hydraulic losses, uniform distribution of ammonia concentration in the volume of boiling liquid, no formation of non-boiling liquid in the evaporator intertube space, and a mean logarithmic distribution of the temperature of the working fluid. Given these uncertainties, the mathematical description of the evaporator is based on well-known equations of heat transfer, material and energy balance. The main equations are as follows [19]:

$$\Phi_0 = M_\Phi i_\Phi + M_Y^{OUT} i_Y^{OUT} - M_X^{IN} i_X^{IN}; \tag{1.45}$$

$$M_X^{IN} \xi_X^{IN} = M_\Phi \xi_\Phi + M_Y^{OUT} \xi_Y^{OUT}; \tag{1.46}$$

$$M_X^{IN} = M_\Phi + M_Y^{OUT}; \tag{1.47}$$

$$\Phi_{MTP} = \alpha_{MTP} F_{MTP} \left(\Theta_{MTP}^{CT} - \Theta_{MTP} \right); \tag{1.48}$$

$$\Phi_{TP} = a_{TP} F_{TP} \left(\Theta_C^{CP} - \Theta_{TP}^{CG} \right); \tag{1.49}$$

$$\Phi_{CG} = \frac{F_{CT}^{CP} \left(\Theta_{TP}^{CT} - \Theta_{MTP}^{CT} \right)}{R_T^{\dot{E}}}; \tag{1.50}$$

$$\Theta_C^{CP} - \Theta_{MTP} = \frac{\left(\Theta_{1C} - \Theta_{MTP} \right) - \left(\Theta_{2C} - \Theta_{MTP} \right)}{ln \left[\frac{\Theta_{1C} - \Theta_{MTP}}{\Theta_{2C} - \Theta_{MTP}} \right]}, \tag{1.51}$$

where M_Φ, M_Y^{OUT}, M_X^{IN} – mass flow rate of phlegm, ammonia vapour at the outlet and liquid refrigerant at the inlet, kg/s; i_Φ, i_Y^{OUT}, i_X^{IN} – enthalpy of phlegm, ammonia vapour at the outlet and liquid refrigerant at

the inlet, kJ/kg; ξ_Φ, ξ_Y^{OUT}, ξ_X^{IN} – weight concentration of phlegm, ammonia vapour at the outlet and liquid refrigerant at the inlet, kg/kg; Φ_{CT}, Φ_{MTP}, Φ_{TP} – heat flows through the pipe wall, from the inter-pipe and pipe space, W; F_{CT}^{CP}, F_{MTP}, F_{TP} – surface area of the average wall, inter-pipe and pipe space, m^2; Θ_C^{CP}, Θ_{TP}^{CT}, Θ_{MTP}, Θ_{MTP}^{CT} – average temperature of the heat transfer fluid and the wall on the tube space side, boiling refrigerant and the wall on the intertube space side, °C.

Equations (1.13)–(1.20), (1.40), (1.41), (1.45)–(1.51), together with formulas for calculating the thermophysical properties of substances and equilibrium dependencies, constitute a complete mathematical model of the evaporator. The research was carried out according to the developed algorithm, the software implementation of which was performed in the MATLAB package [26]. A generalised block diagram of the algorithm is shown in **Fig. 1.7**.

The symbols shown in **Fig. 1.7** correspond to the following physical quantities: V_C – volumetric flow rate of the heat transfer medium, nm^3/s; a_i^{IN} – volumetric concentration of the heat transfer medium components at the inlet, % vol., F = 520 m^2 – total heat exchange surface area; ε = 0.2% – specified calculation error value; $\Delta\Theta = 0.1$°C – temperature change step; Θ_C^{CP} – average refrigerant temperature, °C; $\Delta\Theta^{CP}$ – average logarithmic temperature difference, °C; q_{TP}, q_{MTP} – specific heat flux from the pipe and inter-pipe space, W/m^2; M_{KC}, M_Y^{OUT}, M_X^{IN} – average flow rate of condensed ammonia from the central heating system, refrigerant vapour at the evaporator outlet and liquid refrigerant to the condenser receiver, kg/s; r^{CP} – average heat of condensation of ammonia, kJ/kg; a_{TP}, a_{MTP}, K – heat transfer coefficients from the CH, refrigerant and total heat transfer coefficient, W/(m^2·K); R_T^E – total thermal resistance, (m^2·K)/W; P_C, P_{MTP} – pressure of the central heating system and boiling refrigerant, respectively, MPa; ξ_Φ – weight concentration of phlegm, kg/kg; Θ_{MTP} – boiling temperature of the refrigerant in the intertube space, °C; i_X^{IN}, i_Φ, i_Y^{OUT} – enthalpy of the liquid refrigerant at the inlet, phlegm and ammonia vapour at the outlet, kJ/kg; F_X – effective heat exchange surface, m^2; n = 526 – total number of heat exchange tubes; Φ_{TP}, Φ_{MTP} – heat flow from the pipe and inter-pipe space, respectively, MW. Unlike commonly known algorithms, the developed algorithm allows calculating the effective heat exchange surface F_X of the evaporator under external disturbances using the following formula

$$F_X = \Phi / q. \tag{1.52}$$

The algorithm consists of two main convergence cycles. In the first cycle, the temperature Θ_{2C} is determined and the calculation error δ_1 is estimated under the condition $\Delta M_X^{IN} \geq 0$, when the refrigerant and phlegm flow rates do not exceed the possible inflow of liquid refrigerant to the evaporator from the ARU condenser. The second cycle is related to determining the temperature Θ_{2C} and the effective heat exchange surface in the case $\Delta M_X^{IN} < 0$, i.e. under the conditions of the existing restriction on the consumption of liquid refrigerant from the ARU condenser. At the same time, in both cycles, with a constant level, the overall balance of the evaporator in terms of consumption and energy is maintained.

The applicability of the obtained LTE model is confirmed by the calculation results obtained and presented in **Table 1.8**. A comparison of the experimental data given in **Tables 1.1** and **1.2** and the results obtained in **Table 1.8** using the mathematical model shows that the calculation error does not exceed the

approximation error R_T^E according to equation (1.40). At the same time, the root mean square deviation of the calculated values of Θ_{2C} from the experimental values does not exceed 0.17°C.

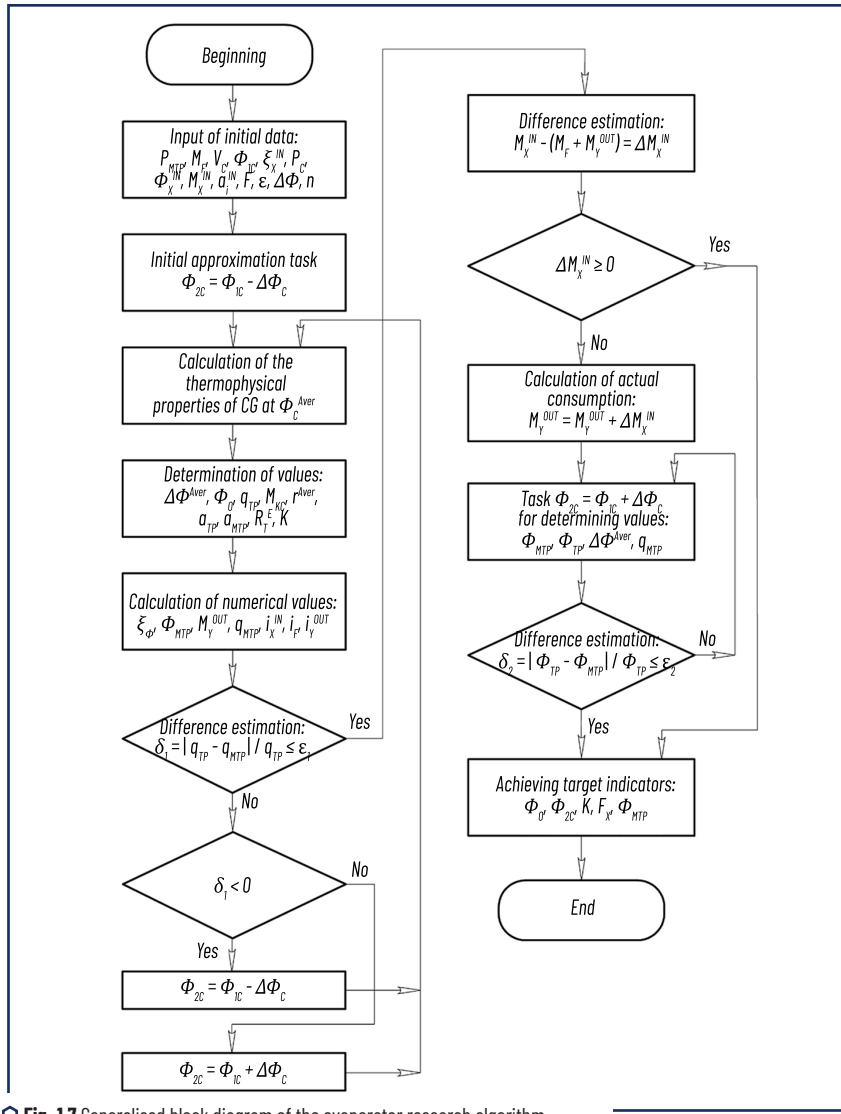

Fig. 1.7 Generalised block diagram of the evaporator research algorithm
Source: [26]

Table 1.8 Calculated indicators of the evaporator operating modes ARU

Indicator name	Mode numbers*						
	1	2	3	4	5	6	7
Ammonia concentration at the inlet $a^{IN}_{NH_3}$, % vol.	9.67	10.15	9.66	9.84	9.14	9.54	8.1
Cooling capacity Φ_0, MW	4.6	5.56	5.04	5.2	3.31	3.26	5.02
Heat transfer coefficient K, W/(m^2·K)	576.05	629.04	579.74	603.54	541.19	544.47	681.67
Boiling point of refrigerant Θ_{MTR}, °C	−14.35	−10.09	−16.51	−14.08	−8.06	−2.87	−16.67
Central heating outlet temperature Θ_{2C}, °C	−4.8	−1.32	−7.57	−5.89	−2.39	4.03	−4.8
Total thermal resistance $R^E_T \cdot 10^4$, (m^2·K)/W	7.125	6.812	7.412	6.941	5.831	6.058	4.746

*Note: *mode numbers correspond to the numbers in **Tables 1.1** and **1.2***
Source: [19]

Mathematical modelling allows us to establish the patterns of influence of variables, both the vector of external disturbances *Z(t)* and the vector of controls *Y(t)*, on the state vector *X(t)* of the evaporator. Moving to the state variable space, these vectors will have the following form:

$$X(t)=\begin{bmatrix}\Theta_{2C}(t)\\ H(t)\end{bmatrix};\quad Z(t)=\begin{bmatrix}\Theta_{1C}(t)\\ a^{IN}_{NH_3}(t)\\ \Theta^{IN}_{X}(t)\\ \xi^{IN}_{X}(t)\\ P_{MTP}(t)\\ V_C(t)\end{bmatrix};\quad Y(t)=\begin{bmatrix}M^{IN}_{X}(t)\\ M_{\Phi}(t)\end{bmatrix}. \tag{1.53}$$

It should be noted that the limitations in the research are due to the range of coordinate changes in the process of developing a mathematical model of the evaporator. The temperature value Θ_{1C} was a constant at 9.2°C, which is ensured by the new technological design of the TCSC.

Fig. 1.8 shows individual research results on the control effect of phlegm flow M_F at different pressures P_{MTP} on the efficiency of the cooling process of the central heating system in the evaporator of the high-pressure turbine under the following restrictions: V_C = 310798 nm^3/s; $a^{IN}_{NH_3}$ = 0.103% vol; $a^{IN}_{H_2}$ = 0.544% vol; $a^{IN}_{N_2}$ = 0.195% vol; $a^{IN}_{CH_4}$ = 0.082% vol; a^{IN}_{Ar} = 0.076% vol; Θ_{1C} = 9.2°C; P_C = 23 MPa; M^{IN}_X = 10 t/h; ξ^{IN}_X = 0.998 kg/kg; Θ^{IN}_X = 26°C.

Fig. 1.9–1.11 show the results of studies on the effect of the control action of the phlegm flow rate M_F on the target indicators of evaporator efficiency, namely the cooling temperature of the refrigerant Θ_{2C} and the cooling capacity of the ARU F_0 under conditions of changing disturbance vector coordinates and under

the above-mentioned restrictions. These are primarily the refrigerant concentration ξ_X^{IN}, the refrigerant flow rate M_X^{IN}, coming from the condenser, and the ammonia concentration in the refrigerant $a_{NH_3}^{IN}$ at the evaporator inlet.

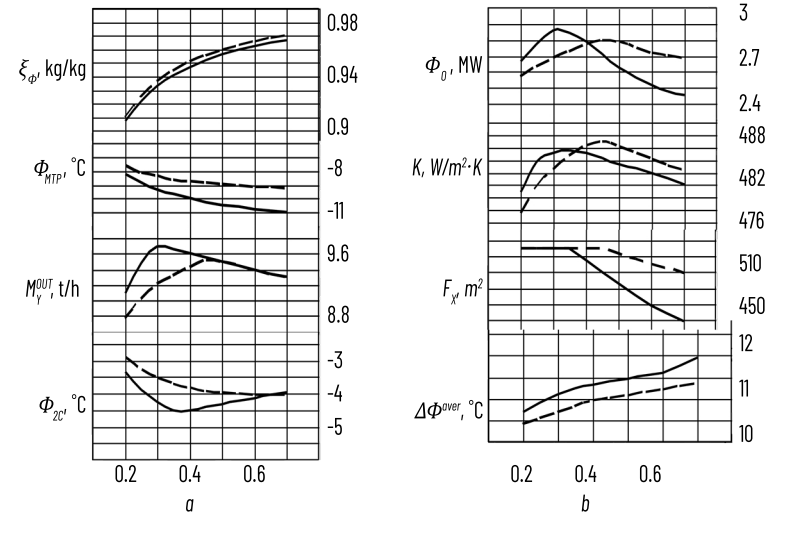

Fig. 1.8 Dependence of the efficiency indicators of the ARU evaporator on the change in pressure P_{MTP} (– – – – P_{MTP} = 0.29 MPa; - - - - - P_{MTP} = 0.3 MPa) and the control action of the phlegm flow rate M_F: *a* — phlegm concentration ξ_Φ, refrigerant boiling temperature in the intertube space Φ_{MTP}, refrigerant vapour flow rate at the evaporator outlet cooling temperature CG Φ_{2C}; *b* — cooling capacity Φ_0, heat transfer coefficient *K*, effective heat exchange surface F_X, mean logarithmic temperature difference $\Delta\Phi^{CP}$
Source: [26]

The dependencies obtained as a result of the research, shown in **Fig. 1.8** for such indicators as cooling capacity Φ_0 and cooling temperature CG Θ_{2C}, are extreme in nature from the control action of the phlegm flow rate M_Φ. This is due, in turn, to the extreme dependence of the refrigerant vapour flow rate M_Y^{OUT}, which increases due to a decrease in the boiling point of the liquid refrigerant Θ_{MTP}. The latter contributes to a decrease in the cooling temperature of the cooling circuit and an increase in cooling capacity.

The values of these coordinates were selected at the levels most characteristic of the summer and winter seasons of operation of the secondary condensation unit, including the ARU.

For example, with an increase in M_F from 0.2 t/h to 0.35 t/h at a constant boiling pressure P_{MTP} = 29 MPa, the average concentration of boiling refrigerant ξ_Φ increases from 0.9071 kg/kg to 0.9408 kg/kg. This, in turn, leads to a decrease in the boiling temperature of the refrigerant Θ_{MTP} from –8.24°C to –9.71°C.

This results in an increase in the average temperature difference of $\Delta\Theta^{CP}$ from 10.68°C to 11.24°C and the consumption of evaporating refrigerant M_Y^{OUT}, from 9.08 t/h to a maximum of 9.65 t/h. Under these circumstances, the temperature Θ_{2C} decreases from –3.36°C to a minimum of –4.5°C, and the cooling capacity Φ_0 increases from 2.66 MW to a maximum of 2.84 MW. The heat transfer coefficient *K* increases and reaches a maximum value of 485.5 W/(m^2·K). This indicates, as is CCown [27], that the critical limit of the bubble boiling regime of the refrigerant has been reached. At the same time, by reducing the temperature of the Θ_{2C} by 1.14°C through the control action on the phlegm flow rate, a reduction in natural gas consumption of 50 thousand nm^3/year is achieved.

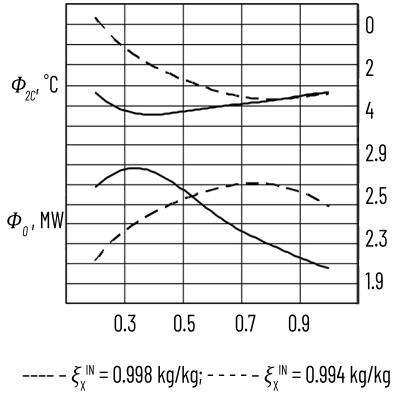

Fig. 1.9 Dependence of the cooling temperature Φ_{2C} and the cooling capacity Φ_0 of the ARU on the control action of the phlegm flow M_Φ at different values of the refrigerant concentration ξ_X^{IN} at the evaporator inlet

A further increase in the control action of M_F, for example to 0.5 t/h, leads to an increase in the concentration of ξ_Φ, a decrease in the temperature of Θ_{MTP} and an increase in the temperature difference $\Delta\Theta^{CP}$ to 0.9562 kg/kg, –10.1°C and 11.32°C, respectively. This reduces the effective heat exchange surface from 520 m^2 to 481.27 m^2 indicating the establishment of a transitional boiling regime for the refrigerant. This mode is characterised by the formation of large vapour cavities on the surface itself. As a result, "dry" areas appear on the surface, which seem to exclude part of the surface from heat exchange. Under such conditions, heat transfer directly to the steam is less intense. This causes a decrease in steam consumption M_Y^{OUT} to 9.52 t/h, heat transfer coefficient K to 482.5 W/(m^2·K), and cooling capacity Φ_0 to 2.63 MW. At the same time, the cooling temperature of the Θ_{2C} will increase to –4.25°C, i.e. by 0.25°C, and the annual consumption of natural gas will increase by almost 77 thousand nm^3.

The increase in pressure is most often caused by an increase in the temperature of the water cooling the absorber. According to **Fig. 1.8**, an increase in pressure P_{MTP} from 0.29 MPa to 0.3 MPa necessitates an increase in the flow rate M_F from 0.35 t/h to 0.45 t/h to establish the critical limit of the bubble boiling regime of the refrigerant. At the same time, due to an increase in the temperature difference $\Delta\Theta^{CP}$ from 10.83°C

to a critical 11.01°C, the cooling capacity will increase from 2.73 MW to a maximum of 2.79 MW, and the cooling temperature of the central heating system Θ_{2C} will decrease from −3.7°C to a minimum of −3.98°C. As a result of this control action on consumption, annual natural gas consumption can be reduced by 88 thousand nm^3/year.

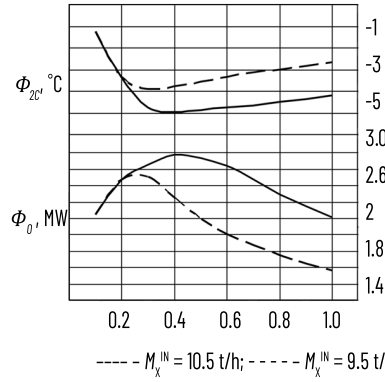

Fig. 1.10 Dependence of the cooling temperature of the central heating system Φ_{2C} and the cooling capacity of the ARU Φ_0 on the control action of the phlegm flow rate M_Φ at different refrigerant flow rate M_X^{IN} at the evaporator inlet
Source: [26]

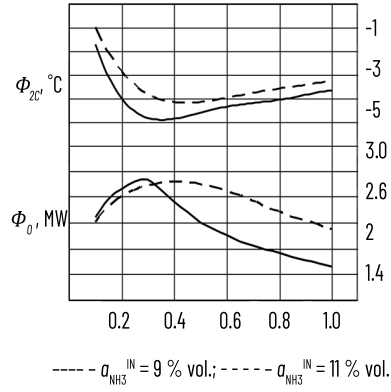

Fig. 1.11 Dependence of the cooling temperature of the central heating system Φ_{2C} and the cooling capacity of the automatic control system Φ_0 on the control action of the phlegm flow rate M_Φ at different values of ammonia concentration in the central heating system Θ_{2C} at the evaporator inlet
Source: [26]

The concentration of liquid refrigerant at the evaporator inlet ξ_X^{IN} also varies within a fairly wide range due to seasonal fluctuations in the air temperature cooling the ARU condenser. As can be seen from **Fig. 1.9**, the extreme (minimum) value of the temperature Θ_{2C} with an increase in the concentration ξ_X^{IN} from 0.994 kg/kg to 0.998 kg/kg decreases from −3.8°C to −4.5°C at a constant pressure P_{MTP} = 0.29 MPa. At the same time, there is a shift towards a decrease in the control action of the phlegm flow rate from 0.8 t/h to 0.35 t/h, at which the minimum values of Θ_{2C} are ensured. Under such conditions, the cooling capacity increases from 2.69 MW to 2.84 MW, and the annual consumption of natural gas can be reduced by 215 thousand nm^3.

With a constant heat supply to the rectifier generator and seasonal fluctuations in condensation pressure, there is also a change in the flow rate of refrigerant vapour entering the condenser and liquid refrigerant entering the evaporator. As a result of these changes in consumption M_X^{IN}, for example, from 9.5 t/h to 10.5 t/h (**Fig. 1.10**), there is also a shift in the required control action of the phlegm consumption from 0.3 t/h to 0.4 t/h, at which the minimum temperature values are achieved Θ_{2C} namely at −3.9°C and −4.98°C. At the same time, the maximum cooling capacities F_0 of 2.71 MW and 2.96 MW, respectively, are ensured. Due to such control action on the phlegm flow rate, the annual natural gas consumption is reduced by 332 thousand nm^3.

The concentration of ammonia in the central heating system changes significantly as a result of the use of air cooling at the primary condensation stage $a_{NH_3}^{IN}$, which causes a change in the heat load of the evaporator. According to the obtained dependencies (**Fig. 1.11**), with a decrease in the concentration of $a_{NH_3}^{IN}$ from 11% vol. to 9% vol., the extreme shifts towards a decrease in the control action of the phlegm consumption, i.e. from 0.4 t/h to 0.3 t/h.

Under these conditions, extreme values of the temperature of the Θ_{2C} are observed at −4.22°C and −4.98°C, respectively, and the cooling capacity reaches maximum values of 2.8 MW and 2.85 MW. At the same time, the annual consumption of natural gas can be reduced by 234 thousand nm^3.

The above studies have proven the significant impact of phlegm consumption for such powerful ARU on the cooling efficiency of the central heating system and, consequently, on the energy efficiency of production. At the same time, the use of control action on phlegm consumption in the range from 0.2 t/h to 0.8 t/h provides a reduction in annual natural gas consumption by an average of 500 thousand nm^3.

The established extreme nature of the dependence of the cooling temperature of the central heating system Θ_{2C} on the control action of the phlegm flow and the shift of the extreme in conditions of changing values of the disturbance vector coordinates *Z(t)* confirms the need to build a system of optimal software control of the cooling temperature regime of the central heating system. The main link in such a system should be an optimisation subsystem for calculating the value of the coordinate of the control action of the phlegm flow rate, which determines the optimal state vector *X(t)* of the evaporator.

Analysis of the above calculation process indicates the possibility of solving a multidimensional optimisation problem using a step-type non-gradient method with one-dimensional extremum search algorithms [28]. Non-gradient methods are, by their nature, most suitable for optimising existing industrial systems. Given the sensitivity of the object to changes in phlegm flow, it is most appropriate to use a scanning method in the space of only one variable. This method guarantees that the extremum will not be missed due

to the use of a small search step [29]. Taking this into account and the dependencies obtained, a search step for phlegm flow rate of 0.02 t/h was adopted. In this case, the block diagram of the algorithm shown in **Fig. 1.7** must be supplemented with a third cycle of searching for a global extremum.

The resulting algorithmic support for minimising the cooling temperature Θ_{2C} of the central heating system allows it to be used in the optimisation subsystem. This subsystem is a key component in the overall technical structure of the computer-integrated system for optimal software control of the ARU evaporator.

1.5 TECHNICAL STRUCTURE OF THE COMPUTER–INTEGRATED SYSTEM FOR OPTIMAL SOFTWARE CONTROL

The TDC-3000 information and control system, which is used in the AM-1360 series ammonia synthesis units operating in Ukraine, covers both the field and technological levels of production control. It includes means for collecting, processing and storing technological information, as well as human-machine interface tools. Information exchange is carried out using communication tools. However, it should be noted that TDC-3000 is a "closed" type control system with pre-installed software. Therefore, it cannot be significantly upgraded. The solution to the task of building a mathematical model in real time and adapting the model to a situation of uncertainty is only possible by supplementing the existing control system with available open-type hardware and software.

Fig. 1.12 shows an option for combining TDC-3000 with the proposed automated system for identification, creation of a mathematical model and minimisation of the temperature regime of the ARU evaporator [19].

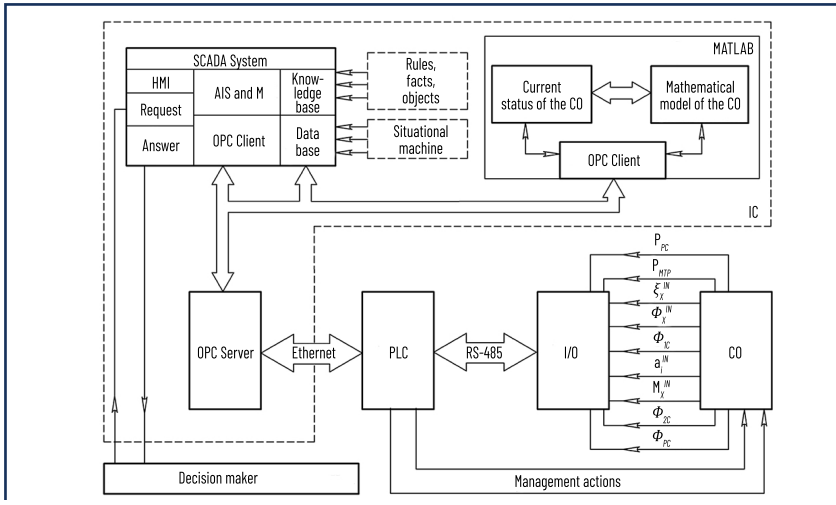

Fig. 1.12 Generalised technical structure of the automated system for optimal software control of the ARU evaporator
Source: [19]

This approach allows the TDC-3000 to be used as a source of operational technological information for filling the database and knowledge base. This is made possible by the use of OPC technology, which allows all the necessary information to be obtained using a client-server method of data access [30]. The SCADA system and the MATLAB software environment perform the client function in the system. With this approach, the SCADA system provides the human-machine interface function, and all the necessary calculations are performed in the MATLAB software environment [31]. As a result, control algorithms can be supplemented with new data regarding the mathematical model, which will ensure the solution of the problem of minimising the temperature regime of the evaporator of the secondary condensation unit in real time.

CONCLUSIONS

Improving the energy efficiency of ammonia production, in particular the secondary condensation process complex (SCPC) as one of the most energy-intensive components, is becoming particularly relevant in the overall process of modernising large-scale synthesis units. The greatest efficiency of modernisation is ensured by the application of a systematic approach through the combination of its systemic-structural and systemic-control positions, the scientific basis of which is mathematical modelling and process identification.

Research has established uncertainties in the operation of the TRU, and algorithms have been developed for forming an information array of experimental data and numerical assessment of uncertainties. The heat exchange processes for the condensation column (CC) and low-temperature evaporators (LTE) included in the TCSC, based on which equations were determined for calculating the heat transfer coefficients, heat transfer and ammonia concentration in the circulating gas at the outlet of the separation part of the CC. It has been shown that, unlike the well-known equations, these equations take into account the condensation thermal resistance in the heat exchange process and the external material and thermal load on the CC. The synthesis of the instrumental and technological design of the TCSC was carried out only with the use of heat-using absorption-refrigeration and steam ejector units, the operation of which is ensured by the utilisation of low (up to 150°C) and ultra-low (up to 90°C) temperature potential of the heat of material flows of the ammonia synthesis unit. The efficiency indicators for the created optimal structure of the TCSC in terms of reducing the total cooling capacity, specific energy consumption of electricity and natural gas, which are 2.66 MW, 60 kW·h/t NH^3 and 1.2 m^3/t NH^3, respectively, have been determined.

Based on the results of mathematical modelling, the dependencies of the evaporator heat exchange efficiency indicators on changes in the phlegm flow control action and the coordinates of the external disturbance vector have been determined. Among these indicators, the following should be highlighted: heat flows, cooling capacity, cooling temperature of the central heating system, temperature head, and heat transfer coefficients. A pattern of extreme dependence of cooling capacity and cooling temperature of the refrigerant on the phlegm flow rate has been established, an increase in which leads to an increase in the temperature head of the evaporator. Achieving maximum cooling capacity, and therefore minimum cooling temperature of the central heating system at a certain temperature head, is determined by the critical regime of bubble boiling of the refrigerant. A further increase in temperature head with an increase in phlegm

flow contributes to the establishment of a transitional boiling regime. This regime is characterised by the appearance of "dry" areas on the heating surface, which leads to a decrease in the effective heat exchange surface, cooling capacity and an increase in the cooling temperature of the central heating system. The obtained dependencies of the cooling temperature of the refrigerant on the control action of the phlegm flow rate characterise the shift of the extreme under conditions of changing values of the disturbance vector coordinates, and, consequently, the change in the energy efficiency indicators of ammonia production (annual natural gas consumption) when changing the disturbance vector coordinates.

Algorithmic support has been developed to solve the problems of identification, obtaining a mathematical model of the HTV evaporator and numerical estimation of the optimal state vector (cooling temperature of the central heating system). The use of the algorithm implemented in the MATLAB package provides a real-time solution to the optimisation problem using a step-type non-gradient method with the application of one-dimensional extremum search methods. The technical structure of a computer-integrated system for optimal software control of the temperature regime of a low-temperature evaporator has been determined, which is adapted to the existing information system of an industrial ammonia synthesis unit.

The scientific results obtained develop the field of knowledge on the creation of energy-efficient technological cooling systems through the utilisation of heat with ultra-low temperature potential and adaptive systems for optimal software control under uncertainty.

REFERENCES

1. Heidlage, M., Pfromm, P. H. (2015). Novel Thermochemical Synthesis of Ammonia and Syngas from Natural Gas. 2015 AIChE Annual Meeting Proceedings, 517b. Available at: https://proceedings.aiche.org/conferences/aiche-annual-meeting/2015/proceeding/paper/517b-novel-thermochemical-synthesis-ammonia-and-syngas-natural-gas
2. Dawson, C. J., Hilton, J. (2011). Fertiliser availability in a resource-limited world: Production and recycling of nitrogen and phosphorus. Food Policy, 36 (1), 14–22. https://doi.org/10.1016/j.foodpol.2010.11.012
3. Dybkjær, I. (2013). 100 Years of Ammonia Synthesis Technology. Ammonia Technical Manual, 101–109. Available at: https://www.scribd.com/document/478848969/011
4. Noelker, D. K., Ruether, J. (2011). Low Energy Consumption Ammonia Production: Baseline Energy Consumption, Options for Energy Optimization. Nitrogen + Syngas Conference 2011, Duesseldorf 14.
5. Singh, U., Singh, S., Malhotra, A. (2010). Successful Operating Experience of CFCL Ammonia Plant Revamped with KBR KRES Technology. Ammonia plant safety (and related facilities). Safety in ammonia plants & related facilities symposium, 121–130.
6. Rouwenhorst, K. (2024). Technology options for low-emission ammonia production from gas. Ammonia Energy Association. Available at: https://ammoniaenergy.org/articles/technology-options-for-low-emission-ammonia-production-from-gas/
7. Mishra, R. S., Dwivedi, A., Ahmad, S. (2017). A thermodynamic analysis of ejector type vapour refrigeration system using eco-friendly refrigerants. International Journal of Research in Engineering and

Innovation, 1 (2), 40–48. Available at: https://ijrei.com/assets/frontend/aviation/[6]%20IJREI_vol-1,%20Issue-2.pdf

8. Babichenko, A. K., Toshynskyi, V. I. (2009). Zastosuvannia matematychnoho modeliuvannia dlia diahnostyky pokaznykiv efektyvnosti protsesiv teplo-i masoobminu v absorberakh teplovykorystuiuchykh kholodylnykh ustanovok ahrehativ syntezu amiaku. Voprosy khymyy y khymycheskoi tekhnolohyy, 6, 107–111.
9. Ladaniuk, A. P. (2015). Suchasni metody avtomatyzatsii tekhnolohichnykh obiektiv. Intehral Lohistyk Ukraina, 408.
10. Wu, H., Wang, W., Ye, H. (2015). Robust state estimation for linear systems with parametric uncertainties and quantised measurements. International Journal of Systems Science, 46 (3), 526–534. https://doi.org/10.1080/00207721.2013.807387
11. Fronk, B. M., Garimella, S. (2016). Condensation of ammonia and high-temperature-glide ammonia/water zeotropic mixtures in minichannels – Part I: Measurements. International Journal of Heat and Mass Transfer, 101, 1343–1356. https://doi.org/10.1016/j.ijheatmasstransfer.2016.05.049
12. Malyshev, V. V., Krietov, V. V., Hladka, T. M. Tekhnichna termodynamika ta teploperedacha. Universytet "Ukraina", 257.
13. Chen H. F., Zhang J.-F. (1990). Stochastic Adaptive Control for ARMAX Systems with Unknown Orders, Time-Delay and Coefficients. IFAC Proceedings Volumes, 23 (8 (2)), 267–272. https://doi.org/10.1016/S1474-6670(17)52019-4
14. Ladaniuk, A. P., Reshetiuk, V. M., Kyshenko, V. D., Smitiukh, Ya. V. (2014). Innovatsiini tekhnolohii v upravlinni skladnymy biotekhnolohichnymy obiektamy ahropromyslovoho kompleksu. Tsentr uchbovoi literatury, 280.
15. Brandt, S. (2014). Data Analysis: Statistical and Computational Methods for Scientists and Engineers. Springer, 523.
16. Babichenko, A., Velma, V., Babichenko, J., Kravchenko, Y., Krasnikov, I. (2017). System analysis of the secondary condensation unit in the context of improving energy efficiency of ammonia production. Eastern-European Journal of Enterprise Technologies, 2 (6 (86)), 18–26. https://doi.org/10.15587/1729-4061.2017.96464
17. Babichenko, A. K., Podustov, M. O., Kravchenko, Y. O., Babichenko, Y. A. (2019). Formation of the information array of the identifier of the adaptive control system of the ammonia production condensation unit with uncertainties. Bulletin of the National Technical University "KhPI" A series of "Information and Modeling", 13 (1338), 24–32. Available at: http://pim.khpi.edu.ua/article/view/2411-0558.2019.13.03
18. Mendenhall, W., Sincich, T. (2002). A Second Course in Statistics: Regression Analysis. Prentice Hall, 880.
19. Babichenko, A., Babichenko, J., Kravchenko, Y., Velma, S., Krasnikov, I., Lysachenko, I. (2018). Identification of heat exchange process in the evaporators of absorption refrigerating units under conditions of uncertainty. Eastern-European Journal of Enterprise Technologies, 1 (2 (91)), 21–29. https://doi.org/10.15587/1729-4061.2018.121711
20. Babichenko, A. K. (2010). Zakonomirnosti teploobminu v protsesi kondensatsii amiaku z tsyrkuliatsionoho hazu u vyparnykakh ahrehativ syntezu. Intehrovani tekhnolohii ta enerhozberezhennia, 1, 47–51.

21. Babichenko, A. K., Podustov, M. O., Kravchenko, Ya. O. (2018). Systemnyi pidkhid shchodo stvorennia optymalnoi struktury ta systemy upravlinnia tekhnolohichnoho kompleksu vtorynnoi kondensatsii vyrobnytstva amiaku. Proceedings of the 8th International Conference Science and society, 145—-155.
22. Babichenko, A. K., Toshynskii, V. I., Krasnikov, I. L., Podustov, M. A. (2007). Enerhosberehaiushchee tekhnolohycheskoe oformlenye bloka vtorychnoi kondensatsyy krupnotonnazhnykh ahrehatoa synteza ammyaka. Intehrovani tekhnolohii ta enerhozberezhennia, 4, 3—6.
23. Garimella, S., Mostafa, S., Sheldon, M. (2012). Ammonia-water desorption in flooded columns. Georgia Institute of Technology, 148.
24. Shukla, A., Mishra, A., Shukla, D., 4Karan Chauhan, K. (2015). C.O.P derivation and thermodynamic calculation of ammonia-water vapor absorption refrigeration system. International Journal of Mechanical Engineering and Technology, 6 (5), 72—81. Available at: https://iaeme.com/MasterAdmin/Journal_uploads/IJMET/VOLUME_6_ISSUE_5/IJMET_06_05_010.pdf
25. Lutska, N. M., Ladaniuk, A. P. (2016). Optymalni ta robastni systemy keruvannia tekhnolohichnymy obiektamy. Lira-K, 288.
26. Babichenko, A., Kravchenko, Y., Babichenko, J., Krasnikov, I., Lysachenko, I., Velma, V. (2018). Algorithmic tools for optimizing the temperature regime of evaporator at absorption-refrigeration units of ammonia production. Eastern-European Journal of Enterprise Technologies, 4 (2 (94)), 29—35. https://doi.org/10.15587/1729-4061.2018.139633
27. Çengel, Y. A. (2007). Introduction to Thermodynamics and Heat Transfer. McGraw-Hill, 922.
28. Hare, W., Nutini, J., Tesfamariam, S. (2013). A survey of non-gradient optimization methods in structural engineering. Advances in Engineering Software, 59, 19—28. https://doi.org/10.1016/j.advengsoft.2013.03.001
29. Ravindran, A., Ragsdell, K. M., Reklaitis, G. V. (2006). Engineering Optimization: Methods and Applications. John Wiley & Sons, 667. https://doi.10.1002/9780470117811
30. Sharma, K. L. S. (2016). Overview of industrial process automation. Elsevier, 492.
31. Pacaux-Lemoine, M.-P., Trentesaux, D., Zambrano Rey, G., Millot. P. (2017). Designing intelligent manufacturing systems through Human-Machine Cooperation principles: A human-centered approach. Computers & Industrial Engineering, 111, 581—595. https://doi.10.1016/j.cie.2017.05.0201814

DOI: 10.15587/978-617-8360-19-1.CH2

Valerii Samsonkin, Valerii Druz, Oksana Yurchenko

CHAPTER 2

MANAGEMENT OF TRANSPORT SYSTEMS AND PROCESSES BASED ON A UNIFIED THEORY OF SELF-ORGANIZING SYSTEMS

ABSTRACT

A comprehensive analysis of processes and control systems in railway transport is presented with an emphasis on their synthesis, modeling and optimization.

Modern approaches to the synthesis, modeling and optimization of processes and control systems in railway transport are revealed. The central place is occupied by the Unified Theory of Self-Organizing Systems, which is used as a methodological basis for the study of complex technical and organizational objects in interaction with the environment. Based on this concept, the Method for Detecting Hidden Statistical Patterns (MDHSP) is proposed, aimed at finding "bottlenecks" in the functioning of transport systems and processes.

The key categories of management are considered — norm, tolerance, system approach, cause-and-effect relationships, which determine new principles for assessing and predicting the state of transport systems. Special attention is paid to the practical application of MDHSP in the field of train safety management, technical condition of infrastructure and organization of the transportation process. It is shown that the use of negative statistics (accidents, failures, failures) as a basis for analysis allows to identify the underlying prerequisites of problems and to form preventive and strategic management solutions.

KEYWORDS

Processes and control systems, modeling systems, railway transport, transport technologies, transport process management, tolerance, statistical regularity, norm of behavior of the system "bottleneck".

The concept of a unified theory of self-organizing systems (UTSS) was to generalize the achievements of the problem of self-organization in various fields of knowledge and to solve gaps, that is, "unresolved issues". The concept of self-organization has been known for quite some time. The peculiarities of studying this concept are that self-organization has become the subject of consideration of many sciences: biology, physiology, physics, systems theory, cybernetics, etc. This led to terminological confusion: the same concepts were defined differently, and vice versa — different concepts were sometimes defined the same way. And language and terminological barriers do not allow the use of achievements in related fields of knowledge.

A systematic "rediscovery" of the same laws, or general principles, has been observed.

The phenomenon of self-organization has remained one of the most mysterious mysteries of nature for many centuries. The diversity of functioning and development of highly organized systems gives reason to believe in the existence of a certain universal mechanism of self-organization. The problem of self-organization is multidisciplinary, that is, it is studied by a number of sciences about living nature, natural and technical sciences. The achievements of biology, physiology, physics, cybernetics, systems theories, synergetics, psychology and other sciences made it possible to highlight the main principles of the process of self-organization within each of them.

By the middle of the twentieth century, generalizing theories of the process of self-organization had developed independently of each other. Despite different approaches to the integration of scientific knowledge at the crossroads of sciences, they successfully complemented each other, practically preparing the basis for building a single theory of self-organization of developing systems. Of particular importance in the integration of scientific knowledge were the works of A. Poincaré, L. von Bertalanffy, P. Anokhin, K. Shannon, L. Zadeh, G. Hacken, I. Prigozhin, J. von Neumann, E. Bauer, E. Schrödinger and others.

Fundamentally new was L. Zadeh's justification of the general theory of self-organization as fuzzy spaces and the introduction of the corresponding measure of uncertainty [1]. In the last quarter of the 20th century, the works of V. Druz and V. Samsonkin comprehensively considered the representation of the norm of self-organization processes, developed the theory of tolerant spaces, and established the connection between the level of tolerance and the possible complexity of developing self-organized systems [2]. At the beginning of the 21st century, they also established the nature of the construction of characteristic semantic spaces with the introduction of a single measure of partial interdependence of functional activity and the viability of the integral complex "functional system — environment". All this in general opened a fundamentally new approach to solving many practical problems that were inaccessible when using classical research methods.

2.1 TERMINOLOGY AND INTERPRETATION IN THE FIELD OF TRANSPORT TECHNOLOGIES, PROCESSES AND SYSTEMS

Railway transport is one of the key elements of the transport system, ensuring the efficient transportation of passengers and cargo over long distances. Its reliability, safety and environmental friendliness make it indispensable in modern conditions of integration of transport networks. Important aspects of the functioning of railway transport are technologies, processes and systems that affect the quality and efficiency of transportation.

The chapter examines the main concepts and terminology related to transport technologies, processes and systems, as well as their interconnections. In particular, such key categories as management, control, monitoring, modeling, simulation and others that play an important role in the development of the railway industry are analyzed.

Management is a generalized concept that encompasses the processes of decision-making, organization, coordination and control to achieve certain goals in transport systems.

Management is an action in the meaning of "to manage"; an administrative institution or department in charge of a certain field of activity [3].

Management is an action in the meaning of "to manage"; administrative institution or department in charge of a certain field of activity; control [4].

Control is a component of management and involves the practical implementation of management decisions by regulating the operation of objects and processes. Control is an action with the meaning of "to control"; leadership; a system or set of devices with the help of which machines, mechanisms, etc. are controlled [5].

Management reflects the strategic aspect of management, which includes analysis, planning, organization, motivation and control of resources in order to increase the efficiency of the transport system. Management is a set of principles, methods, means and forms of production management in order to increase its efficiency and increase profits [6].

Management is a concept used mainly to characterize the processes of management of economic organizations (enterprises). Management — in part 1, a set of principles, methods, means and forms of production management in order to increase its efficiency and increase profits. Management in socio-economic systems; distinguish between general and special management functions; General functions include forecasting and planning, organization, coordination, motivation (stimulation), accounting and analysis, control; special management functions are in principle the same as general ones, but only in a certain (special) field of activity: in the field of circulation, supply, sales, production preparation, production maintenance, etc. [7].

Control is the process of checking the compliance of performed actions with established norms, standards or plans with the possibility of adjustment.

Monitoring is the set of methods used to obtain information on the effectiveness of implementing various activities and the level of achievement of planned results [8].

Bottleneck is a basic concept of the unified theory of self-organizing systems and, accordingly, the Method of detecting hidden statistical patterns. The concept of "bottleneck" in this study is a synonym for a problematic place in the functioning of a management object, or more precisely, the dialectical unity of "object-environment", because the management object (technical means, process, organization) should definitely be considered in unity and interdependence with the surrounding environment.

Reliability theory states that in order to increase the reliability of the functioning of a management object, attention should be paid to the least reliable chain, that is, the bottleneck.

The bottleneck of an organizational structure is the place of maximum resource consumption (material and technical, financial, intellectual) to maintain a stable equilibrium of the functioning of this structure. Recognition of the unity of the laws of development management requires the establishment of the most general system-forming principles regardless of the specific system and specific environment. The principle of bottleneck is one of the system-forming principles.

The principle of bottleneck is considered in conjunction with the principle of least action, which contribute to the selection of the most rational way to achieve the final result of the activity of the management object.

The principle of least action reveals a general law for nature — the desire to ensure functioning in a specific environment with minimal resource expenditure. Dialectically, the principle of least action is related

to the principle of bottleneck, which indicates the need to maximize the expenditure of resources on a problematic (narrow) city in order to maintain the equilibrium stability of the system.

Gaps are information that has not been disclosed in other studies and is disclosed in this one.

Identifying research gaps is an important step in developing knowledge and solving real-world problems. Typically, gaps are identified by examining and analyzing information sources. To do this effectively, several strategies can be used:

1) *thematic analysis* involves organizing existing research findings into topics, allowing for a comprehensive assessment of the literature. By analyzing the extent to which each topic is covered, researchers can identify areas that have received minimal attention or limited research. This approach illuminates "blind spots" in the field, paving the way for new inquiries;

2) *methodological critique* focuses on assessing whether the methodologies used in the current study are sufficiently robust to address key questions or address important problems. This strategy often reveals weaknesses in experimental designs, sampling methods, or analytical tools, offering opportunities for innovation and improvement;

3) *trends* are fertile ground for identifying research gaps. Rapid changes in technology, regulations and environmental conditions create new challenges and opportunities. For example, areas such as the application of artificial intelligence in railway systems or the development of sustainable materials for construction may not yet have been widely explored, leaving a rich field for research;

4) *practical implications* to check whether existing research effectively addresses real-world problems, especially those faced by industries. This includes checking whether research meets the practical needs of industries such as transport or construction, in terms of safety, efficiency and compliance with standards such as CENELEC (European Committee for Electrotechnical Standardization) and TSI (Technical Specifications for Interoperability). Research that bridges the gap between theory and practice is invaluable in promoting innovation and ensuring compliance with regulatory requirements.

A *system* is an order resulting from the correct, planned arrangement and interconnection of parts of something [9].

System — a set of any elements, units, parts, united by a common feature or purpose [10].

A *systems approach* — a methodological approach to the study of objects as systems, which takes into account the relationships between the constituent elements, their hierarchy and integrity [11].

A *systems approach* — a method of studying complex objects by analyzing them as systems, which involves studying the structure, functions, relationships and integrity [12].

System analysis — a set of methodological tools used to prepare and justify solutions to complex economic problems [13].

System analysis — one of the most important means of finding solutions and understanding the problems of social life. It implements the systems approach — the principle of comprehensive study and research of reality — common to any systems of objects: "input", "process", "output", "goal", "feedback", "growth", "interaction", etc. [14].

Model — a reproduction, image, description or imitation of a certain phenomenon, process or object [15].

Modelling is a method of studying objects, processes or phenomena by creating and analyzing their models. This approach allows studying the characteristics and behavior of complex systems using their simplified representations [16].

Model — a simplified representation of a real system or process in the form of mathematical, graphical or physical structures [16].

Modelling is the process of creating and analyzing models to study the characteristics of a system [16].

Simulation is a research method that involves experimentally reproducing the behavior of a system based on its model [16].

Imitation is the reproduction of the functioning of a system in artificial conditions to assess its parameters and optimize solutions [16].

Transport technologies are a set of methods, tools and instruments used to ensure the effective functioning of railway transportation [17].

Transport processes are a sequence of actions aimed at performing transportation, maintaining infrastructure, and managing logistics flows [18].

Thus, the above concepts are basic for the analysis of transport technologies, processes, and systems, as well as for further research into methods for improving the efficiency of rail transport.

2.2 A METHOD FOR DETECTING HIDDEN STATISTICAL PATTERNS IN TRAFFIC MANAGEMENT

Basic terms of the Method for Detecting Hidden Statistical Patterns (MDHSP):

— *system* — any control object (technological process, function, workplace, organizational structure), which is considered in interaction and unity with the environment;

— *final result* — the goal and system-forming factor of the system. In practice, it is one of the parameters of the system's activity, an indicator of the system's state. Its dynamics is a criterion for the similarity of different system states;

— *bottleneck* — the most problematic place in the system's activity, as well as the area of maximum resource consumption to maintain the system's equilibrium stability;

— *norm* in the sense of functional optimum — stereotypical (most probable) behavior of the system;

— *control parameter* — a fixed statistical indicator of the system's activity;

— *statistical pattern* — a trend or a clear tendency in the gradual dynamics of statistical indicators that describe the activity of the railway system;

— *classifier*. Classification — the division of objects (phenomena and concepts) into classes or categories depending on their general characteristics. A classifier is a systematic list in which it is convenient to find a description of each object or phenomenon.

The MDHSP is a multidisciplinary theory that logically follows from the Unified Theory of Self-Organizing Systems.

Fig. 2.1 shows the scientific directions that became the MDHSP basis.

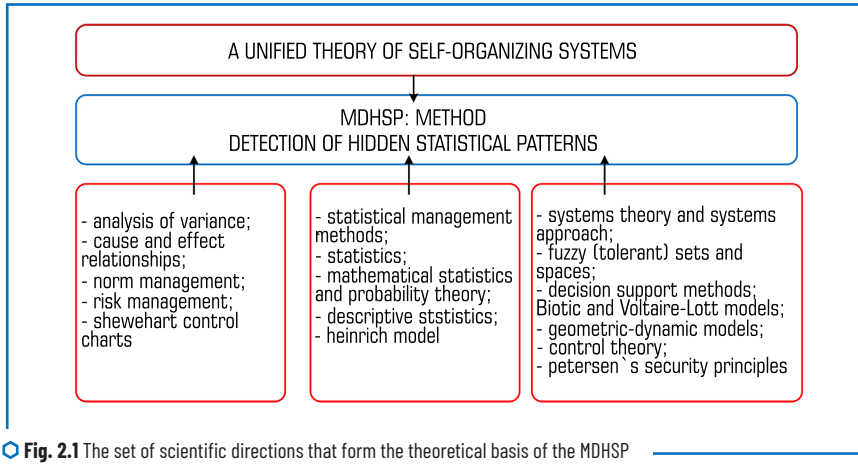

Fig. 2.1 The set of scientific directions that form the theoretical basis of the MDHSP
Source: [2]

2.3 THE CONCEPT AND KEY PRINCIPLES OF THE MDHSP

The MDHSP conducts a search for hidden patterns in the activities of a management object, whether it is an organization as a whole, a structural unit of an organization or even an individual person, a technological process or function.

Regardless of the scale, all these objects (organization, unit, person, process, function, etc.) are considered as a holistic system in *interaction and interconnection with the environment*. The environment can be classified as internal or working (the closest environment) and the general environment (natural and social).

In this chapter, terms with the root "statistics" are often used. Therefore, let's provide its definition. Statistics is a multifaceted concept that includes:

— a branch of social sciences that aims to collect, organize, analyze and compare facts related to a wide variety of mass phenomena;

— a system of indicators;

— a tool for establishing specific patterns;

— numerical/digital data.

— statistical methods used in the collection, presentation, analysis and interpretation of data.

Statistical regularity — the most important category of statistics, which is considered as a quantitative regularity of changes in space and time of mass phenomena and processes of life, consisting of many elements (units or parameters of the set). It is inherent not to individual units of the set, but to the entire set as a whole. For this reason, the regularity is revealed with a sufficiently large number of observations and only on average. Thus, this is an average regularity of mass phenomena and processes. These regularities

arise as a result of the influence of a large number of constantly acting and random causes. Statistical regularities provide researchers with invaluable typical values, which are most often devoid of specificity. But it is known that any general concept is abstract and therefore devoid of specificity: it contains essential features of a class of objects, and the insignificant, which characterizes the single, individual, is not included in it [14].

Thus, a statistical regularity is an objective quantitative regularity of a mass process. It arises as a result of the action of objective laws, expressing causal relationships.

The regularities of the system's behavior allow to establish its state, shortcomings in its functioning, or to confirm its relevance. Therefore, establishing the regularities of behavior is a key stage in system management. These things are obvious, but regularities do not lie on the surface; it is necessary to detect them and prove their reality.

Let's evaluate the behavior of the system by a control parameter. The control parameter is a parameter of the final result, and the final result is considered in the sense of the theory of a functional system [19].

There may be several such control parameters. But let's choose that:

a) depend on the activity of most of the system elements that determine its functionality;

b) change in different periods of supervision, that is, they are not constant, and have a fairly wide range of quantitative manifestation;

c) have methods and means of objective measurement and recording of values over time in the form of statistics, which should preferably be approved by relevant documents in order to be mandatory for the system personnel.

Any control parameter that corresponds to points (a)–(c) can reveal patterns, provided that there is an appropriate amount of statistics. Therefore, in practice, the number of control parameters should be minimal, preferably one. This simplifies the management process and eliminates contradictions in the dynamics of control parameters if there are more than one.

It should be emphasized that the Method belongs to a widespread group of *statistical management methods*. Accordingly, it should be said about the need for the reliability of control parameter statistics. But this fact is not a limitation on the application of the Method, because in most organizations there is a fairly strict responsibility for providing false statistics at both the corporate and state levels.

MDHSP is a theoretical justification for making effective decisions to control functions, processes and structures of systems.

And one more characteristic: MDHSP is a *systems approach*. The concept of a systems approach has been used more and more often in recent years when they want to emphasize the complexity of the task or the complexity of its solution. Analytical methods for managing complex systems that have existed for a long time are ineffective. This is especially true for the tasks of managing production and social systems, given its high responsibility.

The application of a systems approach today is mainly reduced to terminology, the presentation of system elements and their relationships, the declaration of the concept of "dimensionality", mathematical models with simplified implementation conditions. What is missing here? Specifics!

The proposed MDHSP is based on formalized procedures and measurable concepts. It began to be created almost 25 years ago to solve the task of managing traffic safety on the railway transport of Ukraine. The first version of the method was published 20 years ago [20]. Later it became obvious that the established principles, procedures, models and concepts can be used to manage almost any system or function.

The system approach is the opposite of system analysis. The analytical approach studies a separate component of the system, determines its characteristics and management parameters that are effective specifically for this structural subsystem. But this may not correspond to the effective management of the system as a whole. The key principles of MDHSP are given below:

1. Signs of the definition of "bottlenecks".

Having considered the principles of self-organization, one of them can be distinguished – the principle of the bottleneck, which was considered with the principle of least action. Bottlenecks are the most problematic places or places of maximum resource consumption to maintain the stability and safety of its transportation process.

This concept seems to be clear, but how to determine the bottleneck in the statistics of the final outcome parameter. Three signs of a bottleneck are proposed.

Sign 1 – "outlier" (**Fig. 2.2**) of the control parameters for the observation period.

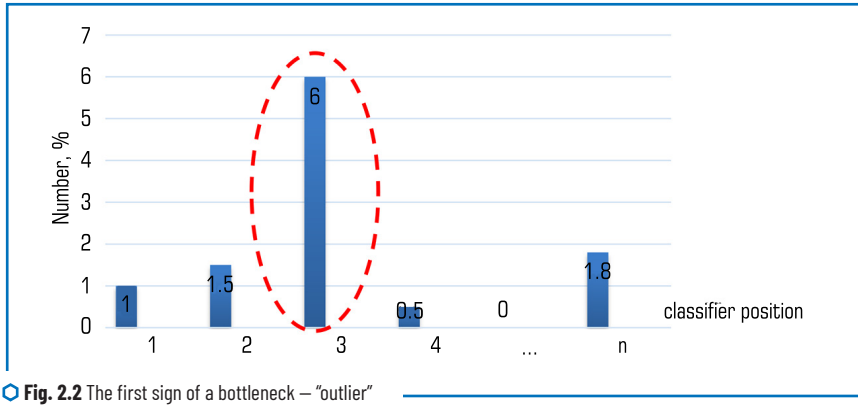

Fig. 2.2 The first sign of a bottleneck – "outlier"

The red line in **Fig. 2.2** indicates the "bottleneck" of the first sign, *n* – the number of elements of the statistical parameter.

Sign 2 – "negative trend" of the dynamics (or time series) of changes in the control parameter being analyzed in adjacent time periods. This sign is shown graphically in **Fig. 2.3**.

Sign 3. If, based on the graphical representation of the statistics of control parameters, a uniform manifestation is observed (i.e., there is no pronounced bottleneck according to Signs 1 and 2) – **Fig. 2.4**, then the sources of improvement of the situation should be sought in the plane of organization of the technological process as a whole.

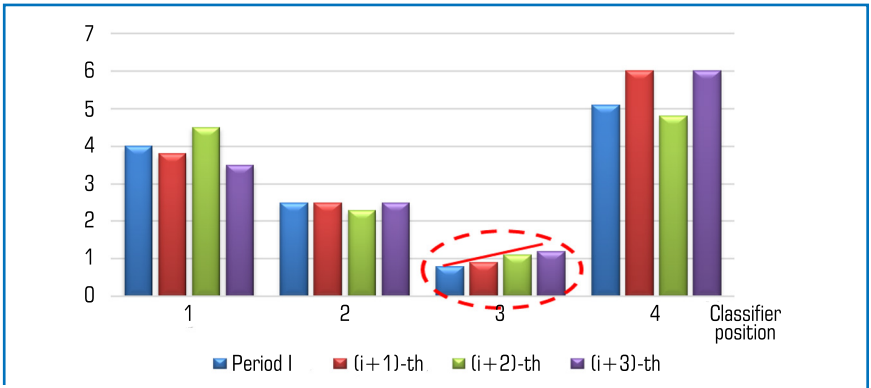

Fig. 2.3 The second sign of a bottleneck – "negative trend" – is marked with a red line for four observation time periods

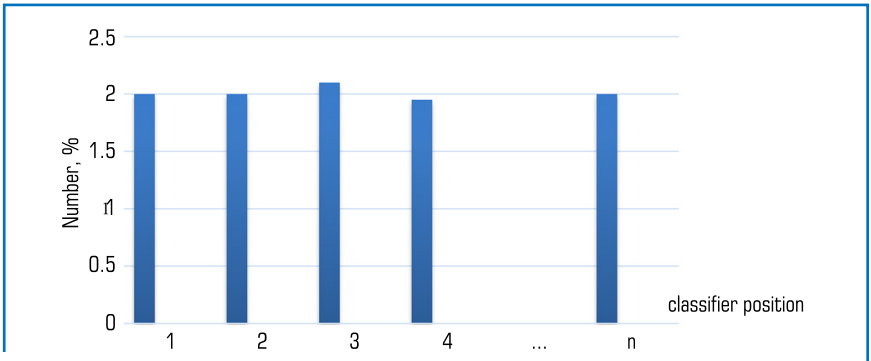

Fig. 2.4 Uniform manifestation of components of the control parameter classifier

There may be several "bottlenecks".

2. Systematization of control parameter statistics.

The problem of using statistical methods is the verbal way of presenting statistics as in the relevant sources of information. Therefore, to use statistical management methods, verbal information must be systematized or formalized.

Statistical data that characterize the final result of the company's activities are quite diverse and their volume is large. For example, the activities of railway transport in Ukraine are characterized by 53 parameters, and taking into account subparameters (components of the parameter) – 114 [21]. These are: volumetric, qualitative, technical, technological indicators that characterize types of transportation, rolling stock indicators, personnel, wages, train delays, etc. All these statistics are approved by regulatory data.

As mentioned above, the MDHSP was initially developed for railway traffic safety management, based on a specific problem that was formulated by the management of the railway company of Ukraine [20]. Therefore, the initial information of the Method used indicators of traffic safety violations (transport incidents/technical failures/delays, etc.), which are found in various sources of information in paper/electronic form in different divisions of the company. That is, negative information about the state of train traffic safety, which related to violations of transportation regulations, was selected as statistics. The reason for the negative information is explained by several thoughts:

– when everything is going well, personnel rarely think about shortcomings and bottlenecks;

– when investigating transport incidents, the circumstances, causes, compliance with service technology, personnel actions, etc. are usually comprehensively studied. And here it is possible to identify hidden shortcomings and shortcomings;

– transport incident statistics are the basis for analyzing the state of traffic safety in railway companies of Ukraine, the EU and many others.

– the statistics that exist in the organization under study are used.

Thus, statistics were used that characterize the negative side of the train traffic safety function, that is, negative statistics. And why negative? Was it possible to use positive statistics? The authors believe that no. Firstly, because companies do not keep statistics of positive actions, because there are a lot of them; secondly, positive statistics are the implementation of technical and technological regulations. That is, it should be so, and such information is of no interest for process management. Thirdly, there is no point in wasting personnel time if everything is going correctly. Thus, it is worth concluding that the initial information for the MDHSP should be statistics of various kinds of failures and violations.

It is proposed to systematize each failure or violation recorded in the statistics of the control parameter in the form of answers to nine questions or in the space of nine parameters (**Fig. 2.5**).

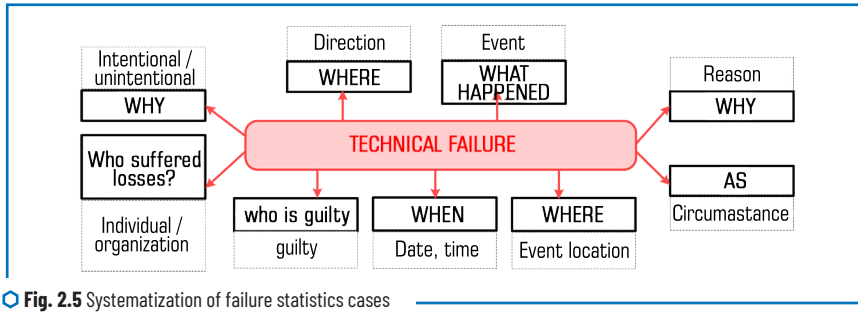

Fig. 2.5 Systematization of failure statistics cases

The parameter "*WHAT happened*" characterizes the event according to the existing classifier and consequences. The geographical location of the event (station, section, section) is assessed by the parameter "*WHERE*". The parameter "*WHEN*" reveals the time of the event. Circumstances ("*HOW*") contain a qualitative characteristic of the event: information about the train (train number, number of cars, tonnage,

number of axles), locomotive, cars, weather conditions, rolling stock condition, infrastructure condition, compliance with load requirements, personnel health, etc. Depending on the technological management process, the characteristics of the circumstances that are necessary can be selected. The parameter "*WHY*" is a possible cause or causes of the event. "*WHO*" is the culprit or violator. The answer to the question "*WHY*" should explain the intentionality or accidental nature of the event. The parameter "*WHO*" should contain information about the targeted nature of the damage. "*WHERE*" is the direction of movement.

3. Identification of patterns.

It is carried out by graphically constructing and further analyzing the following dependencies:

a) dynamics of individual systematization parameters WHAT, WHERE, WHEN, ... in time;

b) variations of the components of nine parameters in time;

c) in the space of two and three systematization parameters (for example, WHAT — WHERE, WHY — WHEN, WHAT — WHO — WHERE, ...).

Different patterns are possible, but in most cases, let's mean patterns that reveal bottlenecks of the type **Fig. 2.2–2.4**. Because it is the bottleneck principle that is the criterion for choosing effective management decisions.

4. Expansion of the formula of causal relationships to four points.

Usually, in the analysis of causal relationships of technological process violations, three points are distinguished: consequences, events, causes. Therefore, identifying the *causes* of violations and, accordingly, the culprit is often the main task of investigating violations of the technological process regulations or management functions. In this case, the *event* is defined clearly: it is classified by *consequences*, that is, the degree of losses from the violation. The cause is revealed as a result of the investigation [22].

The determination of the specific formulation of consequences, events and causes is carried out according to existing classifiers:

— consequences classifier, which determines losses for people (company personnel, users, third parties), the material and technical base of the enterprise, the environment;

— event classifier, which consists of points according to losses, for example: catastrophe, accident, incident for the safety of railway transport. For other types of transport, the event classifier is similar;

— the classifier of causes is either officially approved, as in the EU, or actually exists for individual farms, owners, and those involved.

But in fact, the causes are defined as the last previous event and belong to the space of technological parameters. And therefore, they are random in nature. In order to effectively prevent process violations, it is proposed to introduce a fourth point into the cause-effect relationships: the *prerequisite* of the cause, or the basic cause. The prerequisite lies in the space of organizational support of technological processes. Organizational support is such concepts as personnel selection and training, repair facilities, supply, working and leisure conditions, production culture, management, etc. Organizational support is accumulated for more than one year, it is a function of the company's management system, and it is quite conservative. Causes arise due to shortcomings in the organizational support of technological processes. To prevent negative events, changes should be made to the organizational support, that is, the prerequisites. Accordingly, a classifier of prerequisites is being developed.

Thus, there are *four classifiers*: *losses or consequences, events, causes and preconditions*, the mechanism of interaction of which is shown in **Fig. 2.6**. Each classifier consists of the corresponding elements: *n* preconditions, *m* causes, *i* events and five consequences. As is known, it is by consequences that transport events on modes of transport are classified. The elements of the classifier of consequences are generalized from the classifiers of modes of transport and do not belong to any official document.

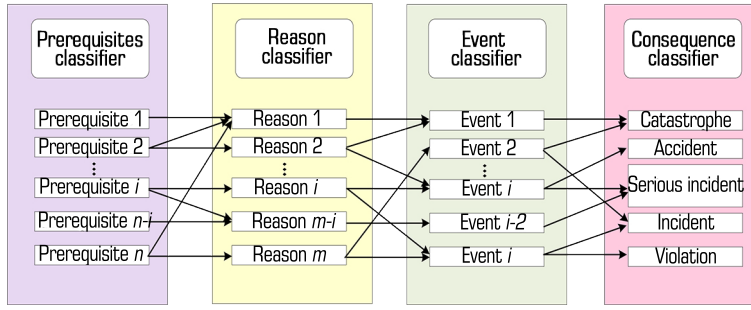

Fig. 2.6 Interaction of cause-and-effect classifiers for transport events

The presence of an arrow in **Fig. 2.6** indicates the corresponding connection. It is known that there is no mutual unambiguous connection between, for example, causes and events. Therefore, for example, event 1 can have two causes: 1 and 2. The *n*-th element of the prerequisite classifier can precede causes *m* and 1.

By the way, the prerequisite or basic cause as a guess is present in various theoretical approaches to process safety management, including D. Petersen's theory, EU railway safety regulations.

5. Tolerance.

Tolerance is understood in the sense of "indistinctness, inaccuracy, blurriness". Large (or high) tolerance is a wide range of manifestation of the control parameter in the normal zone, or low accuracy. Low tolerance is equivalent to high accuracy and dissimilarity.

The source of tolerance of human-machine systems (HMS) is:

a) human activity, which is characterized by untimeliness, insufficient knowledge of the situation, incompetence, shortcomings in the organization of work, errors, etc.;

b) technical means exhibit insufficient reliability, inaccuracy, failures, etc.;

c) the environment, which is characterized by instability, unfriendliness towards humans, negative impact on humans and technology, the need to adapt the boundaries of the equilibrium state, etc.

In general, any HMS, processing the flow of information by comparing input signals with the formed images, allows for a certain inaccuracy. In practice, this inaccuracy should increase as the information becomes more complicated. An intuitively obvious assumption: the more vague the information about the controlled process, the less certain the HMS actions should be.

From the point of view of mathematics, the transition from the indefinite concept of "sameness" to a precisely defined type of relationship is accompanied by the introduction of the term "equivalence" [20]. Similarly, the mathematical point of view that corresponds to our intuitive idea of similarity or indistinguishability is called tolerance.

Equivalence on a finite set $A = \{a_1, a_2, \ldots, a_K\}$ will be called a binary relation. The equivalence relation is generally defined on the set A×A and has the following properties:

1) *reflexivity* : $a_i \approx a_i \left(\forall a_i \in A\right)$;

2) *symmetry* : $a_i \approx a_j \Rightarrow a_j = a_i \left(\forall a_i, a_j \in A, i \neq j\right)$;

3) *transitivity* : $a_i \approx a_j, a_j \approx a_k \Rightarrow a_i = a_k \left(\forall a_i, a_j, a_k \in A, i \neq j \neq k\right)$.

"Tolerance" is a binary relation on the set A×A, which has the following properties:

1) *reflexivity* : $a_i \approx a_i \left(\forall a_i \in A\right)$;

2) *symmetry* : $a_i \approx a_j \Rightarrow a_j = a_i \left(\forall a_i, a_j \in A, i \neq j\right)$; (2.1)

3) *NOT transitivity* : $a_i \approx a_j, a_j \approx a_k \overline{\Rightarrow} a_i = a_k$ *at least for one triad* $\left(i, j, k\right)$.

2.4 THE ESSENCE OF THE IDEA AND USE OF THE MDHSP

Three directions of using the MDHSP for system control (processes/functions/structures) can be identified:
1. Identification of the current state of the system.
2. Justification/support of an effective management decision.
3. System control based on the norm of behavior and bottlenecks.
Let's consider both directions.

2.4.1 IDENTIFICATION OF THE CURRENT STATE OF THE SYSTEM BASED ON THE NORM OF ITS FUNCTIONING

The general scheme of this direction is presented in **Fig. 2.7**. Outwardly, it does not differ from the classical formulation of the control and management task. But in order to understand the features of this direction, it is possible to describe the essence of the presented blocks further: *control parameter* – a fixed indicator of the system's activity, officially approved, on which statistics are kept; *state* – system state; *FOpt* – functional optimum of the system's activity (analog of the norm); *PS* – periodic statistics, or current statistics of the control parameter – the number of values for a certain period of time (week/month/year), which is sufficient to identify the system's state.

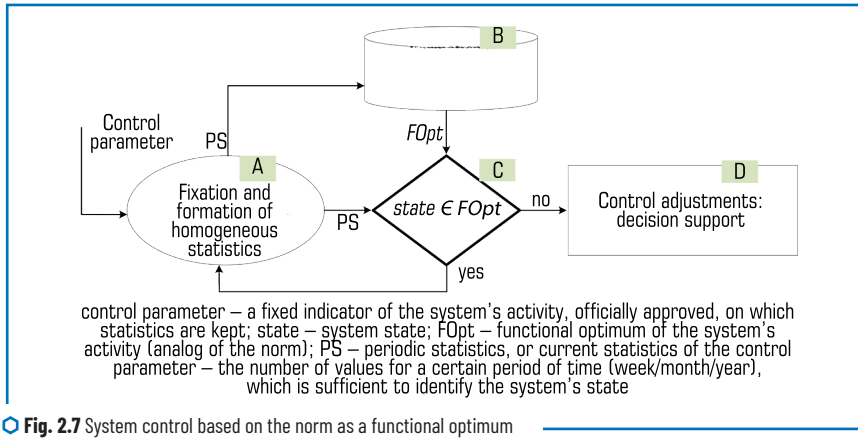

Fig. 2.7 System control based on the norm as a functional optimum

First of all, let's define the terminology. According to [23], the state of a controlled object is understood as the level of activity of its elements in obtaining the final result. It is known that all living systems strive for an equilibrium state, adapting to constant changes in the environment. Equilibrium states are asymptotically stable to weak disturbances (fluctuations). If these fluctuations do not depend on time, then it is possible to speak of a stationary equilibrium state, which characterizes the norm of system behavior. Quantitatively, the state of the system is determined by the numerical value of one or more parameters of the final result of its activity, which it is defined as control parameters.

A few words about the number of control parameters. It is believed that their increase makes the assessment of the state more accurate. However, this is not so. When the environment changes, the range of manifestation increases in some parameters, and decreases in others. The desire to take into account all parameters leads to the expansion of the norm and the inclusion in the list of normal more and more states, which in fact are not such.

If it is about assessing the state of a specific person or the interaction of a specific "human-machine" association, then the ranges of the manifestation of control parameters are individual in nature. Taking into account the adaptive capabilities of the environment leads to a different-vector expansion of the norm in different individuals. The desire to create a general norm for all leads to the need to include in it the manifestation of the control parameters of all individuals. However, this generalized norm for one corresponds to its norm indicators, and for another — not. This is the contradiction of the average statistical norms common in medicine, psychology, technology.

Therefore, the expansion of the norm leads to errors in assessing the state of the system, that is, to its inefficiency. The way out of this problem is often sought in the introduction of an integral indicator in the form of an algebraic sum that combines various parameters with certain weighting factors.

Researchers I. Prigozhin, G. Hacken, A. Dyuldin, V. Druz, and V. Samsonkin have shown that it is possible to consider a minimal number of parameters to describe the final result, and in some cases even

a single parameter. This approach is consistent with the general principles of the π-theorem, as discussed [24]. On the other hand, V. Druz proved that the equipotential value of the final result can be achieved by different participation of the component parameters. Therefore, it is important to have statistics of the behavior of any parameter. By processing this statistic properly, *it is possible to determine the norm of the system behavior using one parameter* in its dynamics.

In fact, the number of control parameters is more than one. It takes a lot of time for people to be convinced of the effectiveness and convenience of just one control parameter.

However, it should be noted that the correct choice of a control parameter is sometimes a non-trivial task. It is necessary to well represent the process or management object. The control parameter must, firstly, be measured, and secondly, vary within fairly wide limits.

And now let's describe the blocks presented in **Fig. 2.7**.

Block A: Fixation and formation of homogeneous statistics.

Each value of the control parameter/parameters is fixed. The sources of fixation are diverse: special journals, databases, computer memory. When using statistical information, there is a need to have a *homogeneous* statistical population. The principle of homogeneity is very important in system control: it is about the homogeneity of information, structure, regulatory and documentary support. The homogeneity of the initial information when controlling the system determines the workability, efficiency, adequacy of management decisions and algorithms. Therefore, it becomes understandable that the management of, for example, railway companies strive for homogeneity (often the sameness) of the structure and regulatory framework of the company's components. Homogeneity is understood at a certain level of tolerance or compliance.

Let's define the concept of *homogeneity of a statistical population*. It is relative and does not mean complete compliance of all units of the population at all, but only implies the proximity of the main property, quality, typicality. The same set of units, for example, can be homogeneous in one characteristic and heterogeneous in another. The homogeneity of units of a statistical set is formed under the influence of certain internal factors and conditions [25].

Let's give an example of the principle of homogeneity of a statistical set, which characterizes the activities of a railway company. When characterizing the activities of a company, much attention is paid to locomotives. But their total number means little. Therefore, locomotives are divided or classified into main and shunting, electric and diesel locomotives, freight and passenger, direct and alternating current. And thus, the categories of freight diesel locomotives, passenger electric AC locomotives, etc. are determined. The purpose of such a classification is to determine homogeneous subsets of locomotives for studying issues of wear, repair base, turnover, load, ..., which will be common to individual subsets of the company's locomotive fleet.

Therefore, at the first stage of system research, attempts are made to make statistical sets homogeneous.

However, it is not always possible to make homogeneous subsets of statistical data by classification. Often, information about violations of the technological process is taken as a control parameter: traffic safety, transportation of dangerous goods, failures and breakdowns of various responsible technical means.

There are classifications of such violations. Taking into account the different consequences of violations, the statistics of the control parameter will not be homogeneous or their classification will lead to small subsets, which will make them unrepresentative.

In this case, various models are used to convert or transform a heterogeneous statistical population into a homogeneous one. This can be done, for example, using the Heinrich model.

Further, depending on the difference in *PS* values in two measurements adjacent in time — the current and previous

$$\delta(t) = PS(t) - PS(t - \Delta t), \tag{2.2}$$

as well as the level of tolerance

$$\Delta = \frac{\max(PS(t)) - \min(PS(t))}{6}, \tag{2.3}$$

the current PS value is added to one of the six sets $M_{-3}, M_{-2}, M_{-1}, M_{+1}, M_{+2}, M_{+3}$. The number six in (2.3) is explained by the "3σ rule" for the Gaussian distribution, meaning 3σ in the positive direction from the center of the distribution of μ and 3σ in the negative direction from μ. Without proof, let's accept the obvious fact that a consecutive series of random *PS* values obeys the Gaussian law. The center of the distribution μ is analogous to the arithmetic mean/mode/median of the Gaussian distribution of the random variable *PS*. Accordingly, the designation of the sets means:

M_{+1} – *the set of PS*(*t*) *values within* $\mu \le \delta(t) \le \mu + \sigma$;

M_{+2} – " ... ... " $\mu + \sigma \langle \delta(t) \le \mu + 2\sigma$;

M_{+3} – " ... ... " $\mu + 2\sigma \langle \delta(t) \le \mu + 3\sigma$;

M_{-1} – " ... ... " $\mu \langle \delta(t) \le \mu - \sigma$;

M_{-2} – " ... ... " $\mu - \sigma \langle \delta(t) \le \mu - 2\sigma$;

M_{-3} – " ... ... " $\mu - 2\sigma \langle \delta(t) \le \mu - 3\sigma$.

The pair $\left(\delta(t), M_j\right)$ *characterizes the current state of the system, i.e.*

$$\delta(t), M_j \equiv state, \tag{2.4}$$

where is defined from (2.2), and j = –1, –2, –3, +1, +2, +3.

Block B: Formation/actualization of the norm.

The term "*norm*" is key in the MDHSP. This concept will be considered in detail below in **Section 2.5**. In the MDHSP, the norm is perceived as a process that determines the optimal mode of functioning of the system, that is, its *functional optimum*. In this concept, the norm is perceived as an interval of optimal functioning of the system with *moving boundaries*. Within these boundaries, optimal communication with the environment and coordinated performance of all system functions are maintained.

The name of the block indicates that the norm is first formed and then constantly updated, theoretically with the appearance at the input of each fixed control parameter or PS. But in fact, the update can be carried out permanently depending on the frequency of receipt of control statistics.

The norm is characterized as the maximum margin of stability of the system. As a deviation from the norm occurs, the system enters a state of tension. At the same time, the variety of compensatory capabilities of the system decreases, and the time of preservation of this particular state is shortened. The reason for this is as follows: an increase in the intensity of the state requires an adequate increase in energy to relieve the tension and transition to the norm. The intensity of the state in which all energy reserves are used to relieve the tension can be taken as the boundary of the functional optimum. After this, irreversible destabilizing processes are observed, which increase with distance from the norm.

By analyzing the location of the norm, it is possible to predict the state of the system and determine its adaptive capabilities. The dependence of the variance of the variation of the control parameter on the functional state allows to consider ***the variance as a criterion for assessing the individual norm and the degree of tension of the system***. This makes the algorithm for controlling the state of the system in the process of continuous activity obvious.

With fatigue, the stability of the system decreases exponentially, the variation of the final result parameter tends to zero. This minimizes the viability of the system.

The norm of the system depends on the environment and therefore changes throughout the life cycle. Since the management object itself and the environment are constantly changing, the norm of the object's behavior should be constantly updated.

Block C: state ∈ FOpt.

The assessment of the equilibrium stability of the system is carried out by comparing the periodic statistics of the control parameter *PS*(*t*) with the norm of the system behavior.

In this case, the norm is considered as a functional optimum (*FOpt*), and the state of the system state is determined from the formula (2.4) described above in block B.

In this case:

— if the state of the system corresponds to the norm (the value of state is inside the surface *FOpt*), then nothing needs to be changed in the system. This is shown by the output "yes" of block C;

— if the state of the system does not correspond to the norm of the behavior of the management object, then changes are necessary in the control of the system (output "no" of block C), and for this purpose a methodology for supporting the management decision has been developed, which will be considered in **Section 2.4.2**.

It should be noted that the discrepancy between the state of the system and the functional optimum *FOpt* may be random: a person was suddenly distracted, equipment failure, etc. Therefore, it is necessary

to make sure that the state of the system has really changed. For additional verification of the reliability of the state deviation from the norm, the authors used the "Shewhart control charts" method [26]. This is possible only if there is no emergency situation (!).

Block D: Control correction: decision-making support.

The essence of this block will be disclosed below in **Section 2.4.2**.

2.4.2 SUBSTANTIATION/SUPPORT OF THE MANAGEMENT DECISION ≡BLOCK D

This direction is devoted to the substantiation or support of the management decision based on the identification of bottlenecks in the operation of the control system. The general scheme of this direction and, accordingly, the previous block D in the form of a separate methodology or sequence of actions is presented in **Fig. 2.8**.

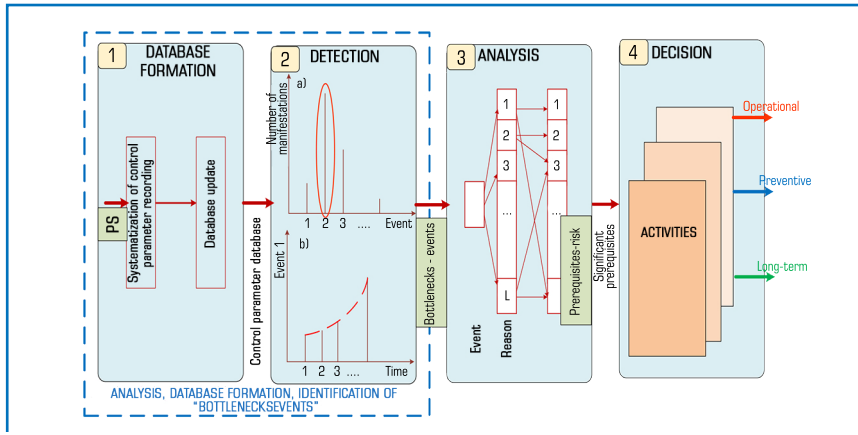

Fig. 2.8 Methodology for substantiating a management decision based on the bottleneck principle

Let's describe the blocks of the methodology in **Fig. 2.8** sequentially.

The input signal of the entire methodology and block 1 is the statistics of the control parameter *PS*(*t*).

Block 1. Formation of the DB.

Systematization of the control parameter record.

As noted above, the control parameter is usually verbal in nature. Even if it can be determined by a number, then in this case it should be specified, for example, date, time, place, classifier item, i.e.

Therefore, for computer analysis of statistics of system performance indicators, each statistical record must be systematized. The key principle "Systematization of statistics of the control parameter" clause 2 of this section suggests systematizing each value of the control parameter in the form of an answer to nine questions:

— WHAT happened — an event that consists in obtaining such a value of the control parameter;

— WHY it happened — the cause of the event;

— HOW it happened — the circumstances of the event;

— WHERE the event took place;

— WHEN the event occurred;

— WHO is responsible for such a value of the control parameter;

— WHO suffered losses or, conversely, income;

— WHY such an event occurred, or a characteristic of the motivation of the responsible person or the structure of the system;

— WHERE — the direction of movement of the process in which the event occurred.

All records of the control parameter are entered into the control parameter database, which consists of nine dimensions and is constantly updated.

By the way, why are there nine questions and, accordingly, nine systematization dimensions? First, nine directions fully describe any event in transport. Second, the sacred Mayan calendar (Tzolk'in) calls the number nine a symbol of periodicity and completeness [27]. Third, in the decimal system, the number 9 is the last among the basic numbers.

Database update.

The structure of the control parameter systematization database (DB) is presented in **Table 2.1**.

Table 2.1 Structure of the control parameter systematization database (DB)

What	Why	How	Where	When	Who	Whom	Why	Whence
1	2	3	4	5	6	7	8	9
Three-car collision	Narrowing of track	Heavy rain	3rd km of section N	June 25, 2017 7:15	Railway track service	1-BIS mine	Inadvertent	From station A to station B
...	...	...	...	...	...	...	...	...

Table 2.1 provides an example that is virtual in nature in order to present the essence of the database elements. In reality, these elements are coded according to classifiers, as will be discussed below. The task of systematization is to determine the number of manifestations and dynamics of measurements of the control parameter for a specific time.

The nine directions of systematization provided in **Table 2.1** are an enlarged systematization. Each direction can be specified. That is, there are first-level parameters (nine directions in **Table 2.1**), and there can be subparameters (second-level parameters), as clarifications or components of the nine first-level parameters. That is, the database should be expanded or specified for the completeness of further analysis and coding of database elements thanks to existing classifiers and enterprise standards. **Table 2.2** provides classifiers that are used in JSC "UZ" and any organization to specify the database of systematization.

Table 2.2 Filling in the refined database

What	Why	How	Where	When	Who	Whom	Why	Whence
1	2	3	4	5	6	7	8	9
Event classifier item	Cause classifier item	List of circum-stances	Railway, station, km	Year, date, time	Unit, staff or private person	Railway, users, environ-ment	Intention-al/unintention-tional	Connection scheme

Thus, for example, the 5th column can be divided into three: year, date, time of the event.

Each value of the control parameter must be systematized and recorded in the database.

The output of block 1 is the current control parameter database taking into account the last *PS(t).*

Block 2. Detection of bottlenecks-events.

The input of the block is the control parameter systematization database.

The task of this block is to detect bottlenecks by features 1 or 2 according to clause 3. The systematization dimension of the WHAT (1st column of **Table 2.2**) of the database is analyzed. The bottleneck is determined for a certain period, depending on the frequency of fixing the control parameter. Bottlenecks are detected for all components of the event (WHAT dimension) according to the event classifier that exists at the enterprise. At the same time, all (!) WHAT components are analyzed both according to option (a) — by *feature 1*, and (b) — by *feature 2*. One or more bottlenecks are selected according to objective mathematical criteria.

The choice according to *feature 1* depends on the experience, skills of the responsible personnel or manager, according to *feature 2* — bottlenecks will be all WHAT components that have "negative" dynamics.

The output of block 2 is one or more identified bottlenecks-events.

Block 3. Analysis of cause-and-effect relationships.

The final result of this block is the determination of the prerequisites (*so-called fundamental/basic/deep and therefore hidden reasons*) that lead to the emergence of bottlenecks-events.

This occurs in two stages:

1) possible causes of bottlenecks-events are determined. These are usually technological reasons — unexpected failure of technical means or infrastructure, driver or dispatcher error, unforeseen environmental disasters;

2) the prerequisites of technological reasons are determined. The prerequisites are related to the organization of the transportation process and do not affect the transportation process itself. These are: the level of personnel training and technical training, the state of technical means, shortcomings in the management system of the structural unit or the system as a whole, outdated material, technical and intellectual base, shortcomings in repair or maintenance, etc.

Identification of negative prerequisites is determined by analogy with block 2 for events. Due to the war, significant causes of "bottlenecks" are formed. This is the risk of an emergency.

As a result of the analysis of the prerequisites, significant prerequisites of bottlenecks are formed. These are real risks that can be eliminated, because prerequisites, unlike causes, are not random in nature.

The organization of the transportation process is formed over the years and it is it that determines errors and failures in technological processes. Changing the organizational principles of the transportation process requires time and significant expenditure of material and nervous resources, because it is associated with the habits of a large number of people.

But controlling prerequisites is the most rational way to increase efficiency and production culture.

The output of block 3 is the most significant prerequisites, which can also be several. Their selection is also a matter of human skill, as well as the use of expert assessments, for example, the Delphi method. The reason for using experts is that there is neither a culture of working with prerequisites nor appropriate prerequisite classifiers at enterprises.

Block 4. Development of management decisions.

This is the formation of management decisions that can reduce or eliminate the impact of significant prerequisites. In practice, three types of management decisions can be identified:

— operational — introduced quickly as a reflex to a bottleneck in order to get rid of negative events-bottlenecks as quickly as possible in the future. As a rule, these are prohibitive decisions;

— preventive, this is the implementation of organizational and technological measures for verification, training, testing, experiments to reduce the impact of bottlenecks in the medium term;

— strategic — this is the development of programs for a fairly long term and their subsequent implementation.

The specific content of this block largely depends on the specific company.

The implementation of the methods of **Fig. 2.7** and **2.8** of operational management in full will become possible with the introduction of digital technologies 4.0 and 5.0: Big Data Analytics, Blockchain, cloud computing, etc. This is a matter of the near future.

2.5 SYSTEM BEHAVIOR NORM

The term "norm" is of key importance in the MDHSP. This term is widely used in natural, social, technical sciences, medicine, mathematics, chemistry (abnormal crystals), in physics (normal oscillations), in mathematics (normalization of vectors and quantities), in biology (adaptive norm, reaction norm), in aesthetics (aesthetic norms), in linguistics (language norms), jurisprudence (norms of law), etc. It is practically impossible to find a science or field of activity in which the term "norm" is not used in one form or another.

Today there is no generally accepted concept of norm. Examples of the use of the concept: ideal, ordinary, average, optimal, rational, etc. The use of this concept in different fields of knowledge and activity is not a terminological coincidence. In all cases of application of this concept, it is possible to speak of a general substantive nature. The following are often used as equivalents to the term norm: "ordinary", "typical", "average", "mass", "correct", "standard", "ideal", "established measure", "recognized order", etc.

Many scientists from different branches of knowledge were engaged in substantiating the norm: G. Hegel, I. Kant, G. Leibniz, C. Lombroso, L. Quetelet.

The main stages of the evolution of the concept of norm:

– visual empirical – in antiquity;

– classification by essential features – typical of the metaphysical stage of the development of science until the 19th century;

– dialectical – typical of the science of the late 19th–21st centuries.

In technology and natural science, the concept of the *average statistical* or *population* norm has become most widespread. Let's dwell in more detail on this interpretation of the norm.

The achievements of the 19th century in the study of the norm have determined its widespread application. The law of large numbers allows to consider each individual event as random in the general process, and the entire set of events that has the stability of reproduction as a necessity. Already at the beginning of the 20th century, a significant number of works appeared that proved the high efficiency of using average statistical estimates of the norm. Statistical commonality increasingly serves as the basis of empirical laws.

The requirements that must be observed in order to form a correct representation of the norm of the phenomenon under study are determined. One of such requirements is the qualitative homogeneity of the set of manifestations of the parameter that characterizes the phenomenon under study. This requirement is closely related to the problem of the boundaries of the set. Mathematical statistics states: the larger the set of manifestations of the parameter being estimated, the more reliable the estimate in the form of the arithmetic mean should be. However, the expansion of this set leads to a wide variation in relation to its average value and an extremely high conditionality of the average statistical estimate.

Therefore, the average statistical norm includes not only the *arithmetic mean*, but also the *variation*, which is most often characterized by *dispersion or standard deviation*.

Actually, a clear idea of the average statistical norm has been formed. It expresses something "limitingly general", "tendency" or "average". In this case, the concept of the norm is not associated with any specific event or property of a specific element of the population, although each of the elements varies within its minimum and maximum, and the average is formed most often. Processes are recognized as normal for the corresponding environment if they occur in most cases.

Naturally, the average statistical norm for a set of phenomena, objects or people cannot correspond to the individual norm of a separate object or person. The more heterogeneous the set of individuals, the more contradictions arise in the understanding and content of the individual and average statistical norm. In a number of cases, such contradictions led to the complete denial of the norm as a category. This is explained by the fact that the formation of the average statistical understanding of the norm took place during the period when the structural representation of the system was absolutized.

The most profound and well-founded interpretation of the *norm as a functional optimum* is considered. Approaches to the quantitative definition of such an understanding of the norm were laid down at the beginning of the 20th century by Academician P. Anokhin in the theory of functional systems [19, 28]. Later, these ideas were developed in the works of K. Sudakov, A. Korolkov, V. Petlenko, N. Amosov, Yu. Antomonov, V. Druz, Japanese scientists Hirata, Kaku, etc. [29]. It is worth noting the works of M. Breitman, who in the 20s of the 20th century, empirically reached the same conclusions, scientifically generalizing them [20].

The functional expediency of the system in achieving the final result is a forming factor in determining standard patterns, orders, and organization of forms of relations, which constitute the norm of the system while maintaining the stability of these relations. In this view, the norm appears not only as an ordered *structure of relations*, but also as a *process* aimed at maintaining a state of stable equilibrium during changes in the environment.

Structural changes in the ordered relations of the system under the influence of the environment lead to the evolution of the system. Such transformations are natural if the system maintains stable relations with the environment, and the process of evolution itself proceeds in accordance with the order inherent in the system. The norm plays the role of a mechanism for managing the relations of the system with the environment. In the event of loss of stability, the system is transformed or destroyed, its orderliness in this environment disappears. This is also the norm of such relations.

The norm changes during the life cycle depending on the environment and its "aging".

Achieving the final result is a factor in shaping the behavior of the system and forms of relations, which constitute the norm of the system with stable relations with the environment. In this view, the norm appears as an ordered structure of relations and as a process aimed at maintaining a state of stable equilibrium with environmental changes.

In this work, *the norm is understood not as a fixed criterion, but as a process that determines the optimal mode of functioning of the system*, that is, its *functional optimum*. In this concept, *the norm is perceived as an interval of optimal functioning of the system with moving boundaries.* Within these boundaries, the optimal connection with the environment and the coordinated performance of all system functions are preserved.

It was previously emphasized that the authors consider the system as a unity of "management object — environment". The question arises of finding statistical patterns that ensure the stability of the continuous process of system adaptation to environmental changes. The optimum of such a process is the norm, and its most stable state (analogy of the mode in Gauss's law) is a reflection of the norm, which can be determined for certainty by the *maximum of the norm.* In this case, the norm characterizes both the qualitative and potential capabilities of the system. The direction of the norm movement determines the qualitative evolution of the system.

The norm characterizes the maximum margin of stability of the system. This is explained by the maximum range of deviations, which nevertheless ensures the return of the system to the previous (normal) state.

When deviating from the norm, the system goes into a state of tension. At the same time, the variety of compensatory capabilities of the system decreases, and the time of preservation of states is shortened. The reason for this is as follows: an increase in the intensity of the state requires an adequate increase in energy to remove the tension and transition to the norm. The tension at which all energy reserves are used to remove it can be taken as the limit of the functional optimum. After this, irreversible destabilizing processes are observed, which increase with distance from the modal state of the system (norm).

System management requires knowledge of the state and level of reliability of the system and each component. **Fig. 2.9** shows the scale of system states from the point of view of stability and reliability of functioning.

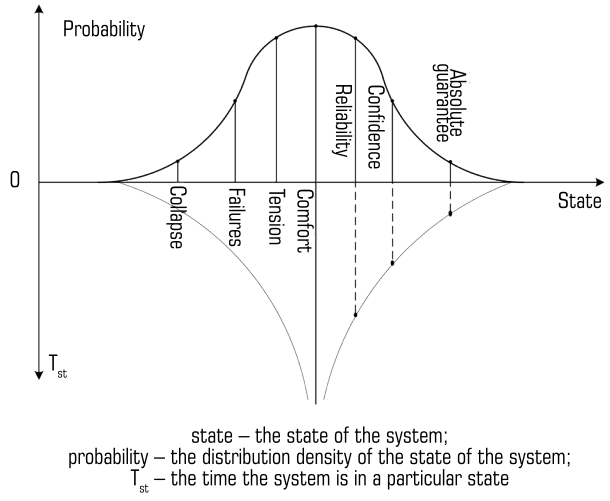

Fig. 2.9 Determination of the probability of the system's activity states and the residence time

Among the set of states, there are two points ("Tension" and "Reliability"), beyond which work becomes unprofitable. They correspond to the inflection points of the normal curve, i.e. $\mu \pm \sigma$. The distance between these points determines the zone of functional optimum, when it is still possible to maintain the equality of income and losses. Approaching these points from the comfort point should cause alarm and take measures to stabilize the activity. This fact allows to establish such a state in which it is necessary to apply measures of increased concern. Outside the zone of functional optimum, there is a mismatch between the capabilities and needs of the system, its individual link or section.

The pattern of change in the probability density of the current statistics of the control parameter *PS* depending on the state of the system is shown in **Fig. 2.10**. Let's explain the graphic construction in **Fig. 2.10**.

1) **Fig. 2.10, *a***.

The density of the PS parameter distribution in the three-dimensional space {*PS*, *state*, *f*} is described by Gauss's law

$$f(PS) = \frac{1}{\sigma\sqrt{2\pi}} e^{-\frac{(PS-\mu)^2}{2\sigma^2}}. \qquad (2.5)$$

On the *PS* axis, the point means the current arithmetic mean of the *PS* parameter. This value is constantly being refined, so it is possible to say that *not only the boundaries of the functional optimum, as mentioned earlier, but also the arithmetic mean* of the control parameter are "*floating*".

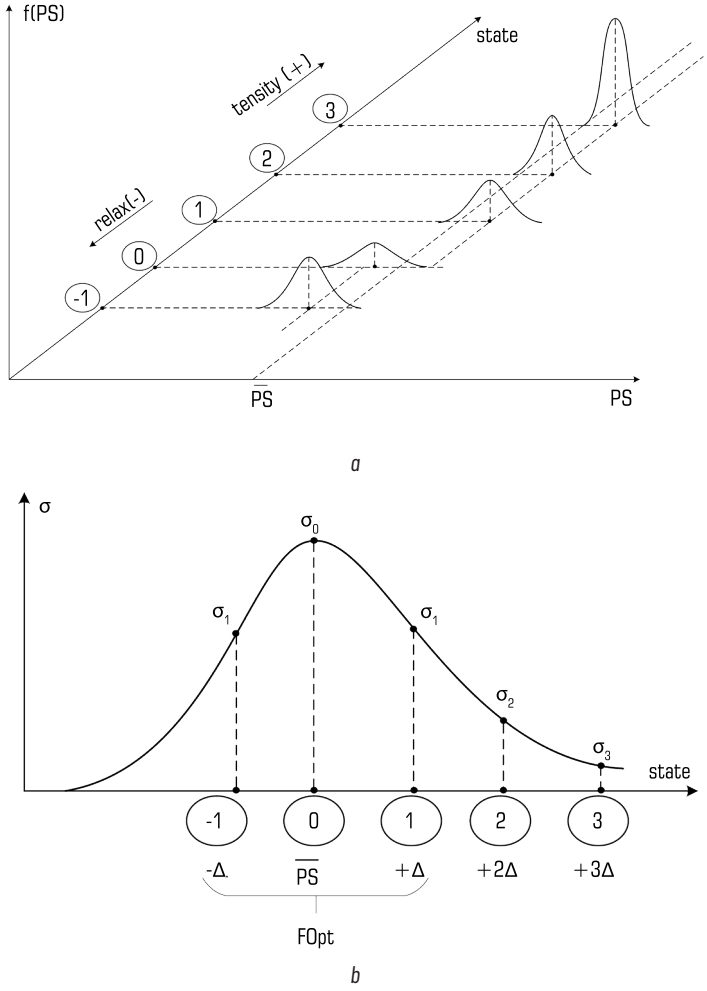

Fig. 2.10 Change in the parameters of the normal distribution of the control parameter depending on the state of the system: *a* — regularity of change in the probability density of the current statistics of the control parameter (PR); *b* — dependence of the PR variation on the state

The "*state*" axis has two directions: tension ("tensity +" and relaxation ("relax —"). Five states are highlighted on the "*state*" axis, which are marked "-1", "0", "1", "2", "3". State "0" corresponds to the "comfort" state in **Fig. 2.9**. This is the optimal state of the system with a large number of options for obtaining the final result.

Therefore, the variance in the distribution (3.3) will be maximum. In the states of tension "1", "2", "3" (in **Fig. 2.9** these are the states "tension", "failures" and "collapse"), the variance gradually decreases in accordance with the state "0". The same considerations can be repeated for the direction of relaxation or "relax". Therefore, all graphical models in the "relax" direction will be symmetrical to the "tensity" direction and are given only for one state "–1", which is symmetrical to the state "1".

Within each removed state, deviations are permissible, which should not exceed inflection points of the curve (3,3), respectively $\mu_{-1} \pm \sigma_{-1}, \mu_0 \pm \sigma_0, \mu_1 \pm \sigma_1, \mu_2 \pm \sigma_2, \mu_3 \pm \sigma_3$. If these deviations go beyond the inflection points, the system passes into a new state with different characteristics of its preservation.

In real operating systems, it is customary to talk about a state of tension, and almost never about relaxation. But from the point of view of the quality and efficiency of activity, these two processes are similar;

2) **Fig. 2.10, *b***.

This figure plots the dependence of the PS variation on the state in the form of the mean square deviation, which corresponds to **Fig. 2.10, *a***). The envelope of the mean square deviations σ of the *PS* parameter also corresponds to the Gaussian law (without proof). This allows to determine the functional optimum as the interval between the points of its inflection of the curve $\sigma(PS)$, which it is possible to define as follows:

$$FOpt = \left[\overline{PS} - \Delta, \overline{PS} + \Delta\right], FP, \tag{2.6}$$

and the value of Δ is determined according to the "3σ rule", by the formula

$$\Delta = \frac{\max PS(t) - \min PS(t)}{6}. \tag{2.7}$$

Thus, formulas (2.6) and (2.7) can statistically characterize the functional optimum of the system. Taking into account the constant refinement of $\overline{PS}$ and Δ, this approach to determining the functional optimum can be called a "floating norm".

The dependence of the dispersion of the distribution law of the control parameter (2.5) on the state of the system (**Fig. 2.9**) allows to consider the dispersion (or the mean square deviation) as a criterion for assessing the norm of the system and the degree of tension or relaxation.

The norm is a living being. It is subject to the influence of the internal and external environment, changes in technology, equipment and personnel, and therefore it changes during the life cycle of the system.

The options for change are as follows:

1) changing the center of the probability density distribution of the control parameter around the axis *state*.

The upper part of **Fig. 2.11** shows the features of changing the location of the distribution of the control parameter PS, which are taken from **Fig. 2.10, *a***, but between the inflection points of the Gaussian curves. From this figure it is obvious that the center of the distribution shifts, and for states of tension in one direction, and for states of relaxation in the other direction. The lower part of **Fig. 2.11** shows the dependence of the center of the probability density distribution μ on the state of the system state.

2) shifting the location and width of the functional optimum interval.

This option is shown in **Fig. 2.12**. The black color shows the option of the functional optimum zone, as shown in **Fig. 2.10, *b***. Further, it is possible to move left or right along the *state* axis without changing the width of the interval (this is shown in blue), or to decrease/increase the width of the functional optimum interval (red).

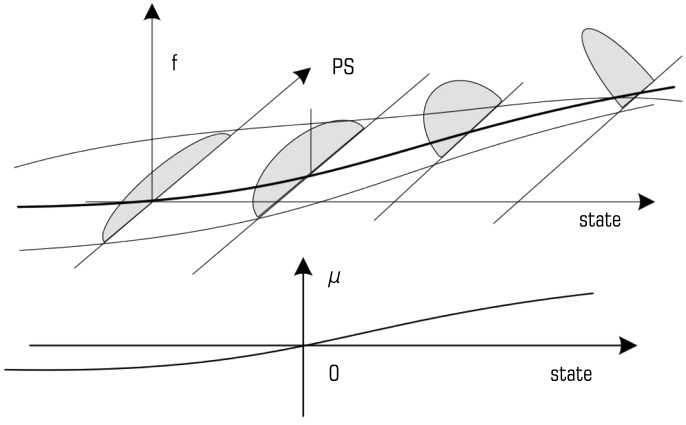

Fig. 2.11 Change of the distribution center according to the increase in tension in the system activity

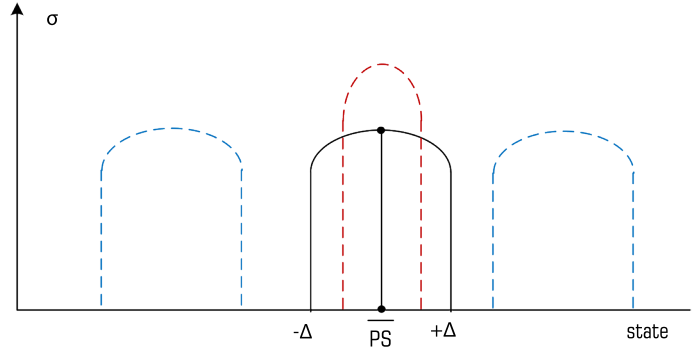

Fig. 2.12 Shift of the location and width of the functional optimum zone

By analyzing the location of *FOpt*, the dynamics and rate of change of the width of the *FOpt* zone, it is possible to predict the state of the system and determine its adaptive capabilities. The dependence

of the dispersion on the functional state allows *to consider the dispersion as a criterion for assessing the individual norm of the system and the degree of tension.* This can be a criterion for controlling the state of the system in the process of continuous activity.

With fatigue, the dispersion in all states decreases, the stability of the system decreases exponentially, the variation of the final result parameter tends to zero. This minimizes the viability of the system.

2.6 INTEGRATED SYSTEM CONTROL MODEL BASED ON NORMS AND BOTTLENECKS

Fig. 2.13 presents an integrated system control model based on the system behavior norm and the bottleneck principle. It is developed by combining (integrating) the directions presented in **Section 2.4.1** (**Fig. 2.7**) and **2.4.2** (**Fig. 2.8**). The numbering of the blocks in **Fig. 2.13** is similar to the numbering of the blocks in **Fig. 2.7** and **2.8**. There are two new blocks: five and six.

The control model in **Fig. 2.13** is not only the result of integration, but also of the synergy of the two directions. Similarly to the style of describing the directions that was used above, let's describe the functions of the blocks in **Fig. 2.13**.

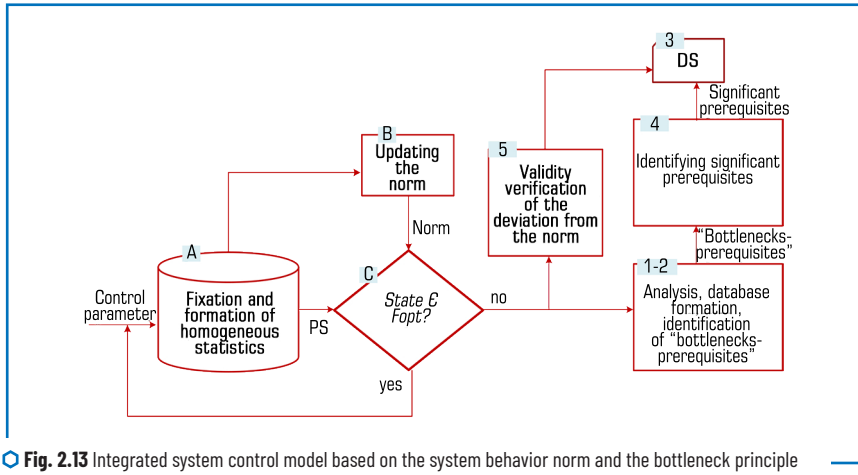

Fig. 2.13 Integrated system control model based on the system behavior norm and the bottleneck principle

Block A: Fixing control parameters and forming homogeneous statistics.

The input signal of block A – control parameter *par*□ – can appear randomly (violation of the regulation, emergency situation, end of technological operation, ...) or periodically (once per hour/day/week/month). The output signal of block A – *PS* consists of a series of adjacent values *par* and is formed periodically, after a certain time Δt according to the existing regulation and the conditions for assessing the state of the system, and is equal to either the number of values *par* in the series, or the *par* statistics are trans-

formed into homogeneous statistics, respectively, for example, (3.2). For example, the value $par\square$ is fixed once a day, and the state assessment is controlled once a month, i.e. $\Delta t = 30$ days. Then $PS(\Delta t) = \sum_{i=1}^{30} par_i$ for the case when the statistics are homogeneous.

Let's describe the sequence of actions of block A in the form of a step-by-step algorithm *PROC FSt*.

PROC FSt.

Step 0: suppose it is necessary to estimate the state of the system at the moment t_k. In this case $t_k - t_{k-1} = \Delta t$.

Step 1: from the moment of the last estimate t_{k-1} to t_k the values $par_1, par_2, ..., par_N$ are fixed and accumulated.

Step 2: at the moment of time t_k, a statistical series of the control parameter $PS(t_k)$ is formed according to the rule:

– if the statistics of the control parameter are homogeneous, then $PS(t_k) = \sum_{i=1}^{N} par_i$;

– if the statistics of the control parameter are not homogeneous, then $PS(t_k)$ is formed into homogeneous statistics, for example, according to formula (2.1) and **Fig. 2.13**.

Step 3: the $PS(t_k)$ value is stored in a one-dimensional array or vector

$$\|PS\| = \langle PS(t_1), PS(t_2), PS(t_3), ..., PS(t_{k-1}), ... \rangle. \quad (2.8)$$

Step 4: PROC FSt.

End.

Formation of the current statistics of the control parameter $PS(t)$ is shown in **Fig. 2.14**. It is important to emphasize that the $PS(t)$ values are remembered and stored (step 3 of *PROC FSt*), because they are used in other blocks, for example block 5:

where t – the time of formation of the statistical series $t_2 - t_1 = t_3 - t_2 = ... = t_k - t_{k-1} = t_{k+1} - t_k = \Delta t$; Δt – the periodicity of the system state assessment.

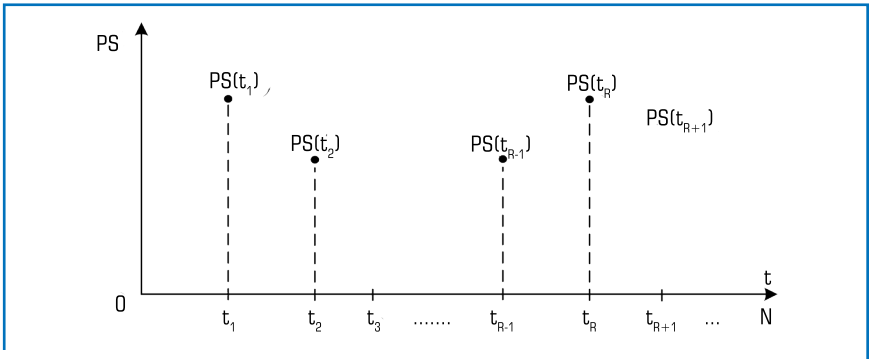

Fig. 2.14 Formation of current statistics of the system status control parameter over time

Block B "Formation/actualization of the norm".

It was noted above that the norm in the MDHSP is perceived as a process that determines the optimal mode of functioning of the system, that is, its *functional optimum*. In this concept, the norm is perceived as an interval of optimal functioning of the system with *moving boundaries*. Within these boundaries, the optimal connection with the environment and the coordinated performance of all system functions are maintained.

The input of this block is $PS(t_k)$. Then the following actions are performed:

Action 1 – the difference between the *PS* values in two measurements adjacent in time – the current and previous ones – is calculated

$$\delta(t) = PS(t_k) - PS(t_{k-1}), \tag{2.9}$$

as well as the tolerance level

$$tol = \frac{\max\|PS\| - \min\|PS\|}{6}. \tag{2.10}$$

The number six in (2.10) is explained by the "3σ rule" for the Gaussian distribution, meaning: "3σ" in the positive direction from the center of the distribution and "3σ" in the negative direction.

Action 2 – Six sets $M_{-3}, M_{-2}, M_{-1}, M_{+1}, M_{+2}, M_{+3}$ are considered. The elements of these sets are formed according to the rules (2.11):

$$\begin{aligned}
&if\ \delta(t) \in \left[0, tol\right], then\ PS(t_k) \to M_1;\\
&if\ \delta(t) \in \left[tol, 2tol\right], then\ PS(t_k) \to M_2;\\
&if\ \delta(t) \in \left[2tol, 3tol\right], then\ PS(t_k) \to M_3;\\
&if\ \delta(t) \in \left[-tol, 0\right], then\ PS(t_k) \to M_4;\\
&if\ \delta(t) \in \left[-2tol, -tol\right], then\ PS(t_k) \to M_5;\\
&if\ \delta(t) \in \left[-3tol, -2tol\right], then\ PS(t_k) \to M_6.
\end{aligned} \tag{2.11}$$

The sign «$\to$» means: becomes an element of the set.

Let's explain the essence of these sets using **Fig. 2.10, *a***. A set M_{-1} is a set of *PS(t)* values in the range between points "-1" and "0" of the *state* axis, M_1 is a set of *PS(t)* values in the range between points "0" and "1" of the *state* axis, M_2 is a set is a set of *PS(t)* values in the range between points "1" and "2" and so on for discrete points of the *state* axis.

Without proof, let's accept the obvious fact that a consecutive series of random PS values in each of the sets $M_{-3}, M_{-2}, M_{-1}, M_{+1}, M_{+2}, M_{+3}$ corresponds to Gauss's law.

In fact, the *pair* $\left(\delta(t), M_j\right)$ *characterizes the current state of the system*, i.e.

$$\delta(t), M_j \equiv state, \tag{2.12}$$

where $\delta(t)$ is determined from (4.1), and the index in the sets M_j= -1, -2, -3, +1, +2, +3.

Action 3 – the arithmetic mean and the standard deviation (SD) are determined in each set $M_{-3}, M_{-2}, M_{-1}, M_{+1}, M_{+2}, M_{+3}$, respectively, $\mu_{-3}, \mu_{-2}, \mu_{-1}, \mu_1, \mu_2, \mu_3$ and $\sigma_{-3}, \sigma_{-2}, \sigma_{-1}, \sigma_1, \sigma_2, \sigma_3$.

The arithmetic mean and SD are calculated using the traditional formulas for sampling $x_1, x_2, ..., x_N$ of a random variable x:

$$\mu = \frac{\sum_{i=1}^{N} x_i}{N}; \sigma = \sqrt{\frac{\sum_{i=1}^{N}\left(x_i - \mu\right)^2}{N-1}}. \tag{2.13}$$

Action 4 – the sample $\sigma_{-3}, \sigma_{-2}, \sigma_{-1}, \sigma_1, \sigma_2, \sigma_3$ is approximated by a Gaussian probability density distribution of the form

$$f(PS) = \frac{1}{\Delta\sqrt{2\pi}} e^{\frac{\left(PS-\overline{PS}\right)^2}{2\Delta^2}}, \tag{2.14}$$

the reliability of which is determined either by kurtosis and skewness, or by the Pearson/Yastremski criterion γ^2. The value Δ from (2.14) characterizes the range of the functional optimum, and the relation

$$\left[\overline{PS} - \Delta, \overline{PS} + \Delta\right] = FOpt \tag{2.15}$$

characterizes the norm of the system as a functional optimum.

Block C "Is the system normal?".

Two input parameters: $PS(t_k)$ and *FOpt* respectively (2.15). This is a classic logic block in algorithm theory, which means checking the condition:

$$IF(PS(t_k) \in FOpt\ GO\ TO\ block\ A; \tag{2.16}$$

$$IF(PS(t_k) \notin FOpt\ GO\ TO\ block\ 5. \tag{2.17}$$

That is, if condition (2.16) is met (the system is normal), then management is transferred to block A in **Fig. 2.13**, and if condition (2.17) is met, then management is transferred to block 5 in **Fig. 2.13**. In (2.16), (2.17) and further in the text "GO TO" means "transition to".

Block 5 "Verifying the validity of the deviation from the norm".

From **Fig. 2.13** it is obvious that in the case when the current state of the system does not correspond to the norm *FOpt* (the output "no" of block C), then block 5 is activated.

But a single exit of the current state of the system beyond the limits of *FOpt* can be random. For example, inaccurate information, or an erroneously recorded failure, or a calculation error. Therefore, it is necessary to make sure of the validity of such an effect, because this happens quite rarely and has a rather negative impact on personnel and generally on the operation of the system. It is for this reason that block 5 "Verifying the validity of the deviation from the norm" is provided.

A procedure for verifying the validity of the state with a multi-level solution is proposed. This procedure is associated with the use of Shewhart control cards [26] in the part called "Verifying structures for special reasons".

The choice of Shewhart control charts is explained by several components of the similarity of this method to the object of the monograph in terms of: process — control of the state of products by control parameters (taken as a random variable), the law of the probability density distribution of the control parameter — the normal law or the Gaussian law.

To interpret the course of control, Shewhart used eight additional criteria, of which three are used in this work. The choice of these three criteria is associated with the operational nature of solving transport system management issues.

In the developed model, the conditions of Shewhart cards are used if the state of the system or process does not correspond to *FOpt*. Let's describe the rules in accordance with the selected three Shewhart criteria.

It should be explained that in the following the letter Δ denotes the mean square deviation of the statistics of the control parameter, respectively (2.14) and (2.15).

Rule 1: One $PS(t_k)$ *value outside the interval* $[-3\Delta,+3\Delta]$. This is a very rare event. It is known that its probability is 0.0027 (0.27% of the general population). This may be an unacceptable (catastrophic) change in the state of the system or process, an unusual environmental phenomenon, military action, destruction of infrastructure, in general force majeure circumstances. In any case, this fact requires immediate intervention depending on the result of the control.

Rule 2: Two of the three consecutive values $PS(t_k)$, $PS(t_{k-1})$, $PS(t_{k-2})$ *are in the interval* $[+2\Delta,+3\Delta]$ *or* $[-2\Delta,-3\Delta]$. The probability of such an event is 0.0428 (or 4.28%). Possible reasons: inadequate personnel behavior, cyberattacks, random emissions.

Rule 3: Four out of five consecutive values of $PS(t_k)$, $PS(t_{k-1})$, $PS(t_{k-2})$, $PS(t_{k-3})$, $PS(t_{k-4})$ *are in the interval* $[+\Delta,+3\Delta]$ *or* $[-\Delta,-3\Delta]$.

This state of affairs can be interpreted as the beginning of an exit from the FOpt state and this should concern the system management.

The criterion for checking according to the three Shewhart rules: if at least one rule works, then the deviation from the FOpt is reliable.

The sequence of checking the reliability of the system deviation from the norm based on the three Shewhart rules is presented below in the form of the PROC Shewhart procedure.

PROC Shewhart.

Step 0: the current $PS(t_k)$ value does not belong to *FOpt*.
The $\|PS\|$ elements from (3.6) are considered:

Step1: IF $[PS(t_k)\langle(\overline{PS}-3\Delta)]$ *OR* $[PS(t_k)\rangle(\overline{PS}+3\Delta]$ *GO TO step* 5.

Step 2: IF $\{(PS(t_k),PS(t_{k-1}))\in[\overline{PS}+2\Delta,\overline{PS}+3\Delta]$ *OR*

$(PS(t_k),PS(t_{k-1}))\in[\overline{PS}-3\Delta,\overline{PS}-2\Delta]\}$ *OR*

$\{(PS(t_k),PS(t_{k-2}))\in[\overline{PS}+2\Delta,\overline{PS}+3\Delta]$ *OR*

$(PS(t_k),PS(t_{k-2}))\in[\overline{PS}-3\Delta,\overline{PS}-2\Delta]\}$ *OR*

$\{(PS(t_{k-1}),PS(t_{k-2}))\in[\overline{PS}+2\Delta,\overline{PS}+3\Delta]$ *OR*

$(PS(t_{k-1}),PS(t_{k-2}))\in[\overline{PS}-3\Delta,\overline{PS}-2\Delta]\}$.

GO TO step 5.

Step 3: IF $\left\{PS(t_k),PS(t_{k-1}),PS(t_{k-2}),PS(t_{k-3})\in[\overline{PS}+\Delta,\overline{PS}+3\Delta]\right.$ *OR*

$PS(t_k),PS(t_{k-1}),PS(t_{k-2}),PS(t_{k-3})\in[\overline{PS}-3\Delta,\overline{PS}-\Delta]\}$ *OR*

$\left\{PS(t_k),PS(t_{k-2}),PS(t_{k-3}),PS(t_{k-4})\in[\overline{PS}+\Delta,\overline{PS}+3\Delta]\right.$ *OR*

$PS(t_k),PS(t_{k-2}),PS(t_{k-3}),PS(t_{k-4})\in[\overline{PS}-3\Delta,\overline{PS}-\Delta]\}$ *OR*

$\left\{PS(t_{k-1}),PS(t_{k-2}),PS(t_{k-3}),PS(t_{k-4})\in[\overline{PS}+\Delta,\overline{PS}+3\Delta]\right.$ *OR*

$\left.PS(t_{k-1}),PS(t_{k-2}),PS(t_{k-3}),PS(t_{k-4})\in[\overline{PS}-3\Delta,\overline{PS}-\Delta]\right\}$ *OR*

$\left\{PS(t_k),PS(t_{k-2}),PS(t_{k-3}),PS(t_{k-4})\in[\overline{PS}+\Delta,\overline{PS}+3\Delta]\right.$ *OR*

$PS(t_k),PS(t_{k-2}),PS(t_{k-3}),PS(t_{k-4})\in[\overline{PS}-3\Delta,\overline{PS}-\Delta]\}$

GO TO step 5.

Step 4: GO TO block "1-2" "deviation from the norm is reliably confirmed".

Step 5: GO TO block "5" "deviation from the norm is random".

Step 6: End of PROC Shewhart.

Block 1–2 "Analysis, database formation, identification of bottlenecks-events" is a combination of blocks 1 and 2 in **Fig. 2.13**, which is shown by a dotted line with a similar name.

Block 3 "Decision support (DS)" is an analogue of block 4 in **Fig. 2.13**.

Block 4 "Identification of significant prerequisites".

The functional structure of this block is shown in **Fig. 2.15**.

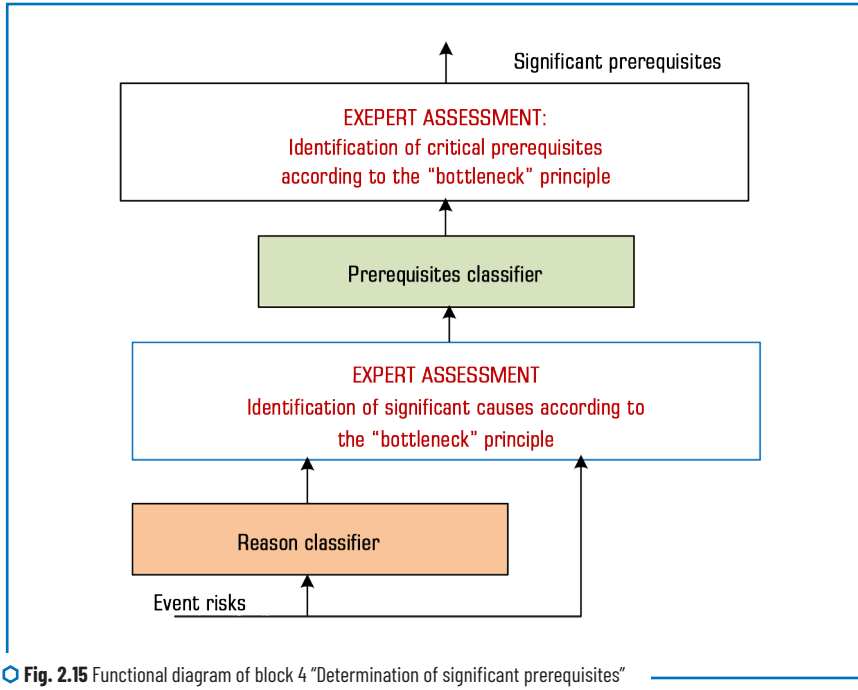

Fig. 2.15 Functional diagram of block 4 "Determination of significant prerequisites"

The input of block 4 is the bottlenecks — events from block 2 in **Fig. 2.8**. Block 4 implements the task of determining the critical or most significant prerequisites in the cause-effect relationships of the control parameter. This is implemented in two stages.

Stage 1: using the cause classifier, the reasons for each position of the bottlenecks — events are identified. And then, using expert assessment, the most significant reasons are identified. The authors have experience using the Delphi methodology to obtain expert assessment [30]. The questionnaire procedure itself takes up to one hour, that is, it is not burdensome.

Stage 2: the interaction of the cause classifiers and prerequisites is analyzed (**Fig. 2.7**). The prerequisites for each of the most significant reasons are identified. And then, using expert assessment, the most significant (significant) prerequisites are identified.

The use of expert methods is due to the absence of (as a rule) classifiers of causes and prerequisites at enterprises, a defined quantitative relationship between their elements, as well as the culture and experience of using such classifiers in analytical work. When this is resolved at the enterprise, then it is possible to do without expert assessments, that is, to detect automatically, or to conduct surveys of experts from time to time.

CONCLUSIONS

The section discusses modern approaches to the synthesis, modeling and optimization of processes and control systems in railway transport.

The application of a unified theory of self-organizing systems as a methodological basis for the study of processes and control systems in railway transport is substantiated. This approach allows to consider the management object in interaction with the environment and ensures the integrity of the analysis.

The essence of the Method for Detecting Hidden Statistical Patterns (MDHSP) is revealed, which is based on the systematization of statistics of management parameters and the identification of "bottlenecks" in the activities of transport organizations. It is proven that the use of this method ensures increased efficiency of management decisions due to the identification of hidden causes of failures and violations.

The practical value of MDHSP for managing traffic safety, the technical condition of the infrastructure and the optimization of the transportation process is shown. Its application allows to move from the statement of negative consequences to the preventive elimination of the prerequisites for violations, which contributes to increasing the level of reliability and stability of the railway system.

The concept of extended causal relationships has been developed, which takes into account not only consequences, events and direct causes, but also deep prerequisites. This opens up the opportunity to form preventive and strategic management decisions aimed at improving the organizational support of the transportation process.

The introduction of the principles of norm, tolerance and a systemic approach to the management of transport systems creates the basis for the use of intelligent information technologies (Big Data Analytics, artificial intelligence, digital management platforms). This allows to increase the adaptability of the transport system to changes in the external environment and ensure its sustainable development.

The results of the study prove that the integration of synthesis, modeling and optimization into a single methodology for managing transport systems creates new opportunities for increasing the efficiency, safety and innovative development of the railway industry.

The obtained provisions can be used in the development of new management methods, as well as in the improvement of regulatory and technical documents in the field of railway transport.

REFERENCES

1. Zadeh, L. A. (1978). Fuzzy sets as a basis for a theory of possibility. Fuzzy Sets and Systems, 1 (1), 3–28. https://doi.org/10.1016/0165-0114(78)90029-5
2. Druz, V. A., Samsonkin, V. M. (2023). Yedyna teoriia system, shcho samoorhanizuiutsia. Kyiv: Talkom, 123.
3. Upravlinnia. Slovnyk ukrainskoi movy. Available at: https://slovnyk.ua/index.php?swrd=управління
4. Upravlinnia. Velykyi tlumachnyi slovnyk suchasnoi movy. Available at: https://slovnyk.me/dict/vts/%D1%83%D0%BF%D1%80%D0%B0%D0%B2%D0%BB%D1%96%D0%BD%D0%BD%D1%8F
5. Keruvannia. Slovnyk ukrainskoi movy. Available at: https://slovnyk.ua/index.php?swrd=%D0%BA%D0%B5%D1%80%D1%83%D0%B2%D0%B0%D0%BD%D0%BD%D1%8F
6. Menedzhment. Velykyi tlumachnyi slovnyk suchasnoi ukrainskoi movy. Available at: https://slovnyk.me/dict/vts/%D0%BC%D0%B5%D0%BD%D0%B5%D0%B4%D0%B6%D0%BC%D0%B5%D0%BD%D1%82
7. Menedzhment. SLOVNYK.ua. Available at: https://slovnyk.ua/index.php?swrd=%D0%9C%D0%B5%D0%BD%D0%B5%D0%B4%D0%B6%D0%BC%D0%B5%D0%BD%D1%82+
8. Shynkaruk, V. D., Piesha, I. V., Sopivnyk, I. V., Halaidiuk, V. V., Koshuk, O. B. (2022). Monitorynh i otsinka u sotsialnii roboti. Kyiv: Komprynt, 360. Available at: https://nubip.edu.ua/sites/default/files/u188/posibnik_monitoring_1673873800.pdf
9. Systema. Slovnyk ukrainskoi movy. Available at: https://slovnyk.ua/index.php?swrd=%D1%81%D0%B8%D1%81%D1%82%D0%B5%D0%BC%D0%B0
10. Systema. Velykyi tlumachnyi slovnyk suchasnoi ukrainskoi movy. Availa-ble at: https://slovnyk.me/dict/vts/%D1%81%D0%B8%D1%81%D1%82%D0%B5%D0%BC%D0%B0
11. Systemnyi pidkhid. Velykyi tlumachnyi slovnyk suchasnoi ukrainskoi movy. Available at: https://irbis-nbuv.gov.ua/cgi-bin/ua/elib.exe?Z21ID=&I21DBN=UKRLIB&P21DBN=UKRLIB&S21STN=1&S21REF=10&S21FMT=online_book&C21COM=S&S21CNR=20&S21P01=0&S21P02=0&S21P03=FF=&S21STR=ukr0000728%5F12
12. Shynkaruk, V. I. (Ed.) (2002). Filosofskyi entsyklopedychnyi slovnyk. Abrys, 842. Available at: https://books.google.com/books/about/Філософський_енциклоп.html?id=iR28AAAAIAAJ
13. Systemnyi analiz. Ekonomichnyi slovnyk. Available at: https://slovnyk.me/dict/economics_dict/%D0%B0%D0%BD%D0%B0%D0%BB%D1%96%D0%B7_%D1%81%D0%B8%D1%81%D1%82%D0%B5%D0%BC%D0%BD%D0%B8%D0%B9
14. Slyusarchuk, A. (2021). Mathematical modelling of a self-assembly in the systems of functionalized nanoparticles. [Extended abstract of PhD thesis; Lviv Polytechnic National University].
15. Kulchytskyi, I. M. (2018). Kontseptualizatsiia poniat «model» ta «modeliuvannia» u naukovykh doslidzhenniakh. Naukovyi zhurnal Lvivskoi politekhniky. Seriia: Pedahohika ta psykholohiia, 829, 273–284. Available at: https://science.lpnu.ua/sites/default/files/journal-paper/2018/jun/12897/19kulchickiy-imkonceptual.pdf
16. Velykyi tlumachnyi slovnyk suchasnoi ukrainskoi movy. Available at: https://slovnyk.me/dict/vts

17. Kyryllova, O. V., Pavlovska, L. A. (2022). Suchasni transportni tekhnolohii. Odesa: Odesa National Maritime University 190. Available at: http://rp.onmu.org.ua/handle/123456789/3958?show=full&locale-attribute=uk
18. Vovk, Yu. Ya., Vovk, I. P. (2021). Osnovy teorii transportnykh protsesiv i system. Ternopil: Ternopilskyi natsionalnyi tekhnichnyi universytet imeni Ivana Puliuia, 104. Available at: https://elartu.tntu.edu.ua/handle/lib/35983
19. Dosenko, S. I. (2019). The principle of functional self-organization of activity intelligent systems. Radioelectronic and Computer Systems, 2 (90), 18–28. https://doi.org/10.32620/reks.2019.2.02
20. Samsonkin, V. N., Druz, V. A. (2005). Metod statisticheskoi zakonomernosti v upravlenii bezopasnostiu dvizheniia na zheleznodorozhnom transporte. Donetck: DIZhT, 158.
21. Dovidnyk osnovnykh pokaznykiv roboty zaliznyts Ukrainy (2015–2023 roky) (2024). Kyiv: AT «Ukrzaliznytsia».
22. STP 07-005:2019. Poriadok sluzhbovoho rozsliduvannia transportnykh podii (2019). Kyiv: AT «Ukrainska zaliznytsia», 82.
23. Bertalanffy, L. von. (2007). General system theory: Foundations, development, applications. New York: George Braziller.
24. Strogatz, S. H. (2018). Nonlinear dynamics and chaos: With applications to physics, biology, chemistry, and engineering. CRC Press. Available at: https://www.biodyn.ro/course/literatura/Nonlinear_Dynamics_and_Chaos_2018_Steven_H._Strogatz.pdf
25. Osnovni statystychni katehorii. Studfile.net. Available at: https://studfile.net/preview/7170223/page:2/
26. DSTU ISO 8258:2001. Statystychnyi kontrol. Karty kontrolni Shukharta (ISO 8258:1991, IDT) (2006). Kyiv: Derzhspozhyvstandart Ukrainy, 38.
27. Arhueles, Kh. (2002). Faktor maiia. Netekhnolohycheskyi put. Kyiv: Sofyia, 272.
28. Filiptsova, K. A., Topchiy, M. S. (2023). Vikova fiziolohiia i valeolohiia. Odesa: Ushynsky University, 383. Available at: http://dspace.pdpu.edu.ua/jspui/bitstream/123456789/16724/1/Filiptsova%20Kateryna%20Anatoliivna.pdf
29. Human Development Report 2020. The Next Frontier: Human Development and the Anthropocene (2020). New York: UNDP. Available at: https://hdr.undp.org/content/human-development-report-2020
30. Samsonkin, V. M., Martyshko, A. M. (2015). Praktychne zastosuvannia vyznachennia «vuzkykh mists» v ubezpechenni rukhu na pidpryiemstvakh zaliznychnoho transportu dlia profilaktyky transportnykh podii. Zaliznychnyi transport Ukrainy, 1, 3–10.

DOI: 10.15587/978-617-8360-19-1.CH3

Vitalii Budashko, Oksana Glazeva, Albert Sandler,
Sergii Khniunin, Valentyn Bogach, Yurii Zhuravlov

CHAPTER 3

IMPROVEMENT OF THE METHOD OF LINEAR-QUADRATIC CONTROL OF AZIMUTHAL DRIVERS OF THE COMBINED PROPULSION COMPLEX

ABSTRACT

The development of the coastal shelf (mining of natural resources, construction of wind and tidal power plants, pelagic fishing, etc.) involves the development of high-tech, science-intensive branches of the marine industry, which involve the construction and operation of ships designed for exploration and drilling, lifting and transport and loading and unloading operations in various operating conditions (the so-called offshore fleet) [1, 2].

Comprehensive monitoring of degradation effects on the lines of propulsion flow has been carried out with the identification of corresponding markers at the intersections of energy flows.

Strategies for all-mode control of power, torque and speed of electric motors of azimuth thrusters (ATS) located in the stern of the combined propulsion complex (CPC) have been developed. Methods for constructing multi-criteria three-level power distribution control strategies in PPC ship power plants (SPP) are proposed [3, 4]. Taking this into account, the following objectives were solved within the framework of the study:

– based on the analysis of the CPC behavior and the ATS efforts in combination with studies of the design features of ships of a similar class, a mathematical model was determined that describes the behavior of the CPC with the ATS in the stern;

– based on the analysis of the principles of modeling and linearization of the ATS control systems and existing methods, the shapes of the state space were determined and the influence of disturbing forces on the characteristics of the controller was tracked;

– physical modeling of the multifunctional CPC with the ATS in the stern was carried out;

– the mathematical model was adapted to the algorithm of the controller and the control system with the corresponding testing of the controller using simulation modeling.

The parametric optimization of the linear-quadratic control of the CPC ATS allowed to increase the efficiency of the CPC SPP operation.

KEYWORDS

Combined propulsion complex, thruster, linear-quadratic control, modeling.

Azimuth thrusters (ATs) are a growing trend in the modern market of sea-based vehicles (SBVs). The AT is a propeller mounted in a nacelle under the SBV hull [5]. This nacelle is capable of rotating around its axis, which allows changing the direction of the force acting on the SBV. This chapter explores the possibilities of improving the control algorithms of large-scale SBV models using the linear-quadratic control principle and linearized hydrodynamics using the example of a model of a multifunctional propulsion complex [6, 7—9] with two ATs in the stern. The controller uses estimates of linear speeds and angular speeds obtained using the Global Positioning System (GPS) and Inertial Measurement Units (IMU) to control the SUV. The input signals are the azimuthal propeller speeds and the angles of the AT stops relative to the SBV diametrical plane. The SBV model is nonlinear in three main parameters: centripetal and Coriolis forces, hydrodynamic damping, and AT input parameters. All these effects are assumed to be approximately linear around the operating points of the controllers [10, 11]. The models are designed to integrate with two different controllers, one of which controls both ATs simultaneously, and the other with differential control. To verify the proposed controllers, simulations are performed where the step responses of the closed-loop system to overload and rotation speed are compared. The first is to verify the model, and the second is to observe how adequately the model and controllers work together [12, 13]. Simulations of speed jumps showed a fairly good response, but the propeller speed showed a more significant effect on the system than the orientation of the motors. When simulating the yaw speed, the behavior of the azimuth angle did not comply with the circular constraints inherent in a device rotating at the appropriate frequency. The calculated angles reached values greater than 2π, which, according to the trigonometric function, gives the same result as the zero angle. In other words, the forces will depend linearly on the azimuth angle. It is concluded that this is a result of the linearization of the actuators, and the proposed solution is to implement a setting reinforcement to better adapt to the AT rotational behavior [14, 15—17]. Another circumstance that contributes to this result is the decoupling between the speed throws, the swing speed and the yaw speed predicted by the linear controller. This is a problem, since in reality they will have some influence on each other. It is concluded that this is the result of using an overly simplified model or an unsuccessfully chosen operating point of the centripetal and Coriolis linearization. Despite these problems, the simulations showed the potential of the model and controller for use in similar situations [18, 19]. Several modifications are also proposed to significantly improve the model and simulations. One of the main changes that could be made is the implementation of predictive control during the linearization of the azimuth motor. This will lead to the fact that the propeller speed will have a greater impact on the directional forces, and the SBV behavior will be more predictable [20, 21].

Unlike the SBV with the AT, most modern ships are propelled by a mechanical system with an internal combustion motor (ICE) or a propeller electric motor (PEM), which drives an underwater propeller (**Fig. 3.1**). The direction of rotation of the propeller is usually fixed relative to the hull of the ship, and control is carried out mainly by a rudder in the stern. Some ships also have a tunnel thruster (TT), installed in the bow or stern and directed sideways to improve maneuverability, for example, when mooring. Another method of movement and maneuvering currently used is the AT. In this system, the propeller is mounted in a nacelle, which is itself mounted under the hull in such a way that it can rotate around a vertical axis. The propeller is driven by a mechanical transmission that connects it to an motor inside the ship or to a PEM installed inside the nacelle itself. This method of motion eliminates the need for a rudder and provides better maneuverability

of the ship in tight sailing conditions [22, 23]. With greater maneuverability, more scenarios for controlling the AT located in the stern appear, which require a more skilled operator or a more complex control system. This chapter describes the study of how adequately a smaller ship with an AT can be controlled using a linear quadratic regulator (LQR). This will require mathematical modeling of both the AT behavior and the behavior of the propeller thrust. Since LQR requires linear models for design, some simplifications and linearizations will be required. Thus, a linearized model will also be implemented to describe the motion of this AT type. The procedure for finding the optimal LQR that can control SBV with the AT in the stern is reduced to comparing its performance with real conditions based on the simulation results. To achieve the result, it is necessary to perform the following objectives in order to get a more complete understanding of the problem:

– determine a mathematical model that describes the behavior of the SBV with the AT in the stern under conditions of incomplete information;

– adapt the obtained mathematical model to work with the LCR in accordance with the algorithmization of the motion controller functioning;

– conduct physical modeling of the SBV with the AT the stern;

– conduct simulation studies that verify the capabilities of the proposed method.

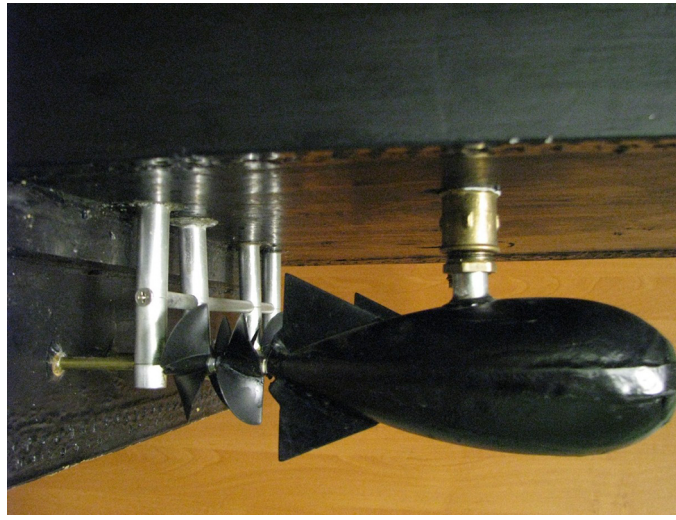

Fig. 3.1 Appearance of the AT physical model located in the stern of the physical model of the multifunctional propulsion complex with a variable structure

To solve the main problem, the main method was divided into five stages:

– analysis of the behavior of seagoing ships and AT efforts in combination with studies of the design features of modern ships of a similar class;

– analysis of the principles of modeling and linearization of AT control systems based on a review of existing methods;

– determination of the shape of the state space and tracking the influence of disturbing forces on the characteristics of the controller;

– testing the controller using simulation;

– analysis of the simulation results and possible changes in the controller settings.

To take into account the existing limitations, it was necessary to make a number of simplifications. Some degrees of freedom (DOF) were excluded, since they were determined to have little effect on the system. Thus, only 3 of the 6 degrees of freedom (DOF) were used in the simulation (sway, pitch, and yaw). Some parts of the resulting mathematical model will be nonlinear, so some linearization is required to make the model work with LQR. In the event that data from a real ship cannot be obtained, the simulation and development of the controller are performed using only nominal values.

The physical simulation begins with defining the coordinate system of the SBV and how certain forces act on the SBV in the aquatic environment. This is followed by an explanation of how the thrust and torque of the AT affect the SBV depending on the angle and speed of rotation. These mathematical models are then combined to form a spatial state vector in which the controller will be applied. This is followed by a description of how LQR works and how to find the optimal controller using the model and the Riccati equations. It is also explained how the subsequent actions of the controller are triggered depending on possible changes in operating conditions. The results of the simulation study with the regulator and controller settings of the reference input signals are analyzed in accordance with the achievement of the desired results. Also, during the simulation, the advantages of choosing different operating points for linearizing the model for different regulator settings are investigated.

3.1 DETERMINATION OF THE MOTION MODEL OF A MARINE VEHICLE UNDER CONDITIONS OF INCOMPLETE INFORMATION

To determine the position, orientation and speed of a marine vehicle, appropriate coordinate systems are required. These are the moving and stationary coordinate systems, which are defined in equations (3.1) and (3.2). The most common representation for the stationary coordinate system is based on the hull symmetry around the X_bZ_b-plane, the approximate symmetry around the Y_bZ_b-plane and the projection onto the Z_b-axis relative to the water surface, as shown in **Fig. 3.2**. The inertial (stationary) coordinate system is used to describe the position and orientation of the ship in global coordinates and Euler angles, as $[x\ y\ z]^T$ and $[\phi\ \theta\ \psi]^T$, respectively. The moving coordinate system describes the forces, torques, linear speeds and angular speeds $[X\ Y\ Z]^T$, $[K\ M\ N]^T$, $[u\ v\ w]^T$, $[x\ y\ z]^T$, and also $[p\ q\ r]^T$, respectively. The motion of a ship can be described by six degrees of freedom, which are divided into two categories: translational motion in three directions: longitudinal displacement (splash), transverse displacement (drift) and vertical displacement (lift), and rotational motion about three axes: roll, pitch and yaw. These are standard notations used in the modeling of marine ships [24].

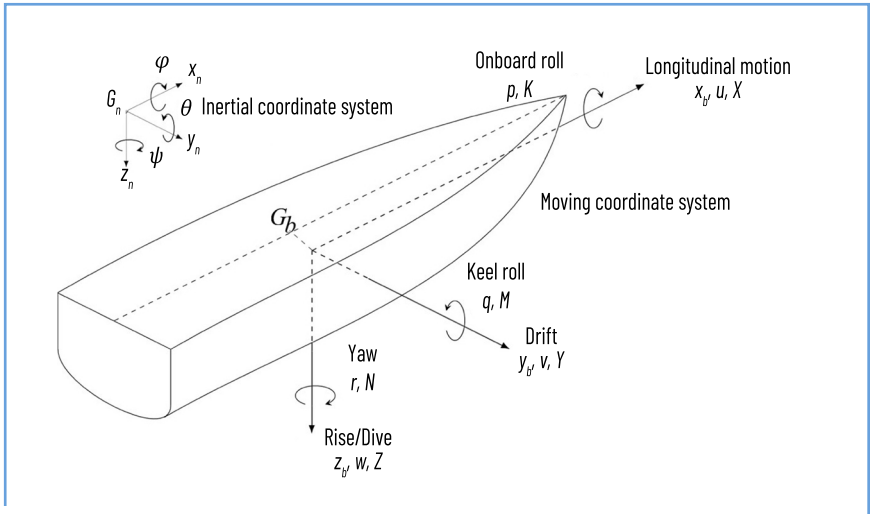

Fig. 3.2 Standard notation for describing the ship's motion according to (3.1) and (3.2)

LINEARIZATION OF THE SHIP'S MANEUVERING MODEL

A common simplification of the model is to neglect vertical motions and longitudinal roll. To obtain a simple model, the roll angle is also assumed to be small. With this in mind, the position orientation vector and the linear-angular speed vector can be defined as:

$$\eta \triangleq \left[x\ y\ \varphi\right]^T, \tag{3.1}$$

$$\nu \triangleq \left[u\ v\ r\right]^T. \tag{3.2}$$

These generalized positions and speeds have a geometric relationship that can be described as

$$\eta = J\left(\eta\right)\nu, \tag{3.3}$$

and the equations of motion of the ship in a fixed coordinate system are as follows

$$M_{RB}\nu = C_{RB}\left(\nu\right)\nu + D\left(\nu\right)\nu = \tau_{act}, \tag{3.4}$$

where M_{RB} – the inertia matrix of the rigid body; $C_{RB}(\nu)\nu$ – the centripetal and Coriolis terms; $D(\nu)$ – the damping matrix; τ_{act} – the vector with generalized external forces.

Initially, for this simple model, the Coriolis terms and the damping matrix will be approximated by a linear function. This system of equations of motion is based on, and the various descriptions of forces are based on [*n*], where models with four degrees of freedom (where roll is an additional degree of freedom) are studied, and not with three, as in our case. For three degrees of freedom, the equations are presented in the following form [25]:

$$J(\eta)=\begin{bmatrix}\cos\varphi & -\sin\varphi & 0\\ \sin\varphi & \cos\varphi & 0\\ 0 & 0 & 1\end{bmatrix}, \tag{3.5}$$

$$M_{RB}=\begin{bmatrix}m & 0 & -y_G\\ 0 & m & mx_G\\ -mx_G & mx_G & I_Z\end{bmatrix}, \tag{3.6}$$

$$C_{RB}(\nu)=\begin{bmatrix}0 & -mr & -mx_Gr\\ mr & 0 & -my_Gr\\ mx_Gr & my_Gr & I_0\end{bmatrix}, \tag{3.7}$$

$$D(\nu)=\begin{bmatrix}X_u & 0 & 0\\ 0 & Y_v & 0\\ 0 & 0 & N_r\end{bmatrix}, \tag{3.8}$$

where the total mass of the ship is taken as m, $r_g = r_G = [x_G, y_G]$; I_z is the moment of inertia about the z-axis, expressed in the b-system; X_u, Y_v and N_r – the scaling damping factors.

LINEARIZATION OF THE FORCE AND MOMENT MODELS OF THE AZIMUTH THRUSTER

On a classic seagoing ship, the driving forces come from the rudder, fixed propellers and thrusters. However, since the type of ship under consideration is driven by AT, the response to the application of forces will be different. The AT is a motor that can rotate 360 degrees around its vertical axis. This allows forces to be applied in the x- and y-directions depending on the AT position and the torque applied to the ship. The following model calculations, which use the input data of the rotation speed and the azimuth angle, are mainly derived from the model calculations used by Ljungberg. One, these approaches were improved by Liang and Andreas, who pay more attention to the azimuthal forces as input data, rather than the rotational speed [26, 27].

Let's suppose that the force N_a of the AT is applied to the ship hull. Let the thruster i be the AT rotating with the propeller speed n_i, and the angle of the applied resultant force α_i. Then the forces in the x_b-direction from the azimuthal motor i can be denoted as (**Fig. 3.3**)

$$F_{x,i} = g_x\left(n_i, \alpha_i, u_{a,i}\right), \tag{3.9}$$

where $u_{a,i}$ – the speed of water passing through the AT in the negative x_b direction. This is necessary because at higher speeds, and when $u_{a,i}$ and $n_i\ cos(\alpha_i)$ have the same sign, there will be efficiency losses. The assumption in the model is a linear relationship between g_x and n_i as

$$g_x\left(n_i, \alpha_i, u_{a,i}\right) = \mu_i n_i \cos\left(\alpha_i\right) - k_i' n_i u_{a,i} \cos\left(\alpha_i\right), \tag{3.10}$$

where μ_i and k_i – positive constants determined by field experiment, and $u_{a,i}$ can be described as

$$u_{a,i} = \left(1-\omega_i\right) u_r. \tag{3.11}$$

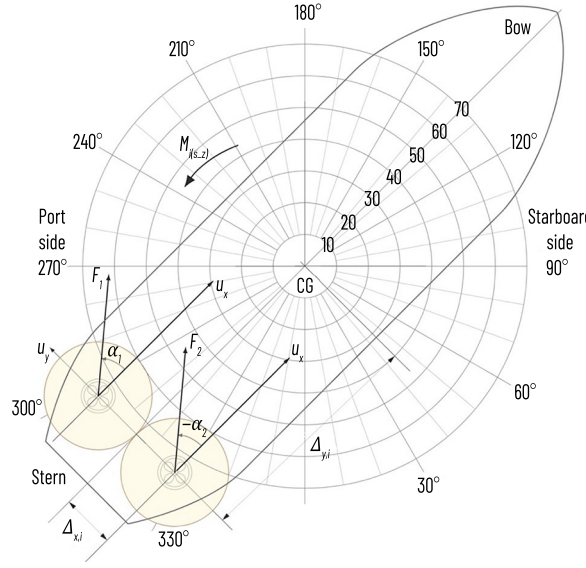

Fig. 3.3 Position and angle of rotation of motor *i*

Here, ω_i – the co-current coefficient, which defines the ratio of the speed of water flowing through the propeller to the speed of the ship u_r – the relative speed between the ship and the surrounding water. Combining the co-current coefficient, it is possible to simplify the second term of (3.10) using

$$k_i = \left(1-\omega_i\right) k_i', \tag{3.12}$$

and substituting this into (3.10)

$$g_x\left(n_i,\alpha_i,u_r\right)=\mu_i n_i\cos\left(\alpha_i\right)-k_i n_i u_r\cos\left(\alpha_i\right). \tag{3.13}$$

Thus, there is a generalized model of the forces from the AT. However, the true function $g_x(\bullet)$ is more complex due to water dynamics, but the approximate function will be adequate for the purposes of this study [28].

Similarly, the force in the Y_b-direction

$$F_{y,i}=g_y\left(n_i,\alpha_i,u_r\right)=\mu_i n_i\sin\left(\alpha_i\right)-k_i' n_i v_{a,i}\sin\left(\alpha_i\right)=\mu_i n_i\sin\left(\alpha_i\right)-k_i n_i u_r\sin\left(\alpha_i\right), \tag{3.14}$$

can be found under the same assumptions as for the *x*-direction. The azimuth motor *i* will also create a torque relative to the ship depending on where it is mounted relative to the ship's center of rotation. The torque can be described as

$$M_i=\Delta_{x,i}F_{y,i}-\Delta_{y,i}F_{x,i}. \tag{3.15}$$

The generalized torque vector is

$$\tau_{act}=\begin{bmatrix}\sum_{i=1}^{N_a}\mu_i n_i\cos\left(\alpha_i\right)-k_i n_i u_r\cos\left(\alpha_i\right)\\ \sum_{i=1}^{N_a}\mu_i n_i\sin\left(\alpha_i\right)-k_i n_i u_r\sin\left(\alpha_i\right)\\ \sum_{i=1}^{N_a}n_i\left[\mu_i\left(\Delta_{x,i}\sin\left(\alpha_i\right)-\Delta_{y,i}\cos\left(\alpha_i\right)\right)-k_i\left(\Delta_{x,i}v_r\sin\left(\alpha_i\right)-\Delta_{y,i}u_r\cos\left(\alpha_i\right)\right)\right]\end{bmatrix}, \tag{3.16}$$

contains the forces and moments from all the azimuthal motors added together. To make the model even simpler, it is possible to neglect the high-speed losses in the 4 direction, since the speeds in this direction are much lower than in the x_b direction.

Also, for simplicity, it is assumed that each motor is equally efficient, and therefore:

$$\mu_i=\mu_j\triangleq\mu\forall i,j=1,N_a, \tag{3.17}$$

$$k_i=k_j\triangleq k\forall i,j=1,N_a. \tag{3.18}$$

Which gives

$$\tau_{act} = \begin{bmatrix} \sum_{i=1}^{N_a} \mu n_i \cos(\alpha_i) - k n_i u_r \cos(\alpha_i) \\ \sum_{i=1}^{N_a} \mu n_i \sin(\alpha_i) \\ \sum_{i=1}^{N_a} \mu n_i \left[\Delta_{x,i} \sin(\alpha_i) - \Delta_{y,i} \cos(\alpha_i)(1 - k u_r) \right] \end{bmatrix}. \quad (3.19)$$

Since τ_{act} depends on u_r, which in turn depends on the rate of drag increase, the model becomes nonlinear. For simplicity, it is possible to neglect these terms and the notation of the generalized torque vector can be simplified to

$$\tau_{act} = \begin{bmatrix} \mu\tilde{\tau}_x \\ \mu\tilde{\tau}_y \\ \mu\tilde{\tau}_\varphi \end{bmatrix} = \begin{bmatrix} \mu \sum_{i=1}^{N_a} n_i \cos(\alpha_i) \\ \mu \sum_{i=1}^{N_a} n_i \sin(\alpha_i) \\ \mu \sum_{i=1}^{N_a} n_i \left[\Delta_{x,i} \sin(\alpha_i) - \Delta_{y,i} \cos(\alpha_i) \right] \end{bmatrix}. \quad (3.20)$$

3.2 ITERATIVE ADAPTATION OF SHIP MOTION MODELS IN ACCORDANCE WITH THE ALGORITHMIZATION OF THE MOTION CONTROLLER FUNCTIONING

LINEARIZATION OF CONTROLLER STATES

Since $C_{RB}(\nu)$ depends on ν, the $C_{RB}(\nu)\nu$ term becomes nonlinear. However, the use of LQR requires a linear model. Thus, linearization is needed to simplify the model further. The linearization is described by the function

$$L(x) = f(a) + f'(a)(x - a), \quad (3.21)$$

where $L(x)$ – the linearized function; $f(a)$ – the function to be linearized evaluated at a; $f'(a)$ – the derivative of $f(x)$ with respect to x evaluated at (a), in this case the Jacobian of the function $f(x)$. Finally, x – the linearization variable (in this case ν), a – the chosen operating point. In this case, the linearizing terms are:

$$f(\nu) = C_{rb}(\nu)\nu = \begin{bmatrix} 0 & -mr & -mx_G r \\ mr & 0 & -my_G r \\ mx_G r & my_G r & 0 \end{bmatrix} \begin{bmatrix} y \\ \nu \\ r \end{bmatrix}, \quad (3.22)$$

$$f(\nu)=\begin{bmatrix} -mr-mx_G r^2 \\ mr\nu-my_G r^2 \\ mx_G ru+my_G r\nu \end{bmatrix}, \tag{3.23}$$

which contain the Jacobian

$$J(\nu)=\begin{bmatrix} 0 & -mr & -mr-2mx_G r \\ mr & 0 & mu-2my_G r \\ mx_G r & my_G r & mx_G u=my_G \nu \end{bmatrix}. \tag{3.24}$$

The operating point depends on the state the system should be in. Since the system will operate at a constant forward speed and with small changes in the AT rotation speed, the corresponding operating point is defined as

$$a=\begin{bmatrix} u_0 \\ \nu_0 \\ r_0 \end{bmatrix}=\begin{bmatrix} 1 \\ 0 \\ 0 \end{bmatrix}. \tag{3.25}$$

Using this operating point and linearizing $C_{RB}(\nu)\nu$, let's find the following

$$L(\nu)=\begin{bmatrix} 0 & 0 & 0 \\ 0 & 0 & m \\ 0 & 0 & mx_G \end{bmatrix}=\begin{bmatrix} u \\ \nu \\ r \end{bmatrix}. \tag{3.26}$$

Then the state matrix (3.26) will replace $C_{RB}(\nu)\nu$ in the state space equation.

LINEARIZATION OF MOTION CONTROLLER INPUT SIGNALS

To control a ship using an AT, it is necessary to process the actuator signals as input signals, so the full equation (3.20) must be combined into a controller with a dependence on n and α. Due to the trigonometric functions cos and sin that are present in (3.21), linearization with the LQR framework is required to make it consistent.

The general case linearization is as follows. Since there are several operating points that can be selected in the simulation, a general case linearization is required. In addition, two different linearizations are required due to the two ways of controlling the ship. One with synchronous control, i.e. the same input signals for both AT, and one with differential (asynchronous) control, where the ATs are controlled independently. Starting with synchronous control, let's use the following variables

$$P_s = \begin{bmatrix} n_i \\ \alpha_i \end{bmatrix}. \tag{3.27}$$

Then (3.21) is integrated into (3.21) with the previously mentioned variable and the generalized operating point a_s:

$$f(p) = \tau(p) = \begin{bmatrix} \sum_{i=1}^{N_a} n_i \cos(\alpha_i) \\ \sum_{i=1}^{N_a} n_i \sin(\alpha_i) \\ \sum_{i=1}^{N_a} n_i \left(\Delta_{x,i} \sin(\alpha_i) - \Delta_{y,i} \cos(\alpha_i) \right) \end{bmatrix}, \tag{3.28}$$

$$J(p) = \sum_{i=1}^{N_a} \begin{bmatrix} \cos(\alpha_i) & -n_i \sin(\alpha_i) \\ \sin(\alpha_i) & n_i \cos(\alpha_i) \\ \Delta_{x,i} \sin(\alpha_i) - \Delta_{y,i} \cos(\alpha_i) & \Delta_{x,i} \sin(\alpha_i) + \Delta_{y,i} \cos(\alpha_i) \end{bmatrix}, \tag{3.29}$$

$$a_s = \begin{bmatrix} \bar{n} \\ \bar{\alpha} \end{bmatrix}. \tag{3.30}$$

which gives the following equation, which includes a constant term

$$L(p) = \sum_{i=1}^{N_a} \begin{bmatrix} \bar{n}\cos\bar{\alpha} \\ \bar{n}\sin\bar{\alpha} \\ \bar{n}\left(\Delta_{x,i} \sin\bar{\alpha} - \Delta_{y,i} \cos\bar{\alpha} \right) \end{bmatrix} + \sum_{i=1}^{N_a} \begin{bmatrix} \cos\bar{\alpha} & -\bar{n}\sin\bar{\alpha} \\ \sin\bar{\alpha} & \bar{n}\cos\bar{\alpha} \\ \left(\Delta_{x,i} \sin\bar{\alpha} - \Delta_{y,i} \cos\bar{\alpha} \right) & \left(\Delta_{x,i} \sin\bar{\alpha} + \Delta_{y,i} \cos\bar{\alpha} \right) \end{bmatrix} \begin{bmatrix} y'n \\ \bar{\alpha} \end{bmatrix}. \tag{3.31}$$

This means that the AT steady state must be at this operating point and the controller will control the deviation from this state. In other words, τ_{act} can be divided into two parts as follows

$$\tau_{act} = \bar{\tau}_{act} + \tilde{\tau}_{act}, \tag{3.32}$$

where $\bar{\tau}_{act}$ – a constant, and

$$\tilde{\tau}_{act} = \sum_{i=1}^{N_a} \begin{bmatrix} \cos\bar{\alpha} & -\bar{n}\sin\bar{\alpha} \\ \sin\bar{\alpha} & \bar{n}\cos\bar{\alpha} \\ \left(\Delta_{x,i}\sin\bar{\alpha} - \Delta_{y,i}\cos\bar{\alpha}\right) & \left(\Delta_{x,i}\sin\bar{\alpha} + \Delta_{y,i}\cos\bar{\alpha}\right) \end{bmatrix} \begin{bmatrix} n \\ \alpha \end{bmatrix}, \tag{3.33}$$

depends on time, which will be determined by the LQ controller. This linearization will force the AT to use the same rotation speed and propeller flow direction angle for both ATs.

For differential (asynchronous) control, the control variable will contain a separate definition of the control signal

$$P_d = \left[n_1\, n_2\, \alpha_1\, \alpha_2\right]^T. \tag{3.34}$$

As before, equation (3.21) is applied and a new Jacobi matrix is derived and the operating point is used. However, for *f(p)* (3.28) is still chosen, since these equations must also undergo the linearization procedure. The revised equations have the form:

$$J(p_d) = \begin{bmatrix} \cos\alpha_1 & \sin\alpha_1 & \Delta_{x,1}\sin\alpha_1 - \Delta_{y,1}\cos\alpha_1 \\ \cos\alpha_2 & \sin\alpha_2 & \Delta_{x,2}\sin\alpha_2 - \Delta_{y,2}\cos\alpha_2 \\ -n_1\sin\alpha_1 & n_1\cos\alpha_1 & n_1\left(\Delta_{x,1}\cos\alpha_1 - \Delta_{y,1}\sin\alpha_1\right) \\ n_2\sin\alpha_2 & n_2\cos\alpha_2 & n_2\left(\Delta_{x,2}\cos\alpha_2 - \Delta_{y,2}\sin\alpha_2\right) \end{bmatrix}, \tag{3.35}$$

$$a_d = \left[\bar{n}_1\, \bar{n}_2\, \bar{\alpha}_1\, \bar{\alpha}_2\right]^T. \tag{3.36}$$

These transformations give a complete linearization

$$L(p_d) = \begin{bmatrix} \bar{n}_1\cos\bar{\alpha}_1 + \bar{n}_2\cos\bar{\alpha}_2 \\ \bar{n}_1\sin\bar{\alpha}_1 + \bar{n}_2\sin\bar{\alpha}_2 \\ \bar{n}_1\left(\Delta_{x,1}\sin\bar{\alpha}_1 - \Delta_{y,1}\cos\bar{\alpha}_1\right) + \bar{n}_2\left(\Delta_{x,2}\sin\bar{\alpha}_2 - \Delta_{y,2}\cosn\bar{\alpha}_2\right) \end{bmatrix} +$$

$$+ \begin{bmatrix} \cos\bar{\alpha}_1 & \sin\bar{\alpha}_1 & \Delta_{x,1}\sin\bar{\alpha}_1 - \Delta_{y,1}\cos\bar{\alpha}_1 \\ \cos\bar{\alpha}_2 & \sin\bar{\alpha}_2 & \Delta_{x,2}\sin\bar{\alpha}_2 - \Delta_{y,2}\cos\bar{\alpha}_2 \\ -\bar{n}_1\sin\bar{\alpha}_1 & \bar{n}_1\cos\bar{\alpha}_1 & \bar{n}_1\left(\Delta_{x,1}\cos\bar{\alpha}_1 + \Delta_{y,1}\sin\bar{\alpha}_1\right) \\ -\bar{n}_2\sin\bar{\alpha}_2 & \bar{n}_2\cos\bar{\alpha}_2 & \bar{n}_2\left(\Delta_{x,2}\cos\bar{\alpha}_2 + \Delta_{y,2}\sin\bar{\alpha}_2\right) \end{bmatrix} \begin{bmatrix} n_1 \\ n_2 \\ \alpha_1 \\ \alpha_2 \end{bmatrix}, \tag{3.37}$$

and the differential (asynchronous) control signal

$$\tilde{\tau}_{act} = \begin{bmatrix} \cos\overline{\alpha_1} & \sin\overline{\alpha_1} & \Delta_{x,1}\sin\overline{\alpha_1} - \Delta_{y,1}\cos\overline{\alpha_1} \\ \cos\overline{\alpha_2} & \sin\overline{\alpha_2} & \Delta_{x,2}\sin\overline{\alpha_2} - \Delta_{y,2}\cos\overline{\alpha_2} \\ -\overline{n_1}\sin\overline{\alpha_1} & \overline{n_1}\cos\overline{\alpha_1} & \overline{n_1}\left(\Delta_{x,1}\cos\overline{\alpha_1} + \Delta_{y,1}\sin\overline{\alpha_1}\right) \\ -\overline{n_2}\sin\overline{\alpha_2} & \overline{n_2}\cos\overline{\alpha_2} & \overline{n_2}\left(\Delta_{x,2}\cos\overline{\alpha_2} + \Delta_{y,2}\sin\overline{\alpha_2}\right) \end{bmatrix}. \quad (3.38)$$

Using such linearization, it is possible to describe the functions of independent changes in the rotation speed and angles of the AT motors.

3.3 ITERATIVE MATCHING OF THE SELECTED POSITION POINT WITH THE MOTION CONTROLLER LINEARIZATION FUNCTION

Since for a simplified model some position points give the best results depending on the expected vehicle maneuver, the simplified trigonometric function of the AT motor orientation is an important aspect when choosing the position point, since they are periodic. After linearization, the trigonometric function loses its characteristic behavior, and a higher value always leads to an increase in torque. Therefore, the obtained simulation behavior should correspond to the position point i in order to obtain the most realistic result. For a sharp turn of the ship, a non-zero value of α for the selected algorithm would be reasonable, and for a sharp change of trajectory, a higher value of n and a zero value of α would be reasonable. These two different approaches will be used for linearization and are described as follows, starting with the algorithm for a sharp change of the ship trajectory (ascending algorithm)

$$\alpha = \begin{bmatrix} 20 \\ 0 \end{bmatrix}. \quad (3.39)$$

Using this position point and substituting the values of Δx_i, and Δy_i, of both motors into (3.33) let's obtain

$$\tilde{\tau}_{act} = \begin{bmatrix} 2 & 0 \\ 0 & 40 \\ 0 & -16 \end{bmatrix} \begin{bmatrix} n \\ \alpha \end{bmatrix}. \quad (3.40)$$

For the ship turning algorithm, the position point is defined as follows

$$\alpha = \begin{bmatrix} 10 \\ \pi/6 \end{bmatrix}, \quad (3.41)$$

adjusted to correspond to the non-zero angle of the AT propellers. The turning speed has also decreased. Inserting this value of $\Delta_{x,i}$ and $\Delta y_{,i}$ into (3.33) let's obtain

$$\tilde{\tau}_{act} = \begin{bmatrix} \sqrt{3} & 10 \\ -1 & 10\sqrt{3} \\ 0.4 & -4\sqrt{3} \end{bmatrix} \begin{bmatrix} n \\ \alpha \end{bmatrix}. \tag{3.42}$$

These will be two different linearizations that will be used during the simulation. Theoretically, the latter should give better results when modeling with an increased search speed. Let's obtain two position:

$$\alpha_d = \begin{bmatrix} 20\ 20\ 0\ 0 \end{bmatrix}^T, \tag{3.43}$$

$$\alpha_d = \begin{bmatrix} 10\ 10\ -\pi/6\ -\pi/6 \end{bmatrix}^T, \tag{3.44}$$

which will also be used for differential linearization and have equivalent values. These position determination points define the following equations:

$$\tilde{\tau}_{act} = \begin{bmatrix} 1 & 1 & 0 & 0 \\ 0 & 0 & 20 & 20 \\ -0.1 & 0.1 & -8 & -8 \end{bmatrix} \begin{bmatrix} n_1 \\ n_2 \\ \alpha_1 \\ \alpha_2 \end{bmatrix}, \tag{3.45}$$

$$\tilde{\tau}_{act} = \begin{bmatrix} \frac{\sqrt{3}}{2} & \frac{\sqrt{3}}{2} & 5 & 5 \\ -\frac{1}{2} & -\frac{1}{2} & 5\sqrt{3} & 5\sqrt{3} \\ \frac{4-\sqrt{3}}{20} & \frac{\sqrt{3}+4}{20} & \frac{1+4\sqrt{3}}{2} & \frac{1-4\sqrt{3}}{2} \end{bmatrix} \begin{bmatrix} n_1 \\ n_2 \\ \alpha_1 \\ \alpha_2 \end{bmatrix}. \tag{3.46}$$

Such linearization can increase the ship maneuverability and create different approaches to solving the control problem.

3.4 ADAPTATION OF DEFINED STATE SPACES ACCORDING TO THE ALGORITHMIZATION OF THE CONTROLLER OPERATION

To use LQR, the model must be defined in the state space form:

$$\dot{x} = Ax + Bu, \tag{3.47}$$

$$y = Cx + Du, \tag{3.48}$$

where x – the controlled states; u – the input signals; y – the output signals; A – the state matrix; B – the input matrix; C – the output matrix; D – the forward coupling matrix. Therefore, if M_{RB} is the inverse matrix, (3.4) must be written as

$$\dot{\nu} = M_{RB}^{-1}\left(-L(\nu) - D(\nu)\nu + \tau_{act}\right). \tag{3.49}$$

Using this equation and substituting the parameters and variables from (3.6), (3.8) and (3.26), it is possible to simplify the equation for τ_{act}. τ_{act} will be replaced by $\tilde{\tau}_{act}$, which is one of the linearized parameters. The equation can be simplified as follows:

$$\dot{\nu} = \begin{bmatrix} \dot{u} \\ \dot{\nu} \\ \dot{r} \end{bmatrix} = \begin{bmatrix} \frac{mx^2 - I_Z}{m^2x_G^2 + m^2y_G^2 - I_Z m} & \frac{x_G y_G}{m^2x_G^2 + m^2y_G^2 - I_Z} & \frac{-y_G}{m^2x_G^2 + m^2y_G^2 - I_Z} \\ \frac{x_G y_G}{mx_G^2 + my_G^2 - I_Z} & \frac{my_G^2 - I_Z}{m^2x_G^2 + m^2y_G^2 - I_Z} & \frac{x_G}{mx_G^2 + my_G^2 - I_Z} \\ \frac{-y_G}{mx_G^2 + my_G^2 - I_Z} & \frac{x_G}{mx_G^2 + my_G^2 - I_Z} & \frac{-1}{mx_G^2 + my_G^2 - I_Z} \end{bmatrix}$$

$$\left(-\begin{bmatrix} 0 & 0 & 0 \\ 0 & 0 & m \\ 0 & 0 & mx_G \end{bmatrix} \begin{bmatrix} u \\ \nu \\ r \end{bmatrix} - \begin{bmatrix} X_u u & 0 & 0 \\ 0 & Y_\nu \nu & 0 \\ 0 & 0 & N_r r \end{bmatrix} + \mu\tilde{\tau}_{act} \right) =$$

$$= \left(\frac{1}{mx_G^2 + my_G^2 - I_Z} \right) \begin{bmatrix} \frac{mx_G^2 - I_Z}{m} & x_G y_G & -y_G \\ x_G y_G & \frac{my_G^2 - I_Z}{m} & x_G \\ -y_G & x_G & -1 \end{bmatrix} \mu\tilde{\tau}_{act} -$$

$$- \begin{bmatrix} \frac{x_u\left(mx_G^2 - I_Z\right)}{m} & Y_\nu x_G y_G & -N_r y_G \\ X_u x_G y_G & Y_\nu\left(mx_G^2 - I_Z\right) & N_r x_G - mx_G^2 - my_G^2 + I_Z \\ -X_u y_G & Y_\nu x_G & -N_r \end{bmatrix} \begin{bmatrix} u \\ \nu \\ r \end{bmatrix}. \tag{3.50}$$

Assuming that the value is sufficiently small, it can be approximated to 0. Then the equation for ν can be simplified even further

$$\dot{\nu} = \begin{bmatrix} -\frac{X_u}{m} & 0 & 0 \\ 0 & -\frac{Y_u}{m} & 1 \\ 0 & 0 & -\frac{N_r}{I_Z} \end{bmatrix} \begin{bmatrix} u \\ \nu \\ r \end{bmatrix} + \begin{bmatrix} -\frac{\mu}{m} & 0 & 0 \\ 0 & -\frac{\mu}{m} & 1 \\ 0 & 0 & -\frac{\mu}{I_Z} \end{bmatrix} \tau_{act}. \quad (3.51)$$

The resulting form can be viewed as a state space representation, where:

$$x = \nu, \quad (3.52)$$

$$A = \begin{bmatrix} -\frac{X_u}{m} & 0 & 0 \\ 0 & -\frac{Y_u}{m} & 1 \\ 0 & 0 & -\frac{N_r}{I_Z} \end{bmatrix}, \quad (3.53)$$

$$u = \begin{bmatrix} n \\ \alpha \end{bmatrix}, \quad (3.54)$$

$$B = \begin{bmatrix} -\frac{\mu}{m} & 0 & 0 \\ 0 & -\frac{\mu}{m} & 1 \\ 0 & 0 & -\frac{\mu}{I_Z} \end{bmatrix} \tau_{act}. \quad (3.55)$$

This is because the sensors used to determine the ship's position and speed are in a moving coordinate system, which leads to the following definitions:

$$y = \begin{bmatrix} u \\ \nu \\ r \end{bmatrix}, \quad (3.56)$$

$$C = \begin{bmatrix} 1 & 0 & 0 \\ 0 & 1 & 0 \\ 0 & 0 & 1 \end{bmatrix}, \quad (3.57)$$

$$D = \begin{bmatrix} 0 & 0 \\ 0 & 0 \\ 0 & 0 \end{bmatrix}. \tag{3.58}$$

B will vary depending on the linearization of the input signal used, for example, if (3.40) and (3.42) are used. From (3.3) and (3.5), these values can be transferred to the *n*-system, where it is assumed that $\psi = 0$.

3.5 STRUCTURING A LINEAR QUADRATIC REGULATOR (LQR) AS A LINEARIZATION OBJECT

The main goal of the problem of adequate ship control is to minimize the design criterion, i.e., to balance it between the magnitude of the tracking error $e = y - r$ and the magnitude of the input signal. Sometimes such a paradigm can be viewed as an optimization problem, when the system is described by a linear differential equation, and the integration relationships are described by quadratic functions. Then the goal is to find the control law $u = -L_x$, where:

$$L = \arg\min \int_0^\infty \left(z^T(t) Q_1 z(t) + u^T(t) Q_2 u(t) \right) dt, \tag{3.59}$$

$$u = -Lx, \tag{3.60}$$

where Q_1 and Q_2 — weight matrices that can be used as design variables for this resulting controller. The optimization problem is solved using the expression

$$L = Q_2^{-1} B^T S, \tag{3.61}$$

where S — a positive semidefinite matrix that solves the Riccati algebra equation

$$A^T S + SA + M^2 Q_1 M - SBQ_2^{-1} B^T S = 0. \tag{3.62}$$

This equation can be solved using software such as MatLab/Simulink.

To achieve the desired design behavior of the system, an iterative modeling process and adjustment according to the observed controller behavior are required to find the optimal value of the constant coefficients. The controller defined above resets the system state to zero, but in this case the controller must follow a given reference signal.

Therefore, it is necessary to integrate the reference signal r in the equations. This can be done by rewriting the input signal as

$$u(t) = -Lx(t) + L_r r(t), \tag{4.63}$$

where L_r is chosen so that the static gain corresponds to the given value. A similar method of using LQR was applied in [29]. The system developed according to the above principle is shown in **Fig. 3.4**.

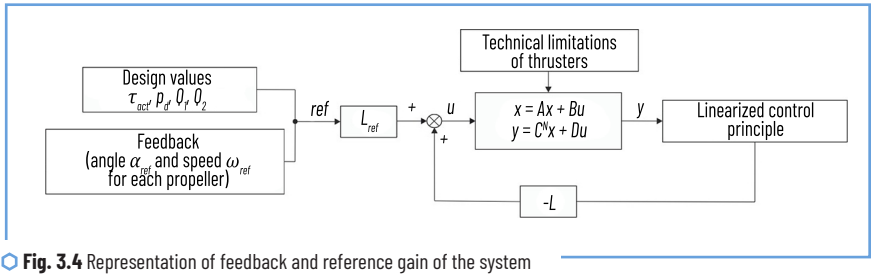

Fig. 3.4 Representation of feedback and reference gain of the system

Every system has uncertainties. Usually these uncertainties are modeled as a random stochastic process ("white noise"), which is a random signal with a constant spectrum. Taking into account the uncertainty, the model can be written as:

$$\dot{x} = Ax + Bu + Nv_1, \tag{3.64}$$

$$z = Mx, \tag{3.65}$$

$$y = Cx + v_2, \tag{3.66}$$

where v_1 and v_2 – white Gaussian noise with zero mean. In order to filter these signals, a state observer can be implemented that uses an estimate of the following form

$$\hat{x} = A\hat{x} = Bu + K(y - C\hat{x}) = (A - KC)\hat{x} + Bu + Ky. \tag{3.67}$$

This problem can be solved by describing it as an optimization problem by analogy with the definition of LQR with minimization of the variance of the estimation error. The estimation error can be denoted as $e = x - \hat{x}$, then the variance will be equal to $E_e(t)e(t)$. If v_1 and v_2 are independent and have zero mean, it is possible to assume that:

$$Ev_1v_1^T = R_1, \tag{3.68}$$

$$Ev_2v_2^T = R_2, \tag{3.69}$$

$$Ev_1v_2^T = 0. \tag{3.70}$$

Then the state observer can be described as:

$$K = PCR_2^{-1}, \tag{3.71}$$

where P — the covariance of the optimal estimator that solves the Riccati equation

$$A^T P + PA + NR_1 N^T - PC^T R_2^{-1} CP = 0. \tag{3.72}$$

The Kalman gain can also be found using Matlab/Simulink. Equation (3.72) is called the Kalman filter, where R_1 and R_2 are design variables and can be tuned to filter out process and measurement disturbances. LQR methods and Kalman filtering are discussed in detail in. The combined use of Kalman filtering and LQR is called Linear-Quadratic-Gaussian control (LQG). Similar approaches to using similar methods to solve such problems are discussed in [30].

MONITORING SYSTEM STRUCTURE

To predict the controller states, it is necessary to use a monitoring system using sensors used in marine navigation. The main monitoring systems used in ship control are the Inertial Measurement Unit (IMU) and the Global Positioning System (GPS).

STRUCTURE OF THE INERTIAL MEASUREMENT UNIT

The IMU uses a combination of accelerometers, gyroscopes, and magnetometers to measure angular speeds, accelerations, and magnetic fields. It is an important device for ship control because ships can move and rotate in all 6 degrees of freedom. The measurements from the gyroscope and accelerometer include some biases that create a systematic measurement error. If the angular speeds and accelerations are integrated, the resulting linear speed errors will increase linearly with time, and the orientation error will increase quadratically. Therefore, it will be difficult to rely solely on the IMU for this purpose over a longer period of time [31].

GLOBAL POSITIONING SYSTEM STRUCTURE WITH SENSOR INTEGRATION FOR CONDITION DETECTION

GPS is a system that uses satellite communication and data exchange with a receiver and provides location and time information in areas with unobstructed direct visibility. The most common GPS has for autonomous vehicles, the development and implementation of a high-integrity navigation system is based on the combined use of GPS and IMU. Improving the integrity of the navigation cycle will be carried out by

detecting possible faults both before and during the synthesis process. The implementation of this fault detection methodology takes into account both low-frequency faults in the IMU caused by sensor drift and device displacement, and high-frequency faults in the GPS receiver caused by multipath errors.

Using a Kalman filter to combine the information provided by the two sensors, it is possible to reduce the negative effects. The IMU offset can be adjusted, and when the GPS sensor is not in line of sight, the controller will rely more heavily on the IMU until the GPS is back in line of sight [32, 33]. However, since most maritime routes pass through open sky areas, the GPS signal will always be present, and therefore the main focus will be on correcting the IMU offset. This type of sensor integration for open air vehicle control is used where land-based vehicles are used instead of the SBV.

3.6 PHYSICAL MODELING OF A MARINE-BASED VEHICLE

The SBV physical scale model based on a controller that uses inputs from the GPS and IMU to determine the ship's position, heading, and speed.

Based on this data, the controller will control the actuators, the Electronically Commutated Motor (ECM), and the servo for each AT. The ECM are connected to the AT screw through gear transmissions (**Fig. 3.5**). The gear ratio between the servo drive and the AT connection is quite large. The main characteristics of the AT formalized physical model are presented in **Fig. 3.6** [34, 35].

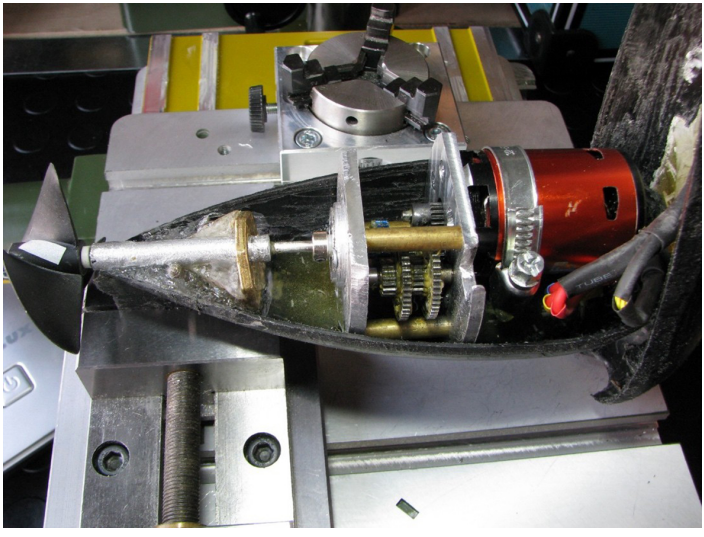

Fig. 3.5 Gearbox connecting the ECM to the AT screw

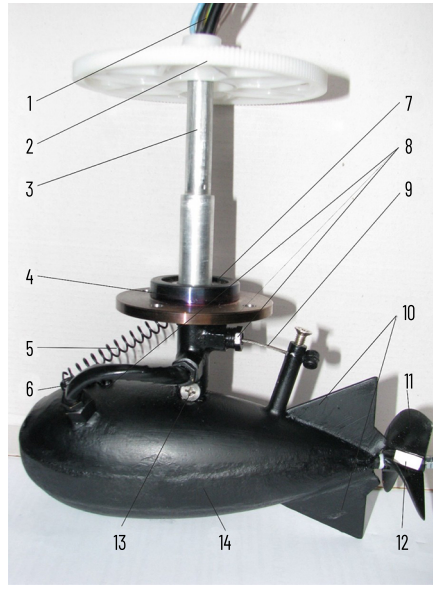

Fig. 3.6 Physical model of the thruster with two degrees of freedom: 1 — ECM power cable and the cable of the drive of changing the angle of inclination; 2 — driving gear of the baller rotation drive; 3 — baller; 4 — bearing shield; 5 — feedback spring of the drive of changing the angle of inclination; 6 — power cable; 7 — support bearing; 8 — gland entries; 9 — cable of the drive of changing the angle of inclination; 10 — stabilizing wings; 11 — GFK; 12 — luminescent tag for remote measurement of the frequency of GFK rotation; 13 — connection point of the baller with the AT body; 14 — AT body with the AT ECM located in the middle

To control the speed and torque of the ECM, the motor currents are measured and the throughput is calculated with high accuracy (**Fig. 3.7, 3.8**). Torque control is an integral part of the design of most applied speed control circuits of AT electric drive systems.

Theoretically, the torque rise time in a frequency converter (FC) with pulse-width modulation (PWM) is limited by the motor inductance in dependent current inverters with a DC link [36].

However, in practice, the controller limits the rate of change of torque to prevent damage to the mechanical part of the electric drive.

Thus, the transfer function of the controller can be described by the dependence [37]:

$$F_p(S) = \frac{1}{\left(1 - t_{FC} S\right)} M_d(s), \tag{3.73}$$

where t_{FC} = 20÷200 ms.

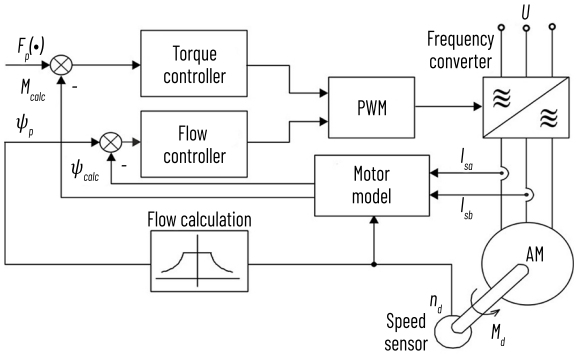

Fig. 3.7 Block diagram of the AT ECM closed-loop torque control system: Ψ_p and Ψ_{calc} — the values of the set and calculated fluxes, I_{sa}, I_{sb} — the measured values of the stator currents

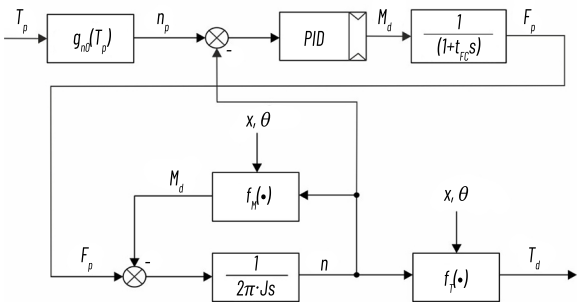

Fig. 3.8 Block diagram of the ECM speed controller

3.7 SIMULATION STUDIES OF THE CHANGE IN THE YAW SPEED BASED ON THE DEFINED STATE SPACE

To investigate the behavior of the physical scale model of the ship during a turn, a setting step is made at the reference yaw speed. To check the possibilities and realistic implementation in practice, two different simulations are performed: one in which there is some "softening" of the settling time and overshoot occurs (peak test), and the other in which the controller tries to adhere to the reference setting as "rigidly" as possible (smooth test). The peak test was adjusted so that all simulations, including this one, had the same settling time of approximately 10 seconds after the start of the setting. Since linearization and simplification of the model were performed, this test may give unrealistic results, but, as before, it is considered to be consistent with the capabilities of the control system [38].

DETERMINATION OF THE ERROR OF SYNCHRONOUS CONTROL WITH ZERO THRUSTER ANGLE FROM THE SELECTED POSITION MATRIX

For the following simulations, the same rotational speed and propeller angle are chosen for both APUs.

In this simulation, the controller uses matrices obtained by linearizing around the operating point with translational motion of the input signals (3.40), which are designed to operate with propeller angles close to zero. Two different settings are used for the controller, which are performed for two objectives: first, for the condition when the input signals are equal to 1, and the reference gain is adjusted to achieve the target value. Another setting eliminates the tracking error for increasing the rotation speed, providing the closest to the reference speed value, while maintaining the input signal level for the lower swing speed value. Therefore, finding the setting limit takes more time, which provides information about the system capability by comparing the evenly and more aggressively tuned system. The matrices of reference coefficients and transfer coefficients, where p and s denote the peak and smoothing indices, respectively, will look like [39]:

$$Q_{1,p} = \begin{bmatrix} 1 & 0 & 0 \\ 0 & 1 & 0 \\ 0 & 0 & 1 \end{bmatrix}, Q_{1,s} = \begin{bmatrix} 1 & 0 & 0 \\ 0 & 0.001 & 0 \\ 0 & 0 & 200 \end{bmatrix},$$

$$Q_{2,p} = \begin{bmatrix} 1 & 0 \\ 0 & 1 \end{bmatrix}, Q_{2,s} = \begin{bmatrix} 1 & 0 \\ 0 & 1 \end{bmatrix},$$

$$L_{r,p} = \begin{bmatrix} 0 & 0 & 1 \\ 0 & 0 & -22.14 \end{bmatrix}, L_{r,s} = \begin{bmatrix} 0 & 0 & 1 \\ 0 & 0 & -14.06 \end{bmatrix}. \quad (3.74)$$

Fig. 3.9 shows the main results of the operation of two different controllers. The maximum value controller provides an overshoot of 7 times the reference value, but stabilizes after 10 s.

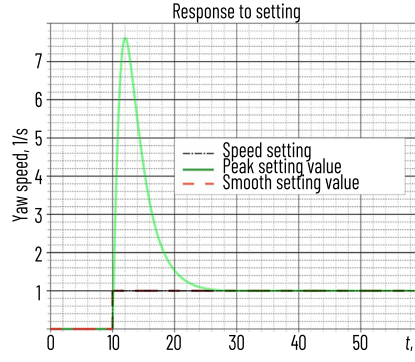

Fig. 3.9 Transient characteristic of zero angle linearization

According to **Fig. 3.10, *b***, the final value of α is $\alpha_p = \alpha_s = 0.065$ rad.

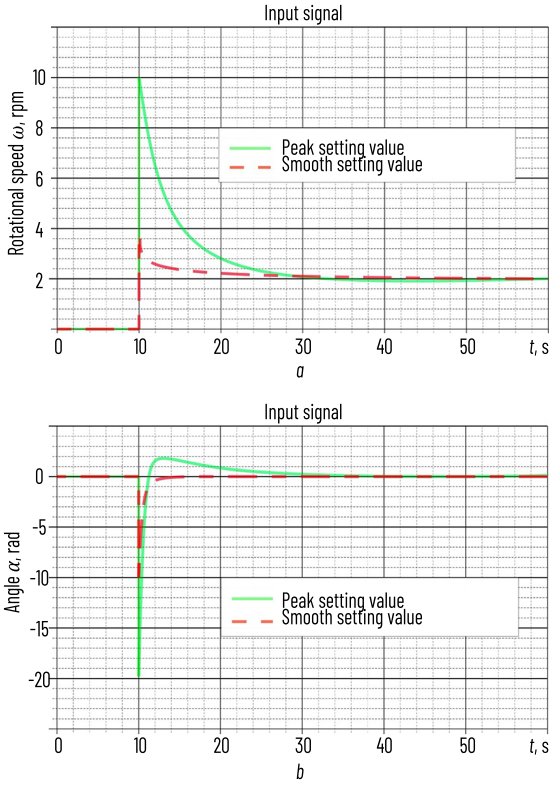

Fig. 3.10 Input signals of zero angle linearization: *a* — rotation speed; *b* — angle α

This is most likely the result of changing the AT angle, as shown in **Fig. 3.10, *a, b***, where α reaches a very high negative value, close to — 20 rad, which is far from the realistic scenario for a real AT.

This fact gives grounds to reassess the need for a more drastic change in the crawl speed over the slow one to counteract the condition when the overshoot reaches such a high value. However, decreasing α is physically reasonable, because a small negative angle will provide a positive torque around the *z*-axis and a positive crawl speed. Although it may be debatable if such a small angle can have such an effect, if a zero angle gives similar results for this controller mode. Another interesting aspect is how separated the rotation

speed and the speed jumps are, since the controller shows the same behavior for both simulations, which for a real AT can significantly affect the results [40].

In a smooth controller, the output value seems to "follow" the reference value, but has two differences from the other controller: the same decrease and restoration of α to the final stabilized value in less than a second, which is not possible for a real AT due to its dynamic properties. In **Fig. 3.11**, the oscillation speed is set much slower, which may indicate that there is some uncoupled behavior, since the input signal to the system is the same time interval of 20 seconds, but the oscillation speed at this time is different. Some unrealistic AT behavior may be associated with the linearization of α and its trigonometric dependence. The trigonometric function, which is periodic and only distributes the forces created by the number of revolutions between the x_b and y_b axes, cannot exceed 1. When applying linearization, the controller "believes" that a higher value of α corresponds to a higher value of the resulting force, which in practice is not true.

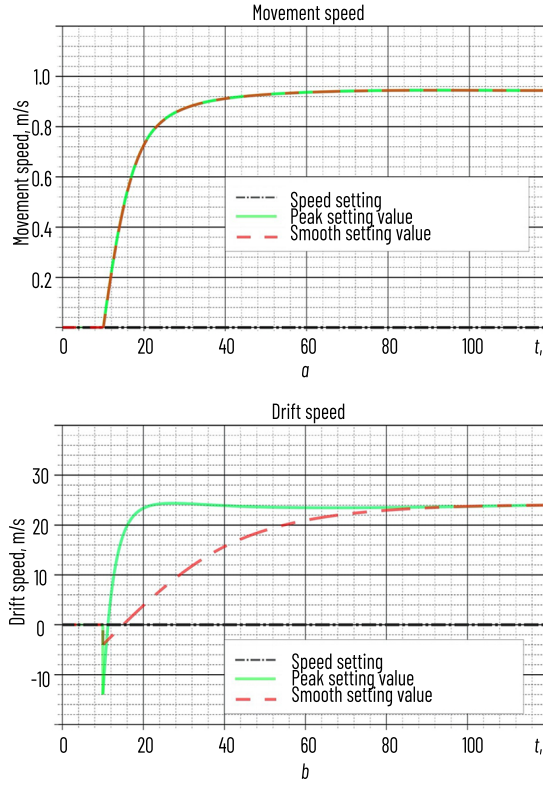

Fig. 3.11 Linearization at zero angle: *a* — speed; *b* — drift speed

DETERMINATION OF THE ERROR OF SYNCHRONOUS CONTROL WITH A NON-ZERO ANGLE OF THE THRUSTERS BY THE SELECTED LOCATION MATRIX

The model is tuned based on the linearization method (3.41), where the angle of the propellers α has a small negative value, which is considered close to the resulting final value for a given simulation of the yaw speed. This is done in order to see if this tuning will give better results than linearization with a zero angle. The design goals of the tuning are similar to the previous simulations. One of the main differences is that the third element in the first row for a given gain value also needed tuning, otherwise the speed jump tends to take a negative value, which requires a different behavior of the model and makes it difficult to compare the two simulations. The weight matrices and gain values for this simulation are as follows:

$$Q_{1,p} = \begin{bmatrix} 1 & 0 & 0 \\ 0 & 1 & 0 \\ 0 & 0 & 1 \end{bmatrix}, Q_{1,s} = \begin{bmatrix} 1 & 0 & 0 \\ 0 & 0.001 & 0 \\ 0 & 0 & 225 \end{bmatrix},$$
$$Q_{2,p} = \begin{bmatrix} 1 & 0 \\ 0 & 1 \end{bmatrix}, Q_{2,s} = \begin{bmatrix} 1 & 0 \\ 0 & 1 \end{bmatrix},$$
$$L_{r,p} = \begin{bmatrix} 0 & 0 & 10 \\ 0 & 0 & -21.6 \end{bmatrix}, L_{r,s} = \begin{bmatrix} 0 & 0 & 3.63 \\ 0 & 0 & -14.09 \end{bmatrix}. \quad (3.75)$$

which gives the results shown in **Fig. 3.12–3.14**.

According to **Fig. 3.13**, the final value of α is: $\alpha_p = \alpha_s = 0.0168$ rad.

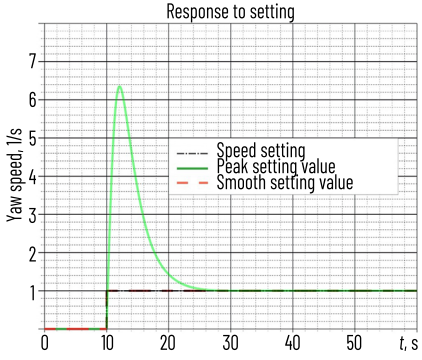

Fig. 3.12 Transient response with non-zero angle α

These results are similar to those obtained but with some differences in the behavior of the model. The peak tuning gives slightly better results, since its overshoot reaches only 6 times the reference value.

The main difference is the higher propeller speed, which is almost ten times more influential on the longitudinal speed. That is, the non-minimum phase response coincides with the fastest response when the maximum peak speed of the setting is reached. The smooth tuning makes the controller response slower than during the "peak tuning" according to $Q_{1,s}$ (3.75).

The most interesting thing in this simulation compared is the input signal graphs in **Fig. 3.13, *a*, *b***. The rotation speed has a much larger value, unlike the angle α, the resulting transient response of which has almost not changed. First, this may be the result of linearization, in which the controller mainly responds to the angle α setting with n maintained at the same level, if there is no need to increase the rotation speed. Second, the input signals show which setpoint values for α are positive, close to zero, but positive. Theoretically, for the simulation process, this should not be the case.

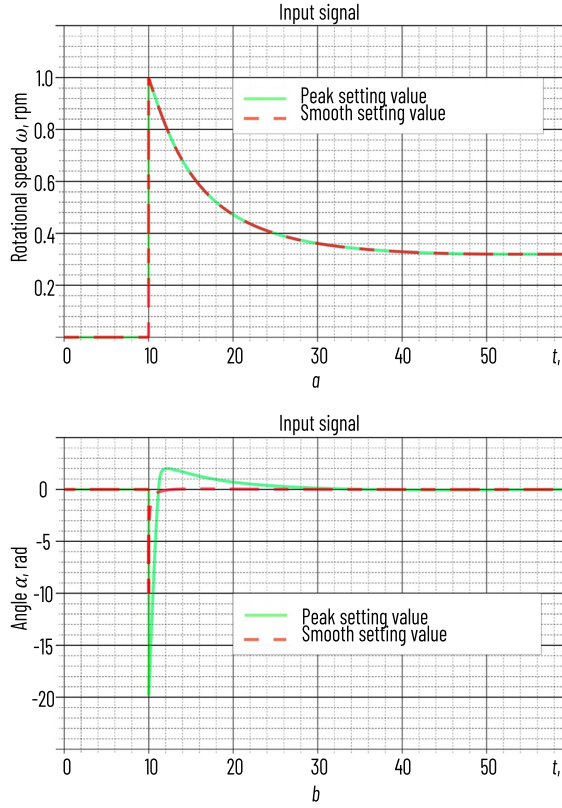

Fig. 3.13 Input signals with non-zero angle α: *a* — propeller rotation frequency; *b* — angle α

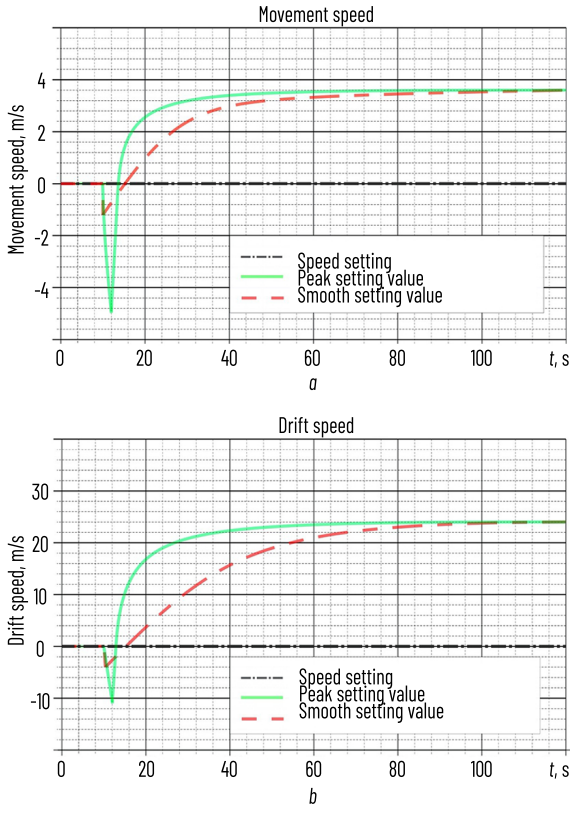

Fig. 3.14 Dependences of speeds with non-zero angle α: *a* — speed of movement; *b* — drift speed

DETERMINATION OF THE ERROR OF ASYNCHRONOUS CONTROL WITH ZERO ANGLE OF THRUSTERS BY THE SELECTED LOCATION MATRIX

The following simulation uses differential control, in other words, the possibility of independent control of the speed and angle of rotation of both ATs.

First, linearization with zero angle α is used for differential (asynchronous) control of the stern ATs. The simulation is carried out according to the same algorithm to study two tuning schemes with different goals. Using differential (asynchronous) control, one can observe a slightly different, potentially more improved behavior of the controller, which is confirmed by the following results:

$$Q_{1,p} = \begin{bmatrix} 1 & 0 & 0 \\ 0 & 1 & 0 \\ 0 & 0 & 1 \end{bmatrix}, Q_{1,s} = \begin{bmatrix} 1 & 0 & 0 \\ 0 & 0.015 & 0 \\ 0 & 0 & 270 \end{bmatrix},$$

$$Q_{2,p} = \begin{bmatrix} 1 & 0 & 0 & 0 \\ 0 & 1 & 0 & 0 \\ 0 & 0 & 1 & 0 \\ 0 & 0 & 0 & 1 \end{bmatrix}, Q_{2,s} = \begin{bmatrix} 1 & 0 & 0 & 0 \\ 0 & 1 & 0 & 0 \\ 0 & 0 & 1 & 0 \\ 0 & 0 & 0 & 1 \end{bmatrix},$$

$$L_{r,p} = \begin{bmatrix} 0 & 0 & 1 \\ 0 & 0 & 1 \\ 0 & 0 & -20 \\ 0 & 0 & -20 \end{bmatrix}, L_{r,s} = \begin{bmatrix} 0 & 0 & 1 \\ 0 & 0 & 1 \\ 0 & 0 & -12.32 \\ 0 & 0 & -12.32 \end{bmatrix}. \quad (3.76)$$

The final values of α_p and α_s (**Fig. 3.15**) are: $\alpha_p = -0.084$ rad, $\alpha_s = -0.41$ rad.

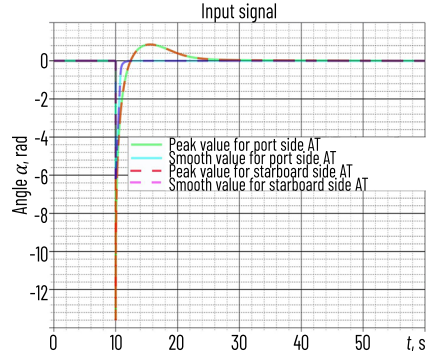

Fig. 3.15 Differential input signals at a given zero angle α

The transient responses for the longitudinal, drift and yaw speeds (**Fig. 3.16** and **3.17**) show the AT operation similar to the synchronous control simulation. Here the step response is lower and the longitudinal speed reaches a higher final value. However, some interesting things can be observed in the input signals. The angle α is the same for both motors with two different settings, despite the AT having differential degrees of freedom. This may be the result of linearization, which makes it the only adequate solution. The large dip shown in **Fig. 17, *b*,** with the simulation is smaller, indicating steps in the right direction. The final value of α for the peak setting is almost the same as for the synchronous control, but the smooth setting is closer to the actual value of $\pi/6$, which is also a good indicator for this controller.

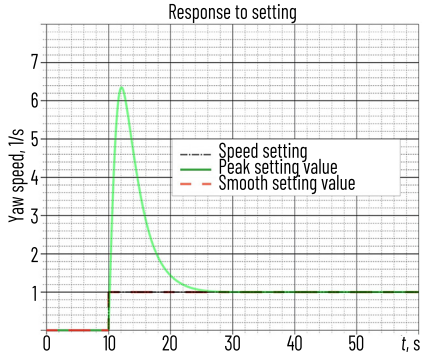

Fig. 3.16 Differential transient response for zero angle α

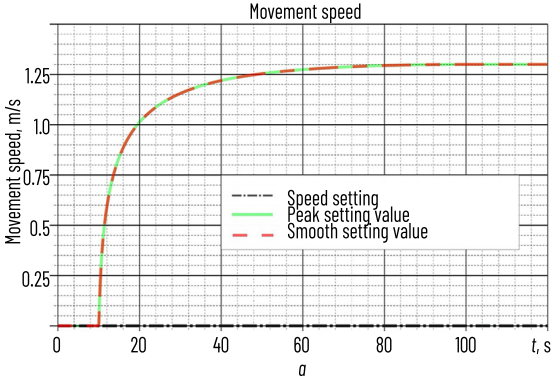

a

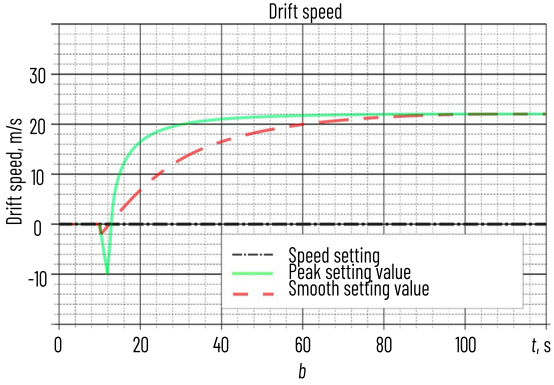

b

Fig. 3.17 Differential speeds at zero angle α: *a* – longitudinal motion; *b* – drift

It is possible to observe completely different indicators n (**Fig. 3.18**), which indicates a smaller influence on the system of this input signal. For both settings, one of the screws rotates at a lower speed, which in practice is an advantage. When one motor provides more thrust, it creates a corresponding torque, turning the ship.

Using this difference in rotation speed, the controller can more effectively regulate the speed of the ship's turn.

The problem that can be seen in this simulation is that any configuration of the values of the AT rotation speed moves the ship "wrongly".

Since motor 1 is located to the right of the x_b axis, and motor 2 to the left, such a run will provide a negative speed of turn.

This is another sign that the controller is counteracting itself, which confirms the consequence of the linearization of the input signal.

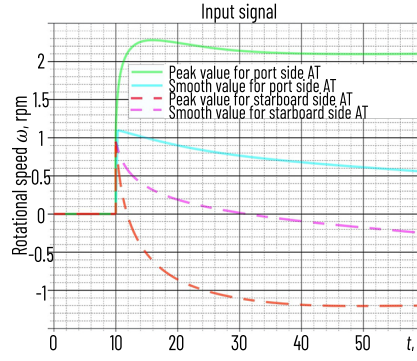

Fig. 3.18 Differential speeds of rotation of the APU at zero angle α

DETERMINATION OF THE ASYNCHRONOUS CONTROL ERROR WITH A NON-ZERO ANGLE OF THE THRUSTERS BY THE SELECTED LOCATION MATRIX

The following settings are based on the model with linearization of the non-zero differential angle (3.41) and have the same tuning aspects as in the previous simulation with the same problem, where the controller required negative speed jumps.

Therefore, this was also corrected by tuning the controller. The weight matrices and the reference gain have the following form:

$$Q_{1,p} = \begin{bmatrix} 1 & 0 & 0 \\ 0 & 1 & 0 \\ 0 & 0 & 1 \end{bmatrix}, Q_{1,s} = \begin{bmatrix} 1 & 0 & 0 \\ 0 & 0.05 & 0 \\ 0 & 0 & 250 \end{bmatrix},$$

$$Q_{2,p} = \begin{bmatrix} 1 & 0 & 0 & 0 \\ 0 & 1 & 0 & 0 \\ 0 & 0 & 1 & 0 \\ 0 & 0 & 0 & 1 \end{bmatrix}, Q_{2,s} = \begin{bmatrix} 1 & 0 & 0 & 0 \\ 0 & 1 & 0 & 0 \\ 0 & 0 & 1 & 0 \\ 0 & 0 & 0 & 1 \end{bmatrix},$$

$$L_{r,p} = \begin{bmatrix} 0 & 0 & 5 \\ 0 & 0 & 5 \\ 0 & 0 & -5.31 \\ 0 & 0 & -5.31 \end{bmatrix}, L_{r,s} = \begin{bmatrix} 0 & 0 & 6 \\ 0 & 0 & 6 \\ 0 & 0 & -9.81 \\ 0 & 0 & -9.81 \end{bmatrix}. \quad (3.77)$$

The simulation results are presented in **Fig. 3.19–3.23**.

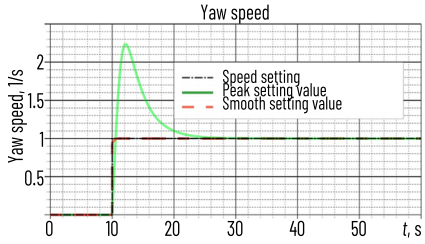

Fig. 3.19 Differential transient response with non-zero angle α

The final values of α_p and α_s (**Fig. 3.22**) are:

$\alpha_{p,1} = 3.64$ rad, $\alpha_{s,1} = 2.68$ rad;

$\alpha_{p,2} = -4.81$ rad, $\alpha_{s,2} = -3.52$ rad.

The simulation results are unique among all the search speed simulations. The peak step shows that the outlier is significantly lower than in any of the previous calculations. This overshoot only reaches twice the reference value. The transient plots in **Fig. 3.22** show similar results to the previous simulations, but with different final values. They can be adjusted by applying a reference gain, which is not necessary, since the goal of the simulation is to find out how the AT behavior affects the system, not what the final values of the angles α are.

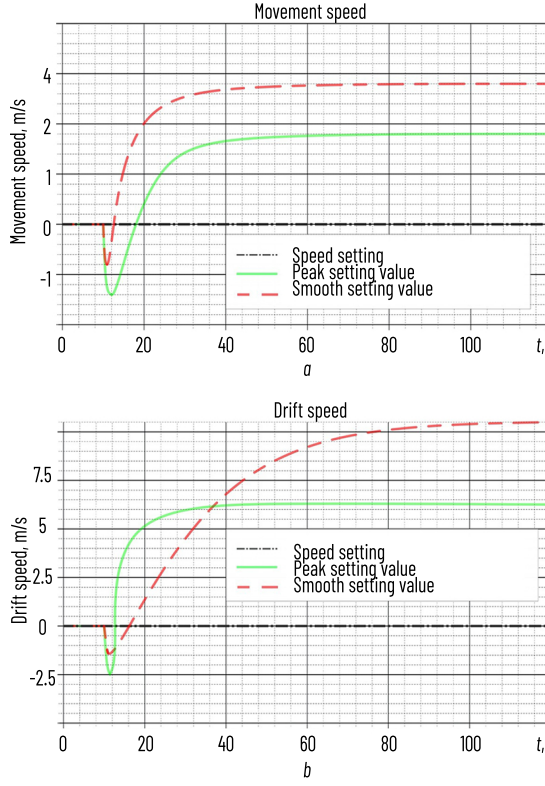

Fig. 3.20 Differential speeds at a non-zero angle α: *a* — longitudinal motion; *b* — drift

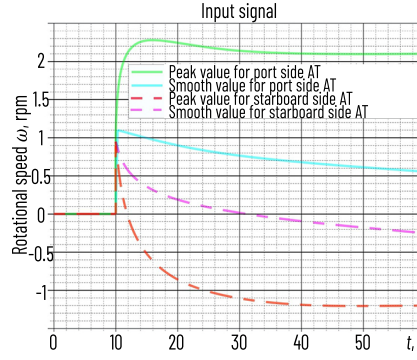

Fig. 3.21 Differential rotational speeds with a non-zero angle

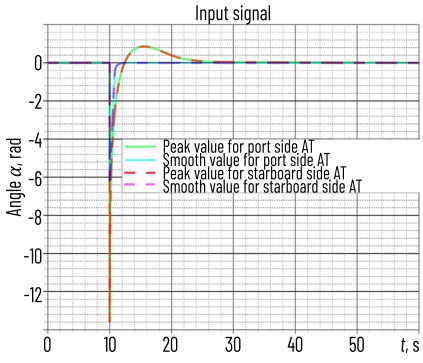

Fig. 3.22 Differential input signals at a given non-zero angle α

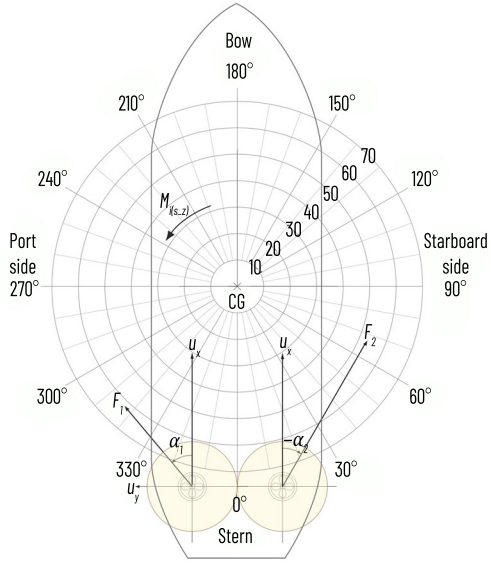

Fig. 3.23 Position and angle of rotation of motor *i*

However, in practice, the input signals "behave" realistically. Both the step and smooth tuning lead to similar transient characteristics, but with different final values. These values have been interpreted and illustrated in **Fig. 3.23**. Here it is possible to see that both AT motors, as in the previous simulations,

counteract each other, but now in a controlled manner. The left AT has a larger angle α compared to the right, which provides a larger torque about the z axis and, therefore, an increase in the turning speed. While the right motor has a higher rotation speed, creating a negative torque about the z axis and, thus, canceling the forces from the left motor. This allows to achieve a constant turning speed. However, the method creates many unnecessary opposing forces in the y_b direction. The angle values are still far from the operating point, which makes the linearization accuracy low. However, the obtained results show trends in the right direction.

DETERMINATION OF THE LIMITING CHARACTERISTICS OF THE CONTROLLER

To further test the capabilities of the system, a controller was developed to set the azimuthal angle limits instead of strictly following the reference sweep speed step. This simulation was performed with differential non-zero angle linearization. The weight and reference gain matrices for this simulation are as follows:

$$Q_1 = \begin{bmatrix} 0.01 & 0 & 0 \\ 0 & 0.01 & 0 \\ 0 & 0 & 1 \end{bmatrix}, Q_2 = \begin{bmatrix} 1 & 0 \\ 0 & 1 \end{bmatrix}, L_r = \begin{bmatrix} 0 & 0 & 6 \\ 0 & 0 & 6 \\ 0 & 0 & -1.31 \\ 0 & 0 & -1.31 \end{bmatrix}. \quad (3.78)$$

The simulation results are shown in **Fig. 3.24–3.27**.

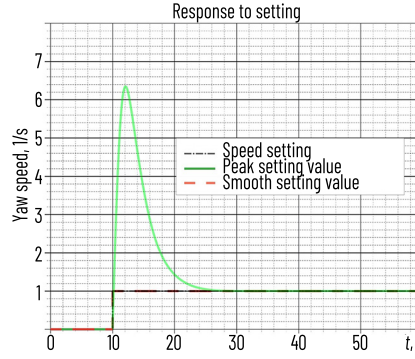

Fig. 3.24 Setting step characteristic limits

The final values of α_1 and α_2 (**Fig. 3.27**) are:

$\alpha_1 = 0.63$ rad, $\alpha_2 = -0.28$ rad.

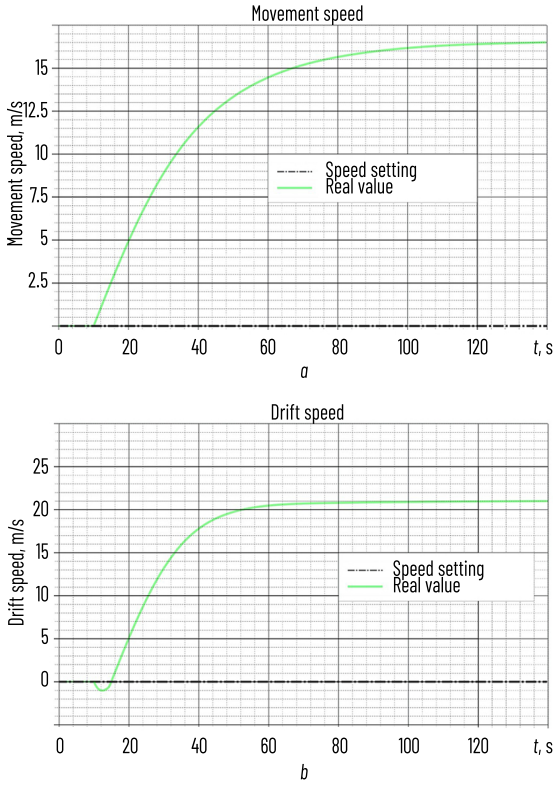

Fig. 3.25 Limit settings: *a* – longitudinal acceleration; *b* – drift acceleration

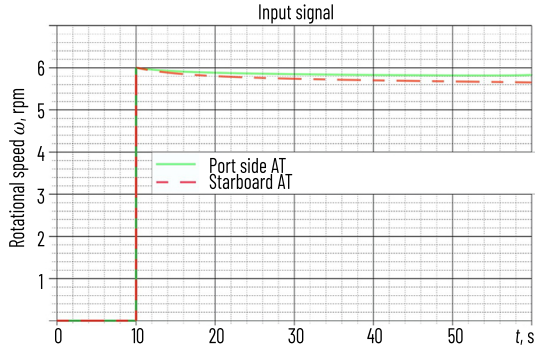

Fig. 3.26 Rotation speed limit settings

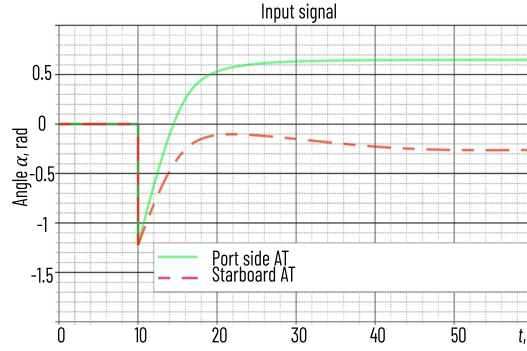

Fig. 3.27 Angle α limit settings

Table 3.1 shows the calculated data and parameters of the SBV physical model *0* (**Fig. 3.1, 3.5, 3.6**) for real-time modeling of the model behavior in the dynamic positioning mode with adequate distribution of the AT thrust and generation of optimal control input data.

Table 3.1 Parameters of the SBV model and thrusters

Name	Designation	Unit	Value
Port side AT	Δ_{yl}	m	–1.22
	Δ_{xl}	m	–0.23
	F_{max}	N	894
	F_{min}	N	0.264
	ω	rev/s	7.96
	α_{lmax}	Rad	3.925
	α_{lmin}	Rad	–0.785
	$\Delta\alpha$	Rad	0.088
	M_p (56)	m/(rev/s)^2	6.6e–4
Starboard AT	Δ_{x2}	M	0.23
	α_{2max}	rad	–0:175
	α_{2min}	rad	–3:054

The SBV model with the AT moved forward with a constant thrust force F_x, and changed course by turning the torque varying in time with a duration of 450 s. Random "noise" was added to the desired generalized force to check the reliability and stability of the given thrust distribution method.

CONCLUSIONS

Improvement of the AT linear-quadratic control method of the ship's propulsion complex consisted in determining the state spaces and linearizing the control system, which allowed to adequately model the ship's yaw rate and track the influence of disturbing forces on the controller characteristics. Moreover, it was found that small negative angles provide a positive torque around the z axis and a positive yaw rate. To take into account the dynamic properties of real AT, it is necessary to be able to regulate the reduction and restoration of the angle α to the final stabilized value. It can also be concluded that when applying linearization, a larger value of α corresponds to a larger value of the resulting force, which in practice does not correspond to reality.

Verification of the model behavior showed that in order to obtain a relatively adequate transient response with minimal overshoot, it is necessary to minimize the tracking error. Studies of the design features of ships of this class confirm that jumps in the speed of AT rotation, which are stabilized with a constant zero angle, lead to a quick response to the jump and the absence of overshoot. Small angles of the AT location relative to the diametrical plane of the ship lead to the fact that both AT motors require a lower speed of rotation to provide a given thrust.

For physical scale modeling, AT physical model in the stern can be implemented on the basis of actuators, an electronically commutated motor and a servo drive for each AT. The electronically commutated motor is connected to the AT propeller through gears. In practice, the controller uses input data from GPS and IMU to determine the position, course and speed of the ship. To regulate the speed and torque of the electric motor, it is necessary to measure the motor currents and calculate the bandwidth of the converters with high accuracy. In practice, it is necessary to provide a limit on the rate of change of torque to prevent damage to the mechanical part of the electric drive.

Independent control of the speed and angle of the AT with linearization with zero or non-zero angle of the AT has proven its greater controllability than synchronous. To reduce the resistance of the AT motors, it is necessary to apply a coordinated change in the angle α with the speed of rotation. And to compensate for the corresponding forces, it is necessary to adjust the speed of rotation, creating a negative torque around the z axis. Increasing the accuracy of linearization is possible by eliminating excess opposing forces in the y_b direction.

Using the predictive gain method in the future will allow, although reducing the versatility of the controller, to increase its realism. To improve the performance of the models, the controller was tuned to more realistic output and input parameters. Changing the principles of linearization of the input signal led to the fact that it acts more like a trigonometric function of predictive gain. The result allowed to clarify the influence of the AT orientation on the ship position, and the linearity of the model on the controller functionality.

REFERENCES

1. Budashko, V., Nikolskyi, V., Onishchenko, O., Khniunin, S. (2016). Decision support system's concept for design of combined propulsion complexes. Eastern-European Journal of Enterprise Technologies, 3 (8 (81)), 10–21. https://doi.org/10.15587/1729-4061.2016.72543

2. Budashko, V. V. (2017). Design of the three-level multicriterial strategy of hybrid marine power plant control for a combined propulsion complex. Electrical Engineering & Electromechanics, 2, 62–72. https://doi.org/10.20998/2074-272x.2017.2.10
3. Budashko, V. (2017). Formalization of design for physical model of the azimuth thruster with two degrees of freedom by computational fluid dynamics methods. Eastern-European Journal of Enterprise Technologies, 3 (7 (87)), 40–49. https://doi.org/10.15587/1729-4061.2017.101298
4. Budashko, V. V. (2016). Increasing control's efficiency for the ship's two-mass electric drive. Electrical Engineering & Electromechanics, 4, 34–42. https://doi.org/10.20998/2074-272x.2016.4.05
5. Budashko, V., Sandler, A., Khniunin, S. (2023). Improving the method of linear-quadratic control over a physical model of vessel with azimuthal thrusters. Eastern-European Journal of Enterprise Technologies, 1 (2 (121)), 49–71. https://doi.org/10.15587/1729-4061.2023.273934
6. Myrhorod-Karpova, V., Hvozdeva, I., Budashko, V. (2022). Multiparameter Approximation Model of Temperature Conditions of Marine Diesel Generator Sets, Based on Markov Chain Monte Carlo. TransNav, the International Journal on Marine Navigation and Safety of Sea Transportation, 16 (4), 779–784. https://doi.org/10.12716/1001.16.04.20
7. Budashko, V., Golikov, V. (2017). Theoretical-applied aspects of the composition of regression models for combined propulsion complexes based on data of experimental research. Eastern-European Journal of Enterprise Technologies, 4 (3 (88)), 11–20. https://doi.org/10.15587/1729-4061.2017.107244
8. Budashko, V., Sandler, A., Glazeva, O. (2024). Improvement of the Predictive Control Method for the High-Level Controller. 2024 IEEE 17th International Conference on Advanced Trends in Radioelectronics, Telecommunications and Computer Engineering (TCSET). Lviv, 294–297. https://doi.org/10.1109/tcset64720.2024.10755561
9. Hvozdeva, I., Myrhorod, V., Budashko, V., Shevchenko, V. (2020). Problems of Improving the Diagnostic Systems of Marine Diesel Generator Sets. 2020 IEEE 15th International Conference on Advanced Trends in Radioelectronics, Telecommunications and Computer Engineering (TCSET). Slavske, 350–354. https://doi.org/10.1109/tcset49122.2020.235453
10. Budashko, V., Shevchenko, V. (2018). Synthesis of the Management Strategy of the Ship Power Plant for the Combined Propulsion Complex. 2018 IEEE 5th International Conference on Methods and Systems of Navigation and Motion Control (MSNMC). Kyiv, 106–109. https://doi.org/10.1109/msnmc.2018.8576266
11. Budashko, V., Hvozdeva, I., Onishchenko, O., Shevchenko, V., Kudelkin, R. (2020). Improvement of the operation for electromechanical system under non-permanent loading. 2020 IEEE 15th International Conference on Advanced Trends in Radioelectronics, Telecommunications and Computer Engineering (TCSET). Slavske, 35–39. https://doi.org/10.1109/tcset49122.2020.235588
12. Budashko, V. (2020). Thrusters Physical Model Formalization with regard to Situational and Identification Factors of Motion Modes. 2020 International Conference on Electrical, Communication, and Computer Engineering (ICECCE). Istanbul, 1–6. https://doi.org/10.1109/icecce49384.2020.9179301
13. Budashko, V., Obniavko, T., Onishchenko, O., Dovidenko, Y., Ungarov, D. (2020). Main Problems of Creating Energy-efficient Positioning Systems for Multipurpose Sea Vessels. 2020 IEEE 6th International

Conference on Methods and Systems of Navigation and Motion Control (MSNMC). Kyiv, 106–109. https://doi.org/10.1109/msnmc50359.2020.9255514

14. Budashko, V., Shevchenko, V. (2021). The synthesis of control system to synchronize ship generator assemblies. Eastern-European Journal of Enterprise Technologies, 1 (2 (109)), 45–63. https://doi.org/10.15587/1729-4061.2021.225517
15. Budashko, V., Shevchenko, V. (2021). Solving a task of coordinated control over a ship automated electric power system under a changing load. Eastern-European Journal of Enterprise Technologies, 2 (2 (110)), 54–70. https://doi.org/10.15587/1729-4061.2021.229033
16. Budashko, V. Diagnosis of the Technical Condition of High-Tech Complexes by Probabilistic Methods [Text] / V. Budashko, I. Hvozdeva, V. Shevchenko, V. Myrhorod, A. Sandler, O. Glazeva // 2022 IEEE 16th International Conference on Advanced Trends in Radioelectronics, Telecommunications and Computer Engineering (TCSET), Slavske, 22-26 Feb. 2022, Ukraine: IEEE TCSET 2022. – P. 7-14. Doi: https://doi.org/10.1109/TCSET49122.2020.235588
17. Budashko, V., Sandler, A., Shevchenko, V. (2022). Optimization of the control system for an electric power system operating on a constant-power hyperbole. Eastern-European Journal of Enterprise Technologies, 1 (8 (115)), 6–17. https://doi.org/10.15587/1729-4061.2022.252172
18. Budashko, V., Sandler, A., Shevchenko, V. (2022). Diagnosis of the Technical Condition of High-tech Complexes by Probabilistic Methods. TransNav, the International Journal on Marine Navigation and Safety of Sea Transportation, 16 (1), 105–111. https://doi.org/10.12716/1001.16.01.11
19. Sir Elkhatem, A., Naci Engin, S. (2022). Robust LQR and LQR-PI control strategies based on adaptive weighting matrix selection for a UAV position and attitude tracking control. Alexandria Engineering Journal, 61 (8), 6275–6292. https://doi.org/10.1016/j.aej.2021.11.057
20. Furmanik, M., Konvičný, D., Rafajdus, P. (2023). Low-Speed Sensorless Control for Six-Phase PMSM Based on Magnetic Anisotropy. Transportation Research Procedia, 74, 892–899. https://doi.org/10.1016/j.trpro.2023.11.222
21. Budashko, V., Sandler, A., Khniunin, S., Bogach, V. (2024). Design of the predictive management and control system for combined propulsion complex. Eastern-European Journal of Enterprise Technologies, 5 (2 (131)), 90–102. https://doi.org/10.15587/1729-4061.2024.313627
22. van Goor, P., Hamel, T., Mahony, R. (2023). Constructive Equivariant Observer Design for Inertial Navigation. IFAC-PapersOnLine, 56 (2), 2494–2499. https://doi.org/10.1016/j.ifacol.2023.10.1229
23. Hemalatha, N., Venkatesan, S., Kannan, R., Kannan, S., Bhuvanesh, A., Kamaraja, A. S. (2024). Sensorless speed and position control of permanent magnet BLDC motor using particle swarm optimization and ANFIS. Measurement: Sensors, 31, 100960. https://doi.org/10.1016/j.measen.2023.100960
24. Sagin, S. V., Semenov, O. V. (2016). Motor Oil Viscosity Stratification in Friction Units of Marine Diesel Motors. American Journal of Applied Sciences, 13 (2), 200–208. https://doi.org/10.3844/ajassp.2016.200.208
25. Lang, X., Mao, W. (2020). A semi-empirical model for ship speed loss prediction at head sea and its validation by full-scale measurements. Ocean Engineering, 209, 107494. https://doi.org/10.1016/j.oceaneng.2020.107494

26. Maidana, R. G., Kristensen, S. D., Utne, I. B., Sørensen, A. J. (2023). Risk-based path planning for preventing collisions and groundings of maritime autonomous surface ships. Ocean Engineering, 290, 116417. https://doi.org/10.1016/j.oceaneng.2023.116417
27. Myrhorod, V., Hvozdeva, I., Budashko, V. (2020). Multi-parameter Diagnostic Model of the Technical Conditions Changes of Ship Diesel Generator Sets. 2020 IEEE Problems of Automated Electrodrive. Theory and Practice (PAEP). Kremenchuk, 1–4. https://doi.org/10.1109/paep49887.2020.9240905
28. Sagin, S. V., Solodovnikov, V. G. (2017). Estimation of Operational Properties of Lubricant Coolant Liquids by Optical Methods. International Journal of Applied Engineering Research, 12 (19), 8380–8391.
29. Myrhorod, V., Gvozdeva, I., Budashko, V. (2022). Approximation - markov models of changes in the technical condition parameters of power and energy installations in long-term operation. Aerospace Technic and Technology, 4, 73–79. https://doi.org/10.32620/aktt.2022.4sup2.11
30. Nikolskyi, V., Budashko, V., Khniunin, S., Nikolskyi, M. (2018). Parametrization and identification of energy flows in the ship propulsion complex. 2018 14th International Conference on Advanced Trends in Radioelecrtronics, Telecommunications and Computer Engineering (TCSET). Slavske, 288–294. https://doi.org/10.1109/tcset.2018.8336205
31. Sandler, A., Budashko, V. (2022). Improving tools for diagnosing technical condition of ship electric power installations. Eastern-European Journal of Enterprise Technologies, 5 (5 (119)), 25–33. https://doi.org/10.15587/1729-4061.2022.266267
32. Budashko, V. V. (2021). Prospektive globale wissenschaftliche Trends: Modern technologies and concepts of researching for ship power plants of combined propulsion complexes. ScientificWorld-NetAkhatAV, 7 (7), 152. https://doi.org/10.30890/2709-2313.2021-07-07
33. Sandler, A., Budashko, V., Khniunin, S., Bogach, V. (2023). Improving the mathematical model of a fiber-optic inclinometer for vibration diagnostics of elements in the propulsion system with sliding bearings. Eastern-European Journal of Enterprise Technologies, 5 (5 (125)), 24–31. https://doi.org/10.15587/1729-4061.2023.289773
34. Boyko, A., Budashko, V., Yushkov, Y., Boyko, N. (2016). Synthesis and research of automatic balancing system of voltage converter fed induction motor currents. Eastern-European Journal of Enterprise Technologies, 1 (2 (79)), 22–34. https://doi.org/10.15587/1729-4061.2016.60544
35. Sáez, D., Cipriano, A. (1998). Fuzzy Linear Quadratic Regulator Applied to the Real Time Control of an Inverted Pendulum. IFAC Proceedings Volumes, 31 (4), 155–160. https://doi.org/10.1016/s1474-6670(17)42150-1
36. Budashko, V. (2015). Implementation approaches during simulation of energy processes for a dynamically positioned ship. Electrical Engineering & Electromechanics, 6, 14–19.
37. Budashko, V. V., Iushkov, E. A. (2015). Mathematic modeling of all-range controllers speed of thrusters for ship power plants in combined propulsion complexes. Electronic Modelin, 37 (2), 101–113. Available at: http://nbuv.gov.ua/UJRN/elmo_2015_37_2_10
38. Sagin, S. V., Kuropyatnyk, O. A., Zablotskyi, Yu. V. Gaichenia, O. V. (2022). Supplying of Marine Diesel Engine Ecological Parameters. Naše More, 69 (1), 53–61. https://doi.org/10.17818/nm/2022/1.7

39. Budashko, V. V. (2020). Ship's power plants of combined propulsion complexes: concepts, technologies, researching. Odesa: NU "OMA", 136.
40. Nikolskyi, V., Budashko, V., Khniunin, S., Nikolskyi, M. (2018). Development of a Computer System of Technical Condition for the Electric Podded Azimuth Thrusters. Information technologies and computer modelling. Ivano-Frankivsk, 157–160.

DOI: 10.15587/978-617-8360-19-1.CH4

Petro Lezhniuk, Viacheslav Komar, Vladyslav Lysyi,
Yuliia Malohulko, Volodymyr Netrebskyi, Olena Sikorska

CHAPTER 4

INTELLIGENTIZATION OF CONTROL SYSTEMS FOR LOCAL ELECTRIC POWER SYSTEMS

Abstract

With the increase in the power of renewable energy sources (RES) in power grids and the introduction of methods and means to compensate for the dependence of their generation on natural conditions, their role and significance in electrical power systems (EPS) is changing. RES are a real opportunity to decentralize electricity generation and provide power supply systems with a reliable source of energy. It has been shown that it is advisable to do this in the form of local electrical systems (LES), which operate in normal modes in parallel with the EPS as balancing groups, and in extreme cases are capable of operating in isolation in autonomous mode. To ensure the reliability and quality of electricity supply to consumers in LES, it is proposed to integrate RES and energy storage systems (ESS) in the form of separate microgrids (MG). To ensure the technical and economic efficiency of MGs, they are combined into an intelligent control system based on the principles of SMART Grid. This allows for more rational use of MG resources, effective interaction with the distribution network, and the use of ESS capabilities as a renewable energy reserve in the process of balancing the LES mode. The paper proposes a hierarchical structure of the intelligent LES system as one consisting of separate agents designed to respond to changing current LES states and form collective actions to ensure reliable power supply to consumers. Autonomous agents make management decisions and form a multi-agent system. Structured in this way, LES with smart grids can, during centralized power supply restrictions, not lose RES, but fully utilize their advantages together with energy accumulation and storage systems for reliable power supply to consumers.

KEYWORDS

Local electrical systems, autonomous mode, renewable energy sources, intelligent control system.

With the RES development in the electrical networks of power systems and the decentralization of generation, it has become possible, and to some extent necessary, to organize local electrical systems based on RES. LES can operate in parallel with the EES as a separate balancing group, consuming or generating electricity into the system. Under certain conditions, LES, based on economic interests or due to extreme conditions in the EES, can operate autonomously as an isolated intelligent system. In the Law of Ukraine

on the electricity market, LES at the level of electricity generation and distribution is considered as a set of microgrids, which are a group of interconnected loads and distributed generation facilities, including mainly renewable energy sources.

Similar problems and tasks arise in local electrical system s as in the EES: balancing the mode, regulating frequency and voltage, reducing power losses and improving its quality, increasing the reliability of power supply, reducing SAIFI and SAIDI. Modern LES are based on renewable energy sources, the majority of which are photovoltaic and wind power plants (PVPP and WPP). Since the generation of electricity by PV and WPP depends on weather conditions, energy storage systems are necessarily used in RES to reduce the imbalance that their variable generation can cause. One way or another, all of the above factors affect the operating modes of RES and the quality of electricity supply to consumers.

The increase in electricity generated by RES in the EPS leads to more frequent and significant power fluctuations in the system and increases its operational risks. Operational dispatching has little chance of coping with the instability of generation. Often, depending on the state of the power system — whether there is a surplus or deficit of electricity — the operator's actions boil down to limiting RES electricity generation or reducing consumer load. This problem is solved in the interests of the electricity producer and consumer if the RES is equipped with means of direct and reverse conversion of electricity. Surplus electricity after balancing can, for example, be stored in the form of electrochemical accumulators or hydrogen obtained as a result of electrolysis. The reverse process of returning electricity to the RES is carried out as necessary, usually during morning and evening peak load modes or during emergency situations. It is impossible for a distribution system operator (DSO) to effectively cope with such a complex process of electricity generation, transmission, distribution, and conversion in order to balance the system mode reliably and without losses. Today, technologies developed on the principles of SMART Grid successfully cope with this problem. The concept of an intelligent system provides greater opportunities for monitoring and controlling the components of the power system, as well as increasing the reliability, quality, and efficiency of electricity supply to consumers. A key feature of an intelligent system is optimal control of system modes in normal mode and self-recovery, which is defined as the ability to automatically recover after failures.

In order to successfully ensure a reliable and economical power supply to consumers, LES faces the task of intellectualizing its mode control system. The aim of this work is to consider: the process of balancing power and electricity in the LES as a necessary condition for ensuring its normal functioning; methods for reducing imbalances between the predicted and actual generation of renewable energy sources in the LES; the formation of an intelligent control system for the LES mode as part of a multi-microgrid; examples of improving the efficiency of electrical networks through their intellectualization.

4.1 CONDITIONS FOR BALANCING POWER AND ELECTRICITY IN THE LES

RES in particular photovoltaic and wind power plants (PVPP, WPP), are not currently guaranteed sources of electricity for EPS. Since RES electricity generation depends on weather conditions, it is necessary to have reserve capacity in order to coordinate their operation with the technological requirements of

the EPS [1–3]. To ensure the effective operation of RES in the EPS and a reliable electricity supply to consumers, it is necessary to have reserve energy sources that could compensate for the natural instability of RES generation. Currently, there are various options available, which differ in their technical and economic characteristics [4–6]. Due to the lack of maneuverable capacity, various methods and means of electricity storage are used in the power system. First and foremost, this involves the storage of electricity generated by RES. Among the most effective storage devices are electrochemical storage devices, hydrogen and biogas technologies [6, 7]. The coordination of RES generation schedules with electricity consumer load schedules can also play an active role in balancing the power system [8, 9]. This is especially true for local electricity systems, which are formed as part of existing distribution networks where RES are being developed and which are acquiring all the characteristics of systems with a certain degree of autonomy [10].

In order to facilitate peak load management, the EES encourages electricity consumers to shift their peak load to hours when the system is operating at minimum load [11, 12]. The participation of "active consumers" in regulating the electricity balance in the EPS can improve frequency and voltage regulation [2, 13]. This is done by setting different electricity tariffs at different times of the day in agreement with the distribution system operator. It has become more difficult to maintain the balance of power and electricity in the EPS when the share of renewable energy sources has grown significantly. In particular, with the development of photovoltaic and wind power plants, which, due to their natural dependence on weather conditions, are not a guaranteed supplier of electricity.

When balancing the EPS regime, it is necessary to take into account the fact that there may be different regulatory conditions for RES generation. They may change in such a way that RES generate electricity in the EPS without any restrictions (restrictions are allowed only due to possible violations of the stability of the EPS), generate electricity in the power system according to a forecast short-term (usually for the next day) hourly schedule or by participating in an auction, or generate electricity according to established rules [14].

Let's consider a case where RES generate electricity according to a forecast hourly generation schedule for the next day. RES operate as part of a balancing group, which total capacity can range from tens to hundreds of MW. The load capacity of electricity consumers in the LES is proportional to the RES capacity. Such a balancing group is, by all accounts, a local electrical system within the IPS. It contains energy sources connected by electrical networks of various voltage classes and electricity consumers, and is connected to the power system by power lines through which it can supply or receive electricity. It is technically and economically feasible and advisable to consider such a LES as a separate balancing group. To do this, it is necessary to determine the methods and means of reducing the instability of RES generation in the LES. These include systems related to the storage and conversion of electricity, and systems for managing electricity generation and consumption schedules. They differ in cost, and therefore it is advisable to use the latter first, namely the coordination of RES generation and electricity consumption schedules. Implementing a method for coordinating electricity generation and consumption schedules can also reduce the required capacity of energy storage devices, which will lower their cost. However, before developing a system for technical implementation and economic motivation of active behavior of electricity consumers in the LES, it is necessary to investigate the effectiveness of coordinating RES generation schedules and electricity

consumption as a measure to balance the LES mode. Thus, it is possible to demonstrate the possibility and feasibility of coordinating RES generation and electricity consumption schedules in the local electrical system as a way to balance power and electricity in it.

Fig. 4.1 shows the composition of the LES, which is a separate balancing group. It includes power sources, power storage facilities, and power consumers. The sources of electricity are solar power plants, wind power plants, small hydroelectric power plants (SHP), as well as centralized power sources from the power grid (nuclear power plants (NPP), thermal power plants (TPP), hydroelectric power plants (HPP), pumped storage power plants (PSPP)). Electrochemical storage devices (ESD), hydrogen and biogas plants (BGP) are used as storage devices and converters of electricity into other types of energy and vice versa. Hydrogen technologies are designed to produce hydrogen through electrolysis, which can be used to generate electricity to maintain the electricity balance in the LES, with the remainder being used in other industries and transportation. BGU can be used as a source of thermal and electrical energy (cogeneration plants). Electricity consumers in RES are industrial and municipal loads, as well as hydrogen technologies and ESD in charging mode.

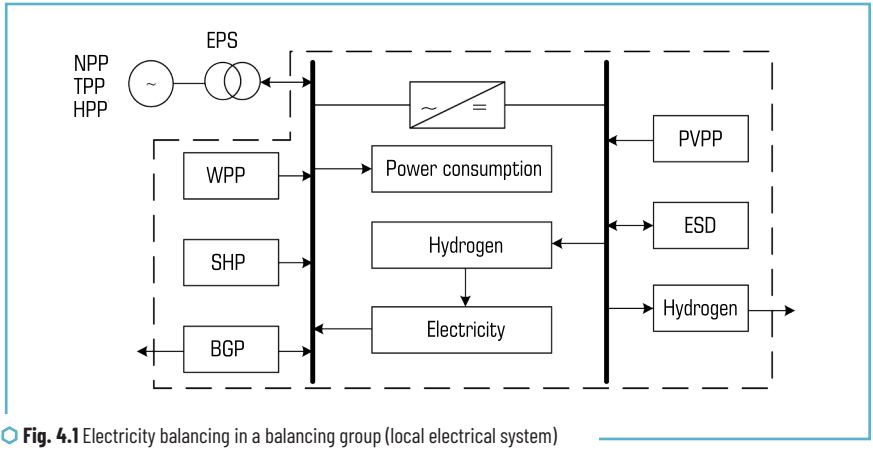

Fig. 4.1 Electricity balancing in a balancing group (local electrical system)

The electricity balance in the LES, as in a balancing group, is recorded as follows:

$$P_{PVPP}(t)+P_{WPP}(t)+P_{SHP}(t)+P_{BGP}(t)\pm P_{EPS}(t)\pm P_{h}(t)\pm P_{ch}(t)-P_{cons}(t)-\Delta P(t)=0 \quad (4.1)$$

where $P_{PVPP}(t)$ – solar power capacity; $P_{WPP}(t)$ – wind power capacity; $P_{SHP}(t)$ – small hydroelectric power capacity; $P_{BGP}(t)$ – electrical capacity of cogeneration plants; $P_{EPS}(t)$ – EPS capacity; $P_{h}(t)$ – hydrogen plant capacity; $P_{ch}(t)$ – electrochemical storage capacity; $P_{cons}(t)$ – power of electricity consumers, including "active" ones; $\Delta P(t)$ – technological losses in electrical networks.

In LES, as in a balancing group, the following principle is implemented: all electricity generated is consumed in LES, and the surplus is transferred to the EPS. To ensure the stability of the LES during periods of maximum (minimum) consumption or limited capacity of the centralized power supply system, when variations in local generation parameters can lead to violations of the restrictions on the parameters of the EPS mode, it is important to optimize RES modes in order to minimize deviations from the centrally set schedule for aggregate RES generation, given the restrictions on primary energy resources and RES characteristics [15]:

$$\int_{t_0}^{t_k} \frac{1}{2}\left(P_{RES}(t) - \sum_{i=1}^{n} P_i(t)\right)^2 dt \to \min \tag{4.2}$$

taking into account the balance sheet restriction:

$$P_{sc(t)} + \sum_{i=1}^{n} P_i(t) - P_{LOAD}(t) - \Delta P(t) = 0,$$

where $P_{RES}(t)$ – total projected RES capacity of the RES, which is provided to the balancing group operator in the form of a generation schedule for the next day; $P_i(t)$ – current value of RES capacity for the time interval t_0–t_k, during which the electricity generated in the RES is monitored; $P_{SC}(t)$ – centralized power supply from TPPs, NPPs, HPPs; $P_{LOAD}(t)$ – total load of electricity consumers; $\Delta P(t)$ – power losses in electrical networks.

Task (4.2) is usually applied to the entire power system. Another option is to allocate several balancing groups in the power system for simpler and more accurate control of PV and wind power generation. In each balancing group, an Automated Commercial Electricity Accounting System (ACEAS) is established for each RES, and an hourly electricity generation schedule for the next day is forecast. That is, for each *i*-th PVPP and WPP, the values of actual and forecast electricity generation for a given period of time are known. Therefore, in accordance with task (2.2), for each *i*-th RES, the task of achieving a certain accuracy between the forecast and actual electricity generation for a certain period of time, for example, one hour, is formulated:

$$\delta_i = \frac{w_i^P - w_i^A}{w_i^S} \le \delta_{PER} \tag{4.3}$$

where w_i^P, w_i^A – predicted and actual values of electricity generation by the *i*-th wind farm per unit of time; δ_i, δ_{PER} – current and permissible error values (the permissible error is set at 0.05 for PVPP and 0.1 for wind power plants).

To control the error value, it is necessary to model two graphs: the predicted and actual generation of the PVPP. The error, as the difference between these graphs, must be within the acceptable range or close to it. The following implementations of this task are possible:

1) the actual graph remains unchanged, and the forecast graph is adjusted every hour or every 15–20 minutes;

2) the forecast graph remains unchanged, and the actual graph is adjusted to the forecast graph, or more precisely, brought into the acceptable range.

However, in the latter case, electricity generation and, accordingly, profits are reduced. It is decided which is better: to lose on electricity generation or to reduce penalties for deviations from the acceptable range?

A third option is also possible, when the forecast schedule is adjusted and the actual generation is changed to bring it into or closer to the acceptable range. In other words, when developing a natural simulation model for researching short-term forecasting processes and operational management of RES generation in the EPS mode balancing system using Smart Grid technologies, it is necessary to consider all options.

To build an effective algorithm for forecasting the electricity output of photovoltaic power plants (**Fig. 4.2**) and successfully automate it, it is necessary to have an appropriate array of source data and software. The first step is to create a mathematical model of the PV plant itself. To do this, it is necessary information about the characteristics of the photovoltaic modules, which are specified in the passport data.

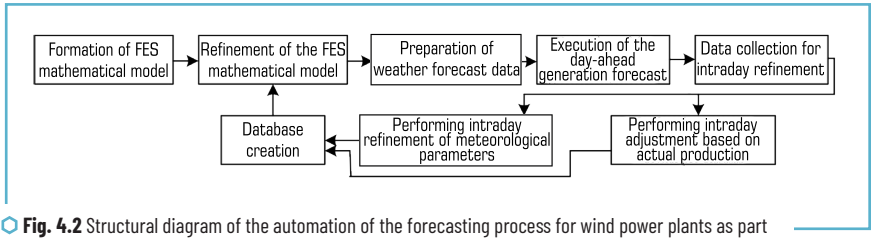

Fig. 4.2 Structural diagram of the automation of the forecasting process for wind power plants as part of a balancing group

Since the operating conditions of wind power plants are constantly changing, their mathematical model is constantly being refined. To automate the process of refining the wind power plant generation forecasting model, a database of parameters is created.

Since the operating conditions of RES are constantly changing, their mathematical model is constantly being refined. To automate the process of refining the RES generation forecasting model, a database (DB) of parameters is created. MySQL is usually used, but it slows down when it is significantly filled. The necessary meteorological parameters from various services are collected in the DB. There are quite a few such services on the market, all of which allow to organize API communication, which automates the data collection process. In addition, there are a significant number of libraries in C#, Python, etc., that implement such communication.

After making a forecast for the next day, no company providing such services can guarantee sufficient accuracy, so it is necessary to use the possibility of intraday adjustment. In different countries, the market accepts the results of this adjustment with varying degrees of discretion. As a rule, this time ranges from 15 minutes to 2 hours. Obviously, the shorter this interval, the better the results. Intra-day adjustments can be made in two ways: by recalculating the generation schedule based on refined meteorological parameters or based on the results of monitoring the current production of electricity from renewable energy sources. The first algorithm requires the use of weather services that adjust their forecasts during the current day.

The second requires the use of telemetry, which can provide polling almost every minute, or ACEAS, which usually works with greater discretion.

After adjustment, the results are sent to the balancing group operator. All data on meteorological parameters, production forecasts, and actual energy production values are also entered into the database for further adjustment of the RES mathematical model. Such adjustments are made during the first month of the forecasting service and then as needed to account for seasonal changes and equipment degradation processes.

The process of automating the forecasting of RES generation schedules and their ongoing adjustment in accordance with changes in operating conditions, primarily weather conditions, is an important element of successful balancing of the power system. As in all dynamic processes related to power systems, in the case under consideration, a special feature is the impossibility of studying them in different modes directly at the facility. Therefore, testing the performance and configuration of the automatic renewable energy generation forecasting system (AREGFS) in order to evaluate its functioning and effectiveness in balancing the state of the power system is only possible through modeling.

Based on the nature of the AREGFS process, it is advisable to use simulation modeling. Since the actual generation value is constantly monitored during balancing using AREGFS, it is possible to use these values during modeling. Such a model can be classified as a physical simulation model. The physical simulation modeling method is considered an experimental research method in which the object itself is not disturbed and studied, but rather a simulation model of the object implemented on a computer.

Fig. 4.3 shows the structure of a full-scale simulation model (FSM) for testing and tuning the AREGFS PVPP. It includes a functional model of the object (FMO), which, together with the AREGFS PVPP, forms a closed system. This allows, with sufficiently accurate modeling of the control object, to achieve maximum reliability of testing the AREGFS PVPP, since in the test system it is possible to reproduce any mode of the object within the permissible range of existence. Along with the advantages, it is necessary to note a certain complexity in the implementation of the structure, which is reflected primarily in the need for not only informational but also physical compatibility between the model and the AREGFS. The correct functioning of the AREGFS in this structure is assessed by comparing the AREGFS outputs with the control data of the real object.

The key link in the organization of the test system's FSM is the construction of a simulator, which is part of the FMO. The simulator is designed to reproduce a specific set of object modes. The PVPP mode is a permissible set of its states and processes of their change. During the transition from one state to another, the current mode indicators (mode parameters) change under the influence of external disturbances (load changes) or control signals to change the actual generation of the PVPP.

When creating and testing a control system based on modeling, the continuous operation of the wind farm is replaced by a set of characteristic modes. Correct implementation of this principle ensures the necessary reliability of the control means verification process. In this case, correctness means the appropriate selection of modes and their number, a set of parameters, and the accuracy of their measurement by the automatic commercial electricity metering system. When signals simulating the parameters of PVPP modes are fed into the control system, the limitations of the transmission system operator (TSO) of the power system are taken into account. First and foremost, this is the state of the EPS in terms of a deficit or surplus in the electricity balance.

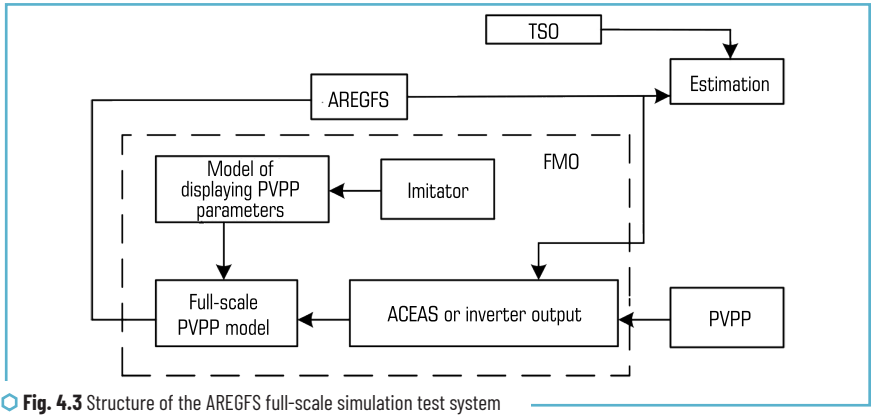

Fig. 4.3 Structure of the AREGFS full-scale simulation test system

At the same time, forecast information on meteorological parameters is taken into account, which is provided by the corresponding subsystem of the automated control system (ACS) [16] and allows for a sufficiently adequate reproduction of the state of RES for a period of up to several days, and then with refinement for a day in advance with intraday correction. Due to this, unstable energy sources such as wind and solar power plants can be represented in the objective functions and constraints of optimal control tasks by the mathematical expectation of the time dependencies of generation $M_{WPP}\{P(t)\}$, $M_{PVPP}\{P(t)\}$, $t \in [t_0; t_k]$.

Despite the fact that the generation of solar and wind power can be predicted fairly accurately, taking into account intraday adjustments, they are unstable in terms of actual electricity production, so a power reserve is necessary in the power system. Such reserves (**Fig. 4.1**) include electrochemical storage devices, hydrogen and biogas technologies, as well as the EPS system reserve. It is also possible to compensate for the instability of RES generation by coordinating their generation schedules with the load schedules of electricity consumers. The question arises as to what methods and means should be used and in what form it is advisable to reserve for the instability of RES electricity generation and to ensure the practical implementation of task (4.2).

In [17], a method was developed for relative comparison of possible ways of reserving renewable energy sources with unstable generation in the power system and assessing the sensitivity of their costs to changes in capacity. To analyze the technical and economic efficiency of various means of reservation, mathematical models were developed based on similarity theory and the criterion method. The criterion method, with minimally available initial information, makes it possible to compare different methods of reserving RES generation and determine the optimal ones. The method allows assessing their comparability and determining the sensitivity of costs to the capacity of the methods of reserving. Criterion models have been developed that allow the construction of dependencies of the costs of means of reserving unstable RES generation on the capacity of the means of reserving. Such dependencies make it possible to choose certain methods of reserving more reasonably in accordance with the characteristics and requirements of the EPS.

4.2 REDUCING IMBALANCES BETWEEN PREDICTED AND ACTUAL RES GENERATION THROUGH A COMBINATION OF METHODS

In electric power systems, the amount of electricity generated and consumed is planned and continuously monitored in order to balance their operation and ensure the required reliability and quality of electricity. Under such conditions, both traditional and renewable energy sources must operate. While modern automated commercial electricity metering systems (ACEMS) make it relatively easy to account for the electricity generated by RES, planning is not so simple. Since the amount of electricity generated by RES depends on the weather forecast, planning turns into forecasting the amount of electricity generated by RES. To date, many methods, algorithms, and programs have been developed for forecasting the generation of electricity from RES, especially solar and wind power plants. Unfortunately, none of them can provide the necessary accuracy, as this is linked to the impossibility of accurately forecasting weather conditions. Therefore, as a solution, it is permissible to adjust the forecast of the hourly schedule for electricity generation by solar and wind power plants for the next day.

Fig. 4.4 illustrates an example of the combined application of methods to reduce the difference between the predicted and actual electricity generation by the balancing group of wind power plants. When the actual value exceeds the forecast for a certain period of time (**Fig. 4.4**, point t_1), it is advisable to reduce this imbalance by storing energy, for example, in the form of hydrogen. Hydrogen can be produced directly at the wind farm, if such a facility is available, or the required amount of hydrogen must be purchased as a service from another producer. The hydrogen option is advisable because, when using, for example, electrochemical storage devices, it is limited by the need to convert the stored energy back into electricity. Whereas in the case of hydrogen, there are more options: use in other industries or in transport, conversion into electricity. When the forecast for a certain time interval is greater than the actual value (**Fig. 4.4**, point t_3), then, after running the forecast refinement program, the predicted generation of the wind power plant is adjusted to the permissible value according to the condition.

For the case shown in **Fig. 4.4**, it is possible to determine the difference between the forecast and actual electricity generation of the wind power plant, which must be compensated for in the task of balancing the power system mode. The amount of electricity generated in excess of the required balance and which can be used for hydrogen production is determined as the area bounded by curves ABC and AC. This is 250.5 MWh.

To calculate the potential volume of green hydrogen production using electrolysis, it is possible to assume that 1 m^3 of hydrogen requires 4.5 kWh of electricity, or 50.56 kWh per 1 kg of hydrogen [18]. For hydrogen production, 250.5 MWh can be consumed, i.e., M = 250.5/50.56 = 4.954 kg of hydrogen per day. If the power system has a deficit in electricity generation, this hydrogen can be used to generate electricity and improve the balance of the power system. If the power system has a surplus, it is advisable to use hydrogen in other industries and in transport. The difference between the forecast and actual generation of wind power plants in the balancing group can be reduced programmatically by correcting the forecast, as shown in **Fig. 4.4**.

There are two ways to reduce the difference between the forecast and actual values of the electricity generation graphs for solar and wind power plants: by influencing the forecast value W_f or the actual value W_{ac}.

The actual generation W_{ac} can only be influenced in the direction of its reduction, which is not economically feasible. Actual electricity generation can only be reduced on the orders of the transmission or distribution system operator when necessary to ensure the stability of the power system. Therefore, under normal conditions, it is only possible to adjust the forecast values of electricity generation for a specific time period Δt. The actual values of electricity generated are approximated for the same time Δt based on preliminary data from ACEAS.

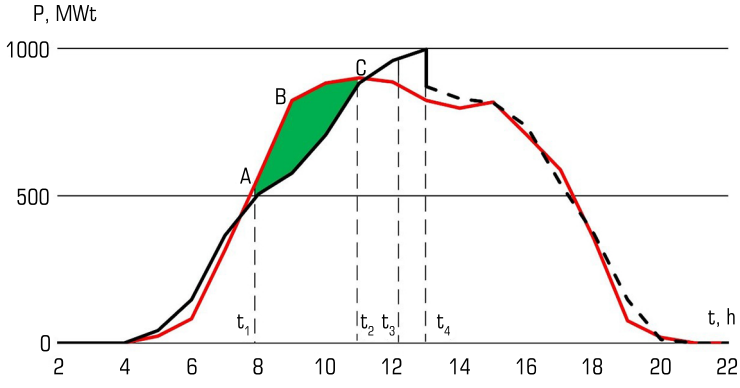

Fig. 4.4 Combination of different methods to reduce imbalance

The logical scheme for calculating the adjusted value of the hourly forecast of wind power generation for the next hour of the current day is illustrated in **Fig. 4.5**. At point t_1, for example, $\delta_1 \succ 0$ and $\delta_1 \succ \delta_{PER}$ then the forecast must be reduced by k. Accordingly, the forecast will be $W_f = k\,W_f$ where $k = 1-\delta_1$ and $\delta_1 = (W_{f1} - W_{ac1}) / W_{ac1}$ At point t_3, for example, $\delta_3 \prec 0$ and $\delta_3 \prec -\delta_{PER}$ then the forecast needs to be increased by k. Accordingly, the forecast will be $W_f = k\,W_f$ where $k = 1-\delta_3$ and $\delta_3 = (W_{f3} - W_{ac3}) / W_{ac3}$ If the difference between the forecast and actual values is within the acceptable range, i.e. $|\delta| \prec |\delta_{PER}|$ then the coefficient k=1 and the forecast values do not need to be adjusted.

The frequency with which the forecasting error is controlled is determined by the capabilities of the automatic control system (ACS) for forecasting the generation schedule of solar and wind power plants, the capabilities of the ACEAS, and the bandwidth of communication channels. Control is carried out evenly in cycles of no more than 1 hour and is organized as follows.

The hour i is determined, from which the i_b begins and the i_e ends of the electricity generation of the PVPP, where i is the current value of the hour number. Next:

– i=i_b, the prediction error for the i-th hour is determined $\delta_i = \dfrac{w_i^f - w_i^{ac}}{w_i^{ac}}$

– i=i+1, the prediction error for the i-th+1 hour is determined $\delta_{i+1} = \dfrac{w_{i+1}^f - w_{i+1}^{ac}}{w_{i+1}^{ac}}$

If $\delta_{i+1} \succ 0$ then:

if $\delta_{i+1} \le \delta_{PER}$, then k=1 and $w^f_{i+1} = k\, w^f_{i+1}$ (that is, the forecast remains the same, within the allowable range);

if $\delta_{i+1} \le \delta_i$, then go to the beginning of the cycle i=i+1 ("forecast" is approaching "fact");

if $\delta_{i+1} \succ \delta_i$ ("forecast" differs from "fact") and $\delta_{i+1} \succ \delta_{add}$, then $k = 1 - \delta_i$ and $w^n_{i+1} = k\, w^n_{i+1}$ and go to the beginning of the cycle i=i+1.

If $\delta_{i+1} \prec 0$, then:

if $\delta_{i+1} \ge -\delta_{PER}$, then k=1 and $w^f_{i+1} = k\, w^f_{i+1}$ (that is, the forecast remains the same, within the allowable range);

if $\delta_{i+1} \succ \delta_i$, then go to the beginning of the cycle i=i+1 ("forecast" is approaching "fact");

if $\delta_{i+1} \prec \delta_i$ ("forecast" differs from "fact") and $\delta_{i+1} \prec -\delta_{PER}$, then $k = 1 - \delta_i$ and $w^f_{i+1} = k\, w^f_{i+1}$ and go to the beginning of the cycle i=i+1.

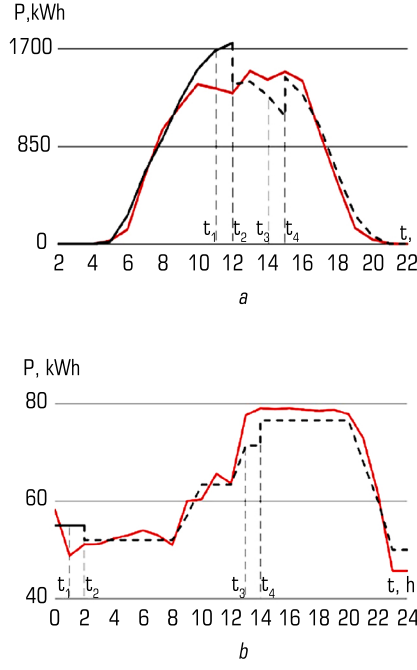

Fig. 4.5 Correction of the forecast graph for: *a* – PVPP; *b* –WPP generation

According to the above algorithm, a program for hourly adjustment of wind and solar power generation forecasts has been developed. **Fig. 4.6** shows an example of the results of hourly forecasting of wind power generation using a program for adjusting forecasts with error compensation δ_i. As can be seen, the error in forecasting PVPP per day decreased from 15.6% to 4.7%.

That is, the algorithm with compensation for hourly errors in forecasting PVPP gives satisfactory results. It can be used in conjunction with the PVPP adjustment based on hourly refinement of daily meteorological parameters.

A local electrical system for the IPS is essentially an active consumer that can be used in generation or consumption mode by the transmission system operator (TSO) or distribution system operator (DSO) as necessary [20].

Another case is when it comes to coordinating generation and consumption schedules in the LES for its internal electricity balancing.

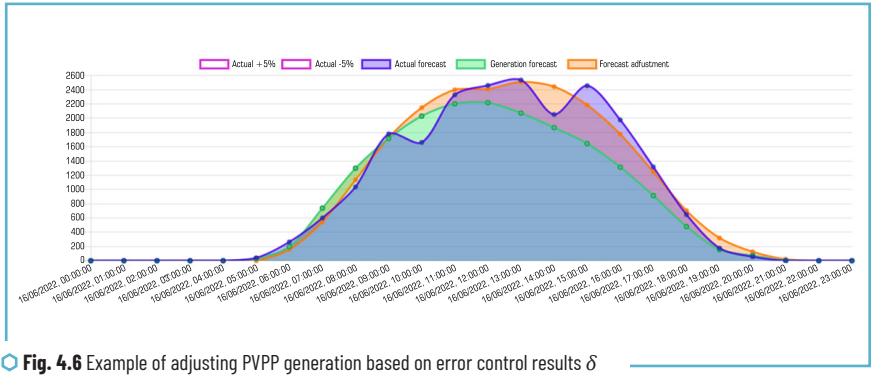

Fig. 4.6 Example of adjusting PVPP generation based on error control results δ

This is especially true when the LES operates separately from the power system, in autonomous mode. In this case, it is necessary to influence not only the generation of renewable energy sources, the consumption/generation of the electricity storage system, but also the electricity consumption schedules of utilities and technological processes.

Influencing load schedules is a complex process that requires changes to the technological processes of electricity consumers. Therefore, changes to the electrical load schedule (ELS) must be thoroughly justified. To do this, it is necessary to select a convenient method for analyzing and comparing load schedules and electricity generation parameters in the LES. In [19], it is shown that the use of a morphometric apparatus for analyzing the unevenness of schedules has a number of advantages and allows for a comprehensive and detailed assessment of the ELS shape. The basis for the application of morphometric analysis is the transition from a rectangular coordinate system to a polar coordinate system (**Fig. 4.7**). Therefore, the aim of the study is to formalize the unevenness of ELS using morphometric analysis, which allows for a more detailed characterization of the unevenness of ELS using indicators that differ from the classical ones describing the nature of the ELS unevenness (dispersion, shape factor, filling coefficient, ELS unevenness coefficient). A detailed analysis of ELS allows for increasing the productivity of energy sources, including renewable energy sources, in the task of covering a specific load schedule within the consumer's balance and, as a result, reducing ELS unevenness.

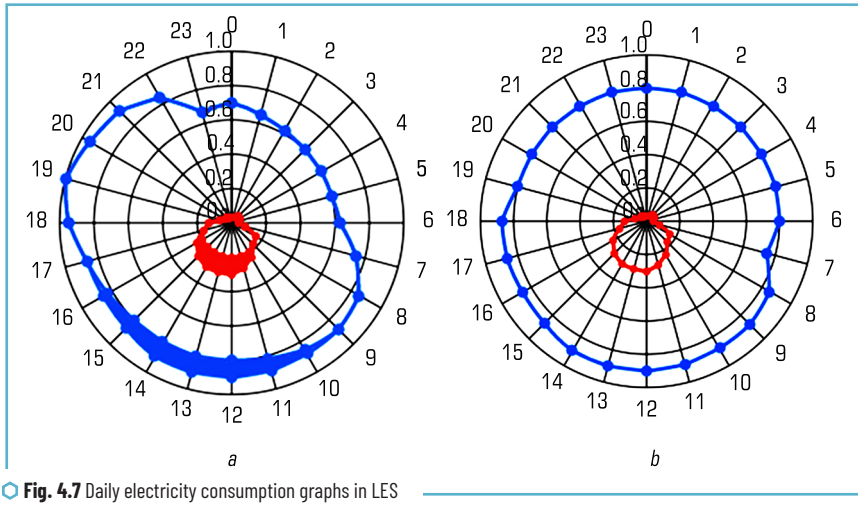

Fig. 4.7 Daily electricity consumption graphs in LES

Fig. 4.7 shows, as an example, the coverage of the daily electricity consumption schedule in the spring-summer period, where consumption and generation by own renewable energy sources and inflows from the EPS are balanced. **Fig. 4.7** is constructed in relative units, where the starting point is the evening peak power.

It is characteristic that in the afternoon, electricity consumption decreases, while RES production increases under favorable weather conditions, i.e., the peak of RES production occurs during the daytime in the load schedule. If the LES mode is currently excessive, "excess" capacity of solar and wind power plants is generated for the purpose of balancing the mode. "Excess" electricity is either stored by the storage system, or the DSO is forced to limit the production of renewable electricity. That is, it is necessary to coordinate the generation and consumption schedules in the RES.

This can be done by consumers, but they must be motivated to shift the daily electricity load schedule to the hours of maximum production of solar and wind power plants. In order to develop a method for coordinating RES generation with the load in the RES, it is necessary to assess the impact of RES generation on the unevenness of the daily electricity load schedule. Integral morphometric indicators of ELS unevenness are used to analyze and evaluate RES in the total load schedule of the power grid [19].

The main incentive is the zonal electricity tariff, according to which the cost of electricity is differentiated by time of day. Consumers can reduce their electricity bills without reducing consumption. This reduces the unevenness of ELS. If the electricity consumer is in a balance group, reducing the difference between the forecast and actual generation schedules using formula (4.3) in the LES is also an additional incentive.

To estimate the cost of displacement of consumption capacity, it is necessary to develop an indicator that would take into account the change in the tariff coefficient of electricity consumption under the zone

tariff. The cost of compensation to the consumer due to changes in the electricity consumption schedule and the cost of electricity losses due to daily balancing of ELS are determined as follows:

$$B_{ij} = P_{sh} \cdot C_t \left(K_{tj} - K_{ti} \right) + \beta \pm \delta P \cdot C_t, \tag{4.4}$$

where P_{sh} – power that the consumer must shift to balance the load schedule of the LES; C_t – electricity tariff of the energy supply company; K_{tj} – electricity cost coefficient according to the zone tariff of the schedule stage from which the power is planned to be transferred; K_{ti} – electricity cost coefficient according to the zone tariff of the schedule stage to which the power is planned to be transferred; β – cost of technological shift in production to be compensated by the power grid; δP – change in power grid losses due to adjustment of the consumer's load schedule.

In order to reduce the overall unevenness of the daily ELS LES and minimize electricity losses, it is proposed to sequentially adjust the load schedule of transformer substations (TS) in accordance with load factors. Obviously, the relative values B_{ij} for each node will differ. In accordance with this task, the objective function is recorded:

$$\sum_{i=1}^{m} \sum_{j=1}^{n} B_{ij} \cdot P_{ij} \rightarrow \min, \tag{4.5}$$

where P_{ij} – power that needs to be shifted from the j-th stage of the load schedule to the i-th; m – hours in which the actual consumption of the TP is greater than the generation of RES; n – hours in which the generation of RES will prevail over the consumption of the TP.

The first set of constraints indicates that the power of any ELS stage must be equal to the total power consumption of that ELS stage. The second set of constraints indicates that the total shift in consumption at this ELS level must fully compensate for production at that level. The possibility of transferring negative values of consumed power is also limited.

To solve this problem, it is possible to use the transportation problem method. A corresponding algorithm and program have been developed. To determine the power regulated by the consumer, a technical minimum is determined for each consumer. Based on this, the transmitted power of the consumer is equal to P_{li} – the difference between the actual power consumption and the technical minimum for a given hour of load P_{tmi}. At the same time, consumers are classified according to the TP utilization coefficient.

Hours when actual TP consumption is lower than RES generating capacity are conventionally referred to as "production hours". That is, hours for which consumption capacity must be transferred. Hours when the load exceeds the generation capacity and the condition $P_{li}(t) - P_{tmi}(t) > 0$ is met are the hours from which electricity can be transferred. It is this difference that determines the excess capacity $P_{exi}(t)$ that can be transferred at a certain price and the capacity $P_{lacki}(t)$ that is lacking at a certain hour of the day to adjust the daily schedule. Based on the identified deficit and excess capacity, a transport matrix is formed to transfer capacity from excess hours to deficit hours in order to adapt the daily load schedule. If the total generation capacity exceeds the capacity that can be transferred to adjust the electricity load schedule, an additional imaginary load generation source (virtual power plant) $P_{viri}(t) = \sum_{i \in \theta} P_i(t) - P_{exi}(t)$ is introduced

for the balanced transportation task (a set of electrical power sources in the LES). If the own production of renewable energy is insufficient to meet the electricity needs of consumers, a conditional source of centralized electricity is introduced:

$$P_{EPSi}(t) = \sum_{i \in \theta} P_i(t) - P_{exi}(t). \tag{4.6}$$

The solution to the transport problem is to recommend shifting the electricity load schedule of consumers that most affects the unevenness of the overall load schedule of the power system. The daily electricity load schedule is adjusted until conditions (4.3) are met. Upon completion, a graphical representation of the morphometric model of the electrical load schedule is displayed, without taking into account the formation of RES, taking into account the RES generation schedule and the adjusted electrical load of the power system and the corresponding morphometric indicators for the listed schedules.

Fig. 4.7, *a* shows the daily electricity consumption schedule, where the unbalanced surplus of RES electricity (highlighted in red) is consumed during the daytime minimum (highlighted in blue). To this end, the necessary changes have been made to the electricity consumption process. **Fig. 4.7, *b*** shows a daily electricity consumption graph, where, in addition to the electricity generated by the wind power plant, the evening maximum electricity consumption is shifted to the nighttime minimum. Thus, the electricity consumption graph can be smoothed out and approximated to a circle.

Thus, it is possible to compensate for the natural instability of RES production in RES not only by means of electricity storage, but also by a method that is not directly related to electricity storage. This involves coordinating electricity generation and consumption schedules in RES. This method is also proposed because energy supply systems have accumulated experience in smoothing load schedules using zonal electricity metering at different tariffs. An algorithm and software have been developed to provide recommendations for coordinating electricity generation and consumption schedules in RES.

4.3 FORMATION OF AN INTELLECTUAL CONTROL SYSTEM FOR THE LES MODE AS PART OF THE ELECTRIC POWER SYSTEM

4.3.1 LES AS AN OBJECT OF AN INTELLIGENT CONTROL SYSTEM

Thanks to the development of renewable energy sources in power systems, in particular in distribution power networks, it has become possible to create consumer power supply systems based on RES. In addition to the fact that this provides certain advantages in terms of energy efficiency of power supply, there is a possibility of forming local electrical systems based on RES as balancing groups in the electric power system [21, 22]. **Fig. 4.1** shows the structure of such a LES, which, in addition to RES, necessarily includes an energy storage (accumulation) system. ESS may include small hydroelectric power plants, electrochemical storage and cogeneration plants running on natural gas and biogas with hydrogen additives.

In LES, the RES generation, which is mainly photovoltaic and wind power plants depends on natural conditions and has an unstable, time-varying capacity. The electricity consumption schedule is also variable in the LES. Even if the average generation and consumption capacities of electricity in such the LES as a balancing group are commensurate, then the problem of mode balancing in it arises. In a LES, it is necessary to create an automated or, taking into account the current state of hardware and software in the industry, an intelligent automatic control system for the LES mode [23]. The functions of the ACS are to maintain the forecasted RES generation schedule for the next day in the LES and coordinate it with the consumption schedule. In this case, active consumers are used, which, by adjusting their technological process, affect the total consumption/generation schedule of the LES in relation to the EPS [24]. When an LES operates with a surplus, the excess electricity is stored in the ESS or can be transferred to the EPS. If, due to their natural limitations, PVPP and WPP cannot cover the load schedule of the LES, then the ESS or EPS services are involved. Under such conditions, LES can maintain their operational capacity and provide electricity to consumers both in normal parallel mode with the power system and in autonomous mode.

Since LES are part of the EPS, they must operate in the conditions and according to the rules, without disrupting the EPS operation, which currently provides a stable electricity supply. This applies to all modes of LES operation. Therefore, it is important, based on the real technical capabilities and the state of generating capacities and electrical networks, to determine with what characteristics and what tasks LES as balancing groups of the EPS can solve. Due to the limited technical and human resources, the process of forming LES can be phased. Individual parts of the system develop according to a certain plan and are formed according to a certain concept. Compliance with the adopted concept is controlled by an integral indicator of the quality of resource use according to the final result [25]. The concept of forming a plan (roadmap) for the formation of LES in the EPS can be based on the "Concept of "smart" electrical networks as an intelligent system". It lays down the technical policy for the development of electric power systems, scientific foundations on the principles of SMART Grid, as well as forms of training qualified personnel.

To substantiate the conditions and principles, it is possible to consider the isolation of a part of the EPS in the form of local electric power systems as an object of an intelligent system [26]. At the first stage of forming a LES with renewable energy sources to balance its capacity, it is advisable to explore the possibilities of using well-proven and relatively inexpensive methods, such as, for example, active consumers [24, 27]. To study the problem of renewable energy consumption, let's consider the LES as a balancing group, which is shown in **Fig. 4.8**. It includes a photovoltaic plant as a source of electricity, an energy storage system and electricity consumers. The sources of electricity are photovoltaic plants, as well as sources of centralized power supply from the EPS (nuclear power plants (NPP), thermal power plants (TPP), hydroelectric power plants (HPP), pumped storage hydroelectric power plants (PSHPP)).

The electricity balance in the LES, shown in **Fig. 4.8**, as in the balancing group, will be written:

$$\pm P_{EPS}(t) + P_{PVPP}(t) \pm P_{ESS}(t) - P_{cons}(t) - P_{accons}(t) - \Delta P(t) = 0, \tag{4.7}$$

where $P_{EPS}(t)$ power from the EPS; $P_{PVPP}(t)$ power of the PVPP; $P_{ESS}(t)$ power of the energy storage system; $P_{cons}(t)$ power of electricity consumers working according to their schedule; $P_{accons}(t)$ power of active consumers working according to the adjusted schedule; $\Delta P(t)$ – technological costs in electrical networks.

Fig. 4.9 shows an example of covering the daily load schedule of the LES, given in **Fig. 4.8**. The task is to form the LES as a balancing group. To do this, forecasting the generation and consumption schedule for the next day, an electricity balance is drawn up (**Fig. 4.9, *a***): $W_L = \sum_{i=1}^{24} \Delta t P_{L_i}$ (t_i – total load electricity, including losses; $W_{PVPP} = \sum_{j=t_s}^{t_e} \Delta t P_{PVP}(t)$ – electricity generated by the PVPP, where t_s, t_e – time of start and end of generation; $W_{ESS} = \sum_{j=t_1}^{t_2} \Delta t P_{PVP}(t) - \sum_{j=t_1}^{t_2} \Delta t P_{L_i}(t)$ – surplus electricity in the LES, which can be transferred to the energy storage system or to the EPS; Δt – in the hourly schedule is equal to 1 hour.

The amount of load electricity is determined in the hours when PVP generation is absent: $W_{EPS} = W_L - W_{PVPP} + \Delta W$ – electricity that must be taken from the EPS or from the ESS for the balance in the PV plant. There are two options here: when the PV plant operates in parallel with the EPS and when it operates autonomously. In the first option, the electricity deficit in the PV plant is covered from the EPS – directly or through the ESS. To operate in autonomous mode, the ESS electricity must be sufficient to cover the load at "night" time. To ensure the autonomous operation of the LES, it is necessary to increase the PVPP power, as shown in **Fig. 4.9, *b***, and, accordingly, increase the ESS capacity. Another way is to limit the power of consumers and use the potential of active consumers, as shown in [24].

The local system isolated in the EPS includes electricity sources, a backup energy storage system and electricity consumers, which are united by developed electrical networks of different voltages. From the point of view of the control system, the LES are a complex distributed object consisting of individual agents designed to respond to the changing current states of the LES and form collective actions to ensure reliable electricity supply to consumers. Autonomous agents make control decisions and constitute a multi-agent system [22, 23, 28].

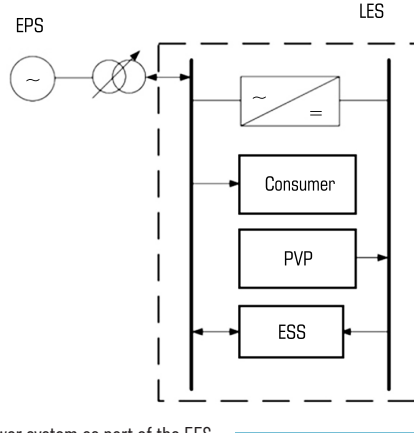

Fig. 4.8 Local electric power system as part of the EES

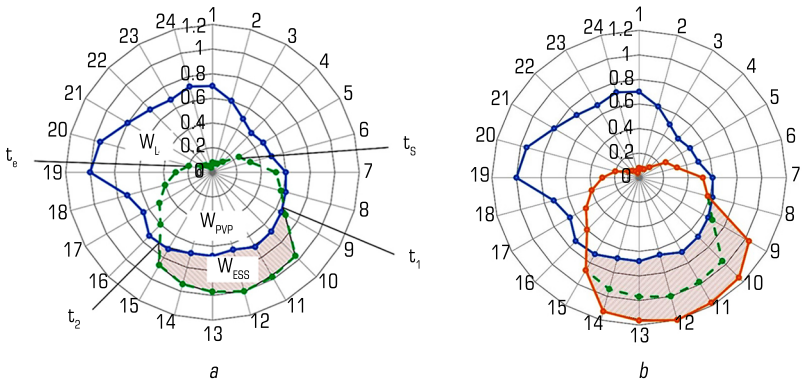

Fig. 4.9 Examples of coverage of the daily electricity consumption schedule of a LES

4.3.2 INTELLIGENT CONTROL SYSTEM OF THE LES MODE

The local system isolated in the EPS includes electricity sources, a backup energy storage system and electricity consumers, which are united by developed electrical networks of different voltages. From the point of view of the control system, LES are a complex distributed object consisting of individual agents designed to respond to changing current states of LES and form collective actions to ensure reliable electricity supply to consumers. Autonomous agents make control decisions and form a multi-agent system [22, 29].

Fig. 4.10 shows the hierarchical structure of the intelligent LES system. At the top level, the local agent LESA is an element of the lower level of the distribution system operator (DSO). Under the condition of parallel operation with the EPS at this level, the LESA performs the functions of a balancing group within the EPS, coordinating its actions with the DSO. At this level, the main current task is to forecast electricity consumption and generation at LES and exchange electricity with the EPS. For this purpose, a database is formed through requests for information from the middle-level agents of the microgrid MGA and MGAi. During the LES separation from the EPS, the tasks and content of the functions to be performed by the ACS change. The LESA are entrusted with the functions of internal balancing of power and electricity and maintaining the technical and economic indicators of the power supply system within permissible values. First of all, this concerns maintaining the frequency and voltage on the consumer buses in the LES. This is carried out by collective actions of the middle-level and technical agents by submitting the relevant work commands to them. Optimal control of active consumers is carried out within the limits of energy consumption W_{ESS}, as well as limiting, if necessary, the power of inactive consumers.

The MGA agent is an agent of the energy storage system, an agent of controlled distributed energy sources, and also within the daily correction of generation by the LESA command. It controls the common ESS, maintaining the frequency, and also controls the reactive power sources, maintaining the voltage.

The MGA agents are microgrids that are responsible for communicating with their agents at the technical level: PVPP, active consumer, inactive consumer, local ESS.

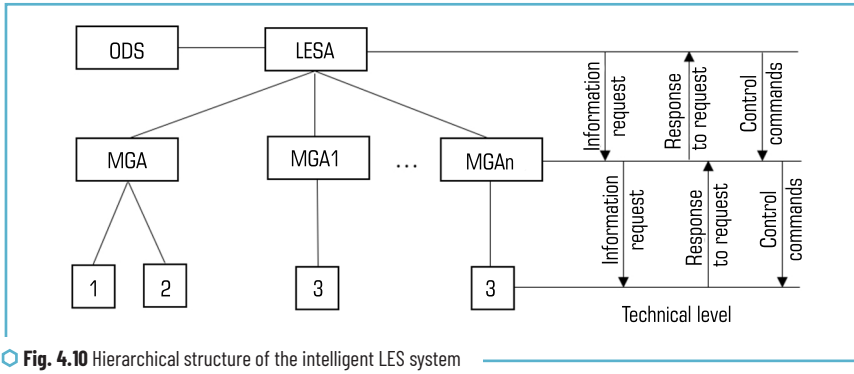

Fig. 4.10 Hierarchical structure of the intelligent LES system

They optimize the technical and economic parameters based on data from local agents and load the optimization result of the corresponding microgrid zone (excess/deficit of power, state of the energy storage, capabilities of the active consumer). They are responsible for communicating to load the relevant data and receive work commands.

The LESA is also entrusted with the functions of switching the LES with the electrical network of the EPS. When the LES and the EPS operate in parallel, the point of their junction is a reference point in terms of voltage. In it, the joint actions of the DSO and LESA maintain a voltage level that ensures the transmission of electricity from the EPS to the LES and vice versa. When transferring the LES to isolated operation, two options are possible: forced, when for some reason the voltage in the electrical network is lost, or in normal mode, when the disconnection of the LES is carried out on the initiative of the DSO or LESA. In these cases, commands are executed on the MGA according to the ACS software and the LES is transferred to autonomous mode. When connecting the LESA to the EPS, all procedures related to the synchronization of the two electrical networks are performed before the command is given to the switch.

Thus, in order to decentralize generation, it is advisable to separate local electric power systems based on RES from the EPS with the creation of intelligent mode control systems in them. It is proposed to form a LES with RES and electricity storage facilities as separate microgrids, which are a key part of the transition to LES operating on the principles of SMART Grid. Local MGs, in addition to generation sources and consumers, also have means of accumulating a certain amount of energy. Due to the hierarchical structure of the intelligent system, the LES can operate both in parallel with the EPS and in isolation from it. Thanks to the intelligent system, the LES implements the principles of SMART Grid and functions as an information and electrical system.

The LES formed in this way can operate as a balancing group within the EES, performing the tasks of the distribution system operator depending on the voltage and power of its MGA components.

In autonomous mode, the LES, depending on the capacity of the energy storage system, can be a full-fledged reserve of renewable energy sources and be used to optimize power flows and maintain frequency and current. The participation of active electricity consumers to coordinate generation and consumption schedules in the LES as a way of balancing power and electricity in it is effective. In the proposed LES with aggregated microgrids and an intelligent control system, its self-recovery after extreme events is implemented and the disturbed load is automatically restored.

The proposed hierarchical structure of the intelligent system of the local electric power system can operate both in parallel with the EPS and in isolation from it. Thanks to the intelligent system, the principles of SMART Grid are implemented in the LES and it functions as an information-electrical system. The LES formed in this way can work as a balancing group within the EPS, performing the tasks of the distribution system operator depending on the voltage and power of its MGA components. In the autonomous mode, the LES, depending on the capacity of the energy storage system, can be a full-fledged reserve of renewable energy sources and be used to optimize power flows and maintain frequency and current. The participation of active electricity consumers to coordinate generation and consumption schedules in the LES as a way of balancing power and electricity in it is effective.

4.4 LOCAL ELECTRIC POWER SYSTEM FORMED FROM MICROGRID

Due to the constant change in time of consumption and generation schedules in LES, it is necessary to create an automated or, taking into account the current state of hardware and software in the industry, an intelligent automatic control system (ACS) for the LES mode [22, 29]. Since LES are part of the EPS, they must operate in conditions and according to the rules, without disrupting the functioning of the EPS, which currently provides a stable power supply. This applies to all modes of operation of LES. Therefore, it is important, based on the real technical capabilities and state of generating capacities and electrical networks, to determine with what characteristics and what tasks LES can solve as balancing groups of the EPS. Due to the limited technical and human resources, the process of forming LES can be phased. Individual parts of the system develop according to a certain plan and are formed according to a certain concept. It lays down the technical policy for the development of electric power systems, scientific foundations, as well as forms of training qualified personnel on the principles of SMART Grid.

Elements of the LES can be formed as separate microgrids. For example, biogas production, its transportation to gas-piston cogeneration plants, distribution heat and electricity networks, system of automatic control (SAC) for this complex can be considered as an independent aggregated object. The same applies to photovoltaic and wind power plants with an electrical network, an hourly generation forecasting system, a backup system to compensate for generation instability due to dependence on weather conditions. The not-so-simple technical and economic task of maintaining the balance of power and electricity in a microgrid is solved more easily if such complexes are implemented and operated as separate microgrids with local SAC, combining them into an intelligent system for controlling the modes of the local electrical system.

Depending on the technical and financial and economic capabilities, LES can be formed in different ways. There are two main options: there is an infrastructure with developed electricity consumption, including industrial, and a distributed generation system is being developed around it; the LES is designed and built practically from scratch with the consumer of electricity and its energy supply. There are real examples. For example, an operating poultry farm as a complex with fattening and processing of raw materials, a feed mill, elevators, etc. with a total capacity of an average of 20–100 MW with power supply from the 10–35 kV power supply (**Fig. 4.11**).

a

b

Fig. 4.11 LES of the MHP complex: *a* – 110/35/10 kV substations; *b* – biogas production complex

Another option – for example, a recreation center is being designed with separate fully electrified houses, a photovoltaic power plant and a power transmission line from the power plant (**Fig. 4.12**). Both the first and second options are characterized by the phased development of renewable energy sources and

backup means for their unstable generation in LES. The question arises of substantiating their composition, power and capacity, and the order of implementation.

Fig. 4.13 shows the structure of a real sufficiently powerful LES at different voltages, which is formed from a microgrid (MG) with its local SAC. Microgrid MGi in various sets can contain photovoltaic and wind power plants, electricity storage systems (ESS), diesel generators for restoring generation of PVPP in an isolated state, cogeneration units (CU) on biogas and electricity consumers (C), including active ones. Powerful microgrid MG_i unite microgrids of lower power mg_i. Depending on the capacity of the stored electricity, the ESS are stored on MG_i buses or on higher voltage busbars. In the latter case, ESS can replenish electricity reserves directly from the EPS as a commercial service. Sources of centralized power supply from the EPS are nuclear power plants (NPP), thermal power plants (TPP), hydroelectric power plants (HPP), and pumped storage hydroelectric power plants (PSHPP). If consumers of electricity from the LES are motivated to receive electricity from RES or from decarbonized sources located in the EPS, then the software is installed in the LES SAC according to the method described in [30].

Fig. 4.12 10 kV LES with microgrid based on photovoltaic modules and energy storage system

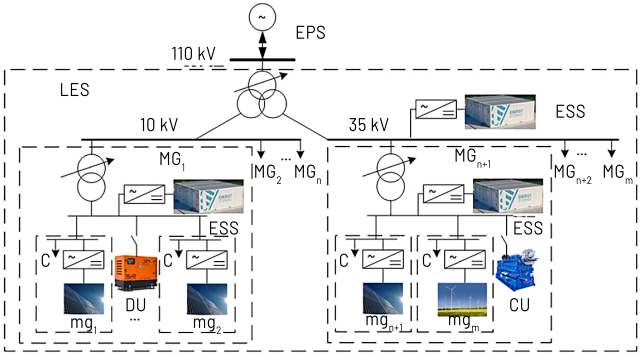

Fig. 4.13 Local electrical system formed from microgrid

In the formed LES based on MG with renewable energy sources and their generation instability backup in the form of ESS, reliability of power supply, as well as observability and controllability of modes are achieved. Due to the LES intellectualization and the use of SMART Grid principles, self-healing is implemented as the ability of the system to automatically recover after failures and resilience as a measure of the ability to withstand emergency situations with severe consequences. As an element of Smart Grid, self-healing is based on the functions of two-way communications in the network, remote monitoring and self-diagnosis of equipment, standards for preventing the development of system accidents, power and voltage flow control, etc.

4.5 INCREASING THE EFFICIENCY OF ELECTRICAL NETWORKS THROUGH THEIR INTELLECTUALIZATION

Fig. 4.14 shows part of the scheme of the district electrical network (DEN) in the area of the 110/35/10 kV substation, in which a local electric power system is being formed. At the first stage, photovoltaic power plants are installed in feeder 12 near substation 63 with a capacity of 2.5 MW and in feeder 13 near substation 122 with a capacity of 5 MW.

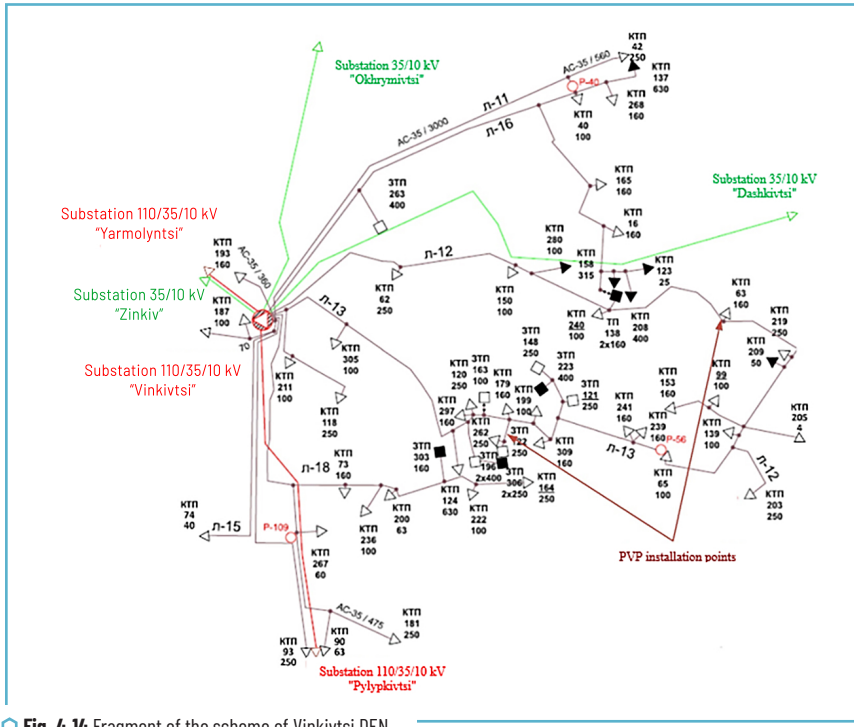

Fig. 4.14 Fragment of the scheme of Vinkivtsi DEN

Both photovoltaic power plants are formed as aggregated microgrids (MG) with local ESS and the use of active consumers. At the next stage, it is planned to install a gas piston unit (GPU) with a capacity of up to 5 MW and a biogas production plant using local raw materials. **Fig. 4.15** shows a structural diagram of such a LES. To ensure the redistribution of active power between feeders 12 and 13, compensation of reactive power in each of the feeders in order to reduce electricity losses, as well as optimal joint use of energy of local GPU in MG_1 and MG_2 and collective GPU in MG_3, a Soft Open Point (SOP) is established. To assess the efficiency of the formation of Vinkivtsi LES, calculations were performed before the installation of the PVPP and after the installation of the PVPP. The calculations were performed using the "Vtrati-110" software package. Below are the results of calculations of the maximum load regime of the 110/35/10 kV substation. The purpose of the calculations is to assess the possibility of installing PVPP and their power, based on the capacity of the power transmission line, the impact on electricity losses and voltage levels.

Fig. 4.16 shows the structure of annual electricity losses by feeders. The largest electricity losses are in F-13 and F-14, followed by F-12, F-15, and F-16.

Fig. 4.17 shows the values of electricity losses in the 110/35/10 kV substation in transformers and 10 kV power lines. Since electricity losses in power transmission lines are quite high, to reduce them, it is advisable to place PVPP closer to the end of the feeder and, preferably, in the area of the active consumer of electricity to enable joint control of generation and consumption schedules.

For the average load mode, the parameters of the feeders of the 110/35/10 kV substations of the "candidates" for the installation of the PVPP were calculated. According to the requirements formulated above (capacity, electricity losses, permissible voltage levels), F-13 and F-12 are appropriate. The sites for the construction of the PVPP with a capacity of 5 MW are located near ZTP-122 and with a capacity of 2.5 MW near substation 63. This also corresponds to the recommendations for the construction of the PVPP in the middle or closer to the end of the feeder, as well as near consumers who may be active in the future.

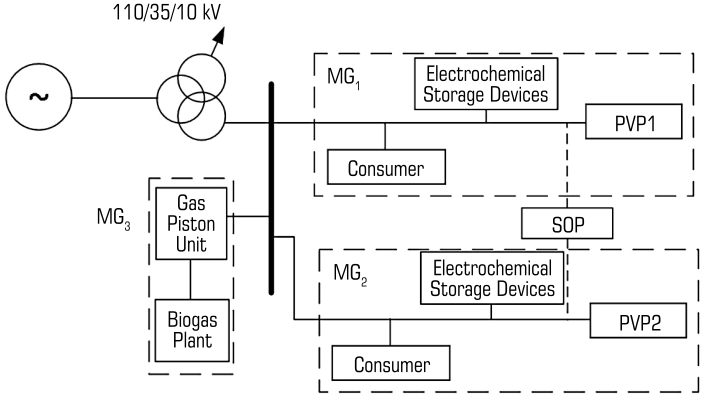

Fig. 4.15 Structural diagram of Vinkivtsi LES

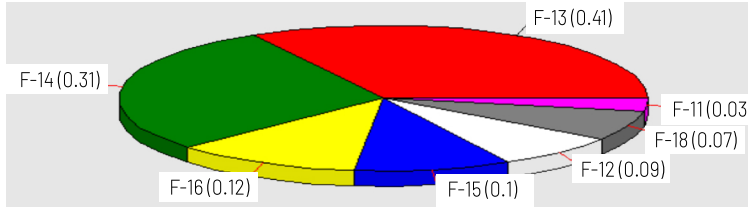

Fig. 4.16 Structure of losses in electrical networks of the Vinkivtsi substation

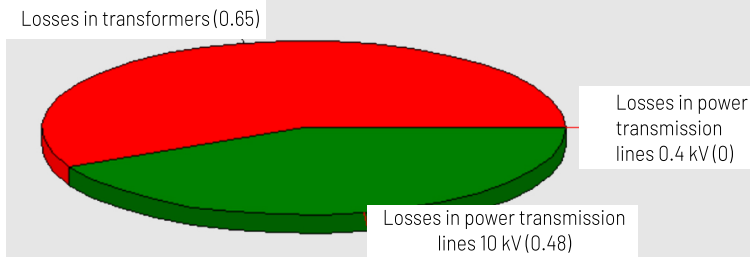

Fig. 4.17 Loss structure at the Vinkivtsi substation in transformers and 10 kV power transmission lines

Calculations were performed under the same conditions as in the previous paragraph, with the exception that in the diagram shown in **Fig. 4.14**, at substations 63 and 122, photovoltaic power plants with a capacity of 2.5 and 5 MW are connected, respectively. **Fig. 4.18** shows the structure of annual electricity losses by feeders. Compared with the previous regime, electricity losses in feeders F-12, F-13 and F-16 decreased the most. Electricity losses in the transformer practically did not change, and losses in the power transmission line of the network decreased by 12% (**Fig. 4.19**).

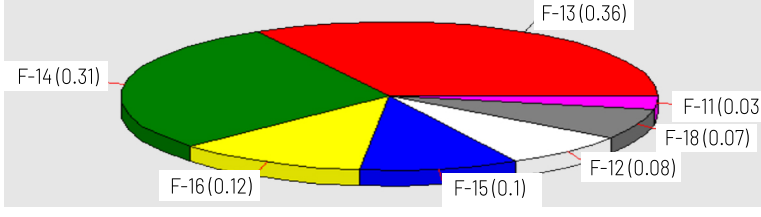

Fig. 4.18 Structure of losses in the electrical networks of the Vinkivtsi substation in the mode with a PVPP

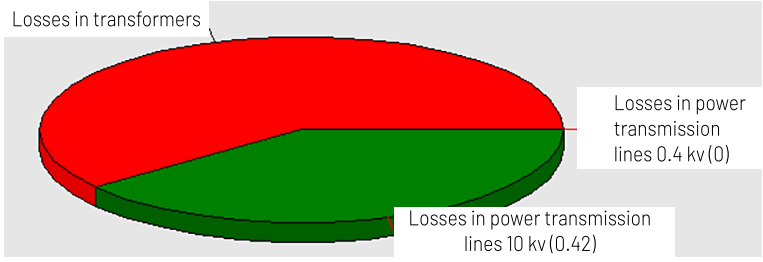

Fig. 4.19 Loss structure at the Vinkivtsi substation in the mode with a PVPP

With normal voltage quality, power losses in F-12 decreased by 25%, in F-13 in different areas power losses decreased from 12 to 24%.

CONCLUSIONS

Distribution electrical networks with an increase in the share of renewable energy sources in them acquire the characteristics of a local electric electrical system and there is a need to create conditions in them to maintain the balance of active and reactive power, taking into account the fact that the generation of electricity from RES depends on natural conditions and is unstable. Since balance reliability as a complex indicator characterizes the quality of the functioning of the power supply system, it is important to provide electrical networks with means that would compensate for the instability of RES generation, especially photovoltaic and wind power plants (PVPP, WPP). The task of choosing methods and means of RES backup is a technical, economic and optimization task.

The feasibility of integrating RES into distribution power grids in the form of separate microgrids (MG), which are a key part of the transition to LES operating on the principles of SMART Grid, is shown. Local MGs, in addition to generation sources and consumers, also have means of accumulating a certain amount of energy. To ensure technical and economic efficiency, MGs are combined into an intelligent control system, which allows for more rational use of MG resources, effective interaction with the distribution network and use the capabilities of active electricity consumers in the process of balancing the LES regime. It is proposed to form the hierarchical structure of the intelligent LES system in such a way that LES with intelligent power grids could not lose RES during the limitation of centralized power supply, but fully use their advantages together with energy storage systems for reliable power supply to consumers.

Calculations and analysis of their results confirmed the positive impact of PVPP on the regime of the distribution power grid under certain conditions. It is shown that the maximum effect of PVPP on the distribution network is achieved when they are connected in the middle or closer to the end of the feeder. It is desirable to choose the feeder with the highest load with consumers, which in the future may be active

and used to coordinate PVPP generation schedules and local electricity consumption. This allows to obtain a number of advantages, such as reducing electricity losses and improving its quality, as well as compensating for the instability of PVPP generation during the day and, accordingly, the negative impact on the balance reliability of the LES. The example of the DEN LES illustrates the effectiveness of the methods and algorithms proposed in the work for determining electricity losses caused by the introduction of PVPP, as well as the formation of the LES in such a way as to ensure the ability of active consumers and other means of reservation to influence its balance reliability as a balancing group.

REFERENCES

1. Basok, B. I., Butkevych, O. F., Dubovskyi, S. V. (2021). Technical and economic aspects of decarbonisation prospects assessing of the interconnected power system of Ukraine. Tekhnichna Elektrodynamika, 5, 55—62. https://doi.org/10.15407/techned2021.05.055
2. Yandulskyi, O., Nesterko, A., Trunina, H. (2020). Determining the reserve capacity of thermal and hydroelectric power stations for frequency and power flows regulation in ISP of Ukraine. Tekhnichna Elektrodynamika, 1, 58—63. https://doi.org/10.15407/techned2020.01.058
3. Shaping the energy transition. Towards a 100% renewable energy future. Wartsila. Available at: https://www.wartsila.com/energy/vision Last accessed: 15.01.2021
4. Kudria, S., Riepkin, O., Rubanenko, O., Yatsenko, L., Shynkarenko, L. (2022). Stages of green hydrogen energy development of Ukraine. Vidnovluvana Energetika, 1 (68), 5—16. https://doi.org/10.36296/1819-8058.2022.1(68).5-16
5. Kan, Z., Li, Z., Li, S., Zhang, T., Zhu, D., Yi, M., Huang, Y. (2020). Research on Grid-Connected/Islanded Control Strategy of PV and Battery Storage Systems as Emergency Power Supply of Pumping Storage Power Station. 2020 IEEE 3rd International Conference on Electronics Technology (ICET). Chengdu, 457—462. https://doi.org/10.1109/icet49382.2020.9119658
6. Zhu, Z., Liu, Z., Duan, Q., Xu, Z., Sun, B., Mei, H. (2021). Capacity Allocation of Energy Storage and Synchronous Condenser for Wind-photovoltaic-thermal-storage Combined Transmission System. 2021 IEEE Sustainable Power and Energy Conference (ISPEC). Nanjing, 239—244. https://doi.org/10.1109/ispec53008.2021.9735446
7. Bolotnyi, N., Loienko, Y., Karmazin, O. (2022). Energy storage systems application for operation management problems in electric power system of Ukraine. Status and development prospects. Vidnovluvana Energetika, 3 (70), 28—35. https://doi.org/10.36296/1819-8058.2022.3(70).28-35
8. Denysiuk, S. P., Derevianko, D. H., Bielokha, H. S. (2022). Synthesis of models of local power systems with distributed generation sources. Tekhnichna Elektrodynamika, 4, 48—53. https://doi.org/10.15407/techned2022.04.048
9. Tomashevskyi, Y., Burykin, O., Kulyk, V., Malogulko, J. (2019). Estimation of the dynamics of power grid operating parameters based on standard load curves. Eastern-European Journal of Enterprise Technologies, 6 (8 (102)), 6—12. https://doi.org/10.15587/1729-4061.2019.184095

10. Yin, S., Jin, M., Chen, X., Guo, X., Feng, J. (2021). Modeling and Simulation of Optimal Configuration of Virtual Power Plant Oriented to Power Internet of Things. 2021 IEEE 4th International Conference on Automation, Electronics and Electrical Engineering (AUTEEE). Shenyang, 751–754. https://doi.org/10.1109/auteee52864.2021.9668812
11. Kuznietsov, M., Karmazin, O. (2022). Optimal planning of hybrid power system at different electricity tariffs. Vidnovluvana Energetika, 3 (70), 6–18. https://doi.org/10.36296/1819-8058.2022.3(70).6-18
12. Jung, J., Villaran, M. (2017). Optimal planning and design of hybrid renewable energy systems for microgrids. Renewable and Sustainable Energy Reviews, 75, 180–191. https://doi.org/10.1016/j.rser.2016.10.061
13. Lezhniuk, P., Komar, V., Hunko, I., Jarykbassov, D., Tussupzhanova, D., Yeraliyeva, B., Katayev, N. (2022). Natural-simulation model of photovoltaic station generation in process of electricity balancing in electrical power system. Informatyka, Automatyka, Pomiary w Gospodarce i Ochronie Środowiska, 12 (3), 40–45. https://doi.org/10.35784/iapgos.3030
14. Pro zatverdzhennia Zmin do postanovy NKREKP (2019). Postanova Natsionalnoi komisii, shcho zdiisniuie derzhavne rehuliuvannia u sferakh enerhetyky ta komunalnykh posluh No. 641. 26.04.2019.
15. Lezhniuk, P., Komar, V., Kravchuk, S., Netrebskiy, V., Lesko, V. (2019). Optimal Integration of Photoelectric Stations in Electric Networks. LAP LAMBERT Academic Publishing, 210.
16. Malvoni, M., Hatziargyriou, N. (2019). One-day ahead PV power forecasts using 3D Wavelet Decomposition. 2019 International Conference on Smart Energy Systems and Technologies (SEST). Porto, 1–6. https://doi.org/10.1109/sest.2019.8849007
17. Lezhniuk, P., Komar, V., Povstianko, K. (2023). Relative assessment of the cost of reservation of renewable energy sources. Power engineering: Economics, Technique, Ecology, 1, 39–45. https://doi.org/10.20535/1813-5420.1.2023.275958
18. Hydrogen Insights A perspective on hydrogen investment, market development and cost competitiveness (2021). Hydrogen Council. Available at: https://hydrogencouncil.com/wp-content/-uploads/2021/02/Hydrogen-Insights-2021-Report.pdf
19. Lezhniuk, P., Kozachuk, O., Komenda, N., Malogulko, J. (2023). Electrical power and energy balance in the local electrical system by using reconciliation of the generation and consumption schedules. Przeglą d Elektrotechniczny, 1 (9), 59–65. https://doi.org/10.15199/48.2023.09.10
20. Smolarz, A., Lezhniuk, P., Kudrya, S., Komar, V., Lysiak, V., Hunko, I. et al. (2023). Increasing Technical Efficiency of Renewable Energy Sources in Power Systems. Energies, 16 (6), 2828. https://doi.org/10.3390/en16062828
21. Kyrylenko, O. V., Blinov, I. V., Parus, E. V., Trach, I. V. (2021). Evaluation of efficiency of use of energy storage system in electric networks. Tekhnichna Elektrodynamika, 4, 44–54. https://doi.org/10.15407/techned2021.04.044
22. Baziuk, T., Blinov, I., Butkevych, O., Honcharenko, I., Denysiuk, S.; Kyrylenka, O. (Ed.) (2016). Intelektualni elektrychni merezhi: elementy ta rezhymy. Kyiv: In-t elektrodynamiky NAN Ukrainy, 399.
23. Jiang, W., Yang, K., Yang, J., Mao, R., Xue, N., Zhuo, Z. (2019). A Multiagent-Based Hierarchical Energy Management Strategy for Maximization of Renewable Energy Consumption in Interconnected Multi-Microgrids. IEEE Access, 7, 169931–169945. https://doi.org/10.1109/access.2019.2955552

24. Lezhniuk, P., Kozachuk, O., Galuzinsky, O. (2023). Use of active consumers for balance of electricity in the electric grid. Herald of Khmelnytskyi national university. Technical sciences, 3, 214—221.
25. Wójcik, W., Lezhniuk, P., Kaczmarek, C., Komar, V., Hunko, I., Sobchuk, N. et al. (2025). Integrated Assessment of the Quality of Functioning of Local Electric Energy Systems. Energies, 18 (1), 137. https://doi.org/10.3390/en18010137
26. Kozachuk, O., Lezhniuk, P. (2024). Formation of local electric energysystems in the composition of the unified energy supply system. Herald of Khmelnytskyi National University. Technical Sciences, 337 (3 (2)), 352—356. https://doi.org/10.31891/2307-5732-2024-337-3-53
27. Denysiuk, S. P., Derevianko, D. H., Bielokha, H. S. (2022). Synthesis of models of local power systems with distributed generation sources. Tekhnichna Elektrodynamika, 4, 48—53. https://doi.org/10.15407/techned2022.04.048
28. Xing, X., Jia, L. (2023). Energy management in microgrid and multi-microgrid. IET Renewable Power Generation, 18 (15), 3480—3508. https://doi.org/10.1049/rpg2.12816
29. Jiang, W., Yang, K., Yang, J., Mao, R., Xue, N., Zhuo, Z. (2019). A Multiagent-Based Hierarchical Energy Management Strategy for Maximization of Renewable Energy Consumption in Interconnected Multi-Microgrids. IEEE Access, 7, 169931—169945. https://doi.org/10.1109/access.2019.2955552
30. Hunko, I., Kudrya, S., Komar, V., Lezhniuk, P. (2024). Mathematical model and algorithm for the determination of the origin of electricity from renewable energy sources in the electric power system. Vidnovluvana Energetika, 2 (77), 6—12. https://doi.org/10.36296/1819-8058.2024.2(77).6-12

DOI: 10.15587/978-617-8360-19-1.CH5

Oleksandr Povazhnyi, Volodymyr Kukhar, Oleksiy Koyfman,
Khrystyna Malii, Volodymyr Pashynsky

CHAPTER 5

IMPROVING CONDITION MONITORING AND MAINTENANCE FRAMEWORK FOR REFRACTORY LININGS IN INDUCTION MELTING FURNACES THROUGH CONTINUOUS IMPROVEMENT METHODS

ABSTRACT

The service life and reliability of refractory linings in coreless induction crucible furnaces are essential factors influencing the efficiency, safety, and cost-effectiveness of metallurgical melting processes. Premature wear of linings, caused by the combined effects of slag composition, molten metal temperature, crucible geometry, electromagnetic stirring intensity, and cooling conditions, inevitably leads to increased maintenance frequency, unplanned production downtime, and higher operational costs. In the context of the global steel industry's decarbonization strategy and the growing demand for resource-efficient technologies, the issue of extending refractory lining durability in induction melting units gains particular relevance. This study presents an improvement of the lining condition monitoring and maintenance decision-making system through the integration of a continuous improvement methodology and heuristic engineering tools, including TRIZ, morphological analysis, the method of control questions, the method of focal objects, the theory of inventive problem solving, and functional–value analysis. The research incorporates both a review of existing industrial practices and an experimental evaluation of innovative technical solutions. A comparative evaluation of monitoring technologies was carried out, with the criteria including measurement accuracy, implementation complexity, cost, and adaptability to harsh metallurgical environments. This assessment resulted in the selection of laser-based 3D profilometry as the most appropriate solution for high-precision wear assessment and digital surface modelling, providing a reliable basis for predictive maintenance planning. The proposed approach combines technical and organizational measures, including optimization of slag formation processes, adjustment of crucible geometry to reduce thermomechanical stresses, improvement of cooling regimes, and systematic wear tracking supported by digital data analysis. An industrial case study involving EGES-type furnaces at Zaporizhzhia Foundry and Mechanical Plant confirmed the applicability and efficiency of the developed framework under real production conditions, ensuring timely maintenance planning, reducing the risk of emergency lining failure, lowering specific energy consumption, and supporting stable quality of the produced steel. The findings demonstrate the potential of combining continuous improvement principles with modern monitoring technologies to create an integrated refractory lining management strategy that enhances durability, minimizes environmental footprint, and strengthens the competitiveness of electrometallurgical production.

KEYWORDS

Induction crucible melting, refractory wear mechanisms, furnace lining durability, 3D laser scanning systems, automated condition monitoring, continuous improvement methodology, digital profiling technologies, TRIZ methodology, morphological analysis, method of control questions, method of focal objects, theory of inventive problem solving, functional-value analysis, slag formation optimization, crucible geometry adjustment, cooling regime improvement.

One of the approaches to reducing greenhouse gas emissions in the fight against climate change, within the framework of the steel production decarbonization strategy, is the transition to electrometallurgical steelmaking technologies, including the production of steel in induction furnaces [1]. Induction heating as a physical principle is universal for a wide range of metallurgical operations — from melting in crucible furnaces [2, 3] to pre-deformation (pre-forming) billet/blank heating and heat treatment of finished products [2, 4]. The principles of current induction are identical: the electromagnetic field of the inductor induces eddy currents in the conductive material, which, due to the Joule effect, heat its volume, and, under certain conditions, also ensure significant electrodynamic stirring of the molten metal [3]. Such intensive circulation is beneficial for achieving chemical homogeneity, but at the same time imposes additional thermomechanical stresses on the refractory lining.

Given the global decarbonization agenda, increasing the operational efficiency and durability of key components in induction furnaces becomes a critical factor for ensuring the competitiveness and sustainability of metallurgical enterprises. Improving refractory lining management directly contributes to both energy efficiency and production reliability.

One of the main limitations hindering the potential full-scale transition to steelmaking in induction furnaces is the relatively low durability of the refractory lining. At the same time, induction steelmaking units are characterized by high productivity and, as demonstrated in practice, are successfully used for the production of relatively small volumes (from 5 kg to 60 tonnes) of high-quality steels in both industrial (foundry shops) and laboratory conditions. The technical literature reports the use of induction furnaces for melting high-alloy heat-resistant steels [5], structural and low-carbon steels [6], non-ferrous metals [7] and special-purpose alloys [8, 9], as well as widespread examples of combined technologies in which, following melting, processes of severe plastic deformation are implemented to improve the mechanical properties of the final products [10, 11]. Induction melting provides intensive stirring of the melt flows and active slag formation, contributing to metal purification. The effect of reducing segregation and modifying non-metallic inclusions can be further enhanced through the use of special additions based on rare-earth metals [12].

A distinctive feature of the operation of an induction crucible furnace is its similarity to a transformer, where the inductor serves as the primary winding and the metal in the crucible — located at the center of the inductor and powered by a high-frequency alternating current generator — acts as the secondary winding. Due to this design, the molten metal, heated by eddy currents, is subjected to radial forces directed towards the center of the molten bath [13]. These forces cause a circulating motion in the vertical plane,

which, on the one hand, facilitates the attainment of chemical homogeneity and the flotation of non-metallic inclusions [14, 15], but, on the other hand, increases the intensity of contact between the molten metal and the refractory lining [13, 16, 17], leading to its accelerated wear.

Active circulation of molten metal positively affects the uniformity of the chemical composition of the produced metals, but has an adverse effect on such a parameter as the durability of the refractory lining in induction furnaces. The lining is located between the molten metal and the inductor (**Fig. 5.1**), and it is evident that the thicker the furnace lining (or its thickening due to build-up deposits), the smaller the magnetic flux penetrating the metal, and consequently the lower the efficiency of electrical energy utilization during melting. Therefore, the lining thickness is subject to certain limitations [18]. The general design of an induction melting furnace is shown in **Fig. 5.1.**

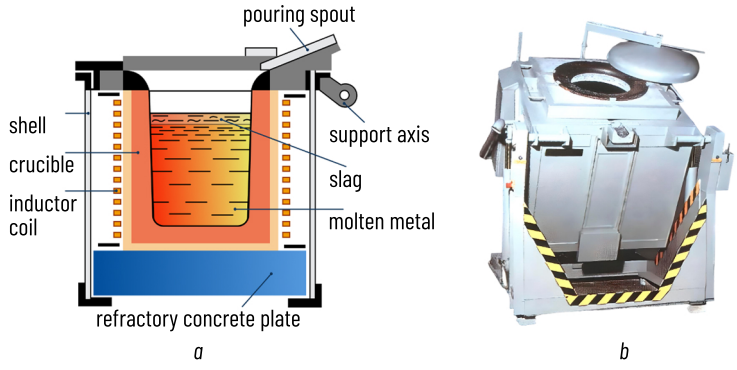

Fig. 5.1 View of a typical coreless induction crucible furnace (modified by the author based on an open-source illustration from KEMA educational resource): *a* — schematic; *b* — general
Source: [17]

The crucible of an induction furnace (**Fig. 5.1**) is manufactured or repaired by ramming or laying with refractory material (bricks). The crucible is positioned directly inside the inductor, which is a water-cooled coil made of copper tubing with a defined number of turns. A rammed crucible made of refractory powder material is fixed in the furnace shell and placed on a base plate made of refractory concrete [17, 18]. The discharge of molten metal is performed through a spout by tilting the furnace together with the shell relative to the support axis. Due to the physical characteristics of heat generation directly within the metal, the maximum melting temperature is mainly limited by the durability of the crucible itself. To increase thermal resistance and reduce thermal stress, water-cooling systems and refractory lining temperature monitoring devices [17, 18] are employed, which may integrate measurement sensors [19] and computer modelling of temperature fields using numerical methods [11, 14]. Such solutions not only extend the crucible's service life but also ensure the stability of the melting process [20]. The crucible is made of refractory materials, which may include ceramics, graphite, or chamotte-graphite [17, 18].

The melting temperatures of steel grades produced in induction furnaces determine the use of three types of crucible linings:

a) acidic;

b) basic;

c) neutral.

Acidic linings (a) are made from refractories based on silicon oxide (90–98% SiO_2), boric acid (1–1.5%), and small amounts of metallic oxides such as Al_2O_3, Fe_2O_3, MnO, and others. The service life of acidic crucibles is typically 80–100 heats. Basic linings (b) are mainly produced from magnesite (up to 85% MgO), water glass, and additives of oxides such as CaO, SiO_2, and others. The durability of such crucibles decreases with increasing furnace capacity and ranges from 20 to 50 heats. Neutral linings (c) are based on Al_2O_3 with magnesite additives. The durability of neutral linings is generally higher than that of the previous two types [17, 18].

Research shows that the behavior of the refractory lining is determined both by the composition of the refractory material and by the nature of its interaction with the molten metal and non-metallic inclusions [12, 21, 22]. Modelling the processes of interaction between the lining, slag, and metal [11, 14, 17] allows for predicting its wear rate and scheduling maintenance in a timely manner.

In the conditions of the intense electromagnetic field of an induction furnace, safety aspects must be taken into account – including personnel electrical safety, the effects of electromagnetic radiation, and the safe operation of power systems [20, 23]. Addressing these issues involves the implementation of risk control and protection systems based on the principles of industrial safety and occupational health standards.

Sources [24, 25] also highlight, among the advantages of induction crucible furnaces, their broad potential for automation using controllers, as well as the high environmental performance of these units, while citing the low durability of the refractory lining as a disadvantage. According to the author of [26], an important part of maintenance, ensuring equipment efficiency and reliability, and maintaining process safety during melting, is the automated monitoring of lining wear. At the same time, the low durability of the refractory lining once again appears among the main drawbacks, which is why current research focuses on developing methods to improve it, including the application of heuristic approaches, functional value analysis (FVA), and TRIZ tools to optimize the monitoring and maintenance of melting units [27, 28].

Based on the above, the analysis of industrial experience in improving refractory lining durability and the development of recommendations for enhancing the efficiency of lining wear monitoring in induction crucible melting furnaces is a relevant scientific and practical task. The aim of the study is to substantiate and implement a methodological approach to the synthesis and improvement of a condition monitoring and maintenance system for refractory linings in induction melting furnaces, based on continuous improvement methods, in order to enhance the reliability, durability, and operational stability of the induction melting process.

CHAPTER 5

5.1 TECHNICAL BACKGROUND AND METHODS FOR IMPROVING LINING DURABILITY

Induction steelmaking furnaces are widely used in the metallurgical industry, in glass production, and in waste processing. Considering the prospects and the objective necessity for the development of electro-

metallurgical technologies, the scope and volume of their application are expected to increase. For example, at *Zaporizhzhia Foundry and Mechanical Plant LLC*, an induction steelmaking furnace manufactured by EGES (Turkey) with a capacity of 3.0 tonnes has been installed. **Fig. 5.2** shows the furnace in operation, and **Fig. 5.3** – during tapping. The technical specification s of the furnace equipment are presented in **Table 5.1**.

a *b* *c*

Fig. 5.2 Melting in a 3-tonne induction furnace produced by EGES (Turkey): *a* – overall appearance of the unit; *b* – the crucible is enclosed to minimize heat loss and limit the escape of metal vapors into the work area; *c* – the interior of the furnace visible after tapping

a *b* *c*

Fig. 5.3 Steel casting using a 3-tonne induction melting furnace from EGES (Turkey): *a* – pouring molten metal from the furnace into a ladle; *b* – skimming slag from the surface of the melt; *c* – filling molds during the casting stage

Among the main causes of crucible failure in an induction steelmaking furnace, the following should be highlighted:

– thermal stress: during the steel melting process in the crucible, significant heating and cooling occur. These heating and cooling cycles induce thermal stresses in the crucible material, leading to its damage and wear;

— mechanical impacts: during the charging of the charge material and scrap, impacts occur when the material falls onto the refractory lining. The steel melting process is accompanied by mechanical effects, such as the intensive movement of metal in the crucible. This also causes crucible damage and wear;

— corrosion (erosion): certain constituents of steel or additives used during melting may be corrosively active towards the crucible material, resulting in its wear;

— uneven heating: uneven heat distribution within the crucible during melting also generates thermal stresses, which may cause cracking of the refractory lining;

— contact with metal: direct contact with unmelted metal (at the beginning of melting) and with molten metal during the process leads to mechanical wear of the lining through friction.

Fig. 5.4 shows the process of ramming a 3-tonne crucible of an induction furnace under the operating conditions of *Zaporizhzhia Foundry and Mechanical Plant LLC*.

Table 5.1 Specifications of EGES induction furnaces (Turkey) with crucible capacities of 1 tonne and 3 tonnes

Furnace		**Electric converter**		**Melting rate, kg/h**		**Melting time, min**	
Model	Capacity, kg	Power, kW	Frequency, Hz	Cast iron at 1450°C	Steel at 1600°C	Cast iron at 1450°C	Steel at 1600°C
EGP 1000 SE	1000	600	1000	1137	1043	53	58
EGP 3000 SE	3000	1750	500	3305	3062	54	59

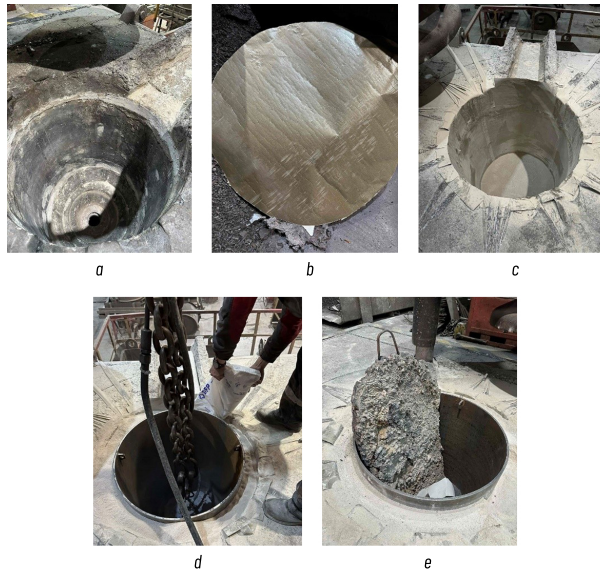

Fig. 5.4 Relining of a 3-tonne capacity induction furnace (produced by EGES, Turkey): *a* — inductor workspace prepared for lining; *b* — meconite being readied for application to the furnace lining; *c* — lining the furnace bottom; *d* — placing the furnace lining machine inside the unit using a crane; *e* — charging the furnace for the sintering stage

5.2 METHODS FOR IMPROVING THE DURABILITY OF REFRACTORY LININGS

Improving the durability of the crucible requires a comprehensive approach, which includes both the selection of appropriate materials and the proper management of the operating process. The general methods and strategies used to enhance the durability of the refractory lining in industrial and laboratory induction furnaces, identified as a result of the analysis of literature sources and practical experience, are summarized in **Table 5.2**.

Table 5.2 Systematization of methods for improving the durability of refractory linings in induction steelmaking furnaces

No.	Method for improving durability	Essence of the method
1	2	3
1	Selection of appropriate crucible material	Use of high-quality materials with high thermal resistance and mechanical strength that meet the requirements of the specific process. Application of special materials, such as silicon carbide or zirconium oxide, which may offer improved thermal and chemical resistance [18, 29]
2	Thermal insulation	Ensuring effective thermal insulation of the refractory lining to prevent heat losses, overheating, and wear under high-temperature conditions. Applied to concentrate heat in the required areas. Thermal insulation coatings are used to reduce heat losses and retain heat within the inner region of the crucible. These materials can help maintain stable temperature conditions and reduce energy consumption [20, 26, 30]
3	Cooling systems	Use of cooling systems to control the temperature of the refractory lining and prevent overheating [18, 31, 32]. This includes lining with integrated channels for water cooling, pumping and circulating a coolant (water), introducing a cooling medium (cold gas) directly into the crucible, and employing additional active cooling methods (e.g., using Peltier elements [33])
4	Temperature regime monitoring and automated control	Installation of temperature monitoring systems for continuous tracking of operating parameters and timely detection of anomalies to avoid sudden temperature changes that may cause thermal shock to the crucible. This includes maintaining a stable temperature regime and ensuring gradual heating and cooling. The method involves installing thermocouples and sensors for continuous crucible temperature monitoring and prompt response to any changes, as well as using automatic temperature control systems capable of adjusting the supply of cooling liquid or gas as required [19, 25, 26, 34]
5	Optimisation of melting processes and crucible design	Analysis and optimization of technological processes to reduce excessive hydrodynamic friction and thermal impact on the refractory lining. This involves studying the hydrodynamics of melting to identify areas where excessive friction occurs, and using computer modelling to analyze and improve hydrodynamic processes and thermal models in order to determine heat distribution and identify zones with excessive thermal impact. Modifications to the shape and configuration of the lining are introduced to reduce frictional resistance. Ensuring proper crucible design takes into account parameters such as wall thickness, shape, and dimensions. The risk of thermal shock is minimized by selecting optimal design parameters [35]

Continuation of Table 5.2

1	2	3
6	Expert assessment, monitoring of wear and deformations	Engagement of specialized experts for systematic assessment of the refractory lining condition and identification of any signs or risks of wear. This includes conducting visual inspections to detect any traces of wear or deformation, as well as using non-destructive testing methods (e.g., ultrasonic inspection) to identify internal defects [13, 18, 26, 36]
7	Regular maintenance and repair	Regular maintenance of the refractory lining to ensure timely detection of wear signs or defects and to maintain its durability. This includes scheduled repairs, refurbishment, or replacement of the crucible [26, 37]
8	Application of protective coatings	Application of protective coatings to reduce the effects of chemical reactions and wear on the crucible surface [30, 38, 39]. Graphite coatings are used to protect the crucible from erosion and oxidation at high temperatures, as graphite is chemically stable and withstands high temperatures, making it an effective material for crucible protection. Ceramic coatings are applied to create a thermally and chemically resistant layer that shields the crucible from aggressive environments (some types of ceramic coatings have high thermal shock resistance). Oxide-ceramic materials, such as aluminum oxide or zirconium oxide, are employed to protect the crucible from oxidation and aggressive reactions at elevated temperatures. Some manufacturers offer specialized coatings designed specifically for metallurgical applications and induction melting, which can be optimized for particular operating conditions. Enamel and ceramic coatings with a low coefficient of friction may also be used to reduce frictional resistance and improve crucible performance
9	Electromagnetic field management	Optimization of crucible design and positioning to reduce the impact of the electromagnetic field on its durability [40, 41]. Transition to innovative electromagnetic cold crucible (EMCC) solutions [40], i.e., the use of a segmented, water-cooled copper crucible for induction melting in a vacuum or controlled atmosphere without the use of refractory materials. EMCC technology is being adopted in two types of industrial applications: (a) as batch crucibles for melt preparation, and (b) as bottomless cylindrical molds for continuous casting. The advantages of EMCC include: reduced friction effects in the forming system (minimized contact between the melt and the crucible), which significantly increases crucible durability; absence of contamination and inclusions in the melt; creation of fluid flow conditions that can control grain structure and accelerate online chemical treatment (resulting in high-quality castings); and reduction of cycle time [41]

The selection of the optimal solution is recommended to be carried out after consultation with manufacturers or specialists in metallurgical equipment.

5.3 METHODS FOR MONITORING THE CONDITION OF REFRACTORY LININGS

Regular and comprehensive monitoring of the refractory lining condition allows timely detection of any changes and helps to avoid potential accidents or production issues. Based on practical experience and the analysis of information from the sources listed in **Table 5.2**, the methods for monitoring the condition of refractory linings in induction steelmaking furnaces have been systematized. The results of this systematization are presented in **Table 5.3**. It should be noted that the effectiveness of wear monitoring depends on the systematic nature, accuracy, and timeliness of the measurements and inspections performed.

Table 5.3 Methods for monitoring the condition of refractory linings in induction steelmaking furnaces

No.	Monitoring method	Type of work under the monitoring method
1	Visual inspection	Conducting regular inspections of the refractory lining for the presence of cracks, spalling, or any signs of mechanical damage. Checking for uniform wear of the lining and identifying any possible unevenness that could lead to a loss of durability
2	Measurement of crucible thickness and geometric parameters	Carrying out regular measurements of the refractory lining thickness to detect wear (a reduction in crucible wall thickness may indicate the need for replacement). Monitoring other geometric parameters of the crucible (height, diameter) to detect deviations from standard values. The use of appropriate equipment is required to ensure precise measurements
3	Thermal (thermographic) monitoring	Using thermal imaging cameras to identify potential overheating zones or areas of uneven heat distribution, which may indicate problems in the refractory lining. Measuring the temperature on the lining surface and in the contact zone with molten metal when monitoring thermal parameters
4	Tracking of furnace operating parameters	Tracking operating parameters such as operating time, power, and temperature regime to detect anomalies that may indicate problems with the refractory lining. Sudden temperature changes or overheating can accelerate lining wear
5	Non-destructive testing	Using non-destructive testing methods, such as ultrasonic inspection or radiography, to detect internal defects in the refractory lining. Magnetic testing methods can also be effective for identifying cracks and defects in the lining structure
6	Petrographic analysis of refractory lining material composition	Sampling refractory lining material for subsequent petrographic analysis to identify structural changes in the material and determine the degree of ageing, which affects strength and thermal resistance
7	Testing of refractory lining material properties	Measuring the elastic characteristics of the refractory lining material to assess the degree of ageing and durability. Conducting strength tests on the lining to determine its mechanical properties and strength reserve
8	Vibration monitoring	Installing a vibration monitoring system to detect potential vibrations, impacts, or other anomalies that may affect the condition of the refractory lining
9	Scheduled maintenance	Establishing a regular schedule for planned maintenance, including inspection and monitoring of the refractory lining

5.4 HEURISTIC METHODS APPLICATION

To address the problem of improving the durability of the refractory lining of an induction furnace, heuristic methods [42, 43] were used, including:

a) method of control questions (MCQ);

b) morphological analysis / focal objects method (MO/FOM);

c) algorithm for solving inventive problems (ASIP);

d) functional value analysis (FVA).

Heuristic methods are widely used for solving inventive problems and making design decisions. Their essence lies in a set of logical, methodologically justified techniques aimed at achieving a goal under conditions of limited initial data. The solutions obtained are not definitive and require consideration of the specific context and accumulated experience.

5.4.1 METHOD OF CONTROL QUESTIONS (MCQ)

The method of control questions is used to stimulate and verify the understanding of information. The essence of the MCQ lies in creating or using a prepared list of questions that allow the problem to be examined from different perspectives, stimulate critical thinking, systematize the search process, and identify possible solutions to the problem. To ensure a comprehensive exploration of the problem, the questions should be structured to reflect the key aspects of the topic, considered step by step, varied in form and complexity, promote active application of knowledge and creativity, provide feedback to correct misunderstandings, and encourage discussion during collective review (for example, when applied in brainstorming techniques).

At various times, different authors have developed different sets of questions used to stimulate creative thinking within the MCQ framework. These include question lists by authors such as A. Osborn, T. Eiloart, D. Pearson, G. Polya, R. Busch, and others. Below, selected questions (five sample questions) from the lists of A. Osborn and T. Eiloart are presented, with responses based on industrial experience.

Consideration of the problem using A. Osborn's checklist of questions.

"What in the technical object can be changed? What and to what extent can be replaced: using another ingredient, material, process, energy source, arrangement, colour, sound, lighting?"

Answer: As indicated in the literature review, the durability of the refractory lining depends on the lining material. Thus, an increase in durability can be achieved by ensuring the correct selection of refractory material according to the steel grades being produced.

"What in the technical object can be reduced or replaced? Can anything be compressed, condensed, miniaturized, shortened, narrowed, separated, broken down?"

Answer: The thermal resistance of the lining can be increased by performing hot repairs on specific areas of the lining as it wears, namely hot patching in zones of intensive wear — usually in the scrap charging area and near the spout. In such repairs, the hot patch in the form of a briquette is placed on the problem area, where it melts under high temperatures and fills the repaired section. When performed correctly, hot patching can achieve a service life of up to 100 heats.

"What can be transformed in the technical object? Which components can be replaced? Can the model, layout, arrangement, sequence of operations be changed? Can cause and effect be swapped, or can speed, pace, or mode be altered?"

Answer: Instead of briquettes for hot patching, the semi-dry gunning repair method can be used. This method can be applied to repair any zone, and the operation takes less time than hot patching. However, the lining restored by gunning has a lower durability — up to 40 heats — but allows for more selective repairs.

"Is it possible to solve the inventive problem through adaptation, simplification, reduction? What does the technical object resemble? Does the analogy suggest a new idea? Are there similar problematic situations from the past that can be applied? What can be copied? Which technical object needs to be outperformed?"

Answer: A relatively new and advanced method for increasing furnace lining lifetime is the use of laser systems [44–46] (e.g., ZoloSCAN system [47]) to monitor the residual lining thickness. This allows early determination of the need for local repairs and the required amount of repair material, thereby optimizing repair time.

"What modifications to the technical object are possible? Would modification through rotation, bending, twisting, or turning be acceptable? What changes in function, movement, colour, odour, shape, or outline can be applied? Are other changes possible?"

Answer: By controlling slag quality and its chemical composition, the service life of lining materials can be extended. The highest intensity of lining failure is observed during the slag formation period when the basicity CaO/SiO_2 = 1.0–1.5 and oxidation level is high (up to 30% FeO). This indicates the need, in the initial stage of melting, to form a slag with the maximum MgO concentration for the given temperature conditions, as close as possible to saturation.

Consideration of the problem using T. Eiloart's checklist of questions.

"Define the ideal solution, develop possible ones."

Answer: One practical method that can be considered "ideal" for industrial conditions is to increase the durability of the refractory lining through the use of refractories with a longer service life and lower cost. For example, chamotte brick has the highest durability. Although its maximum refractoriness is not as high as that of basic brick (1690–1730°C compared to 2000°C), it withstands temperature fluctuations well and is cheaper.

"Try different types of materials and types of energy."

Answer: From the standpoint of the energy used in induction melting, its utilization is sufficiently efficient. Regarding the use of alternative materials, known methods for improving lining durability include steel melting with slags enriched in MgO, when the slag is formed at MgO saturation levels. Slags of such composition are less aggressive towards the furnace refractory lining.

"Mentally get inside the mechanism."

Answer: When examining the kinetics of slag saturation with magnesium oxide, during the interaction of MgO-C refractory material, modelling the process of adding magnesian flux shows a significant slowdown – by 2–2.5 times – in the rate at which magnesium oxide enters the slag. Industrial trials have made it possible to assess the degree of dissolution of basic refractories in slag depending on its magnesium oxide content, revealing a pattern in which the transition of magnesium oxide from the lining into the slag decreases with increasing MgO saturation.

"Modify the problem solution in terms of time (faster or slower), size, viscosity, etc."

Answer: The geometry of the crucible and compliance with dimensional tolerances during lining installation have an additional impact on lining durability. The crucible may undergo pre-assembly at the facility manufacturing the refractory structures, which can also contribute to increasing the number of heats.

"Identify alternative problems and systems that remove a specific link from the chain, thus creating something entirely different and leading to the desired solution."

Answer: It is evident that the refractory lining undergoes the most severe wear (softening and slag build-up) in zones with elevated temperatures. Therefore, one approach aimed at extending lining service life is targeted cooling in these zones.

5.4.2 FOCAL OBJECTS METHOD (FOM)

The focal objects method is intended for improving a selected object – called the focal object (because it is the focus of attention) – by transferring the characteristics of randomly chosen objects onto the focal object [48]. This is a method for generating new ideas, notable for its simplicity and potential for repeated application. With the goal of improving the durability of the refractory lining of an induction furnace, which average service life is around 50 heats, the system for monitoring the residual lining thickness was chosen as the focal object. The selection of random objects and their defined properties is presented in **Fig. 5.5**.

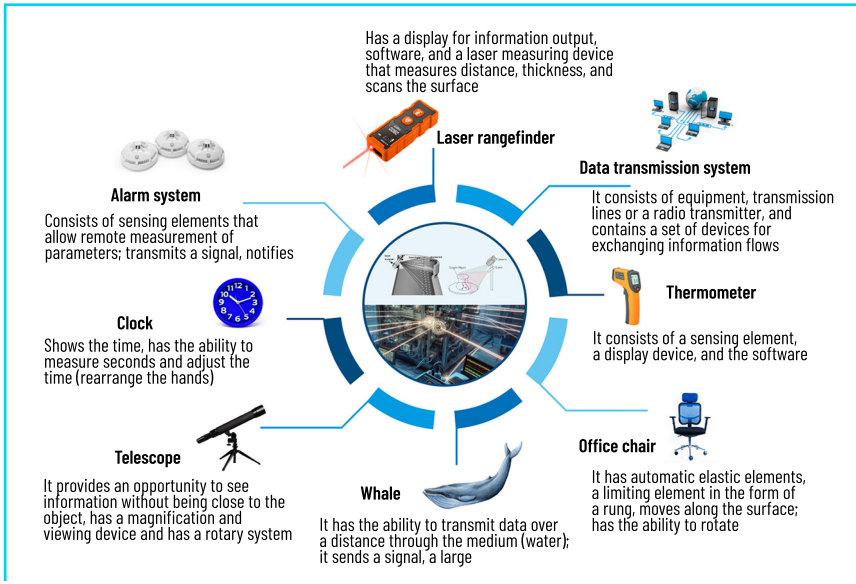

Fig. 5.5 Improvement of the system for monitoring the residual refractory lining thickness using the focal objects method: analysis of the properties of randomly selected objects

By generating ideas through the addition of variable properties from randomly selected objects (**Fig. 5.4**) to the focal object, the feasibility of implementing laser systems was determined.

The experience in developing and successfully applying a laser system for monitoring the condition of an induction furnace crucible is presented in [49]; in [46], a similar laser system was implemented for measuring the wear of a blast furnace lining.

Notable manufacturers of laser systems with the required functions include: DELTA (Sensors and Systems for the Steel Industry), SAVEWAY, Luoyang Songdao Induction Heating Technology Co., Ltd, MTI Corporation, and Acuity, among others.

For practical industrial application, the LR 2000 Delta CCS laser scanning unit was selected for implementation to monitor the residual thickness of the refractory lining. The system is based on the principle of a 3D scanner for constructing the lining profile [49], which enables the determination of residual dimensions. This allows early identification of the need for local repairs, optimization of repair time, and calculation of the required amount of lining materials.

5.4.3 ALGORITHM FOR SOLVING INVENTIVE PROBLEMS (ASIP)

The ASIP is a sequence of systematically executed actions (steps, stages) aimed at solving an inventive problem, which, in the context of this work, is improving the efficiency of monitoring the condition of an induction furnace refractory lining. The application of ASIP is reduced to the rational search for new technical solutions within a given system, achieving effective problem resolution with minimal cost, minimal modification of the original technical system, and economically justified expenses when implementing the developed solution.

The creation of a new technical solution is based on a technical contradiction within the system, which must be resolved during the implementation of ASIP. The essence of ASIP lies in comparing the ideal and actual states of the object, identifying a specific technical contradiction or its root cause — a physical contradiction. The algorithm involves determining the specific parameters that are in conflict, translating them into standardized general parameters, and using G. S. Altshuller's contradiction matrix to search for standard solutions (inventive principles) to eliminate the identified contradiction. This is followed by selecting a rational option and returning from standardized to specific parameters, with a description of the developed solution [42, 43].

Below is the solution to an inventive problem related to the implementation of a modern laser monitoring system (adopted from the results obtained using the focal objects method) for assessing the lining condition. In this context, new promising ideas are proposed, the feasibility of which will depend on the state of development of science and technology. **Fig. 5.6** presents the algorithm applied for solving the inventive problem using G. S. Altshuller's matrix (tables). **Fig. 5.7** contains information on the formulation of the technical contradiction using the "If — Then — But" formula (I, **Fig. 5.6**), with the identification of which specific parameters (II, **Fig. 5.6**) are improved and which are worsened when using a laser system for measuring lining thickness.

The transition from specific to generalized parameters (III, **Fig. 5.6**) listed in G. S. Altshuller's matrix [42, 43] may include the options (with the corresponding matrix number) given in **Table 5.4**: **F** — parameters to be improved (generalized: 27, 28, 33, 36, 38, 39), **G** — parameters to be worsened (generalized: 19, 22).

The contradictions (IV, **Fig. 5.6**) between generalized parameters according to G. S. Altshuller's matrix make it possible to determine the numbers of generalized inventive principles **H** (VI, **Fig. 5.6**), the names of which are provided in the note to **Table 5.4**.

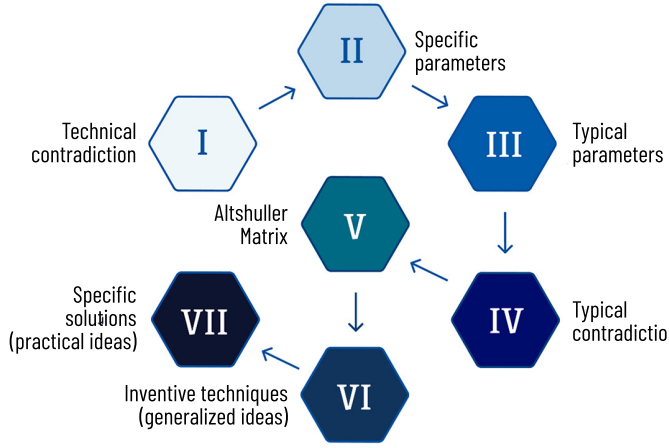

Fig. 5.6 Procedure for solving an inventive problem using G. S. Altshuller's matrix (ASIP)

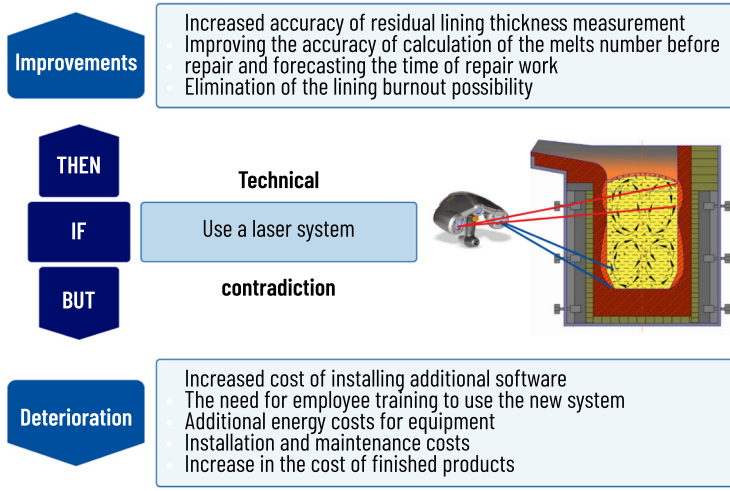

Fig. 5.7 Formulation of the technical contradiction using the "If – Then – But" formula when applying a laser system for measuring the thickness (3D scanning of the condition) of the refractory lining

Table 5.4 Application of ASIP to the use of a laser system for determining the lining thickness of an induction steelmaking furnace

Parameter	What is improved, F	What is worsened, G	Typical contradiction (IV, Fig. 5.6), F – G	Numbers of generalized inventive principles, H (VI, Fig. 5.6)*	Frequency of occurrence of the generalized inventive principle, N (times)	Numbers of generalized inventive principles, H (VI, Fig. 5.6)*
Specific (II, **Fig. 5.6**)	Accuracy, reliability of prediction	Costs, energy consumption, and expenditure	27–19	11, 19, 21, 27	5	2
Generalized (III, **Fig. 5.6**)	27 – reliability; 28 – measurement accuracy; 33 – ease of operation; 36 – device complexity; 38 – degree of automation; 39 – productivity	19 – energy consumption by a stationary object; 22 – energy losses	27–22	10, 11, 35	4	10, 13, 35
			28–19	3, 6, 32	3	19, 27, 28, 32
			28–22	26, 27, 32	2	3, 11, 29
			33 – 19	1, 13, 24	1	1, 6, 21, 24, 26, 38
			33 – 22	2, 13, 19		
			36 – 19	2, 27, 28, 29		
			36 – 22	2, 10, 13, 35		
			38 – 19	2, 13, 32		
			38 – 22	2, 3, 28		
			39 – 19	10, 19, 35, 38		
			39 – 22	10, 28, 29, 35		

*Note: *names of the generalized inventive principles (H) according to their numbers in G. S. Altshuller's classification. Principles: 1 – "Segmentation"; 2 – "Extraction"; 3 – "Local quality"; 6 – "Universality"; 10 – "Preliminary action"; 11 – "Cushion in advance"; 13 – "The other way round"; 19 – "Periodic action"; 21 – "Skipping"; 24 – "Intermediary"; 26 – "Copying"; 27 – "Cheap short-life instead of expensive long-life"; 28 – "Replacement of a mechanical system"; 29 – "Use of pneumatic and hydraulic structures"; 32 – "Change of colour"; 35 – "Change of physical and chemical parameters of the object"; 38 – "Use of strong oxidizing agents"*
Source: [42, 43]

Each contradiction corresponds to a certain set of generalized inventive principle numbers, and from the full list, those occurring with a frequency of one to five times were selected (**Table 5.4**). It can be assumed that the inventive principles that occur most frequently should be given more attention, as they address a relatively larger number of technical contradictions – the higher the frequency of occurrence of a generalized inventive principle, the greater its relevance.

From the generalized inventive principles, we then proceed to specific solutions (VII, **Fig. 5.6**) in the form of practical and promising ideas, considering each case in the order of decreasing frequency of occurrence (**Table 5.4**). The results of the analysis are presented in **Table 5.5**.

Table 5.5 Numbers and names of inventive principles and proposed solutions

No.	Name of Principle	Solution (Idea) (VII, Fig. 5.4)
1	**2**	**3**
		N = 5
2	Extraction	a) establishment of a dedicated service (outsourcing [50]) or training one or several specialists to operate the laser system and maintain several furnaces (possibly not only induction furnaces but also basic oxygen converters, blast furnaces, electric arc furnaces, etc.); b) relocation of the laser system outside the unit (furnace), ensuring mobility of the measuring device
		N = 4
10	Preliminary action	a) focus the sensors and laser scanning on areas of maximum wear and dimensional changes in the refractory lining, as identified from operational experience; b) perform measurements only in areas subject to maximum wear, deformation, and changes; c) take measurements several heats before the known critical number that characterizes the minimum durability of the lining; d) pre-scan the initial shape of the lining (crucible) or its critical shape and periodically compare with the actual condition to determine wear
13	Inversion (reverse, the other way round)	Reorient the sensors and embed them "in the armor" outside the refractory lining, directing the laser (or an acoustic system, ultrasonic testing [51], etc.) not from the outside onto the lining, but rather from beneath the lining outward
35	Parameter changes (changing the physical or chemical parameters)	a) controlling slag build-up on the refractory lining [52] by adding fluxes during the melting process; b) modifying the crucible shape during repairs, taking into account slag build-up ("freezing-on"), in combination with Principle 10 (*Preliminary action*); c) adjusting the relative position of the inductor coil and the crucible to anticipate slag deposits; d) in the case of acidic linings, avoiding the use of fluorspar (CaF_2) and borax ($Na_2B_4O_7$) in the slag to prevent a sharp decrease in lining durability; e) reducing the porosity of the lining and selecting appropriate raw materials, e.g., using high-quality quartzite linings with boron anhydride for alternating melting of cast iron and alloyed (corrosion-resistant, chromium–nickel) steels
		N = 3
19	Periodic action	a) operating the sensors (laser system) not in a continuous mode, but only when measurements are required, for example, before the predicted critical heat corresponding to the minimum durability of the lining; b) effective when applied in combination with Principle 13 (*Reverse — The other way round*); c) alternating melting of cast iron and alloyed steels
27	Cheap short-living instead of expensive long-living	The use of inexpensive laser sensors is hardly feasible. Replacing the laser system with mechanical measurement is unproductive, unsafe, outdated, and contradicts the task requirements

Continuation of Table 5.5

1	2	3
28	Replacement of a mechanical system (with an optical or acoustic one)	In certain cases, it is reasonable to consider replacing a costly laser system with a more affordable ultrasonic system [51] for measuring the lining thickness
32	Change of colour	Changing the color of the laser beam depending on the lining thickness (the color changes together with the thickness). This is possible when using an ionic liquid (molten salts, sodium chloride at 800°C) [53] and controlling the state of the ionic liquid via feedback ("laser – lining thickness – laser")
		N = 2
3	Local quality	Differentiated gunning during repairs
11	Cushion in Advance	Disabling or preventing the start-up of a furnace, which lining thickness is below or above the critical value
29	Use of pneumatics and hydraulics	Application of gas, liquid, and other types of lasers [53, 54]. Liquid lasers enable continuous adjustment of emission wavelengths, i.e., beam color (used in conjunction with Principle 32 – color change)
		N = 1
1	Segmentation	a) perform measurements not in a continuous mode, but at specific time intervals (see also Principle 19 – Periodic Action); b) since the lining thickness changes unevenly, more detailed measurements should be taken in areas of intensive thickness variation (see also Principle 10 – preliminary action)
6	Universality	Use lasers capable of varying their power over a wide range, both for scanning the lining profile as its thickness changes and for performing repair work such as overlaying a protective glaze on worn areas and/or selectively melting slag deposits. In the future, apply laser melting for metal processing ("laser furnaces"), considering current developments in laser sintering and casting [55]
21	Skipping	Following earlier proposals, use a high-power laser for both repair [56] and scanning [57] of the lining condition in a "skip" mode, allowing much shorter measurement times
24	Intermediary	Apply a controllable laser amplifier [58] to enable seamless switching between "scanning-measuring" and "repair-modification" modes
26	Copying	Study lining wear using photocopies and scanned images. Create a holographic model of the crucible for further analysis
38	Use of strong oxidants	Employ laser ionization methods [59]. Although oxidation is harmful to both the metal and the lining (crucible material), future laser technology could ionize the layer between the lining and the molten metal [60], preventing direct contact. Combining this with Principle 6 – Universality, one can envision melting units based on variable-power lasers that can: a) scan the lining condition; b) repair and modify the lining; c) ionize the contact layer; d) melt metal

It should be noted that some of the ideas presented in **Table 5.5** are formulated with consideration for the innovative development of science and technology, demonstrating the prospects of using laser systems for monitoring the thickness of the lining and expanding their technological capabilities.

5.5 FUNCTIONAL VALUE ANALYSIS

Functional Value Analysis (FVA or ABC-Method) is a method for evaluating the efficiency of a technical system in terms of its functionality and cost. In order to optimize the expenses for the technology of repairing worn-out linings of induction crucible furnaces, FVA is expedient to apply for determining the relationship between the functionality of cost components (materials) used for repair and their price. The main stages of FVA for evaluating the effectiveness of materials for repairing the worn lining of an induction crucible furnace are given in **Table 5.6**.

Table 5.6 Main stages of FVA in evaluating the effectiveness of materials for repairing the lining of an induction crucible furnace

No.	FVA stage	Description of the FVA stage
1	Identification of the functions of the repair materials	See **Table 5.7**
2	Evaluation of the importance of functions	Determining the degree of importance of each function for restoring the lining and ensuring the efficient operation of the induction crucible furnace, using the ABC principle. Assessing the impact of each function on furnace productivity and operational safety
3	Cost analysis of functions	Considering the costs of materials, their manufacturing, and installation. Evaluating the efficiency of different materials in terms of service life extension, resistance to aggressive environments, and lining cost
4	Identification of alternatives	Reviewing various types of thermal insulation, structural, and heat-resistant materials that may be used for lining repairs. Comparing their technical characteristics and cost
5	Selection of the optimal option	Selecting the material that ensures the highest efficiency at an affordable cost
6	Optimization and continuous improvement	Implementation of the selected material. Monitoring the material's performance. Adjusting the material specification if necessary

The wear of the crucible lining in an induction furnace is influenced by the severe operating conditions it is subjected to: thermal, erosive, and corrosive impact of the hot molten metal; the chemical corrosion processes caused by slag; the effect of the static pressure of the molten metal column (up to 40–80 kPa [18]); the effect of dynamic friction during molten metal stirring; mechanical impacts during charging of scrap and alloying elements; as well as during the collapse of bridges formed during melting.

The object of improvement considered is a 3t induction crucible furnace operated in the melting department of the foundry shop of *Zaporizhzhia Foundry and Mechanical Plant LLC*.

Thus, FVA makes it possible to select the optimal material for repairing worn lining, ensuring process efficiency and economic feasibility in resource utilization. The furnace lining must typically be replaced on a monthly basis. The following components are required for the repair: refractory mass, refractory concrete, ramming mass, a mold for furnace ramming, and a crucible (which has its own service life and requires replacement after wear).

The functionality of the materials was assessed in terms of their significance for achieving the goal (effect) of extending the intervals between repairs. An expert assessment method was applied to evaluate the functionality of the elements. Following the Eisenhower-Pareto principle, functions (see item 1 in **Tables 5.6** and **5.7**) were categorised by their contribution to achieving the goal, assigned to specific ABC classes, denoted as follows: **A** — main functions, **B** — secondary functions, **C** — unnecessary or redundant functions.

Table 5.7 Distribution of repair material functions for furnace lining (as per item 1 in **Table 5.6**) according to the ABC principle for the target objective of extending the inter-repair period

No.	Components	Functions						
		F1	F2	F3	F4	F5	F6	Total by components
1	Crucible	B	A	A	A	A	B	4A–2B
2	Refractory mass	B	B	–	A	–	B	A–3B
3	Refractory concrete	–	B	B	A	–	C	A–2B–C
4	Ramming mass[1]	A	C	–	C	–	–	A–2C
5	Furnace ramming mould[2]	A	–	–	–	–	–	A

Note: [1]mineralizers and binding agents; [2]welded from sheet material.
F1 — restoration of the lining's dimensions and shape; F2 — recovery of the lining's thermal insulation properties operating across the entire working temperature range (200…1650°C); F3 — provision of mechanical strength to retain the melt and withstand impacts; F4 — ensuring resistance to high-temperature exposure; F5 — protection against erosion, aggressive media, and wear caused by hydrodynamic stirring of the molten metal; F6 — restoration of heat-reflective characteristics
Source: [61]

Thus, the materials are considered according to the expenditure incurred for furnace repair. Owing to fluctuating prices, nondisclosure policies, and the likelihood of trade secrecy affecting the repair cost, **Table 5.8** presents the distribution of repair expenditures as resulting percentage values. The costs for items 2–3 in **Table 5.8** are given per tonne of material. In addition, the materials used for furnace repair were evaluated in terms of their functional significance for achieving maximum lining durability. The evaluation was performed on a tenpoint scale. A survey was conducted among employees of various shop departments, namely: the section foreman, representatives of the procurement department, and repair crews. The average expert scores for significance are provided in **Table 5.8**. Based on the obtained results, a significance coefficient was calculated for the constituent materials used to repair the induction crucible furnace (**Table 5.8**). The data obtained are presented graphically in **Fig. 5.8** as a functional-value diagram.

Table 5.8 Calculation of cost coefficients for constituent materials used to repair an induction crucible furnace

No.	Components	Repair costs		Expert assessment of the significance		Cost ratio
		Share in total costs, STC (%)	Class	Average score (10-point scale)	Significance, SIG (%)	Cost coefficient, CC = STC/SIG
1	Crucible	81	A	7.6	21	3.85
2	Refractory mass	6.2	A	8.3	24	0.25
3	Refractory concrete	3.5	B	7	20	0.17
4	Ramming mass	5	A	7.6	21	0.20
5	Furnace ramming mold	4.3	C	5	14	0.30
Total		100	–	35.5	100	–

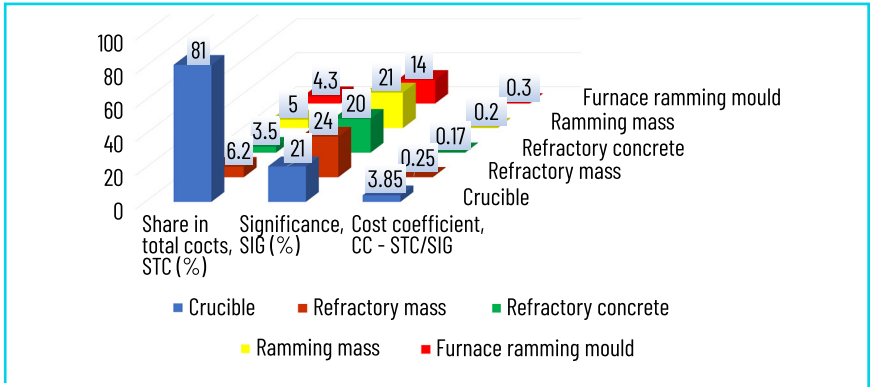

Fig. 5.8 Functional-value diagram for the repair of an induction crucible furnace

For an optimal technical system, the ratio of the specific weight in total costs to the significance of each individual parameter (component) should not exceed 1.0. Based on the obtained results, it was established that the cost coefficient (CC) for crucible replacement is 3.85, which indicates the need to search for alternative crucible suppliers with lower prices. It should be noted that crucible replacement does not take place during every repair. Therefore, in the future, it is advisable to refine the above-mentioned FVA methodology to recalculate costs per tonne of steel produced.

As an organizational optimization measure, recommendations have been developed to ensure compliance with crucible operating rules to extend the intervals between repairs and to carry out maintenance by re-ramming the furnace without crucible replacement. The cost coefficient for other components is considered favorable (<1.0).

CONCLUSIONS

In the context of global decarbonization, this study addresses the improvement of electrometallurgical steelmaking processes, particularly the operation and reliability of induction melting furnaces used for high-quality steel and alloy production. These units combine high productivity with stable process control and lower environmental impact, yet the durability of the refractory lining remains a limiting factor for operational efficiency and reliability.

The improvement of induction furnace performance primarily depends on optimizing the crucible design and refractory lining properties, including resistance to thermal shocks, slag corrosion, and mechanical stresses, as well as maintaining minimal wear during melting. Based on the operational experience of *Zaporizhzhia Foundry and Mechanical Plant LLC*, a methodological framework for systematic condition monitoring and maintenance decision-making of refractory linings was developed and tested. This framework integrates engineering practice with heuristic analysis and continuous improvement principles to identify actionable measures for enhancing lining durability and stability of melting processes.

The application of the method of control questions (MCQ) enabled identification of critical operational and design factors affecting refractory wear. These findings formed the basis for the monitoring logic, linking observed wear symptoms with preventive and corrective actions — selection of optimal refractory materials, implementation of local hot repairs, control of slag quality and chemical composition, and optimization of crucible geometry and cooling zones. Using the focal objects method (FOM), innovative technical concepts were generated, particularly the feasibility of introducing a laser-based system for real-time monitoring of the residual lining thickness. This system, functioning as a diagnostic element of the proposed monitoring framework, allows continuous tracking of the lining profile and thickness, enabling early detection of critical wear areas and precise scheduling of maintenance operations.

The TRIZ/ARIZ methodology contributed to the synthesis of the overall monitoring and maintenance framework by connecting heuristic problem-solving with the structural definition of decision-support stages — data acquisition, condition assessment, and corrective planning — within a continuous improvement loop. In turn, the Functional–Value Analysis (FVA) enabled the evaluation of the cost-efficiency of maintenance and repair operations for a 3-tonne induction crucible furnace, identifying cost drivers and establishing decision criteria for supplier selection, resource allocation, and maintenance optimization.

Organizational improvements were also proposed, focusing on standardized maintenance protocols and adherence to operational parameters to extend crucible service life. These measures facilitate the transition from reactive to predictive maintenance strategies, improving process stability and the overall efficiency of the equipment.

The integration of the developed condition monitoring and maintenance decision-making framework, grounded in continuous improvement principles, enables a systematic increase in process reliability, reduction of unplanned downtime, and improvement of refractory lining durability. The obtained results confirm the effectiveness of combining analytical, heuristic, and managerial methods in advancing electrometallurgical process control systems and serve as a practical foundation for further development of decision support tools for maintenance planning and optimization of refractory management in induction melting furnaces.

REFERENCES

1. Zhang, J., Guo, H., Yang, G., Wang, Y., Chen, W. (2025). Sustainable Transition Pathways for Steel Manufacturing: Low-Carbon Steelmaking Technologies in Enterprises. Sustainability, 17 (12), 5329. https://doi.org/10.3390/su17125329
2. Mariani, A., Malucelli, G. (2023). Insights into Induction Heating Processes for Polymeric Materials: An Overview of the Mechanisms and Current Applications. Energies, 16 (11), 4535. https://doi.org/10.3390/en16114535
3. Hauck, A., Schmitz, W. (2018). The basic properties of the coreless induction furnace and its application in recycling production scrap. World of Metallurgy — ERZMETALL, 71 (6), 309—317.
4. Kukhar, V., Prysiazhnyi, A., Balalayeva, E., Anishchenko, O. (2017). Designing of induction heaters for the edges of pre-rolled wide ultrafine sheets and strips correlated with the chilling end-effect. 2017 International Conference on Modern Electrical and Energy Systems (MEES), 404—407. https://doi.org/10.1109/mees.2017.8248945
5. Ren, W., Wang, L. (2022). Precipitation behavior of M23C6 in high nitrogen austenitic heat-resistant steel. Journal of Alloys and Compounds, 905, 164013. https://doi.org/10.1016/j.jallcom.2022.164013
6. Wang, B., Zhang, Y., Qiu, F., Cai, G., Cui, W., Hu, Z. et al. (2022). Role of trace nanoparticles in manipulating the widmanstatten structure of low carbon steel. Materials Letters, 306, 130853. https://doi.org/10.1016/j.matlet.2021.130853
7. Chelariu, R. G., Cimpoeșu, N., Birnoveanu, T. I., Istrate, B., Baciu, C., Bejinariu, C. (2022). Obtaining and Analysis of a New Aluminium Bronze Material Using Induction Furnace. Archives of Metallurgy and Materials, 67 (4), 1251—1257. https://doi.org/10.24425/amm.2022.141049
8. Li, H., Wang, A., Liu, T., Chen, P., He, A., Li, Q. et al. (2021). Design of Fe-based nanocrystalline alloys with superior magnetization and manufacturability. Materials Today, 42, 49—56. https://doi.org/10.1016/j.mattod.2020.09.030
9. Aikin, M., Shalomeev, V., Kukhar, V., Kostryzhev, A., Kuziev, I., Kulynych, V. et al. (2025). Recent Advances in Biodegradable Magnesium Alloys for Medical Implants: Evolution, Innovations, and Clinical Translation. Crystals, 15 (8), 671. https://doi.org/10.3390/cryst15080671
10. Markov, O. E., Khvashchynskyi, A. S., Musorin, A. V., Markova, M. A., Shapoval, A. A., Hrudkina, N. S. (2022). Investigation of new method of large ingots forging based on upsetting of workpieces with ledges. The International Journal of Advanced Manufacturing Technology, 122 (3-4), 1383—1394. https://doi.org/10.1007/s00170-022-09989-1
11. Kukhar, V., Balalayeva, E., Hurkovska, S., Sahirov, Y., Markov, O., Prysiazhnyi, A., Anishchenko, O. (2019). The Selection of Options for Closed-Die Forging of Complex Parts Using Computer Simulation by the Criteria of Material Savings and Minimum Forging Force. Intelligent Communication, Control and Devices. Singapore: Springer, 325—331. https://doi.org/10.1007/978-981-13-8618-3_35
12. Kalisz, D., Żak, P. L., Semiryagin, S., Gerasin, S. (2021). Evolution of Chemical Composition and Modeling of Growth Nonmetallic Inclusions in Steel Containing Yttrium. Materials, 14 (23), 7113. https://doi.org/10.3390/ma14237113

13. Patil, D. D., Ghatge, D. A. (2017). Parametric Evaluation of Melting Practice on Induction Furnace to Improve Efficiency and System Productivity of CI and SGI Foundry- A Review. International Advanced Research Journal in Science, Engineering and Technology, 4 (1), 159–163. https://doi.org/10.17148/iarjset/ncdmete.2017.36
14. Sinelnikov, V., Szucki, M., Merder, T., Pieprzyca, J., Kalisz, D. (2021). Physical and Numerical Modeling of the Slag Splashing Process. Materials, 14 (9), 2289. https://doi.org/10.3390/ma14092289
15. Dou, W., Yang, Z., Wang, Z., Yue, Q. (2021). Molten Steel Flow, Heat Transfer and Inclusion Distribution in a Single-Strand Continuous Casting Tundish with Induction Heating. Metals, 11 (10), 1536. https://doi.org/10.3390/met11101536
16. Liang, X., Li, M., Cheng, B., Wu, F., Luo, X. (2023). Effects of induction furnace conditions on lining refractory via multi-physics field simulation. Applied Physics A, 129 (8). https://doi.org/10.1007/s00339-023-06808-6
17. Kozlov, H. O., Topolov, V. L., Kozlov, O. H. (2025). Konstruktsiia elektrometalurhiinykh ahrehativ. Nikopol Professional College of the Ukrainian State University of Science and Technology. Available at: https://kema.at.ua/book1.html#fig73
18. Shiqi, L., Weili, L.; Kuangdi, X. (Ed.) (2024). Induction Furnace Melting. The ECPH Encyclopedia of Mining and Metallurgy. Singapore: Springer, 929–931. https://doi.org/10.1007/978-981-99-2086-0_967
19. Khrebtova, O., Shapoval, O., Markov, O., Kukhar, V., Hrudkina, N., Rudych, M. (2022). Control Systems for the Temperature Field During Drawing, Taking into Account the Dynamic Modes of the Technological Installation. 2022 IEEE 4th International Conference on Modern Electrical and Energy System (MEES). IEEE, 1–6. https://doi.org/10.1109/mees58014.2022.10005724
20. Savchenko, I. V., Shapoval, O., Kuziev, I. (2022). Modeling of High Module Power Sources Systems Safety Processes. Materials Science Forum, 1052, 399–404. https://doi.org/10.4028/p-24y9ae
21. Artiukh, V., Mazur, V., Kukhar, V., Vershinin, V., Shulzhenko, N. (2019). Study of polymer adhesion to steel. E3S Web of Conferences, 110, 01048. https://doi.org/10.1051/e3sconf/201911001048
22. Shapoval, A., Kantemyrova, R., Markov, O., Chernysh, A., Vakulenko, R., Savchenko, I. (2020). Technology of Production of Refractory Composites for Plasma Technologies. 2020 IEEE Problems of Automated Electrodrive. Theory and Practice (PAEP). IEEE, 1–4. https://doi.org/10.1109/paep49887.2020.9240830
23. Kruzhilko, O., Volodchenkova, N., Maystrenko, V., Bolibrukh, B., Kalinchyk, V., Zakora, A. et al. (2021). Mathematical modelling of professional risk at Ukrainian metallurgical industry enterprises. Journal of Achievements in Materials and Manufacturing Engineering, 1 (108), 35–41. https://doi.org/10.5604/01.3001.0015.4797
24. Pachkolin, Y., Bondarenko, A., Levchenko, S. (2018). Practical application of mathematical models of electro-thermo-mechanical processes in industrial induction furnaces with the aim of increasing their energy efficiency. Technology Audit and Production Reserves, 5 (1 (43)), 28–33. https://doi.org/10.15587/2312-8372.2018.146484
25. Razzhivin, O., Markov, O., Subotin, O. (2022). Automated Melt Temperature Control System In Induction Furnace. 2022 IEEE 4th International Conference on Modern Electrical and Energy System (MEES). IEEE, 1–4. https://doi.org/10.1109/mees58014.2022.10005650

26. Dötsch, E.; Rudnev, V. T., Totten, G. E. (Eds.) (2014). Operation of Induction Furnaces in Iron Foundries. Induction Heating and Heat Treatment. ASM International, 491–520. https://doi.org/10.31399/asm.hb.v04c.a0005904
27. Achkan, V. V., Vlasenko, K. V., Chumak, O. O., Sitak, I. V., Kovalenko, D. A. (2022). A model of learning the online course "Creative Thinking through Learning Elementary Maths." Journal of Physics: Conference Series, 2288 (1), 012020. https://doi.org/10.1088/1742-6596/2288/1/012020
28. Hsia, T.-C., Huang, S.-C. (2011). Using the Theory of Inventive Problem-Solving (TRIZ) to Implement Safety Improvements in Foundry Engineering Pouring Procedures. 2011 International Conference on Management and Service Science. IEEE, 1–4. https://doi.org/10.1109/icmss.2011.5999352
29. Refractory lining materials for induction furnaces (2024). Refractories Materials. Available at: https://refractoriesmaterials.com/refractory-lining-materials-for-induction-furnaces
30. Park, H.-S., Dang, X.-P. (2013). Reduction of heat losses for the in-line induction heating system by optimization of thermal insulation. International Journal of Precision Engineering and Manufacturing, 14 (6), 903–909. https://doi.org/10.1007/s12541-013-0119-6
31. Umbrasko, A., Baake, E., Nacke, B., Jakovics, A. (2008). Numerical studies of the melting process in the induction furnace with cold crucible. COMPEL – The International Journal for Computation and Mathematics in Electrical and Electronic Engineering, 27 (2), 359–368. https://doi.org/10.1108/03321640810847643
32. Dötsch, E., Nacke, B.; Rudnev, V. T., Totten, G. E. (Eds.) (2014). Components and Design of Induction Crucible Furnaces. Induction Heating and Heat Treatment. ASM International, 447–461. https://doi.org/10.31399/asm.hb.v04c.a0005899
33. Nesarajah, M., Frey, G. (2016). Thermoelectric power generation: Peltier element versus thermoelectric generator. IECON 2016 – 42nd Annual Conference of the IEEE Industrial Electronics Society. IEEE, 4252–4257. https://doi.org/10.1109/iecon.2016.7793029
34. Demin, D. (2020). Constructing the parametric failure function of the temperature control system of induction crucible furnaces. EUREKA: Physics and Engineering, 6, 19–32. https://doi.org/10.21303/2461-4262.2020.001489
35. Przyłucki, R., Golak, S., Oleksiak, B., Blacha, L. (2011). Influence of the geometry of the arrangement inductor – crucible to the velocity of the transport of mass in the liquid metallic phase mixed inductive. Archives of Civil and Mechanical Engineering, 11 (1), 171–179. https://doi.org/10.1016/s1644-9665(12)60181-2
36. Sadri, A., Ying, W. L., Erskine, J., Macrosty, R. (2016). Smelting furnace non-destructive testing (NDT) and monitoring. 19th World Conference on Nondestructive Testing. Munich, 1–12. Available at: https://www.ndt.net/article/wcndt2016/papers/th4e5.pdf
37. Ung, D. (2023). Enhancing crucible performance in non-ferrous applications. Foundry Practice, 272, 13–17. Available at: https://27097971.fs1.hubspotusercontent-eu1.net/hubfs/27097971/FP%20272%20en.pdf
38. Tamura, S., Ochiai, T., Matsui, T., Goto, K. (2008). Technological philosophy and perspective of nano-tech refractories. Nippon Steel Technical Report, 98, 18–28. Available at: https://www.nipponsteel.com/en/tech/report/nsc/pdf/n9804.pdf

39. Prstić, A., Aćimović-Pavlović, Z., Terzić, A., Pavlović, L. (2014). Synthesis and Characterization of New Refractory Coatings Based on Talc, Cordierite, Zircon and Mullite Fillers for Lost Foam Casting Process. Archives of Metallurgy and Materials, 59 (1), 89–95. https://doi.org/10.2478/amm-2014-0015
40. Buliński, P., Smolka, J., Golak, S., Przyłucki, R., Palacz, M., Siwiec, G. et al. (2017). Numerical and experimental investigation of heat transfer process in electromagnetically driven flow within a vacuum induction furnace. Applied Thermal Engineering, 124, 1003–1013. https://doi.org/10.1016/j.applthermaleng.2017.06.099
41. Durand, F. (2005). The electromagnetic cold crucible as a tool for melt preparation and continuous casting. International Journal of Cast Metals Research, 18 (2), 93–107. https://doi.org/10.1179/136404605225022883
42. Savransky, S. D. (2000). Engineering of creativity: Introduction to TRIZ methodology of inventive problem solving. CRC Press, 408. https://doi.org/10.1201/9781420038958
43. Altshuller, G. S. (1984). Creativity as an exact science. CRC Press, 320. https://doi.org/10.1201/9781466593442
44. Wu, X., Ma, J., Wang, J., Song, H., Xu, J. (2025). Mobile Tunnel Lining Measurable Image Scanning Assisted by Collimated Lasers. Sensors, 25 (13), 4177. https://doi.org/10.3390/s25134177
45. Tucci, G., Conti, A., Fiorini, L.; Parente, C., Troisi, S., Vettore, A. (Eds.) (2020). Refractory Brick Lining Measurement and Monitoring in a Rotary Kiln with Terrestrial Laser Scanning. R3 in Geomatics: Research, Results and Review. Springer, 296–310. https://doi.org/10.1007/978-3-030-62800-0_23
46. Kuo, S.-K., Lee, W.-C., Du, S.-W. (2008). Measurement of Blast Furnace Refractory Lining Thickness with a 3D Laser Scanning Device and Image Registration Method. ISIJ International, 48 (10), 1354–1358. https://doi.org/10.2355/isijinternational.48.1354
47. Andrade, J., Viale, M., De los Santos, C., Butler, R., Kan, M., Rambo, M., Corbari, R. (2015). EAF application of SmartFurnace and ZoloSCAN laser off gas measurement technology at Vallourec Star (Tech. Rep. No. PPMS001_2018). AMI. Available at: https://www.amiautomation.com/PPMS001_2018
48. Angelova, D. (2021). Experimental application of the method of focal objects in design education. Innovation in Woodworking Industry and Engineering Design, 2 (20), 82–87. Available at: https://www.cabidigitallibrary.org/doi/pdf/10.5555/20220215904
49. Schmitz, W., Donsbach, F., Henrik, H. (2006). Development and use of a new optical sensor system for induction furnace crucible monitoring. Proceedings of the 67th World Foundry Congress: "Casting the Future". Institute of Cast Metals Engineers. Curran Associates, Inc., 653–662. Available at: https://www.iftabira.org/pdfs/15%20W.Schmitz_441168101.pdf
50. Pererva, P., Kuchynskyi, V., Kobielieva, T., Kosenko, A., Maslak, O. (2021). Economic substantiation of outsourcing the information technologies and logistic services in the intellectual and innovative activities of an enterprise. Eastern-European Journal of Enterprise Technologies, 4 (13 (112)), 6–14. https://doi.org/10.15587/1729-4061.2021.239164
51. Sadri, A., Ying, W. L., Erskine, J., Macrosty, R. (2016). Smelting furnace non-destructive testing (NDT) and monitoring. 19th World Conference on Nondestructive Testing. Munich, 1–12. Available at: https://www.ndt.net/article/wcndt2016/papers/th4e5.pdf

52. Prijanovič Tonkovič, M., Lamut, J. (2020). Build-up formation in an induction channel furnace. Materiali in Tehnologije, 54 (2), 167–171. https://doi.org/10.17222/mit.2019.233
53. Zhang, H., Zhang, C., Vaziri, S., Kenarangi, F., Sun, Y. (2021). Microfluidic Ionic Liquid Dye Laser. IEEE Photonics Journal, 13 (1), 1–8. https://doi.org/10.1109/jphot.2020.3044861
54. Biswas, D. J. (2023). Molecular Gas Lasers. A Beginner's Guide to Lasers and Their Applications. Cham: Springer, 261–285. https://doi.org/10.1007/978-3-031-24330-1_11
55. Yang, L., Tang, S., Fan, Z., Jiang, W., Liu, X. (2021). Rapid casting technology based on selective laser sintering. China Foundry, 18 (4), 296–306. https://doi.org/10.1007/s41230-021-1099-2
56. Mudge, R. P., Wald, N. R. (2007). Laser engineered net shaping advances additive manufacturing and repair. Welding Journal, 86 (1), 44–48. Available at: https://www.researchgate.net/publication/285913676_Laser_engineered_net_shaping_advances_additive_manufacturing_and_repair
57. Chang, K.-S., Lu, S.-T., Wu, Y.-P., Chou, C. (1992). Correction algorithms in a laser scanning dimension measurement system. IEE Proceedings A Science, Measurement and Technology, 139 (2), 57–60. https://doi.org/10.1049/ip-a-3.1992.0011
58. Zuo, J., Lin, X. (2022). High-Power Laser Systems. Laser & Photonics Reviews, 16 (5). https://doi.org/10.1002/lpor.202100741
59. Hu, S., Huang, K., Zhu, F., Gai, B., Li, J., Tan, Y., Guo, J. (2023). Temporal evolution of laser-induced ionization and recombination processes in argon-helium mixture. Optics Continuum, 2 (12), 2516. https://doi.org/10.1364/optcon.506849
60. Oukach, S., Pateyron, B., Pawłowski, L. (2019). Physical and chemical phenomena occurring between solid ceramics and liquid metals and alloys at laser and plasma composite coatings formation: A review. Surface Science Reports, 74 (3), 213–241. https://doi.org/10.1016/j.surfrep.2019.06.001
61. Gorokhovskii, A. V., Meshcheryakov, D. V., Burmistrov, I. N., Sevryugin, A. V. (2019). Heat-Reflecting Ceramic Materials Based on Potassium Polytitanate and Silicon Oxide. Refractories and Industrial Ceramics, 59 (6), 663–666. https://doi.org/10.1007/s11148-019-00292-3

Edited by
Igor Krasnikov

PROCESSES AND CONTROL SYSTEMS: SYNTHESIS, MODELING, OPTIMIZATION

Anatolii Babichenko, Igor Krasnikov, Juliya Babichenko, Oleksandr Dzevochko, Yana Kravchenko, Ihor Lysachenko, Valerii Samsonkin, Valerii Druz, Oksana Yurchenko, Vitalii Budashko, Oksana Glazeva, Albert Sandler, Sergii Khniunin, Valentyn Bogach, Yurii Zhuravlov, Petro Lezhniuk, Viacheslav Komar, Vladyslav Lysyi, Yuliia Malohulko, Volodymyr Netrebskyi, Olena Sikorska, Oleksandr Povazhnyi, Volodymyr Kukhar, Oleksiy Koyfman, Khrystyna Malii, Volodymyr Pashynskyi

Monograph

Technical editor I. Prudius
Desktop publishing T. Serhiienko

TECHNOLOGY CENTER PC®
Published in December 2025
Enlisting the subject of publishing No. 4452 – 10.12.2012
Address: Shatylova dacha str., 4, Kharkiv, Ukraine, 61165
